NEIGHBORING GROUP PARTICIPATION IN THE REDOX MECHANISMS OF THIOETHERS AND THEIR TRANSITION METAL COMPLEXES

by

Sanaullah

B.Sc., Jahanzeb College, Swat, PAKISTAN, 1976
M.Sc., University of Karachi, PAKISTAN, 1981

Submitted to the Department of
Chemistry and the Faculty of the
Graduate School of the University
of Kansas in partial fulfillment
of the requirements for the degree
of Doctor of Philosophy

ABSTRACT

This report addresses the structural and redox properties of thioethers and their coordination compounds. The low temperature x-ray studies of the hexacoordinated $[Cu^{II}(TTCN)_2]$ (a $Cu(II)S_6$ type chromophore, TTCN = 1,4,7-trithiacyclononane) with a chiral counter ion ((+)-3-bromocamphor-10-sulfonate) failed to reveal Jahn-Teller distortion. The complex ion crystallizes in the space group $P2_12_12_1$. The point group symmetry of the complex ion is C_i. The electrochemistry of $[Cu^{II/I}(TTCN)_2]$ system reflects conformational changes following the electron transfer reaction. The crystallographic studies of $[Cu^{I}(TTCN)_2]$ has shown the reduced form to be tetrahedral (space group $P2_1/n$). Comparing the crystallographic data of $[Cu^{I}(TTCN)_2]$, $[Cu^{I}(TTCN)(SODTCN)]$ (SODTCN = 1-sulfoxide-4,7-dithiacyclononane) and $[(Cu^{I}(TTCN))_2(1,4\text{-Dithiane})]$ revealed that the mode of coordination of the monodentate thioether in all three cases is almost the same. However the NMR studies of $[Cu^{I}(TTCN)_2]$ has shown an extremely fluxional conformation of the complex ion. Pulse radiolysis was employed to study in detail the absolute kinetics of the conformational changes associated with the electron transfer reactions of $[Cu^{II/I}(TTCN)_2]$ system.

Cyclic voltammetry of structurally constrained thioethers, tricyclo[2.2.1.0]heptane-1,5-dithiocane (NorDTCO) and 2-*endo*-naphtho-6-*endo*(methylthio)bicyclo[2.2.1]heptane, has shown a strong dependence of the redox

chemistry of the thioethers on the neighboring lone-pair and π-electrons as well as on the solvent. The acid/base chemistry, presumably involving the $-^{+\cdot}S-C_{\alpha}-H$ proton, has also been studied.

The electrochemistry of the more flexible thioether, methionine, is shown to strongly depend on pH of the solution. However, there is no influence of pH when the carboxylate and ammine moieties of methionine are coordinated to Co(III). These observations have been justified in terms of neighboring group participation in the redox chemistry of thioethers. The crystallographic asymmetric unit of $[Co^{III}(en)_2(L\text{-}Met)]$ contains two independent enantiomeric structural units (Δ and Λ). The electrochemistry of $[Co^{III}(trien)(L\text{-}Met)]$ as well as that of a bimetallic complex $[(trien)Co^{III}(L\text{-}Met)Ru^{II}(NH_3)_5]$ is also presented.

To my grandpa, Qazi Sabitur Rahman and my father-in-law Sarbiland Khan whose dedication to teaching has benefitted hundreds of people. To my father, Dilber Khan, my mom, and my uncle and teacher, Mohammad Ismail.

ACKNOWLEDGEMENTS

Many people in the Chemistry Department have contributed to this work with their knowledge and expertise but first of all I praise and thank The almighty God for keeping me on the right track.

I would like to express my heart felt gratitude to Dr. George Wilson for his guidance, patience and caring. His scientific wisdom and a desire to maintain simplicity and clarity without losing the scientific rigor has been a catalyst in extracting all the fine details from the collected data.

The keen interest and spontaneous chemical intuition of Dr. Richard Glass has saved me lot of trouble and time and his enthusiasm has always been a source of motivation. I express my deep appreciation to Dr. Glass and members of his research group for all the encouragement and guidance.

The painstaking perusal of this work by my defense committee (Drs. Daryle Busch, Richard Glass, Cynthia Larive, Craig Lunte, Christian Schnöneich and George Wilson) has brought this work to its final shape. I would like to express my appreciation to all of them for their assistance and patience. I would also like to thank Dr. Fusao Takusagawa, Dr. David Vander Velde, Dr. Joseph Heppert and Martha Morton for their help in x-ray crystallography, NMR spectroscopy, and electrochemistry in a dry box. The invaluable input to this work and to my understanding of the redox chemistry by Drs. K.-D. Asmus and Hartmut Hungerbühler is greatly appreciated. I could not have made it without them.

My special thanks go to the members of Dr. Wilson's research group (1988 - 1992) and I have to acknowledge the invaluable help of Brian Hill and Dr. Caroline Scolari who got me started on my road to this destination. I would also like to extend a note of appreciation to Dr. Fitratullah Khan, Kapila DeSilva and Iffaz Salahuddin for cheering me up in moments of depression.

Drs. M. Ghaziuddin, Syed A. Malik, M. Abu Anwar Usmani, Shabbir A. Zubairi, and Stanley C. Neely definitely get the credit for encouraging me to continue my studies abroad toward the Ph.D. degree. Their contribution to this process is greatly appreciated.

Finally I thank my parents, uncles, brothers and sisters for all the encouragement and help both at home and abroad. My long absence from them has put them into a tough ordeal but I hope one day I will be able to make it up. My long hours at work have also made Rukhsana and our children Hafsa, Safia and Zakaullah pay their share. Bringing up our children has made me appreciate the greatness of my parents and their commitment to my well-being. Also the occasional silly curiosity of Hafsa, Safia and Zakaullah has been a source of joy and ammusement.

TABLE OF CONTENTS

LIST OF FIGURES

LIST OF SPECTRA

LIST OF PLOTS

LIST OF TABLES

LIST OF SCHEMES

LIST OF ABBREVIATIONS

bipy ..... bipyridine

$CamphSO_3$ ..... (+)-3-bromocamphor-10-sulfonate

$CamphSO_3H$ ..... (+)-3-bromocamphor-10-sulfonic acid

CPE ..... Controlled potential electrolysis

CV ..... Cyclic voltammetry/voltammogram

DES ..... Diethylsulfide

DMS ..... Dimethylsulfide

DTBP 2,6-Di-*tert*-butylpyridine

en ..... Ethylenediamine

ET ..... Electron transfer

HTCOD 1,4,7,10,13,16-hexathiacyclooctadecane

HTFA ..... Trifluoroacetic acid

HTFMS ..... Trifluoromethanesulfonic acid

Met ..... L-Methionine

NMR ..... Nuclear magnetic resonance

NorDTCO ..... tricyclo[2.2.1.0]heptane-1,5-dithiocane

OAc ..... Acetate

O-phen 1,10-phenanthroline

PMS ..... Pentamethylene sulfide

RDE ..... Rotating disc electrode

RRDE ..... Rotating ring disc electrode

SODTCN 1-sulfoxide-4,7-dithiacyclononane

TBAHFP ..... Tetrabutylammoniumhexafluorophosphate

TFMS ..... Trifluoromethanesulfonate

THT ..... Tetrahydrothiophene

trien ..... triethylenetetraamine

TTCN 1,4,7-trithiacyclononane

CHAPTER 1

GENERAL INTRODUCTION

The high polarizability of sulfur has led to the classification of sulfur centered nucleophiles as soft bases and their general reactivity has been defined along this line[1,2]. The presence of one or more S atoms in an organic molecule entitles it as a member of organosulfur class of compounds. However, the variability of functional groups with sulfur gives rise to such different compounds as thiols, sulfides, sulfones, thiones, and many others with distinct chemical and physical properties. But basicity and polarizability are still popular in defining the nucleophilic reactivity of organosulfurs[3,4].

Organic sulfides are defined as poorer nucleophiles than thiolate anions, because of their much lower basicity. Nevertheless, the reactivity of these centers is highly dependent on their structural environment. A classical example of the nucleophilic participation of the sulfide function as an anchimeric group is the hydrolysis of β-chlorosulfides (Eq.1.1)[5]. Anchimeric assistance is strong when three,

$$RS\text{-}CH_2\text{-}CH_2\text{-}Cl \xrightarrow{^-OH} [R\text{-}S(\text{-}CH_2\text{-}CH_2) + Cl] \longrightarrow RS\text{-}CH_2\text{-}CH_2\text{-}OH \qquad (1.1)$$

five-, or six-membered rings can be formed[6]. Similarly the influence of the neighboring group and its spatial position on the numerical value of the redox potential and on the electrochemical reversibility of the $R_2S/R_2S^{\cdot+}$ redox couple is well documented[7]. Therefore, structural effects are more important in defining the

electronic properties of sulfur centers than mere classification into "polarizable" vs "non-polarizable" functions.

Sulfur centered radical cations are normally unstable towards nucleophilic attack. The cation radical generated by one-electron oxidation of R_2S accommodates the unpaired electron in the sulfur *p*-orbital. This highly reactive species tends to stabilize itself by interacting with an available *p*-electron lone pair to form an inter or intramolecular 3 electron bond. The cation radical thus generated can accommodate the unpaired electron in the corresponding σ^* orbital resulting in a weaker σ bond[8]. The participation of free radicals from sulfur-containing compounds is implicated in a number of important biological processes[9].

The present work was inspired by the desire to understand the electronic properties of thioethers in a variety of environments. Part of this report will be devoted to the anodic oxidation of a number of thioethers, tailored to provide specific information. The redox properties of the thioethers **1.1** and **1.2** were extensively studied in order to see how the presence of lone pair and such π electrons must

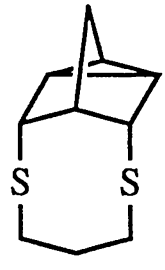

1.1

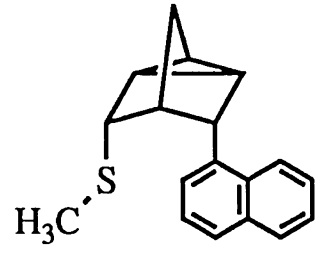

1.2

stabilize the electrochemically generated thioether cation radical. Such knowledge may

be very useful in providing first hand qualitative information about the ionization of different thioethers and about the fate of the ionization product and may also be of vital interest in the mass spectrometry of thioethers[10].

A significant part of bioenergetics is contributed by electron transfer reactions through protein assemblies. Sulfur containing amino acids in the protein backbone serve to stabilize, through disulfide bonds, the three dimensional structure of proteins and to hold the metal centers in certain configuration in metalloproteins. For example in ferricytochrome c one of the axial positions on iron is coordinatively held by methionine[11] and in plastocyanine[12] and azurine[13] the Cu(II) center involves cysteine, methionine and two histidines. The specific three dimensional structure and the ligand environment about the metal center in these proteins uniquely defines their position in the biological electron transport chain.

Until the early 1980's the coordination chemistry of thioethers was not as extensively investigated as that of the phosphine and amine complexes[14]. This can be imputed to the general conception that thioethers are poor donors to transition metal ions, probably due to the increased repulsion between the metal based electrons and the ligand based uncoordinated pair(s) of electrons. Thus the coordination capability of the potential ligands decreases in the order $R_3P > R_2S > RCl$. The importance of this stereoelectronic repulsion can be appreciated from the increased strength of the Metal-S bond in $[Br_2Pt(SEt_2)_2PtBr_2]$ where both lone pairs are involved in bonding[15]. The donation is further discouraged by the lower effective electronegativity of sulfur

which fails to relieve the increased negative charge on the metal ion. Because of the low donor ability, thioethers fail to displace effectively even noncoordinating anions from the coordination sphere of the first row transition metals [16-20].

By considering the electronic structure of thioethers, one would expect the uncoordinated pair of electrons to be readily available for π-donation. Also the empty *d* orbital on sulfur can be expected to act as π-acceptor (Figure 1.1). However, there has been very little evidence of π-donation.

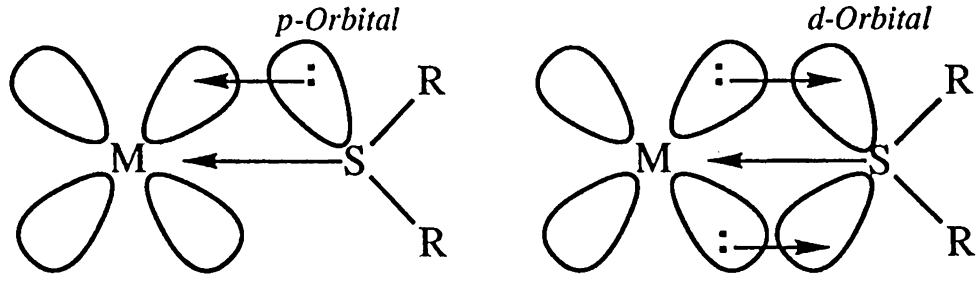

Figure 1.1. Metal-thioether bonding assuming sp^3 hybridization at S.

An interesting aspect of thioether coordination chemistry is its π-acidity. The outer electron configuration of sulfur in the ground state is $3s^2\ 3p^4\ 3d^0$. The empty *d* orbital might have the correct symmetry to take part in π back-donation from metal to ligand[21]. There has been no unequivocal evidence to support this, nevertheless, there are some aspects of the structure and reactivity of thioether complexes with transition metals that can be simply explained in such terms[22].

The realization that the *macrocyclic effect* can provide extra stability to the complexes even with unusual coordination geometry or unusual oxidation state of a

metal ion is responsible for the renewed interest in the coordination chemistry of thioethers[22,23]. However, the tedious routes to the synthesis of crown thioethers has been the major stumbling block until recently. Advances in the synthetic methodology and the routine availability of x-ray diffraction facilities has spurred investigation of the coordination chemistry of crown thioethers.

The active research on crown-type ligands has also enabled study of the effect of the size of the macrocycle on the stability, electron transfer (ET) properties, and the ability to cause the constriction or dilation of the coordination sphere. Spectral properties of thioether complexes with a wide variety of metal ions have been characterized[24]. The study of the macrocyclic effect has provided some insight into how the metalloenzymes and metal containing redox proteins function. In this report an attempt has been made to demonstrate a delicate balance between the structural and functional characteristics of a metal center in complex molecules. $[Cu^{II/I}(TTCN)_2]$ molecule is used as a model (TTCN = 1,4,7-trithiacyclononane). This choice is based upon (i) the plasticity of the coordination geometry of Cu(II), (ii) the apparently significant difference in the stereochemical properties of Cu(II) and Cu(I), and (iii) the fairly rigid conformation of TTCN macrocycle.

TTCN, which in most of its complexes sandwiches the metal ion between two TTCN molecules, is a very versatile macrocyclic ligand. The number of coordination sites and the structural rigidity of the molecules can be expected to favor Cu(II) state whereas the nature of the coordination points would appear to prefer the Cu(I)

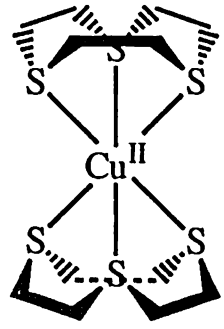

1.3

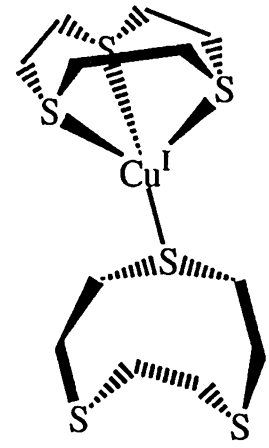

1.4

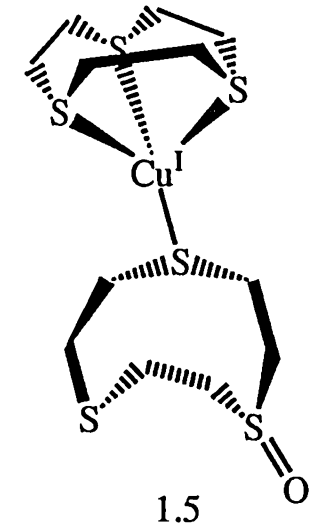

1.5

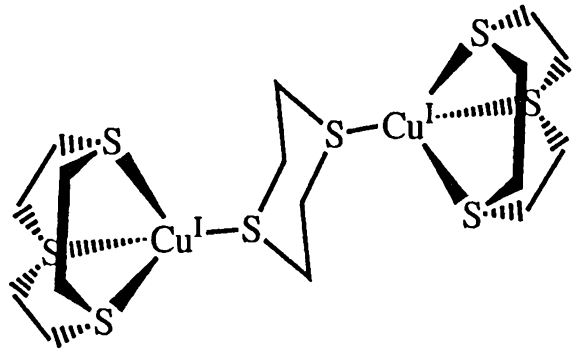

1.6

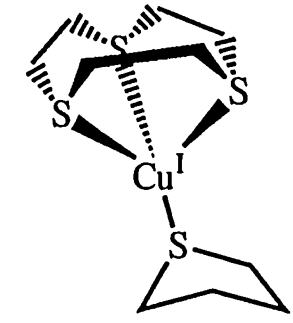

1.7

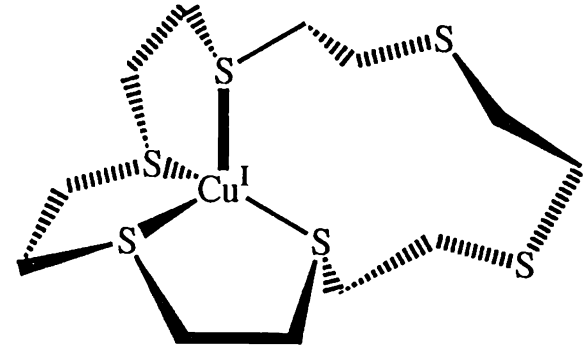

1.8

oxidation state. In order to see if the structural characteristics of copper-TTCN system are exclusively controlled by the ligand, an extensive electrochemical investigation of the system (**1.4 - 1.6**) has been carried out. The electrochemical studies have shown that even TTCN is not rigid enough to retain the coordination geometry regardless of the oxidation state of copper ion. These results have been supported by x-ray crystallography of $[Cu^{I}(TTCN)_2]$ which is tetrahedral unlike the octahedral $[Cu^{II}(TTCN)_2]$ complex.

Unfortunately none of the electrochemical techniques available is fast enough to facilitate a detailed study of the intermediate. However, pulse radiolysis is fast enough to study reactive intermediates and was, therefore, employed to study this system in detail. In pulse radiolysis the oxidation and reduction can be carried out by a hydroxyl (or any other appropriate) radical or hydrated electron, respectively. Pulse radiolytic oxidation of $[Cu^{I}(TTCN)_2]$ has indicated that the oxidized complex passes through an intermediate state before it collapses to the stable octahedral geometry.

Due to the intense color of $[Cu^{II}(TTCN)_2]$ a small decrease in the optical density resulting from the reduction process is hard to detect. Therefore, pulse radiolysis of only Cu(I)-thioether complexes (**1.5 - 1.8**) has been carried out to unambiguously assign the intermediate structure.

The fundamental comprehension of ET in metalloproteins has come from the research done on simple chemical systems. These studies primarily provided unequivocal evidence for the significance of the ET distance and the associated

driving force to evaluate the validity of theoretical models for long range ET[25-27].

The classification into outer sphere (OS) and inner sphere (IS) mechanisms provided a clear distinction between these two mechanistically different fundamental processes of ET[28]. Typically in the OS mechanism the redox partners, the *donor* (**D**) and the *acceptor* (**A**), communicate with each other as distinct bodies at least during the ET step, while in the IS mechanism they share one or more coordination sites along the ET pathway. In any case several elementary steps are required to achieve the ET as depicted in Eq. 1.2 - 1.4[29]. Any of these forward or reverse steps can be rate-limiting.

$$D + A \rightleftharpoons [DA] \tag{1.2}$$

$$[DA] \rightleftharpoons [D^{z+}A^{z-}] \tag{1.3}$$

$$[D^{z+}A^{z-}] \rightleftharpoons A^{z+} + D^{z-} \tag{1.4}$$

These accompanying elementary processes can complicate elucidation of the elementary ET step.

Obviously it was very hard to meet strictly the conditions necessary for such a study through intermolecular ET, therefore, attention was turned to the intramolecular ET in which the electron is transferred through a common bridging ligand between **D** and **A** thereby keeping them at a fixed and known distance from each other. The elegant approach to intramolecular ET which was taken by Isied and Taube some twenty years ago was to chemically synthesize a stable encounter complex i.e. a precursor to the ET step which is now a common practice[30]. However,

there are many difficulties associated with this approach with regard to finding appropriate **D** and **A** pairs in terms of oxidation states, redox potentials, substitution properties, self exchange rate constants, and ruggedness of the synthetic precursor.

The bridging molecule can serve four main purposes: (i) to act as a medium for the electron to flow through, (ii) to facilitate the outer-sphere electron transfer by bringing the coordination spheres of the metal centers in contact either through a rotation about the C-C single bonds, or through a helical orientation about a common axis as in polyproline bridges, (iii) to hold the two centers rigidly at a fixed distance and allow for the electron tunnelling across the intervening matter directly between the coordination spheres of the two metal centers and (iv) to hold the two metal centers at fixed positions in space with no intervening matter and allow to study through space ET.

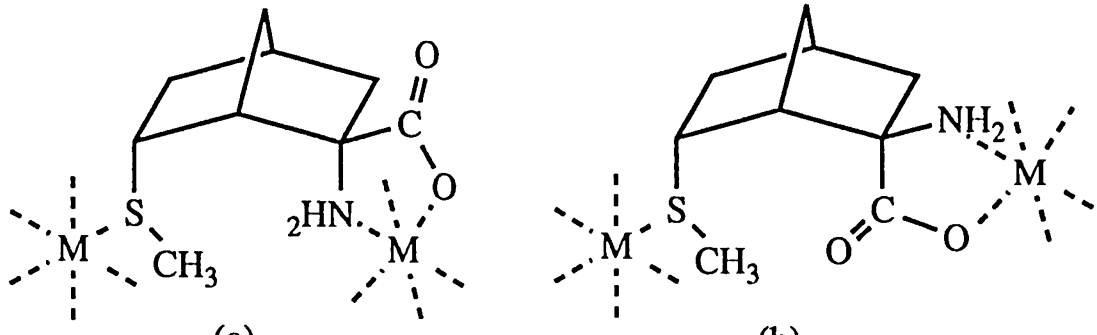

1.9

A norbornyl derivative of methionine in which the two ends, glycinic and thioether, are held rigidly in position provides a potential bridging molecule to hold

the two metal centers at a fixed distance by a saturated system as in **1.9**. This permits the study of through space ET reactions. However, the highly dissymmetric and chemically different ends of the molecule can deter the interaction between the metal centers. Because of this the two metal centers can behave independently from each other. This study includes the synthesis and characterization of a binuclear complex in which the metal centers are bridged by methionine.

A greater incentive for the study of the coordination chemistry of thioethers stems from the role of thioethers at the metal binding centers of the metalloproteins like blue copper proteins[31]. In copper proteins, however, the metal binding center is intrinsic which means that the skeleton of the protein fabricates the cavity for the metal ion to provide stability to both oxidation states for an efficient ET and appropriate accessibility of the metal center, to fit the physiological function of the protein[12]. As a consequence of this intrinsic nature of the copper center these proteins often exhibit unique geometric, spectral, and redox properties compared to the normal copper complexes which makes it very hard to mimic the detailed features of copper proteins in a single synthetic analogue. Nevertheless, the binding of copper to macrocyclic thioethers has led to a greater understanding of Cu-thioether(S) interaction and the associated stereochemical preferences.

CHAPTER 2

EXPERIMENTAL

1. Reagents

The following materials were purchased from the indicated vendor. All the chemicals from Aldrich were reagent grade and purus grade from Fluka, unless otherwise indicated.

(+)-3-bromocamphor-10-sulfonic acid	Fluka
1,4-dithiane	Aldrich
1,4,7,10,13,16-Hexathiacyclooctadecane	Aldrich
L-methionine	Aldrich
Pentamethylene sulfide	Aldrich
Tetrabutylammonium hexafluorophosphate	Fluka
Tetrabutylammonium perchlorate	Fluka
Tetrabutylammonium tetrafluoroborate	Fluka
Tetraethylammonium perchlorate	Fluka
Tetrahydrothiophene	Aldrich
1,4,7-trithiacyclononane	Aldrich

Purification of Solvents and Gases.

Acetonitrile (Fisher, HPLC grade) was distilled over calcium hydride at 82°C. The distillate was collected after 5 hours of reflux over calcium hydride. The distilled acetonitrile was directly delivered from the distillation head.

Methylene chloride (Fisher, reagent grade) was purified and delivered the same way as acetonitrile.

Water. Highly pure (18 MΩ) water was obtained by passing house distilled deionized water through a Barnstead Nanopure II system (Sybron/Barnstead, Boston, MA).

Argon (99.995%, Burnox) was deoxygenated by passing it through an activated column of Ridox, Oxygen Scavenger, (Fisher Scientific) and bubbled through the solvent of the medium. For non-aqueous systems the gas was dried by passing through blue silica gel before bubbling through the solvent. Other gases were used as obtained.

Zinc/mercury amalgam. Zinc shots (Baker) were submerged in 0.2 M trifluoroacetic acid (HTFA) solution for about 5 minutes with occasional swirling. The acid solution was decanted and the zinc was covered with a satd. solution of mercuric chloride for about 15 minutes with occasional swirling. The amalgamated zinc was washed thoroughly with water and dried on blotting paper before use.

2. Syntheses

1-sulfoxide-4,7-dithiacyclononane (SODTCN). TTCN (200 mg, 1.11 mmol) was dissolved in 10 mL of dioxane in a 100 mL round bottom flask. Sodium persulfate (264 mg, 1.11 mmol) was dissolved in 20 mL of water. The persulfate solution was added slowly and dropwise over a period of 1 h to the TTCN solution with constant stirring. Any turbidity appearing during the addition was redissolved with dioxane. The stirring was continued overnight. The solvent mixture was

evaporated on a rotary evaporator at room temperature. The residue was extracted with 20 x 4 mL of chloroform. Chloroform was evaporated on rotary evaporator and the thick oily residue was refrigerated overnight. The solid material was crushed and dried under vacuum for 1 h. The residue was dissolved in a minimum volume of methylene chloride and the product recrystallized under a gentle stream of argon.

$[Cu(TTCN)_2](CamphSO_3)_3.H_3O.3CH_2Cl_2$. To a solution of 140 mg (0.78 mmol) of TTCN in 30 mL of methylene chloride was added 500 mg (1.5 mmol) of (+)-3-bromocamphor-10-sulfonic acid ($CamphSO_3H$) at 4°C followed by the addition of 40 mL of more methylene chloride to dissolve the acid completely. 75 mg (0.38 mmol) of $Cu(OAc)_2.H_2O$ were added to the above solution with stirring and the stirring was continued for about 3 h at 4°C and then 3 h at room temperature. The reaction was cooled down to 4°C and filtered by gravity. 150 mL of diethyl ether were carefully deposited on top of the filtrate and refrigerated overnight. The supernatant was decanted completely. The crystalline product was redissolved in 10 mL of methylene chloride and filtered by gravity. This saturated solution was refrigerated overnight.

Anal. Calcd for $Cu_{45}H_{75}S_9O_3Br_3Cl_6$: C, 33.18; H, 4.64; S, 17.68. Found: C, 33.64; H, 4.79; S, 18.37.

$[Cu(TTCN)_2]PF_6$. The synthetic procedure recommended by Clarkson *et al*[2] was adapted for synthesis of the title complex. To a solution of TTCN (200 mg, 1.11 mmol) in methanol (20 mL, Aldrich sure seal) under argon, was added

$[Cu(CH_3CN)_4]PF_6$ (200 mg, 0.54 mmol). The reaction mixture was stirred under argon for about 2 h. The volume of the reaction was reduced to about 3 mL. The white crude product was filtered out, washed sequentially with methanol, ethanol, and finally with diethyl ether under argon.

The above product was dissolved in 1 - 2 mL of nitromethane, prepurged with argon. 20 mL of methanol was added slowly and allowed to mix slowly with the solution while refrigerated. The volume was reduced on a rotary evaporator to about 3 mL and the microcrystalline product was filtered and washed as described above. The yield was 90%.

Anal. Calcd for $C_{12}H_{24}S_6CuPF_6$: C, 25.32; H, 4.25; S, 33.79; F, 20.02. Found: C, 25.24; H, 4.11; S, 33.62; F, 19.73.

[Cu(TTCN)(SODTCN)]PF_6. To a solution of TTCN (80 mg, 0.443 mmol) and SODTCN (90 mg, 0.458 mmol) in 30 mL deaerated methanol (Fisher, HPLC Grade) was added $[Cu(CH_3CN)_4]PF_6$ (165 mg, 0.443 mmol). The reaction mixture was stirred for 3 h under argon. The white powdery product was filtered out under argon and washed sequentially with methanol and diethyl ether and dried under vacuum. Yield 77 %.

Anal. Calcd for $C_{12}H_{24}S_6OCuPF_6$: C, 24.63; H, 4.13; S, 32.87; P, 5.29; F, 19.48. Found: C, 24.48; H, 4.04; S, 32.99; P, 5.22; F, 19.33.

[(TTCN)Cu(1,4-dithiane)Cu(TTCN)]$(PF_6)_2$. To a solution of 200 mg (1.11 mmol) of TTCN and 70 mg (0.58 mmol) of 1,4-dithiane in 25 mL of methanol

prepurged with argon were added 410 mg (1.1 mmol) of $[Cu(CH_3CN)_4]PF_6$ with stirring. The stirring was continued for about 2 h under argon. 10 mL of nitromethane were added to dissolve the precipitate. Any undissolved material was filtered out under argon and the filtrate was concentrated on a rotary evaporator until crystallization started. After refrigerating overnight, the crystalline product was filtered out. The product was washed with ether and the filtrate was carefully covered with an equal volume of ether and refrigerated overnight. The crystalline product was processed as before under argon. The overall yield was 42 %.

Anal. Calcd for $C_{16}H_{32}S_8Cu_2P_2F_{12}$: C, 21.40; H, 3.59; S, 28.56; P, 6.90; F, 25.39. Found: C, 21.32; H, 3.60; S, 28.43; P, 6.83; F, 25.44.

[Cu(TTCN)(PMS)]PF_6. To a solution of 200 mg (1.11 mmol) of TTCN and 205 mg (2 mmol) of pentamethylene sulfide (PMS) in 40 mL of methanol prepurged with argon, were added 410 mg (1.1 mmol) of $[Cu(CH_3CN)_4]PF_6$ with stirring. The stirring was continued for about 3 h. The reaction mixture was concentrated on a rotary evaporater until crystallization started and then left overnight at -40°C. The crystalline product was collected on a sintered funnel under argon, washed with ether and desiccated. The yield was 55.55%.

Anal. Calcd for $C_{11}H_{22}S_4CuPF_6$: C, 26.91; H, 4.52; S, 26.12; P 6.31; F, 23.21. Found: C, 26.81; H, 4.48; S, 26.44; P, 6.52; F, 23.01.

[Cu(TTCN)(THT)]PF_6. Exactly the same procedure and quantities of reactants were used for the synthesis of the tetrahydrothiophene (THT) complex as those for the

synthesis of the PMS complex, described above. The yield was 41 %.

Anal. Calcd for $C_{10}H_{20}S_4CuPF_6$: C, 25.18; H, 4.23; S, 26.88; P, 6.49; F, 23.90. Found: C, 25.16; H, 4.16; S, 26.95; P, 6.50; F, 23.71.

[Cu(HTCOD)]PF_6 was synthesized according to the literature procedure[3].

[Co(trien)(TFMS)$_2$](TFMS). The literature method for the synthesis of a triflato complex of Cr(III) was followed[4]. To 5.0 g (14.26 mmol) recrystallized α-[Co(trien)$(NO_2)_2$]Cl.H_2O[5] in a 50 mL round bottom flask was carefully added anhydrous trifluomethansulfonic acid (HTFMS) (Aldrich) (50 mL) in a fume hood. The mixture was stirred gently for about 3 days under a gentle stream of argon and then transferred to a 1 L flask. 300 mL anhydrous diethylether was added very carefully (the process is very exothermic) and slowly with vigorous stirring. The supernatant was decanted and the product treated several times with 300 mL portions of diethyl ether until a colorless supernatant was obtained. The product was filtered out first by gravity and then under suction after the deposition of a layer of the precipitate. This was washed with 4 x 20 mL of diethyl ether and desiccated. Yield: 95%.

Anal. Calcd: C, 16.56; H, 2.76; N, 8.59; S, 14.72; F, 26.23. Found: C, 16.47; H, 2.89; N, 8.35; S, 14.78; F, 26.48.

[Ru$(NH_3)_6$]Cl_3. To a slurry of 5 g (mol) $RuCl_3.3H_2O$ (Aldrich) in 25 mL ammonia in 1 L flask was added 50 mL Hydrazine hydrate dropwise with constant stirring. The stirring was continued for about 30 more minutes. The reaction mixture

was then refluxed until the evolution of gas finished (about 1 h). The solution was cooled down to room temperature and filtered by gravity. Air was bubbled through the filtrate for 3 h. 25 mL of concentrated HCl was added to the solution and the product was filtered out with suction, washed sequentially with ethyl alcohol and diethyl ether and air dried. Yield: 67.5%

Anal. Calcd: N, 27.14; H, 5.86; Cl, 34.35. Found: N, 26.94; H, 5.85; Cl, 34.44.

$[Co(en)_2(Met)](ClO_4)_2$. A solution of 0.6 g of $[Co(en)_2(CO_3)]NO_3$[6] in 5 mL water was slowly reacted with 0.7 mL of 70% perchloric acid with slow stirring. The stirring was continued at 35°C for 1 h. The pH was adjusted to 5 with 5 M NaOH solution and 0.3 g L-methionine was added. The heating and stirring was continued for one more hour during which the pH was maintained at 5-5.5. The pH was then raised to 7 and maintained for 1 h. 0.5 mL of 5 M NaOH was added and the reaction was run at 35°C overnight. The resulting precipitate was filtered, washed with ethanol, then with ice-cold 1 M NaOH solution, again with ethanol and finally with diethyl ether following air drying. Yield: 55%.

Anal. Calcd: C, 19.82; H, 5.14; N, 12.84; S, 5.87; Cl, 13.03. Found: C, 20.13; H, 5.07; N, 12.78; S, 5.74; Cl, 13.08.

$[Co(trien)(Met)](ClO_4)_2$. 0.6 g of the corresponding carbonato complex[5] was treated exactly the same as for the synthesis of $[Co(en)_2(Met)](ClO_4)_2$.

Anal. Calcd: C, 23.88; H, 5.1; N, 12.66; S, 5.78; Cl, 12.84. Found: C, 23.95; H, 5.12; N, 12.69; S, 5.87; Cl, 12.94.

[Co(trien)(Met)](TFMS)$_2$. 2 g (3 mmol) of [Co(trien)(TFMS)$_2$](TFMS) was dissolved in 15 mL water on a steam bath. 0.6 g L-methionine was dissolved in the above solution. The pH was adjusted to 8 with 2 M NaOH and the heating was continued on the steam bath for 2 h to reduce the volume to about 5 mL, maintaining the pH at 7-8. This solution was cooled down to room temperature and pH was adjusted to 10-11. After stirring the reaction mixture at room temperature for 1 h, the product was filtered out, washed with 0.5 mL chilled 2 M NaOH solution and then with diethyl ether followed by drying under vacuum. Yield: 63 %.

Anal. Calcd for $CoC_{13}H_{28}N_5S_3O_8F_6$: C, 23.96; H, 4.33; N, 10.75; S, 14.76; F, 17.5. Found: C, 23.97; H, 4.29; N, 10.8; S, 14.73; F, 17.15.

[(trien)Co^{III}(Met)Ru^{II}(NH$_3$)$_5$](PF$_6$)$_4$. A solution of [Ru(NH$_3$)$_5$(TFMS)](TFMS)$_2$[4] (0.247 g, 0.5 mmol) in a minimum volume of water was purged with argon for 30-45 minutes. 2 g of amalgamated zinc was dropped into the above solution which was then purged for 30-45 minutes. In another flask a solution of [Co(trien)(Met)](TFMS)$_2$ (0.327 g, 0.5 mmol) in 15 mL water was purged well with argon. The reduced ruthenium complex was transferred to the cobalt complex solution through a cannula under argon pressure. This reaction mixture was then stirred for 5 h. 0.327 g (2 mmol) NH_4PF_6 was added and the stirring was continued overnight under argon. The product was filtered out under argon and dried in a vacuum oven. This complex was characterized only electrochemically.

3.. Instrumentation and Techniques

Electrochemistry. Electrochemical experiments were carried out using a computer controlled Cypress Electroanalytical system Model CS-1090.

A Princeton Applied Research (PAR) Model 273 potentiostat/galvanostat equipped with digital coulometer was used for the controlled potential electrolysis (CPE) and chronocoulometric experiments.

Pine Instruments bipotentiostat Model AFRDE4 and rotator Model AFASR were used for rotating ring disk electrode (RRDE) experiments. A Kipp & Zonen (Holland) X-Y recorder was used to record the RRDE voltammograms.

Aqueous electrochemistry was performed in a three- compartment cell separated by medium porosity frits and sodium nitrate salt bridges. No corrections were made for the liquid junction potential.

The potentials were measured against Ag/(AgCl, satd. NaCl) reference electrode. The auxiliary electrode consisted of a large platinum flag and the working electrode consisted of glassy carbon press fitted into a Kel-F shroud (Bioanalytical System). Pine Instruments Model AFDTO6GCPT glassy carbon disk, platinum ring working electrode was used for the RDE and RRDE.

Non-aqueous electrochemistry was performed in three-necked one-compartment cell on glassy carbon vs Ag/0.1 M $AgNO_3$ (acetonitrile) reference electrode using platinum flag as a counter electrode. For strictly anaerobic and dry electrochemistry cyclic voltammetric experiments were performed in a dry box using 88 % distilled methylene chloride, 10 % trifluoroacetic anhydride (Sigma) and 2 % anhydrous

trifluoroacetic acid (Sigma, protein sequencing grade) as a medium, with 0.2 M in TBAHFP as supporting electrolyte.

For the controlled potential electrolysis (CPE) of thioethers, the rotator head of the RDE assembly and the electrochemical cell were specially designed to avoid exposure to the air and moisture. To ensure the maximum possible exclusion of air and moisture, the electrolysis was performed in a glove bag under an inert gas (argon) atmosphere.

Digital Simulation of the Cyclic Voltammograms. Simulation programs were developed to fit the entire experimental voltammogram to the theoretical curve and calculate the corresponding kinetic and thermodynamic parameters. The programs were designed to analyze systems with concurrent chemical reactions. For the one-step multielectron transfer case a correction for disproportionation can be made and K_{disp} calculated.

The normal explicit finite difference digital simulation technique was employed in the calculation of current-potential curves[7]. In the curve-fitting analysis of voltammograms, the dumping Gauss-Newton method was applied as a non-linear least squares technique[8]. Digital simulation and curve-fitting analysis of the cyclic voltammograms have previously been described[9]. All computer programs were written in Turbo Pascal by Dr. Kenji Kano.

The calculations were carried out on a Gateway 2000 VGA 386 or an NEC PC-9801RA microcomputer equipped with Math coprocessor. The calculation interval

(ΔE_{calc}) was 1 mV unless otherwise stated. The experimental current-potential (*i-E*) data acquired on the Cypress System were corrected for the background current every 5 mV.

X-ray Crystallography. Single crystal x-ray structures of the following compounds were determined.

$[Cu^{II}(TTCN)_2](CamphSO_3)_3.H_3O$ **2.1**

$[Cu^{I}(TTCN)_2]PF_6$ **2.2**

$[(Cu^{I}(TTCN))_2(1,4\text{-Dithiane})](PF_6)_2$ **2.3**

$[Cu^{I}(TTCN)(SODTCN)]PF_6$ **2.4**

$[Co^{III}(dien)_2Met](CLO_4)_2$ **2.5**

In each case a single crystal of the corresponding compound was mounted on a glass fiber, fixed with epoxy glue and ultimately centered on the goniometer head. All the diffraction measurements were made on a Rigaku AFC5R diffractometer equipped with graphite monochromated Kα radiation and a 12 KW rotating anode generator.

Cell constants and orientation matrices for data collection were obtained from least square refinement using the setting angles of a number of carefully centered reflections in an appropriate range of 2θ. The space groups were determined from the systematic absences.

The ω - 2θ scan technique was used, to a maximum 2θ value of 112.5°, to collect the data[10]. Weak reflections were rescanned (maximum of 3 rescans) and the counts were accumulated to insure good counting statistics. Scan speeds were adjusted according to the size of the crystal. Stationary background counts were recorded on each side of the reflection. The ratio of the peak counting time to background counting was 2:1.

In case of $[Cu^{I}(TTCN)_2](PF_6)$ the intensities of three representative reflections which were measured after every 150 reflections declined by 15%. A linear correction factor was applied to account for the decline. In all the other cases the intensities remained constant throughout the data collection. This was considered as an indication of the stability of the crystal and the electronics. Therefore, no decay correction was applied. Lorentz and polarization corrections were applied to all the reflections. ORTEP[11] and PLUTO[12] representations are used for drawing the crystal structures.

The final cycle of full-matrix least-squares refinement for each crystal was converged with the unweighted and weighted reliability factors, R and R_w respectively.

$$R = (\Sigma \; | \; |F_o| - |F_c| \; |)/\Sigma \; |F_o|$$

$$R_w = [\Sigma \, w(|F_o| - |F_c|)^2/\Sigma \, wF_o^2]^{1/2}$$

The weighting scheme was based on counting statistics and included a factor (p) to downweigh the intense reflections. The goodness of fit (GOF) is represented as the standard deviation of an observation of unit weight.

$$GOF = [\Sigma \, w(|F_o| - |F_c|)^2/(N_o - N_v)]^{1/2}$$

where

N_o = Number of observations

N_v = Number of variables.

$[\Sigma w(|F_o| - |F_c|)^2$ = Function minimized

$w = 4F_o^2/\sigma^2(F_o^2)$ = Weighting factor

$\sigma^2(F_o^2) = [S^2 (C + R^2B) + (pF_o^2)^2]/L_p^2$

S = Scan rate; C = Total integrated peak count;

R = Scan Time/Background counting time;

B = Total background count; p = p-Factor;

L_p = Lorentz-polarization factor

Neutral atom scattering factors were taken from Cromer and Weber[13]. Anomalous dispersion effects[14] were included in F_{calc}. The values of $\Delta f'$ and $\Delta f''$ were those of Cromer[15]. All calculations were performed using the TEXAN crystallographic software package of Molecular Structure Corporation[16] and/or KUDNA crystallographic software package developed at KU[17]. No unusual trends in any structure were observed in plots of $\Sigma w(|F_o| - |F_c|)^2$ vs $|F_o|$, reflection order in data collection, sin θ/λ, and various classes of indices.

Crystallography of $[Cu^{II}(TTCN)_2](CamphSO_3)3.H_3O.3CH_2Cl_2$. A brown plate single crystal having approximate dimensions of 0.352 x 0.211 x 0.015 mm was picked from the recrystallized compound, as described in the synthesis section, and mounted on a glass fiber. The unit cell parameters corresponded to an orthorhombic

system. Based on the systematic absences at $h00$ for $h \neq 2n$, at $0k0$ for $k \neq 2n$ and at $00l$ for $l \neq 2n$, the space group was determined to be $P2_12_12_1$ (#19).

The data were collected at a temperature of -160 ± 1°C. ω-scans of several intense reflections, made prior to collection, had an average width of 0.55°,at half height, with a take-off angle of 6.0°. Scans of (1.78 + 0.30 tan θ)° were made at a speed of 32.0°/min. The weak reflections ($I < 10.0\sigma(I)$) were rescanned. A total of 4781 reflections was collected.

The structure was solved by direct methods[18]. The non-hydrogen atoms were refined either anisotropically or isotropically. The final cycle of full-matrix least-squares refinement was based on 4748 observed reflections ($I > 0.00$), out of which 3776 reflections are above $3\sigma(F)$, and 686 variable parameters. The largest parameter shift in the final cycle was 0.32 time its esd, the estimated standard deviation. The maximum and minimum peaks on the final difference Fourier map corresponded to 0.33 and -0.28 $e^-/Å^3$, respectively.

The TTCN ligands have been found to be disordered. The occupancy factors of each disordered fragment were estimated such that the temperature factors of the ligands were approximately the same. The counter ion was also found to be disordered. The method of refinement that was employed is used in protein crystallography[17]. The bond angles and distances of the disordered fragments are restrained to the ideal values. The function minimized is given by:

$$\Sigma\, w(|F_o| - |F_c|)^2 + \Sigma\, k(|D_o| - |D_c|)^2$$

where D_o is the ideal atom-atom distances and D_c is the calculated atom-atom distances in the disordered fragment and

$$k = 0.25\ \Sigma\ w(|F_o| - |F_c|)^2/\Sigma\ (|D_o| - |D_c|)^2$$

Further structural details are outlined in Table A1.1 - A1.5.

Crystallography of $[Cu^I(TTCN)_2]PF_6$. A white plate single crystal having approximate dimensions of 0.300 x 0.200 x 0.050 mm was mounted on glass fiber. The unit cell parameters corresponded to a monoclinic system. Based on the systematic absences at *h*0*l* for $h+l \neq 2n$ and at 0*k*0 for $k \neq 2n$, the space group was determined to be $P2_1/n$ (#14).

The data were collected at a temperature of 23 ± 1°C. ω-scans of several intense reflections, made prior to collection, had an average width of 0.49° at half height with a take-off angle of 6.0°. Scans of (1.47 + 0.30 tan θ)° were made at a speed of 8.0°/min (in ω). A total of 4781 reflections was collected.

The structure was solved by a combination of the Patterson method[19] and direct methods[18]. The non-hydrogen atoms were refined anisotropically. The final cycle of full-matrix least-squares refinement was based on 2792 observed reflections ($I > 3.00\ \sigma(I)$) and 469 variable parameters. The largest parameter shift in the final cycle was 0.05 time its esd. The maximum and minimum peaks on the final difference Fourier map corresponded to 1.18 and -0.77 $e^-/Å^3$, respectively.

The crystal structure has pseudo-symmetry. Two crystallographically independent complexes were located at x,y,z and x,y,(1/2)z, respectively. Further

structural details are outlined in Table A2.1 - A2.5.

Crystallography of $[Cu^{I}(TTCN)(SODTCN)](PF_6)_2$. A white prism single crystal having approximate dimensions of 0.200 x 0.300 x 0.400 mm was mounted on a glass fiber. The unit cell parameters corresponded to a monoclinic system. Based on the systematic absences at $0k0$ for $k \neq 2n$, the space group was determined to be $P2_1$ (#4).

The data were collected at a temperature of 23 ± 1°C. ω-scans of several intense reflections, made prior to collection, had an average width of 0.45° at half height with a take-off angle of 6.0°. Scans of (1.78 + 0.30 tan θ)° were made at a speed of 8.0°/min (in ω). The weak reflections ($I < 10.0\sigma(I)$) were rescanned. A total of 1667 reflections was collected.

The structure was solved by direct methods. The non-hydrogen atoms were refined either anisotropically or isotropically. The final cycle of full-matrix least-squares refinement was based on 1389 observed reflections ($I > 0.01\ \sigma(I)$) and 234 variable parameters. The largest parameter shift in the final cycle was 0.40 time its esd. The maximum and minimum peaks on the final difference Fourier map corresponded to 0.18 and -0.12 $e^-/Å^3$, respectively.

The SODTCN ligand is disordered. The structure was refined with the restrain method in which the bond angles and bond distances are restrained to the ideal values[17]. Further structural details are outlined in Table A3.1 - A3.5.

Crystallography of $[(Cu^{I}(TTCN))_2(1,4\text{-Dithiane})](PF_6)_2$. A white needle single crystal having approximate dimensions of 0.200 x 0.200 x 0.500 mm was mounted on a glass fiber. The unit cell parameters corresponded to a monoclinic system. Based on the systematic absences at *hkl* for $h+k \neq 2n$ and at *h0l* for $l \neq 2n$, the space group was determined to be $C2_1/c$ (#15).

The data were collected at a temperature of -160 ± 1°C. ω-scans of several intense reflections, made prior to collection, had an average width of 0.41° at half height with a take-off angle of 6.0°. Scans of (1.57 + 0.30 tan θ)° were made at a speed of 32.0°/min (in ω). The weak reflections ($I < 10.0\sigma(I)$) were rescanned. A total of 2188 reflections was collected.

The structure was solved by direct methods[18]. The non-hydrogen atoms were refined anisotropically. The final cycle of full-matrix least-squares refinement was based on 1993 observed reflections ($I > 0.01\ \sigma(I)$) and 246 variable parameters. The largest parameter shift in the final cycle was 0.19 time its esd. The maximum and minimum peaks on the final difference Fourier map corresponded to 0.14 and -0.11 $e^-/Å^3$, respectively.

The complex has a center of symmetry. The full complex can be obtained by performing the symmetry operation 0.5 - x, 0.5 - y, -z on the coordinates of the half complex. Two half PF_6^- counterions are found in the asymmetric unit. A full PF_6^- ion can be obtained by applying 1-x, y, 1.5-z symmetry operation. Several short C—H---F contacts are observed which are probably weak H-bonds. Further structural details are

outlined in Table A4.1 - A4.5.

Crystallography of $[Co^{III}(en)_2(Met)](ClO_4)_2$. An orange prism single crystal having approximate dimensions of 0.100 x 0.100 x 0.300 mm was mounted on a glass fiber. The unit cell parameters corresponded to a monoclinic system. Based on the systematic absences at $0k0$ for $k \neq 2n$, the space group was determined to be $P2_1$ (#4).

The data were collected at a temperature of 22 ± 1°C. ω-scans of several intense reflections, made prior to collection, had an average width of 0.38° at half height with a take-off angle of 6.0°. Scans of (1.05 + 0.30 tan θ)° were made at a speed of 4.0°/min (in ω). The weak reflections ($I < 10.0\sigma(I)$) were rescanned. A total of 3275 reflections was collected.

The structure was solved by direct methods. The non-hydrogen atoms were refined either anisotropically or isotropically. The final cycle of full-matrix least-squares refinement was based on 2187 observed reflections ($I > 3.00\ \sigma(I)$) and 521 variable parameters. The largest parameter shift in the final cycle was 0.59 time its esd. The maximum and minimum peaks on the final difference Fourier map corresponded to 0..57 and -0.58 $e^-/Å^3$, respectively.

The unit cell contains two independent molecules in a crystallographic asymmetric unit. The two molecules are related by a pseudo-center of symmetry. Further structural details are outlined in Table A5.1 - A5.5.

Spectroscopy.

Ultraviolet and visible absorption spectra were obtained at room temperature

on a Varian Model Cary 219 spectrophotometer.

^{1}H and ^{13}C NMR spectra were recorded on a Bruker AM NMR Spectrometer at 500.13 and 125.03 MHz respectively.

Pulse radiolysis was carried out at the Radiation Laboratory of the University of Notre Dame, Indiana and at The Hahn-Meitner Institute, Berlin, Germany.

CHAPTER 3

ANODIC OXIDATION OF ALIPHATIC THIOETHERS HAVING NEIGHBORING LONE-PAIR OR π-ELECTRONS

Introduction:

One of the first reactions discovered in the field of organosulfur chemistry was the oxidation of sulfides to sulfoxides[1,2]. The sulfoxide functional group activates adjacent carbon-hydrogen bonds toward attack by base and the resulting anions can be alkylated[3,4] or acylated[4,5] with high diastereoselectivity.

The effect of the neighboring *carboxylate* and *amine* functions on the oxidizability of a thioether group has been studied extensively[6]. A brief discussion of similar interactions will also be presented in Chapter 6 of this report. However, in those studies the main focus has been on how a neighboring substituent can facilitate the oxidation of thioethers. Moreover, in a biological molecule the sulfide function could be a part of a giant molecular assembly which could bring a variety of functional groups into the neighborhood of the target sulfide. Compound **1.1** and **1.2** were chosen to study respectively, the effect of a neighboring lone-pair (sulfide) or a π system of electrons on the anodic oxidation of aliphatic thioethers. The structural rigidity of the molecular backbone carrying the potentially interacting functional groups is an important factor in the choice of these model compounds.

There is a great deal of interest in the use of organic sulfides as substrates in

oxidation mechanisms where they may function as antioxidants. Such studies can also provide better understanding of the stereoselectivity of the *in vivo* oxidation of sulfides via the action of certain enzymes as well as under more destructive conditions involving the action of ozone, singlet oxygen and other exogenous oxidants. A comprehension of the biological oxidation-reduction chemistry of sulfides is essential to the understanding of the metabolism of sulfur-containing L-amino acids, certain vitamins and drugs, and even some toxic compounds. A detailed understanding of the redox properties of model organic sulfides is, therefore, essential to the understanding of the susceptibility of biological thioethers toward oxidation.

Normally the redox potentials of ordinary sulfides lie outside the oxidizing capability of biological oxidants. Nevertheless, sulfoxidation represents a major route of mammalian metabolism of sulfur-containing xenobiotic compounds, and the resulting sulfoxides often possess defined absolute stereochemistry at sulfur[7]. The ability of mammalian enzymes to oxidize sulfides has been recognized for many years, and was first reported as early as 1940 in the context of the metabolism of sulfur-containing pharmaceuticals[8,9].

The microbial sulfoxidation of sulfur-containing heterocycles such as dibenzothiophene has been studied from the perspective of the microbial metabolism of sulfur-containing fused ring polycyclic aromatic environmental pollutants[10], and as a model for the use of microbial agents in the desulfurization of coal[11].

Sulfides are known to undergo photosensitized oxidation to their corresponding

sulfoxides[12]. This oxidation, which has been found to be induced by singlet oxygen, is of particular interest because methionine is one of the amino acids which is attacked most rapidly in photodynamic action (the destructive action of dye sensitizers, light and oxygen on organisms)[13-15]. Other amino acids such as S-methylcysteine and lanthionine are also known to give sulfoxides on photooxygenation[16]. The environment and accessibility of the thioether sulfur play a significant role in its oxidizability. Jori and coworkers[17] have found protein elastase, which contains two methionine units (position 41 and 172), to be unaffected under neutral pH photooxidation conditions. This has been ascribed to the location of the two methionyl side-chains in internal hydrophobic regions. At pH 3.5, methionine-172 undergoes photooxidation, presumably because at this pH the tertiary structure is loosened allowing access of the photooxidizing agent to that particular site. At pH 2.5 both methionine-172 and -41 are oxidized and irreversible loss of enzymatic activity occurs. Further research has indicated that sensitized or nonsensitized photooxidation of sulfides can also occur via a nonsinglet oxygen mechanism[18,19]. Such unsensitized photooxidation of sulfides can even occur in the solid state[20].

It is known that electron transfer (ET) is facilitated by neighboring lone-pair donors such as *thioethers*, *carboxylate* and *amino* groups[21,22]. Therefore, it is quite conceivable that the immediate environment or the neighboring group must be playing a significant role in the metabolism of thioethers in biological systems.

Discussion

Following is the general outline of the redox chemistry (oxidation) of aliphatic thioethers (Eq. 3.1 & 3.2) and a number of anticipated chemical steps (Eq. 3.3 - 3.9) that could follow the electron transfer step.

a. **One electron oxidation**

$$R_2S \rightleftharpoons R_2S^{\bullet+} + e^- \qquad E^{\circ\prime}_A \qquad (3.1)$$

$$R_2S^{\bullet+} \rightleftharpoons R_2S^{2+} + e^- \qquad E^{\circ\prime}_B \qquad (3.2)$$

b. **Dimer formation**

$$2R_2S^{\bullet+} \rightleftharpoons R_2S : SR_2]^{2+} \qquad \text{(diamagnetic)} \qquad (3.3)$$

$$R_2S^{\bullet+} + R_2S \rightleftharpoons R_2S \therefore SR_2]^{\bullet+} \qquad \text{(paramagnetic)} \qquad (3.4)$$

c. **Disproportionation/Comproportionation**

$$2R_2S^{\bullet+} \rightleftharpoons R_2S^{2+} + R_2S \qquad (3.5)$$

d. **Adduct formation**

$$R_2S^{\bullet+} + ROH \rightleftharpoons R_2S \therefore OR + H^+ \qquad (3.6)$$

$$R_2S^{\bullet+} + RNH_2 \rightleftharpoons R_2S \therefore NHR + H^+ \qquad (3.7)$$

e. **Nucleophilic attack**

$$R_2S^{2+} + H_2O \rightarrow R_2S{=}O + 2H^+ \qquad (3.8)$$

$$2R_2S^{\bullet+} + H_2O \rightarrow R_2S{=}O + R_2S + 2H^+ \qquad (3.9)$$

f. **Further oxidation of sulfoxide**

$$R_2S{=}O \xrightarrow[H_2O]{\text{-2e-}} R_2S(=O)_2 + 2H^+ \qquad (3.10)$$

Scheme 3.1. General outline of the redox chemistry of thioethers.

Sulfur centered radical cations are normally very reactive toward nucleophilic attack. The cation radical generated by one-electron oxidation of R_2S, termed here as the "*primary cation radical*", accommodates the unpaired electron in the sulfur *p*-orbital. This highly reactive species tends to stabilize itself by interacting with an available *p*-electron lone-pair of another atom to form an intramolecular (transannular) or intermolecular (dimeric) 3-electron bond. The cation radical thus generated can accommodate the unpaired electron in the corresponding σ^* orbital resulting in a weaker σ bond (bond order = 1/2).

Because of the high reactivity of the primary cation radical, resulting from the anodic oxidation of thioether the cathodic peak is seldom observed. Most of the time the reactivity of the primary cation radical also frustrates further oxidation to the dication. However, it can be stabilized if allowed to interact with an appropriate neighboring nucleophilic substituent in the same molecule to convert to what is termed here as the "*transannular cation radical*". A proper orientation of the neighboring nucleophile would allow the primary cation radical to form a transient transannular 3-electron bond. This process, however, may be subject to a competing reaction with another potential nucleophile. The potential contenders are the analyte itself, the solvent, oxygen, or traces of water, supposing that there is no other impurity present.

Figure 3.1. Variation of the cyclic voltammograms of tricyclo[2.2.1.0]heptane-1,5-dithiocane (NorDTCO) with [NorDTCO] and scan rates in methylene chloride, 0.1 M in tetrabutylammonium hexafluorophosphate (TBAHFP), on glassy carbon vs Ag/(0.1M $AgNO_3$ in CH_3CN). The numbers in parentheses indicate μA corresponding to the scale given in top left corner.

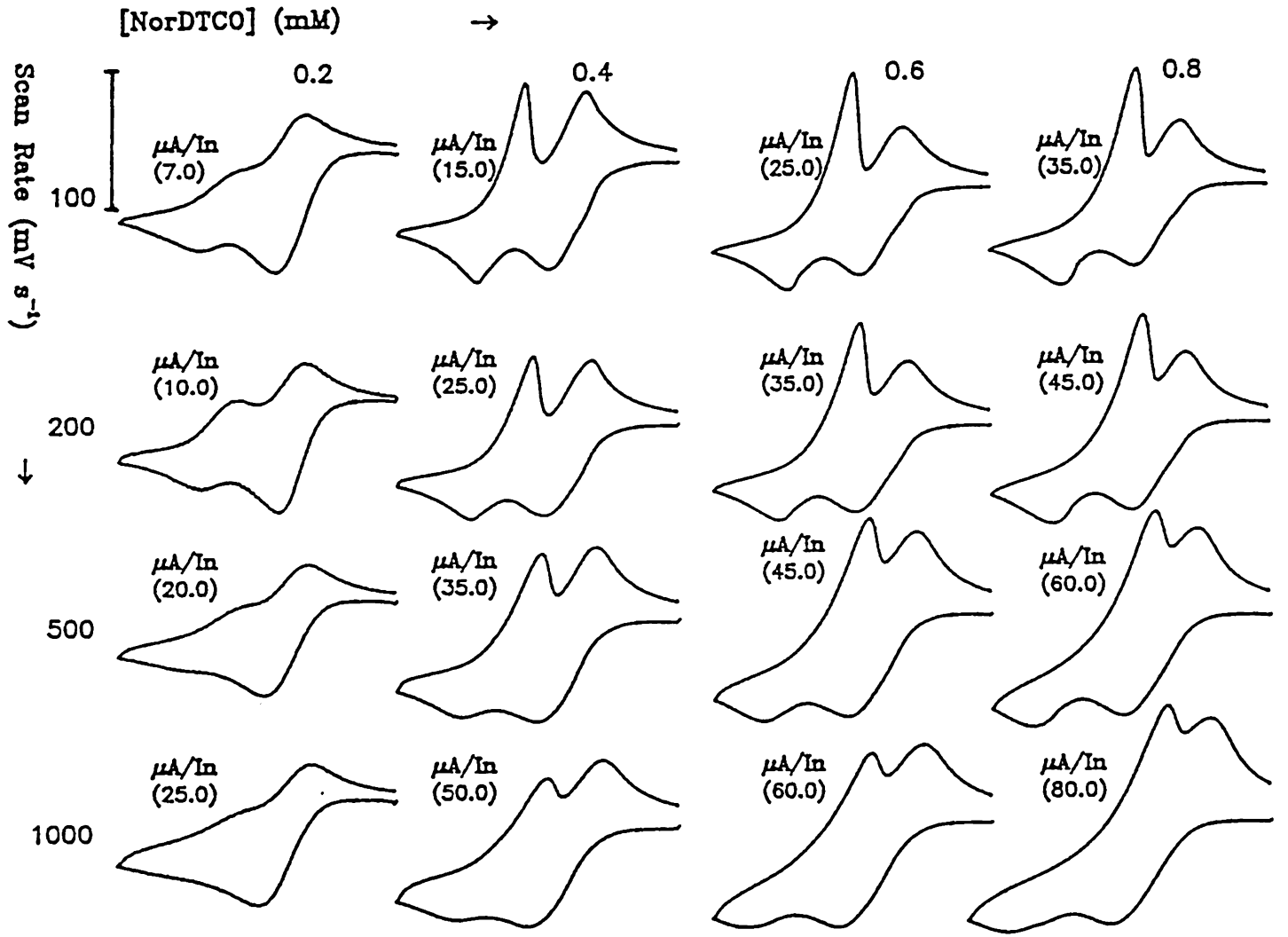
[NorDTCO] (mM) →
0.2
0.4
0.6
0.8
Scan Rate (mV s⁻¹) ↓
100
200
500
1000
μA/In (7.0)
μA/In (15.0)
μA/In (25.0)
μA/In (35.0)
μA/In (10.0)
μA/In (25.0)
μA/In (35.0)
μA/In (45.0)
μA/In (20.0)
μA/In (35.0)
μA/In (45.0)
μA/In (60.0)
μA/In (25.0)
μA/In (50.0)
μA/In (60.0)
μA/In (80.0)

Electrochemistry of NorDTCO in Methylene Chloride. Figure 3.1 summarizes the CV data for NorDTCO in methylene chloride for a concentration range of 0.2 to 0.8 mM and scan rate varying from 0.1 V to 1.0 V s^{-1} over a potential range of 250 - 850 mV. The CV was carried out on a glassy carbon electrode vs Ag/(0.1 M Ag^{+}/CH_3CN), using 0.1 M TBAHFP (Electrochemical grade) as supporting electrolyte. The working electrode surface was polished with 0.3 μm deagglomerated alumina (Buehler) then sonicated and finally dried before starting the experiment. No cleaning of the electrode was done between the scans because no fouling of the electrode was noticed.

The voltammograms are clearly resolved into two electron transfer (ET) steps. The thermodynamic driving force provided by the neighboring sulfur for the initial oxidation is evident from the substantially lower redox potentials of the system. The presence of the well resolved cathodic peaks on the reverse scan at a scan rate as low as 10 mV s^{-1} and concentrations as low as 0.2 mM is an indication of the kinetic stability of the oxidation products in methylene chloride.

Reversal of the direction of the potential sweep after the first anodic peak (peak I) reveals the corresponding cathodic peak (peak IV) (Figure 3.2). The sharp cathodic counterpart (peak III) of the second anodic peak (peak II) is characteristic of a faradaic reaction involving an adsorbed species. This strongly suggests the oxidation of the cation radical to a dication. The high positive charge on the dication may make it less readily soluble in the essentially nonpolar methylene chloride. The decreased

solubility of the dication would result in its transitory accumulation at the electrode surface. This phenomenon might account for the shape of the voltammetric peaks at higher concentrations and lower scan rates.

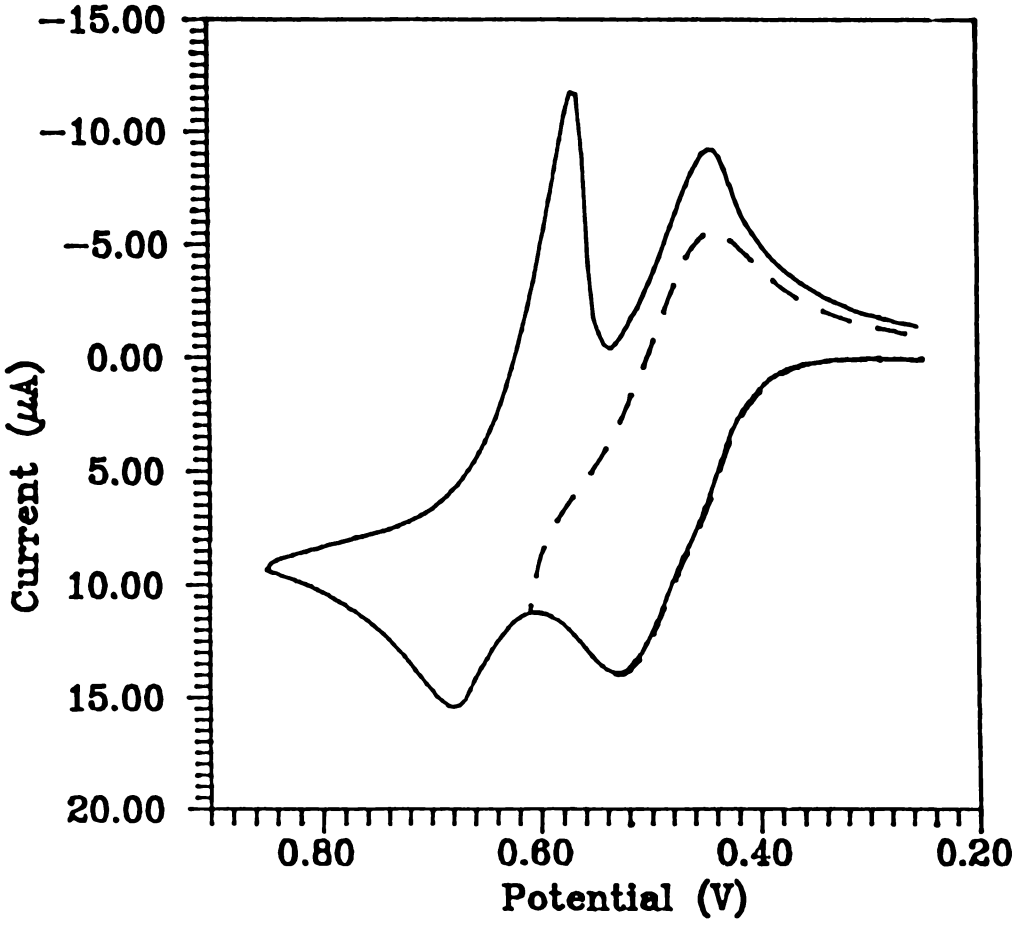

Figure 3.2. Typical CV's of NorDTCO in CH_2Cl_2 at 100 mV s^{-1} Scan Rate ([NorDTCO] = 0.5 mM).

The number of electrons in the first ET process (n_1) and for the second ET step n_2 were determined from the logarithmic analysis of the RDE data of 0.2 mM NorDTCO at 900 rpm and 10 mV s^{-1} scan rate. A plot of $\log\{i/(i_l - i)\}$ vs E for the

first ET step yielded a straight line. The slope of this line is 61.5 mV which corresponds to n_1 = 1.04 electrons. Similarly the logarithmic analysis of the second step afforded n_2 = 0.85 electrons. The Levich plot for the first anodic wave yielded a straight line passing through the origin which suggests that the process is diffusion controlled. The diffusion coefficient of the neutral molecule was calculated from the Levich plot to be 9.25 x 10^{-6} cm^2 s^{-1}.

The RDE data for concentrations of NorDTCO above 0.2 mM were highly irreproducible and also too complex to be analyzed in detail. This could also be due to the decreased solubility of the oxidation product of NorDTCO beyond the first oxidation step. The RDE results for the first ET step are further supported by the semi-integration of the cyclic voltammetric data in methylene chloride.

Semi-integration of the voltammetric data results in the transformation of the whole voltammetric curve to what has been termed a neopolarogram[23] defined by the following equation for the Nernstian process[24]:

$$E = E_{1/2} + (RT/nF) \ln\{(F_t - F(t))/F(t)\} \qquad (3.11)$$

where F(t) is the convolution transform of the experimental i(t) data and is given by

$$F(t) = 1/(\pi)^{1/2} \int_0^t (i(u)/(t - u)^{1/2})\, du \qquad (3.12)$$

and

$$F_t = nFAD^{1/2}C^{\infty} \quad (3.13)$$

where n is the number of electrons, F is the Faraday constant (C mol^{-1}), A is the electrode surface area (cm^2), D is the diffusion coefficient (cm^2 s^{-1}) and C^{∞} is the bulk concentration of the analyte in mol cm^{-3}.

ν (mV s^{-1}) / C (mM)	50	100	200	500	1000
0.2	1.04	1.02	1.00	1.06	0.99
0.4	1.1	1.11	1.13	1.17	1.17
0.5	1.02	1.06	1.09	1.08	1.21
0.6	1.06	1.06	1.13	1.11	1.30
0.8	1.11	1.01	1.13	1.10	1.11

Table 3.1. Number of electrons involved in the first ET step of NorDTCO in CH_2Cl_2 calculated from the semi-integration of the voltammetric data at different concentrations and scan rates.

Logarithmic analysis can be carried out on the semi-integral cyclic voltammograms in much the same way as with the steady state voltammograms at stationary or rotating electrodes[25,26] in which the *i-E* relationship for the anodic Nernstian process is defined as:

$$E = E_{1/2} - (RT/nF) \ln \{i/(i_\ell - i)\} \quad (3.14)$$

The results of the logarithmic analyses of the semi-integral voltammograms are presented in Table 3.1 which lists the number of electrons (n_1) for different concentrations of NorDTCO at various scan rates (ν). Based on these observations the likely mechanism of the redox reactions of NorDTCO is predominantly EE in nature. According to such a mechanism NorDTCO is first oxidized to the primary cation radical (Eq. 3.15).

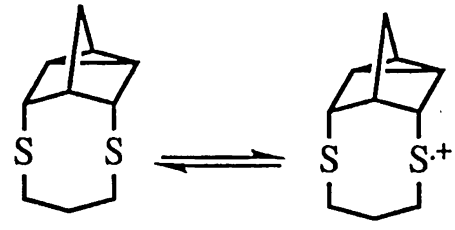

(3.15)

The primary cation radical is further oxidized to what is termed here the "*localized biradical dication* " at a higher potential as shown in Eq. 3.16.

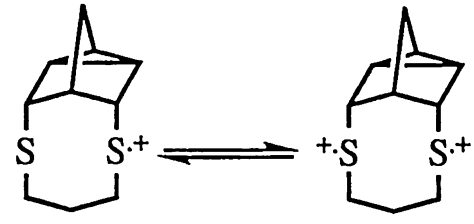

(3.16)

The voltammograms in Figure 3.1 may suggest the possibility of the dependence of the redox behavior of NorDTCO on its concentration. However it is not evident because both the anodic and cathodic peaks are as well resolved at the

lowest concentration as they are at the highest concentration. Moreover, the reversibility of the peaks, n_1 and the peak potentials corresponding to the first ET process are not strongly influenced by concentration.

However, the fractional number of electrons calculated from the logarithmic analysis of the RDE data (n_2 = 0.85) for the second oxidation step suggests a limited consumption of the primary cation radical by the formation of a dimeric species. This is supported by a similar analysis of the semi-integral voltammetric data. Analysis of the semi-integral voltammograms, at 200 mV s^{-1} scan rate, of 0.2, 0.4, 0.6 and 0.8 mM NorDTCO gave 1.06, 0.85, 0.89 and 0.89 electrons, respectively, involved in the second ET step.

The broadening of the second anodic peak associated with the suppression of the corresponding cathodic peak at higher scan rates could be explained in two ways:

(i) The first oxidation step is followed by a chemical step the product of which can further be oxidized to a dication. If the follow-up chemical step is slow enough to become rate limiting at high scan rates and if only the product of the chemical step can be oxidized further, then at higher scan rates the chemical step becomes progressively less influential. Therefore, at higher scan rates the yield of the second oxidizable species would be lowered. This would result in a decreased peak current for the second ET step relative to the first one. Since the effect of concentration is not so significant, the product of the chemical step could be the transannular cation radical.

Because of the presence of an electron in the σ* orbital of the >S∴S<]$^{+}$ three-electron bond, the oxidation of the transannular cation radical to the corresponding dication should be as easy as that of the parent thioether or even easier[21,27,28]. Thus in a purely thermodynamic sense the redox process would seem to be a one-step two-electron process rather than two resolved peaks. Under the condition of slow kinetics of the second electron transfer (ET) step the two oxidation peaks, if resolved at all, would tend to merge at slower scan rates[29] due to the thermodynamically facile oxidation of such a species. Apparently this is not the case here. Therefore the broadening of the second anodic peak cannot be ascribed to the kinetics of a chemical reaction following the initial oxidation to produce a second electroactive species. This also rules out the likelihood of slow kinetics of the second ET step to be responsible for the resolution of the constituent ET steps, involving the formation of the transannular cation radical.

(ii) The broadening of the second anodic peak may be ascribed to a slow ET involving the direct oxidation of the second sulfur of NorDTCO]$^{+}$ (Eq. 3.16). However at such a high overpotential the rate of ET step should not be rate limiting. Nevertheless, the increased solution resistance and/or decreased diffusion coefficient for the primary cation radical compared to the neutral NorDTCO molecule cannot be ruled out as reasons for the observed behavior. This second possibility seems more plausible.

All these arguments amount to the fact that in methylene chloride the two ET

steps are predominantly localized following the EE type redox mechanism. The oxidation products of NorDTCO gain thermodynamic stability from the neighboring thioether function in the molecule whereas the kinetic reactivity does not seem to be of great consequence. The resolution of two oxidation steps is achieved because the first oxidation step makes the second step harder. This would cause the second oxidation to take place at a relatively higher potential[30,31].

The formal potential of the two ET steps roughly differ by 0.14 V as estimated from the CV of 0.5 mM NorDTCO at 50 mV s^{-1} scan rate. This can provide some information about the possibility of comproportionation in solution as outlined below.

$$\text{NorDTCO} \rightleftharpoons \text{NorDTCO}^{\bullet+} + e^- \qquad E^{\circ\prime}_1 \qquad (3.17)$$

$$\text{NorDTCO}^{\bullet+} \rightleftharpoons \text{NorDTCO}^{2+} + e^- \qquad E^{\circ\prime}_2 \qquad (3.18)$$

$$\text{NorDTCO}^{2+} + \text{NorDTCO} \rightleftharpoons 2\,\text{NorDTCO}^{\bullet+} \qquad K_{com} \qquad (3.19)$$

$$K_{com} = \text{Exp}(F/RT)\,(E^{\circ\prime}_2 - E^{\circ\prime}_1) \qquad (3.20)$$

The K_{com} is estimated to be 234 indicating that the cation radical should be fairly stable electrochemically.

Electrochemistry of NorDTCO in Acetonitrile. The oxidation of NorDTCO was studied on a glassy carbon working electrode vs Ag/(0.1M Ag^+/CH_3CN), using 0.1 M tetrabutylammonium hexafluorophosphate (TBAHFP) (Fluka, Electrochemical

grade) as supporting electrolyte. The working electrode surface was cleaned after every run by squirting it with a jet of acetonitrile then polishing on Kimwipes for about 3 min, sonicating in acetonitrile for about 3 min, and finally rinsing with dry acetonitrile. Without such cleaning the response of the electrode kept decreasing progressively with repeated scans and the voltammograms were highly distorted.

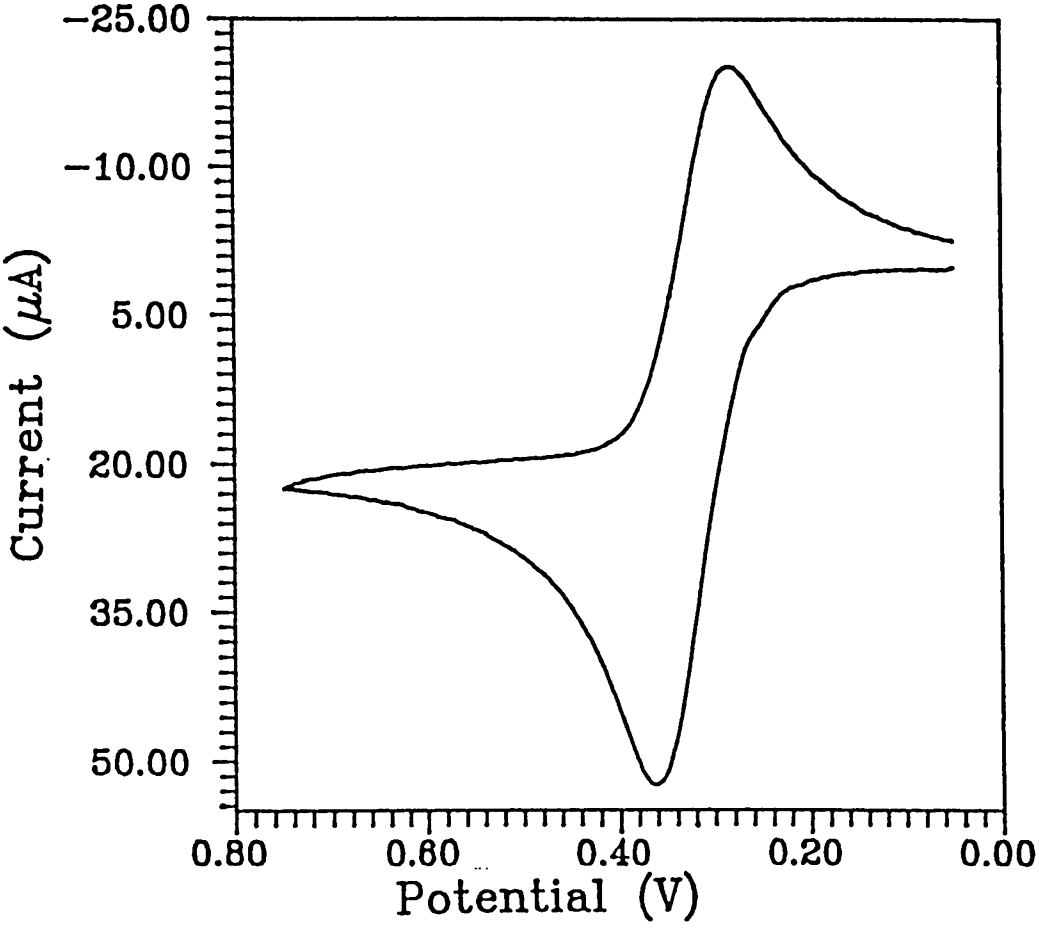

Figure 3.3. Cyclic Voltammogram of 1.0 mM NorDTCO in Acetonitrile at 100 mV s^{-1} Scan Rate.

Intramolecular Pathway. Figure 3.3 shows the redox behavior of 1.0 mM

NorDTCO at 100 mV s^{-1} scan rate. This is a normal concentration for cyclic voltammetry, in acetonitrile. The symmetrical shape of the voltammogram and the smaller positive value of the apparent redox potential relative to those of simple aliphatic thioethers are indicative of a substantial interaction between the neighboring sulfides. At first glance it would seem that the primary cation radical which is produced by the initial oxidation of NorDTCO (Eq. 3.15) gains stability and a driving force by interacting with the lone pair of electrons on the neighboring sulfur to form the transannular cation radical(Eq. 3.21).

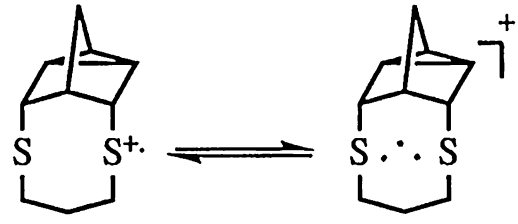

(3.21)

The transannular cation radical can either be reduced back to NorDTCO or it can undergo further oxidation to a dication. However, the analysis of the voltammogram in Figure 3.3 yielded 1 electron involved in the redox process which is indicative of either no further oxidation or the involvement of a following chemical process which can account for overall one-electron oxidation. This will be explained later.

Figure 3.4 shows the crystal structure of the title compound (**1.1**)[32]. It is clear from the structure that the molecule is apparently twisted and the two sulfurs may appear not to promote effective mutual orbital overlap. This twist may either be arising from the structural constraints imposed by the norbornyl backbone or may be

a consequence of the lone pair - lone pair electronic repulsions between the two sulfur atoms which are tightly held in position by the norbornyl back bone. The driving force for the transannular interaction following the formation of the primary cation radical may derive from a change in the electron density at the sulfur due to oxidation and thus relieving the structural constraints. This could facilitate the through space orbital interaction between the two sulfurs. This would seem to be responsible for the remarkably facile oxidation of the target sulfide.

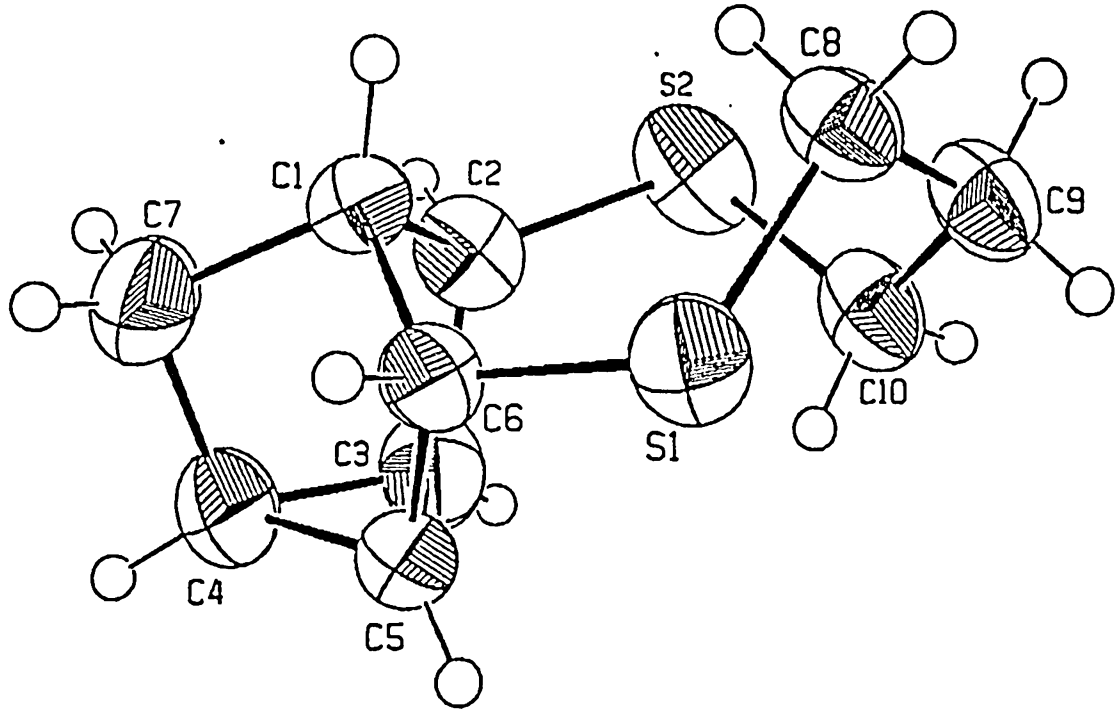

Figure 3.4. Crystal Structure of **1.1** (NorDTCO)[32] (ORTEP Drawing).

Increasing the scan rate has a remarkable effect on the voltammetric results. The dependence of the voltammograms on the scan rate is such that the height of the

cathodic peak decreases relative to that of the anodic peak with increasing scan rate and is ultimately completely suppressed at 20 V s^{-1} scan rate (Figure 3.5). This can be explained by the generation of an electroinactive species on the anodic scan which can convert to its electroactive conformer in a rate limiting step. The effect of increasing scan rate on the overall number of electrons in the anodic process is such that n increases with increasing scan rate until it reaches 2. However, there is no indication of a second ET step in the anodic peak. This suggests that the product of initial oxidation can be oxidized further to a dication at the potential of initial oxidation.

The oxidation of NorDTCO to the primary cation radical would tend to encumber its further direct oxidation (no 3-electron-bond formation) to the dication[30,31] because of the coulombic interaction between two positive charges. Therefore, two-electron oxidation of NorDTCO via the formation of only the primary cation radical, at the same potential would seem unlikely. However, such an oxidation via the formation of the transannular cation radical is feasible because of the presence of an electron in the σ^* orbital of the >S∴S<]$^+$ species[21,27,28] (Eq. 3.22).

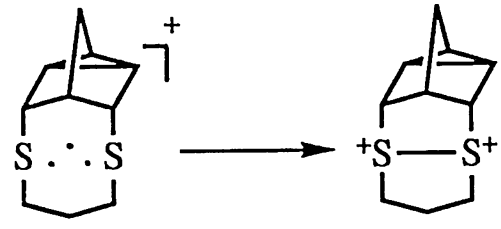

(3.22)

The transannular dication (Eq. 3.22) might be the electroinactive species

Figure 3.5. Variation of the cyclic voltammograms of NorDTCO with [NorDTCO] and scan rates in acetonitrile, 0.1 M in TBAHFP, on glassy carbon vs Ag/(0.1M $AgNO_3$ in CH_3CN). The numbers in parentheses indicate μA corresponding to the scale given in top left corner.

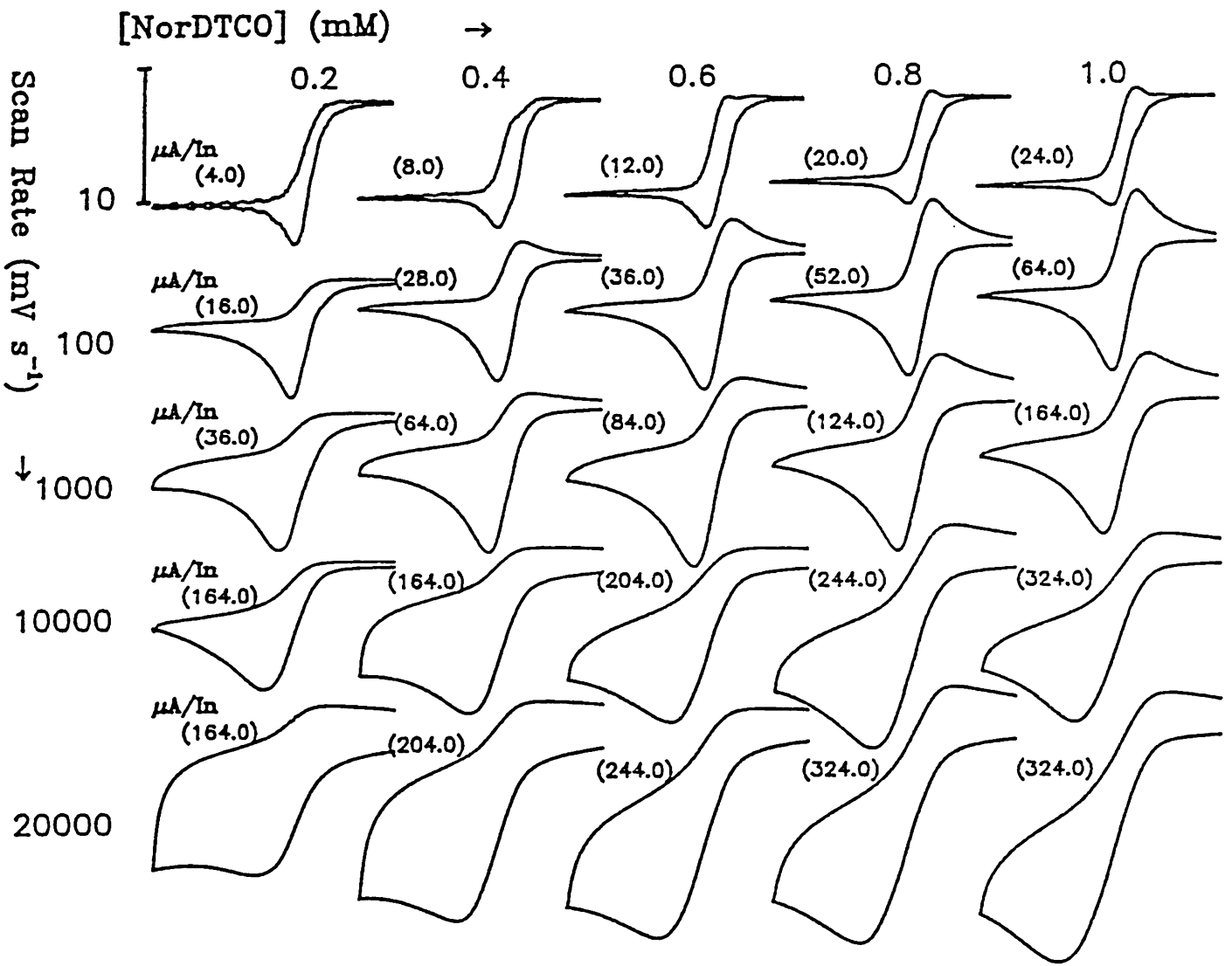
[NorDTCO] (mM) →
0.2
0.4
0.6
0.8
1.0
Scan Rate (mV s⁻¹)
↓
10
100
1000
10000
20000
μA/In
(4.0)
(8.0)
(12.0)
(20.0)
(24.0)
μA/In
(16.0)
(28.0)
(36.0)
(52.0)
(64.0)
μA/In
(36.0)
(64.0)
(84.0)
(124.0)
(164.0)
μA/In
(164.0)
(164.0)
(204.0)
(244.0)
(324.0)
μA/In
(164.0)
(204.0)
(244.0)
(324.0)
(324.0)

because the oxidation of the transannular cation radical to the transannular dication will result in an increased bond-order between the two sulfurs which could introduce significant conformational changes in the molecule. Therefore the transannular dication has to convert into the localized biradical dication (Eq. 3.23) to undergo reduction on the reverse scan in the experimental potential range.

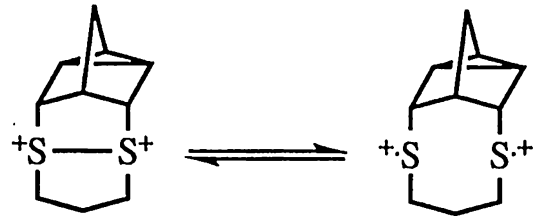

(3.23)

At slow scan rates the system would be both in chemical and electrochemical equilibrium but at higher scan rates the conversion of the transannular dication to the localized dication (Eq. 3.23) could become rate limiting. Thus the effect of increasing the scan rate would be to "beat" the rate of backward reaction in Eq. 3.23. This seems to be responsible for the lowering of the cathodic peak current[33].

Intermolecular Pathway. Figure 3.5 summarizes the cyclic voltammetric data of the title compound in acetonitrile at different concentrations and scan rates. An intramolecular interaction should not depend on the concentration of the analyte. Because of the dependence on concentration of the cathodic peak-height relative to that of the anodic peak, the redox chemistry of NorDTCO in acetonitrile cannot be explained only by the intramolecular interaction.

Table 3.2 presents the logarithmic analysis of the semi-integral voltammograms of NorDTCO, in acetonitrile. This table indicates an increase in the apparent number of electrons from a minimum of 1 electron to a maximum of 2 electrons with increasing scan rate (100 mV - 20 V s^{-1}) but increasing the concentration (0.2 mM - 2.0 mM) of NorDTCO did not show any significant influence on "*n*" at a given scan rate (Table 3.2).

ν (V s^{-1}) / C (mM)	0.1	0.2	0.5	1.0	2.0	5.0	10.0	20.0
0.2	1.06	1.15	1.41	1.36	1.54	1.73	1.66	1.88
0.4	1.05	1.07	1.13	1.27	1.35	1.59	1.69	2.08
0.6	1.06	1.14	1.27	1.21	1.41	1.65	1.88	2.09
0.8	1.11	1.09	1.13	1.26	1.41	1.76	1.88	2.11
1.0	1.13	1.12	1.18	1.34	1.46	1.64	1.86	2.11
2.0	1.20	1.27	1.28	1.41	1.63	1.84	1.78	1.98

Table 3.2. Number of electrons involved in the anodic oxidation of NorDTCO in CH_3CN calculated from the semi-integration of the voltammetric data at different concentrations and scan rates.

Because the thermodynamic feasibility of the oxidation of the transannular cation radical should not depend on the scan rate, the number of electrons involved in the overall redox process should remain the same both at higher and lower scan

rates (even more so at lower scan rates). Because the number of electrons involved in the overall anodic process decreases with decreasing scan rate, it must mean that at higher scan rates the transannular cation radical can be further oxidized to the corresponding dication whereas at lower scan rates the transannular cation radical is subject to a chemical reaction which can count for only one electron per molecule in the overall oxidation. Since upon decreasing the scan rate the system apparently gains more and more reversibility, the follow-up chemical process cannot simply be the decomposition of the transannular cation radical.

Alternatively the intramolecular chemical step, following the formation of the primary cation radial, is progressively handed over to the impending, relatively facile, intermolecular dimerization process as the concentration increases. The availability of the favorable intermolecular dimerization pathway can outweigh the intramolecular dimerization. The ephemerality of the transannular cation radical in favor of a dimeric cation radical can be ascribed to a possible structural strain associated with the former. An improper alignment of the two neighboring sulfurs relative to each other could be responsible for such a strain. However, in the case of the intermolecular dimerization the steric factors should also be taken into account. Thus the intramolecular pathway which presumably prevails at low concentration and high scan rates may not be playing a dominant role in the overall redox mechanism at higher concentrations and lower scan rates.

There are two different potential candidates to take part in the intermolecular

pathways following the formation of the transannular cation radical. (i) Neutral NorDTCO molecule and (ii) the transannular cation radical itself.

The interaction of the transannular cation radical with a neutral NorDTCO molecule to give the dimeric cation radical is shown in Eq. 3.24.

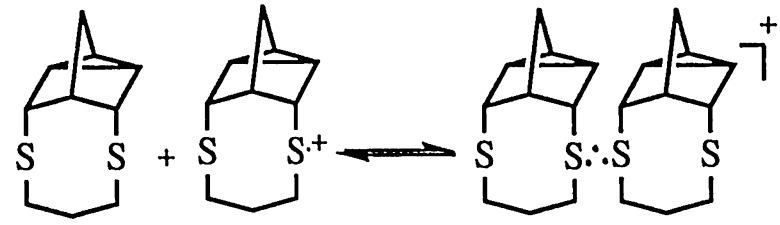

(3.24)

Further oxidation of the dimeric cation radical can account only for overall one electron per molecule (Eq. 3.25).

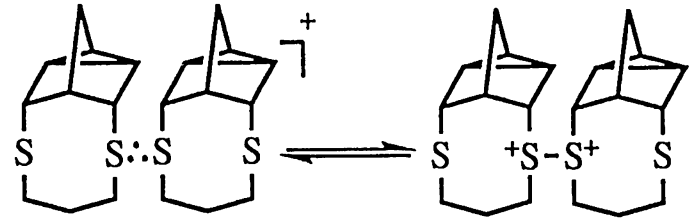

(3.25)

The chemical interaction between two transannular cation radicals can either lead to the formation of the dimeric dication (Eq. 3.26)

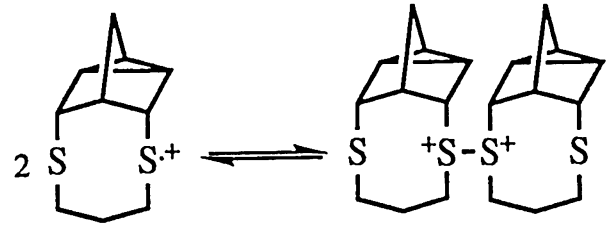

(3.26)

or it can end up in the dimeric biradical dication (Eq. 3.27).

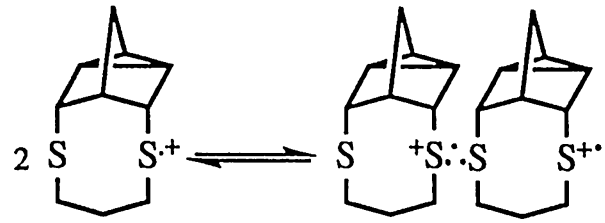

(3.27)

The dimeric dication resulting from Eq. 3.26 may not be further oxidized at the potential of initial oxidation for the reasons presented above regarding the direct oxidation of the primary cation radical. This process would also ultimately lead to an overall one electron oxidation. The dimeric biradical dication from Eq. 3.27 will undergo further oxidation as shown in Eq. 3.28.

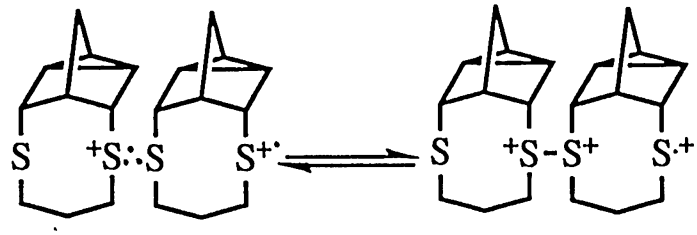

(3.28)

The oxidation product of Eq. 3.28 can then undergo the following reaction (Eq. 3.29). This process can account for a total of one electron for the overall oxidation.

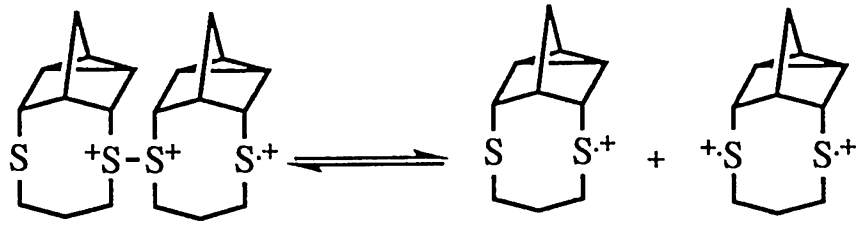

(3.29)

Nevertheless the product of Eq. 3.27 could also be a polymeric species $((NorDTCO)^{+})_n$ where n = 2, 3,...). This species can undergo further (n-1)-electron

oxidation. Therefore the overall redox process involving Eq. 3.27 could involve 1.5 $\leq n < 2$. Because the formation of polymeric species along the intermolecular pathway would be favorable at higher concentrations, n should increase with increasing concentration at a given scan rate. The dependence of n only on the scan rate regardless of the concentration of NorDTCO (Table 3.2) appears to rule out the formation of the polymeric species. Therefore, the intermolecular pathways could involve only $1 \leq n \leq 1.5$.

The effect of increasing the concentration of NorDTCO would be to increase the chances of encounter between two species. This would provide kinetic stability to the cation radical through the formation of the dimeric species which can then undergo further oxidation. It is evident from Table 3.2 and Figure 3.5 that higher scan rates lead to 2 electron oxidation and no cathodic processes regardless of the concentration. This suggests that the immediate product of the chemical reaction following the formation of the primary cation radical is the transannular cation radical the formation of which should follow first order kinetics. The transannular cation is then oxidized to the electroinactive transannular dication at the same or lower potential. Only such a scenario can account for the first order behavior as well as the increasing irreversibility and increasing n with increasing scan rate.

The overall number of electrons involved in the oxidation of NorDTCO via the formation of only the transannular cation radical is 2. The data from table 3.1 at low scan rates suggest a process which can account only for overall one electron

oxidation. Therefore, the intermolecular pathway involving Eq. 3.26 might be the dominant route in the slow scan rate regime. At a very low scan rate the neutral molecule may get enough time to diffuse to the electrode surface and react with the monomeric cation radical. Alternatively the cation radical can diffuse into the solution to react with the neutral molecule to produce the dimeric cation radical which would then diffuse back to the electrode and undergo further oxidation to give an overall one-electron oxidation. In the intermediate range of scan rates the monomeric cation radical (primary or transannular) would have just enough time to react with another cation radical according to Eq. 3.26 or Eq. 3.27. The pathway involving Eq. 3.27 can account for an overall $n = 1.5$. At very high scan rates the cation radical may not have enough time to undergo intermolecular reaction and, therefore, the intramolecular pathway would become the dominant route.

Other potential reactions following the formation of the transannular cation radical. ***Reaction with a simple aliphatic thioether.*** Tetrahydrothiophene (THT) is electroinactive in the potential range where NorDTCO is electroactive. CV's of 0.2 mM NorDTCO were run in the presence of THT to explore the possibility of intermolecular interaction of the oxidation product of NorDTCO with another thioether. Figure 3.6 shows a number of such voltammograms, in methylene chloride, superimposed on the voltammogram of pure NorDTCO run under the same experimental conditions. There is obviously a trend in the peak potential, a shift to

Figure 3.6. Variation of the cyclic voltammograms of 0.5 mM NorDTCO tetrahydrothiophene (THT) added, in methylene chloride at 100 mV s^{-1} scan rate. (---) No THT added; (◇◇◇) 0.2 mH THT; (○○○) 0.4 mM THT; (▽▽▽) 0.6 mM THT; (—) 0.8, 1.0 mM THT. (0.1 M in TBAHFP, on glassy carbon vs Ag/(0.1M $AgNO_3$ in CH_3CN)).

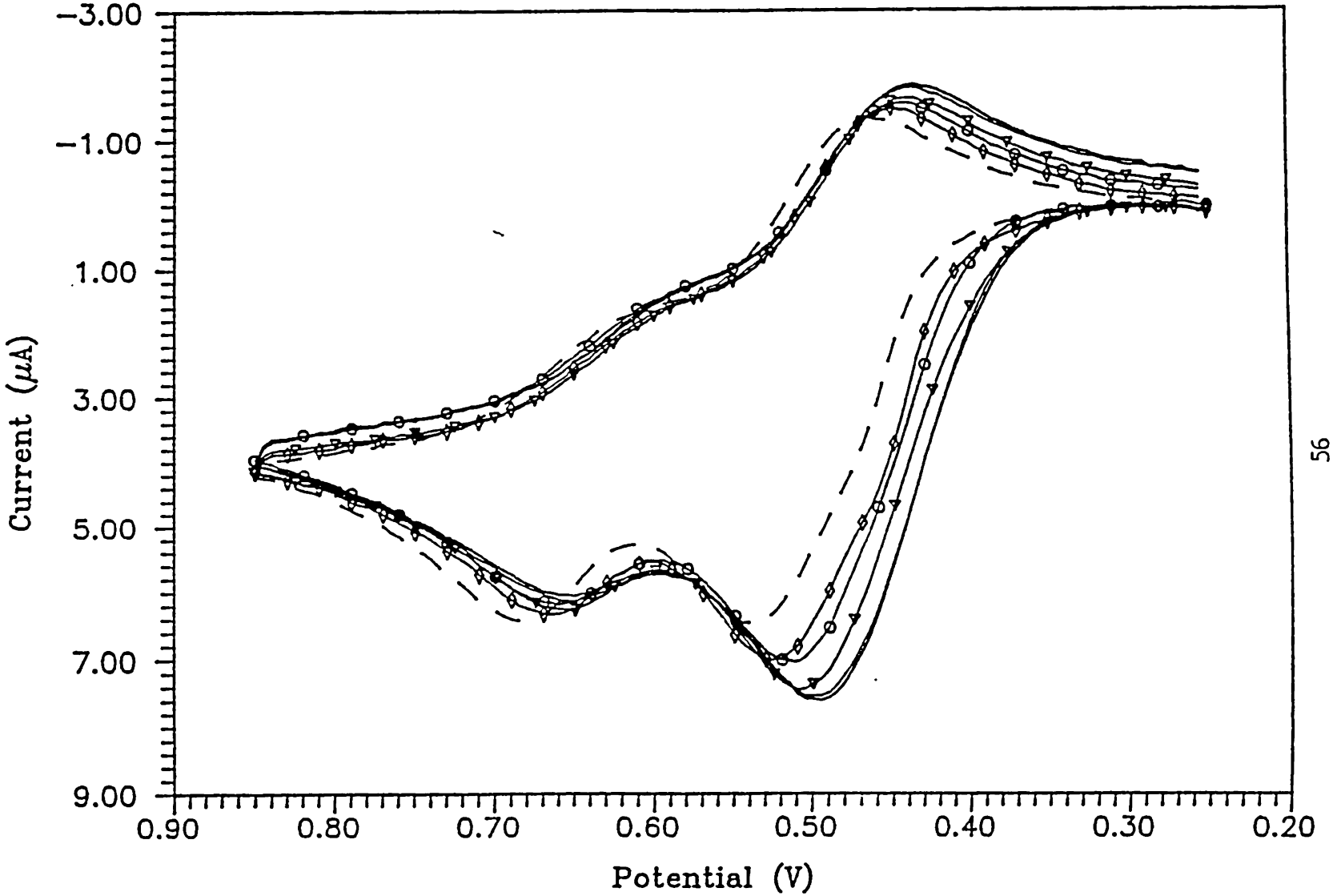
−3.00
−1.00
1.00
3.00
5.00
7.00
9.00
Current (μA)
0.90
0.80
0.70
0.60
0.50
0.40
0.30
0.20
Potential (V)

less positive values with increasing concentration of THT up to 0.8 mM [THT]. Such a shift is consistent with comsumption of the primary cation radical in a follow-up chemical reaction.

The lack of such a trend in the CV's of NorDTCO itself, in methylene chloride, with its increasing concentration is another manifestation of the kinetic stability of the primary cation radical which would lead to the presumed EE mechanism. However, the effect of increasing NorDTCO concentration can also be an increased ***iR*** drop due to increased Faradaic current. The ability of THT to interact with the cation radical can be attributed to its smaller size. The fact that THT itself is not electroactive in the experimental potential range may be another reason that its potential nucleophilicity is uninterrupted by a redox process.

In acetonitrile the concentration of NorDTCO has been shown to have a substantial influence on its redox chemistry. The reason that we do not see such a shift in the peak potentials in acetonitrile may be that the cation radical is already subject to a follow-up chemical reaction. The data in acetonitrile is strongly suggestive of the formation of the transannular cation radical immediately after the initial oxidation. Besides that, the interacting species which is NorDTCo itself is also electroactive. Interestingly the presence of THT apparently had no effect on the redox behavior of NorDTCO in acetonitrile. This is a further indication of the formation of the transannular cation radical, a first order process, immediately after the initial oxidation. Thus a variation in concentration of NorDTCO or the presence of any other

thioether apparently has no effect on the oxidation of NorDTCO in acetonitrile.

Solvent effect. Acetonitrile has been shown previously to be a potential nucleophile for the anthracene cation radical[34]. Under ordinary conditions the anthracene cation radical has been shown to be susceptible not to acetonitrile but to attack by traces of water. However in "super dry" acetonitrile the oxidative acetamidation product of anthracene has been isolated. The pseudo-first-order rate constant, obtained from the RDE data, for the reaction between anthracene cation radical and acetonitrile at room temperature was found to be ca. 125 s^{-1} which is not a fast process. Such a nucleophilic process has been shown to be avoidable either at high rotation speed or by running the experiments in dry methylene chloride.

It has been reported in the literature that certain redox systems undergoing two-electron transfer reactions display a single two-electron wave in acetonitrile and resolved one-electron waves in methylene chloride. This thermodynamic discrimination has been defined as to be arising from unequal solvent dependence of the corresponding formal potentials[35].

The substantial negative shift in the anodic peak potential relative to the oxidation of simple aliphatic thioethers can be accounted for in terms of the thermodynamic stability provided by the intramolecular communication between the neighboring sulfurs. However, the irreversibility of the voltammograms in acetonitrile at low concentration suggests that the interaction may not be able to provide enough kinetic stability to the primary cation radical.

Figure 3.7. Variation of the cyclic voltammograms of 0.5 mM NorDTCO with acetonitrile in methylene chloride at 100 mV s^{-1} scan rate. (A) No CH_3CN added (B) 0.5 % (C) 1 % (D) 5 % μL added (E) 10 % (F) H_2O added to (A). (0.1 M in TBAHFP, on glassy carbon vs Ag/(0.1M $AgNO_3$ in CH_3CN)).

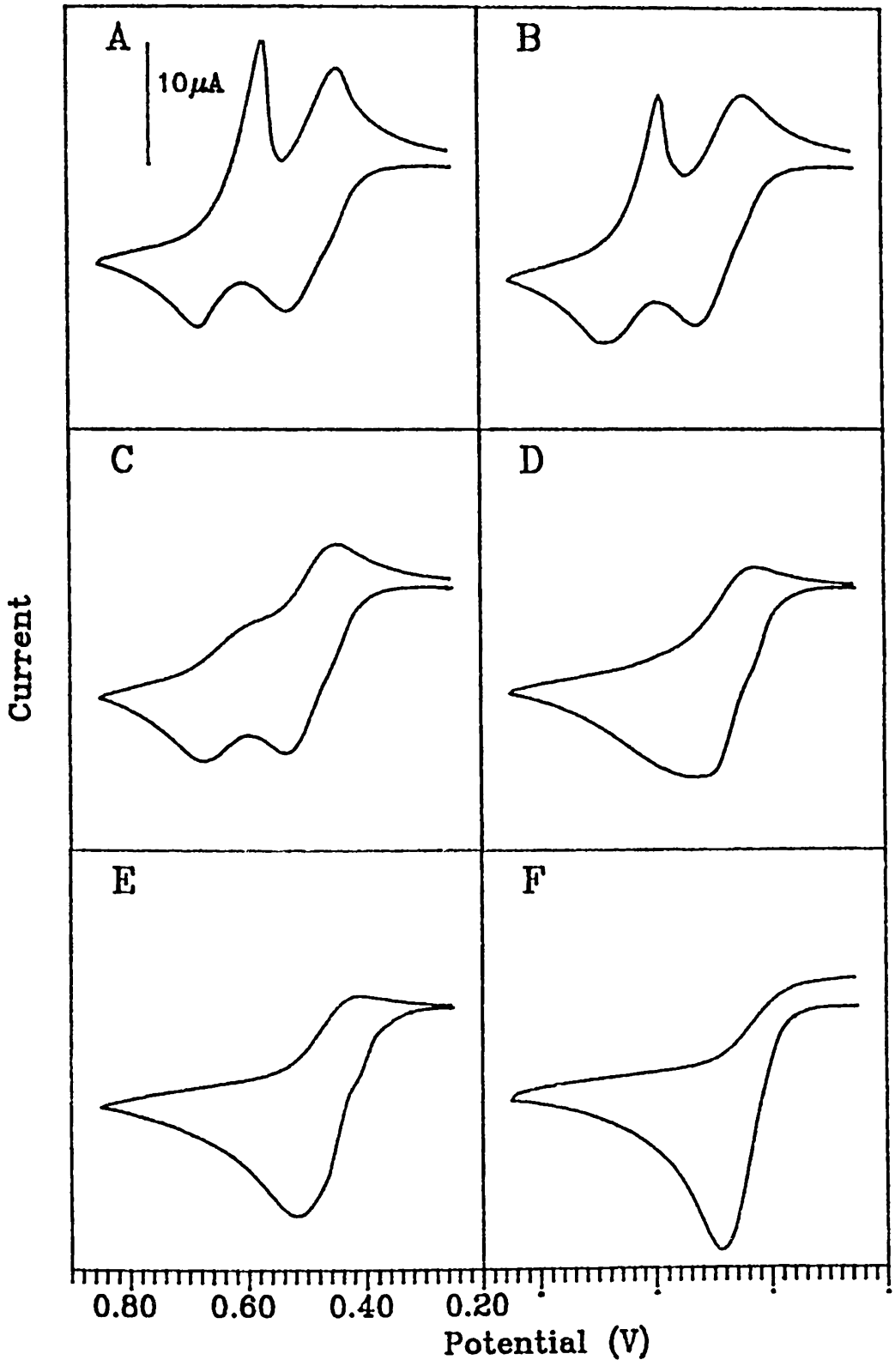
A
10μA
B
C
D
E
F
Current
0.80
0.60
0.40
0.20
Potential (V)

The fact that the voltammograms cannot be reproduced in acetonitrile unless the electrode is thoroughly cleaned between the runs could also suggest that the oxidation product of NorDTCO is subject to decomposition. The product of the decomposition could deposit/adsorb on the electrode surface. This could lower the electrode response as well as affecting its ET properties. Nevertheless, in methylene chloride the voltammograms can be retraced at any time during the experiment which also obviates the need for cleaning the electrode between runs.

Figure 3.7 demonstrates how the presence of acetonitrile in methylene chloride can switch the EE mechanism to the ECE mechanism which seemingly prevails in acetonitrile. It is obvious from Figure 3.7 that the two well resolved steps progressively merge into a single step with increasing concentration of acetonitrile in methylene chloride. This provides further support to the suggestion that the first oxidation step would render the subsequent oxidation harder especially when the two oxidation centers are within an interacting range. Most probably the way in which the two-electron oxidation in acetonitrile is accomplished in a single step is only through the formation of intra- or intermolecular >S∴S<$^{+}$ species.

Acid-base chemistry of the system. The one electron oxidation of a heteroatom (A) in an organic molecule weakens the AC_{α}-H bond by hyperconjugative interaction with the formally half-filled *p* orbital of the heteroatom[36]. For less stabilized cases, the dissociation of this proton is often the rate limiting reaction for the decomposition of the cation radical. The rate of this process which also depends on the dihedral angle

Figure 3.8. Variation of the cyclic voltammograms of 1.0 mM NorDTCO with added 2,6-di-*tert*-butylpyridine (DTBP) in acetonitrile at 100 mV s^{-1} scan rate. (A) No DTBP (B) 0.16 mM (C) 0.32 mM (D) 0.48 mM (E) 0.64 mM (F) 0.96 mM. (0.1 M in TBAHFP, on glassy carbon vs Ag/(0.1M $AgNO_3$ in CH_3CN)).

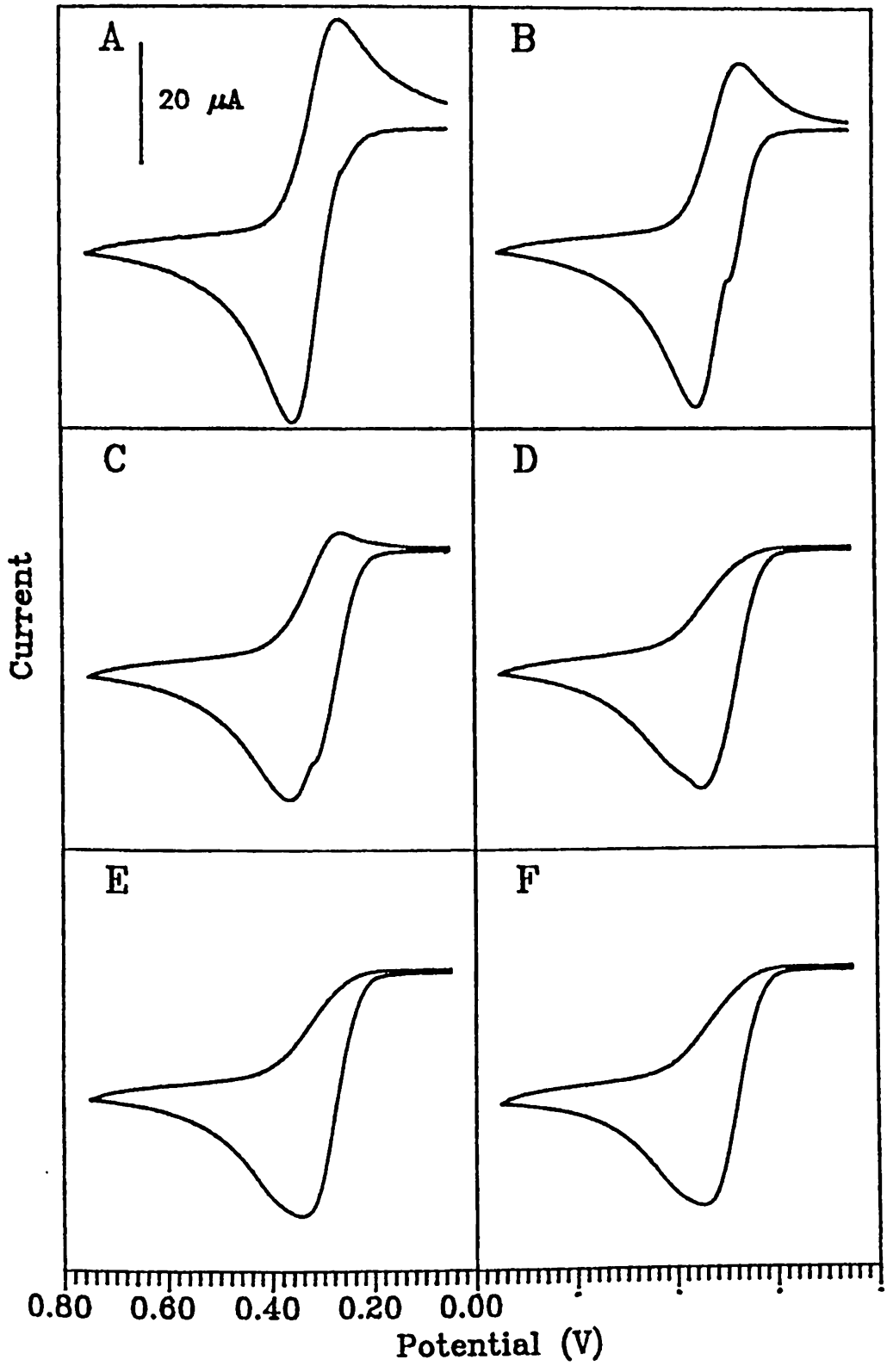
A
20 μA
B
C
D
E
F
Current
0.80
0.60
0.40
0.20
0.00
Potential (V)

between the C_{α}-H and the half-filled *p* orbital could have been slowed down for the bridgehead hydrogens in NorDTCO system but the hydrogens on the α methylene group may not be protected from cleavage. The dissociation of any of these α protons can have a detrimental effect on the electrochemical reversibility of the system.

Since acetonitrile is more basic and has a higher dielectric constant than methylene chloride, it is also reasonable to assume that dissociation of the $-^{+\cdot}SC_{\alpha}$-H proton would be more facile in acetonitrile than in methylene chloride. Therefore, the slow deterioration of the immediate product of oxidation of NorDTCO can be circumvented by using methylene chloride as the medium.

Figures 3.8 and 3.9 show the effect of adding the sterically hindered base, 2,6-Di-*tert*-butylpyridine (DTBP), to the NorDTCO solution. Figure 3.8 shows a new anodic peak in the CV of 1.0 mM NorDTCO at lower potential. The new peak grows progressively at the expense of the original anodic peak with the addition of base until the base concentration reaches 0.64 mM. At the same time the cathodic peak diminishes until it is completely suppressed at 0.48 mM base concentration. In Figure 3.9 the base concentration is kept constant at 0.32 mM and the concentration of the analyte is varied from 0.2 to 1.0 mM. The effect of increasing the analyte concentration is a progressive restoration of the original shape of the voltammetric curve. This suggests the involvement of slow acid/base chemistry concurrent with the ET reaction. However, the apparent base-effect might as well have been due to traces of water present in the DTBP.

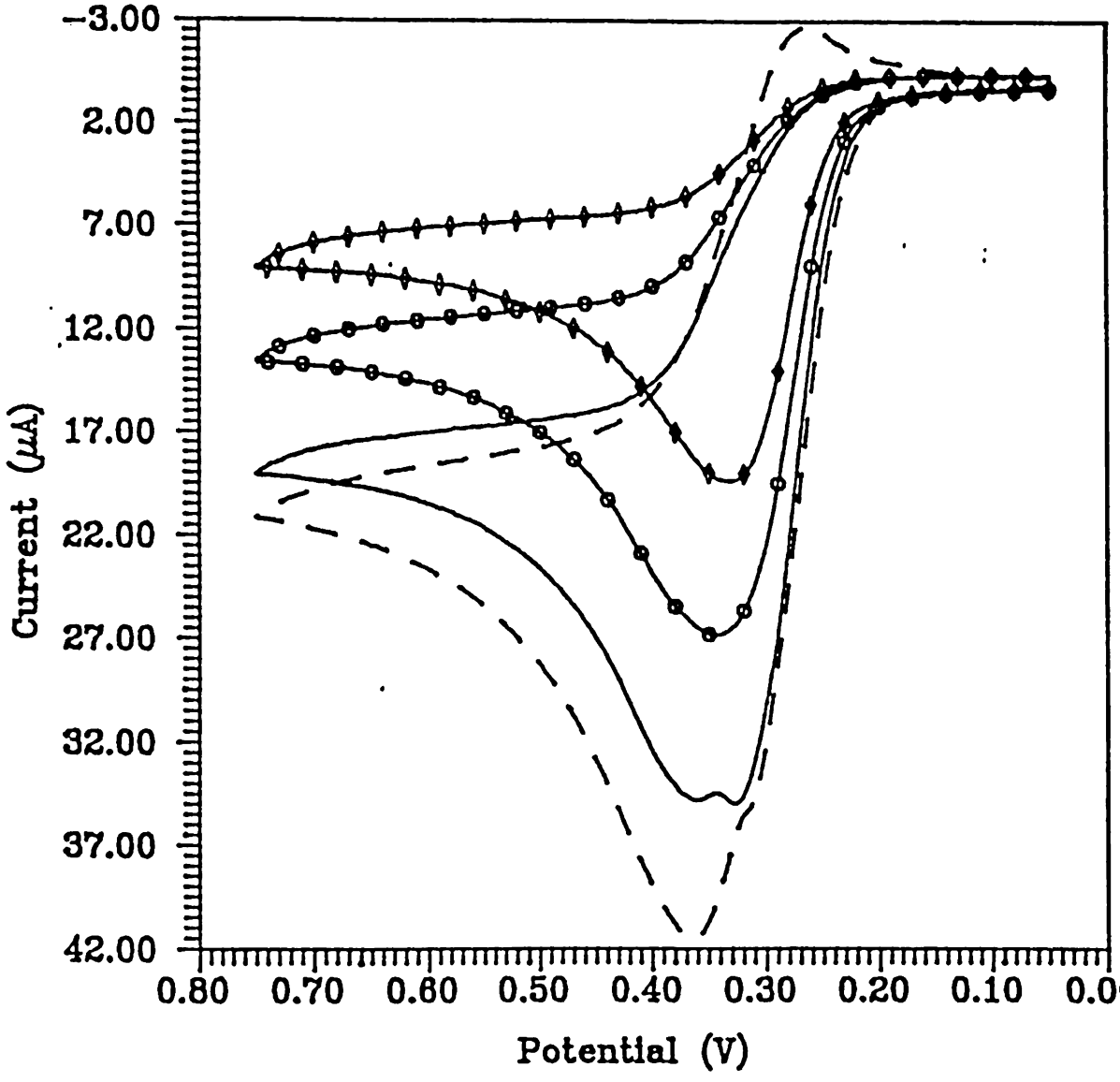

Figure 3.9. Variation of the Cyclic Voltammograms of NorDTCO in CH_3CN with [NorDTCO] at 100 mV s^{-1} Scan Rate,and [DTBP] = 0.32 mM. (◇◇◇) 0.4 mM; (○○○) 0.6 mM; (—) 0.8 mM; (---) 1.0 mM.

The effect of added water. While water can behave both as a base or a nucleophile, the latter seems to be the dominant factor in view of the high reactivity of the

Figure 3.10. Variation of the cyclic voltammograms of 1.0 mM NorDTCO (10 mL) with added water, in acetonitrile at 100 mV s^{-1} scan rate. (A) No water added (B) 5 μL added (C) 10 μL added (D) 15 μL added (E) 20 μL added. (0.1 M in TBAHFP, on glassy carbon vs Ag/(0.1M $AgNO_3$ in CH_3CN)).

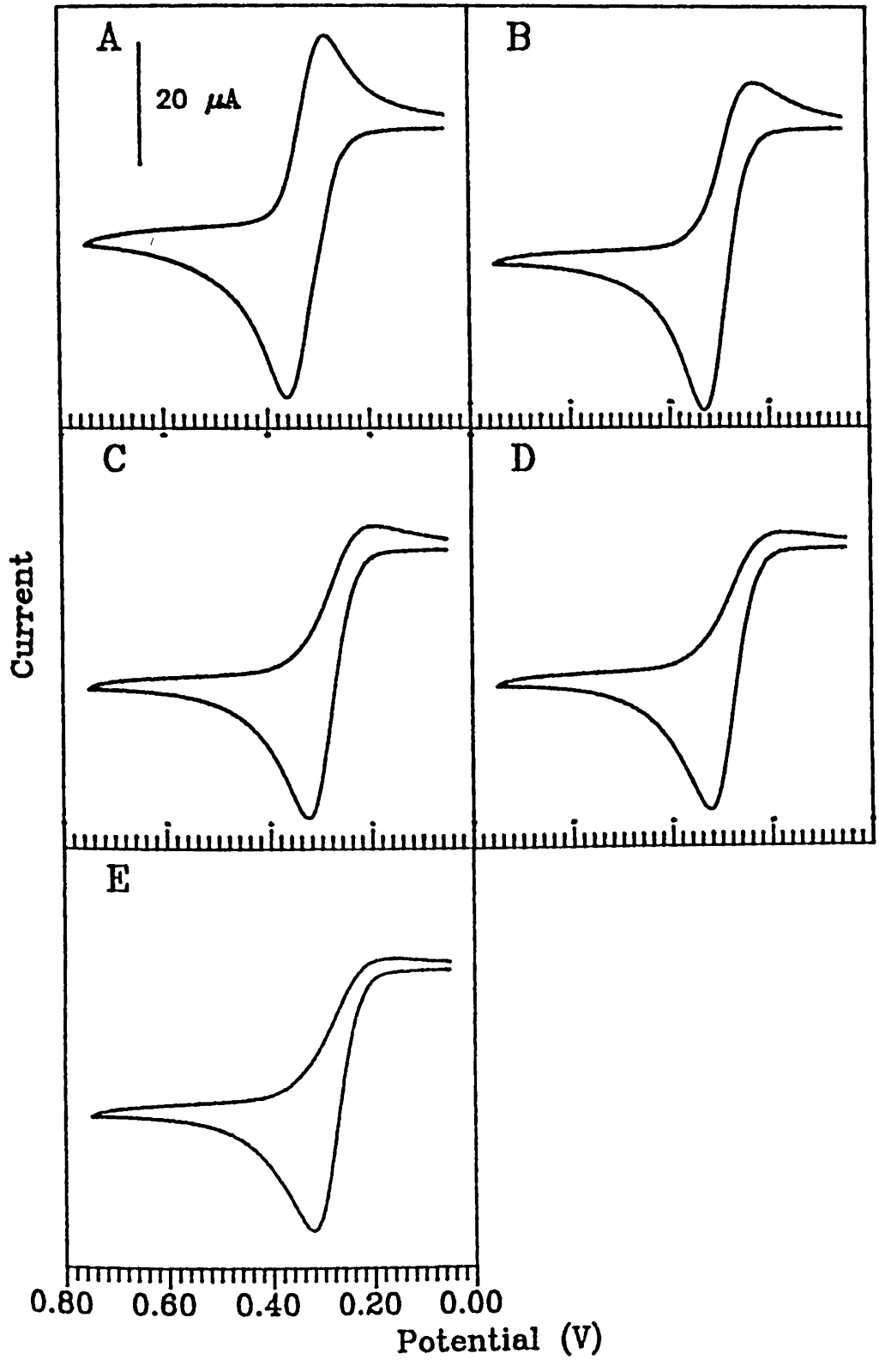
A
20 μA
B
C
D
E
Current
0.80
0.60
0.40
0.20
0.00
Potential (V)

thioether cation radical. Figure 3.10 shows the effect of adding water to 10 mL of ≈ 1.2 mM NorDTCO solution. For the cathodic peaks Figures 3.10 B, C (added water) and Figures 3.8 B, C (added DTBP) are comparable, however, in the case of added water the peak has shifted more negatively. The shift in the anodic peak for added water is relatively more negative than observed for added base. More importantly, there is no split or shoulder in the anodic peak in the case of added water. This suggest a difference in the mechanisms of the base effect and water effect and, therefore, the distortion of the voltammograms resulting from the addition of base may not be merely due to the presence of traces of water in DTBP.

It is also interesting to see that the effect of water on the voltammograms of NorDTCO can be partially reversed by the addition of an acid to the solution. Figure 3.11 shows the effect of adding 48 % aqueous tetrafluoroboric acid solution to 10 mL of ≈ 1.2 mM analyte solution with 20 μL of water already present. Even with the addition of 1 μL of the acid solution the appearance of the anodic wave corresponding to the oxidation of NorDTCO in dry acetonitrile is discernible. This wave then grows into a peak, at exactly the same position as that of the analyte, with further addition of the acid solution. However the regenerated cathodic peak is at a potential significantly more negative relative to the original peak position.

Comparing both the base and water effect, it can be concluded that due to steric hinderance, DTBP can function only as a base abstracting the $-SC_{\alpha}-H$ proton whereas the attack of water takes place directly at the $>S^{\bullet+}$ center. The dissociation

Figure 3.11. Variation of the cyclic voltammograms of 1.0 mM NorDTCO (10 mL + 20 μL water) with added HBF_4 (48 %), in acetonitrile at 100 mV s^{-1} scan rate. (A) No HBF_4 added (B) 1 μL added (C) 3 μL added (D) 5 μL added (E) 10 μL added (F) 20 μL added. (0.1 M in TBAHFP, on glassy carbon vs Ag/(0.1M $AgNO_3$ in CH_3CN)).

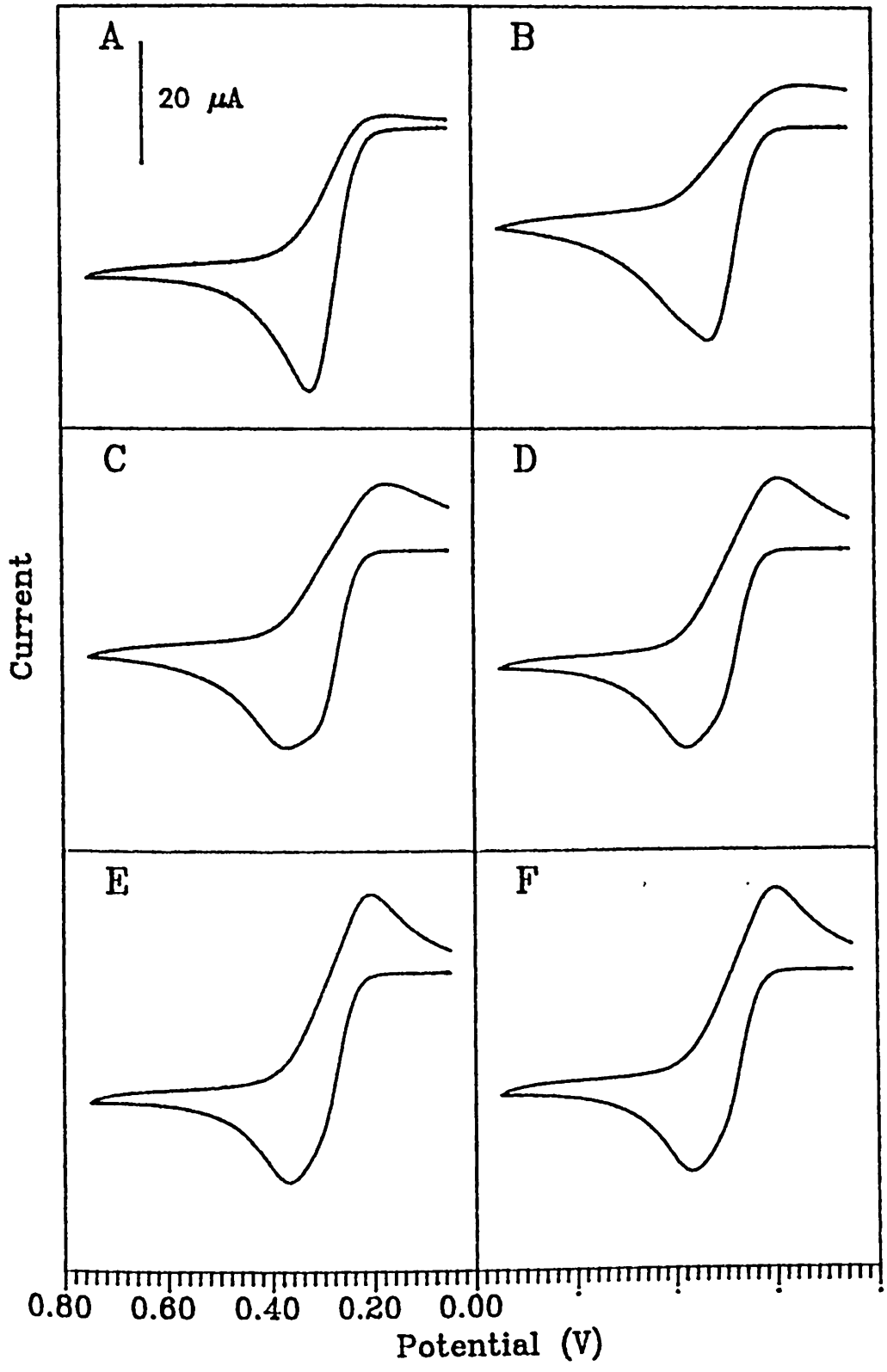
A
20 μA
B
C
D
E
F
Current
0.80
0.60
0.40
0.20
0.00
Potential (V)

of the α-proton which seems not to be as efficient as the nucleophilic attack of water

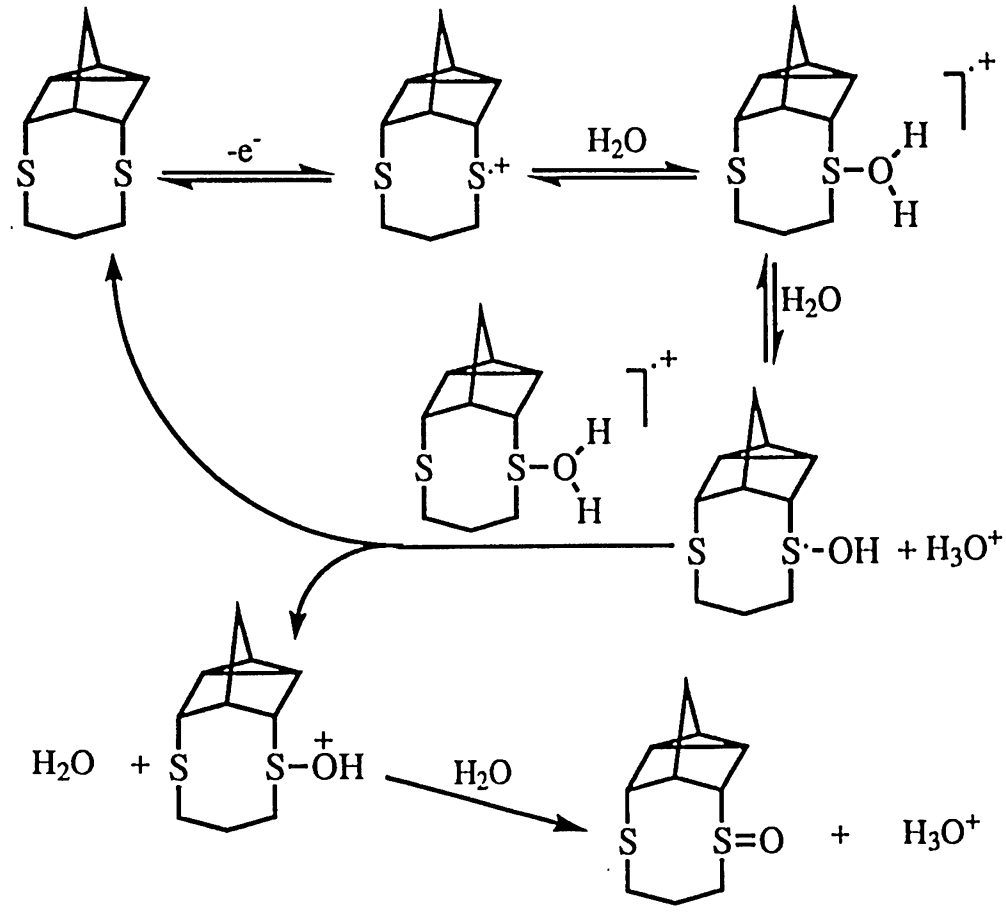

Scheme 3.2. The Mechanism for the Nucleophilic Attack of Water on NorDTCO$^{\cdot+}$.

on >S$^{\cdot+}$, can be reversed by acidifying the medium. The acidic medium might also have a role in suppressing the nucleophilic process by protonating the water molecules even if the acid is itself a 48 % aqueous solution. The mechanism depicted in Scheme 3.2 can be proposed for the nucleophilic reaction of water with the NorDTCO cation radical. As we can see the sulfoxidation process entails the

production of protons. The role of acid in partial re-establishment of the electrochemical reversibility can also be ascribed to the reversal of the sulfoxidation process by adding protons to the solution.

Sulfoxidation reaction as proposed here follows the first ET step, probably due the high reactivity of the cation radical. According to the above mechanistic scheme the second electron rather than being transferred at the electrode, is exchanged homogeneously to regenerate the neutral analyte molecule. An alternative pathway is the disproportionation of two cation radicals to produce a single-sulfur-centered dication and a neutral molecule (Eq. 3.30).

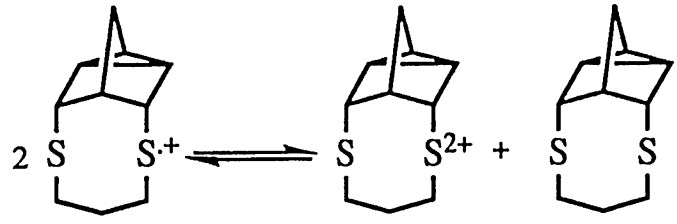

(3.30)

This is also a solution electron transfer process. The dication thus produced will react with a water molecule to give the corresponding sulfoxide as outlined in Eq. 3.31.

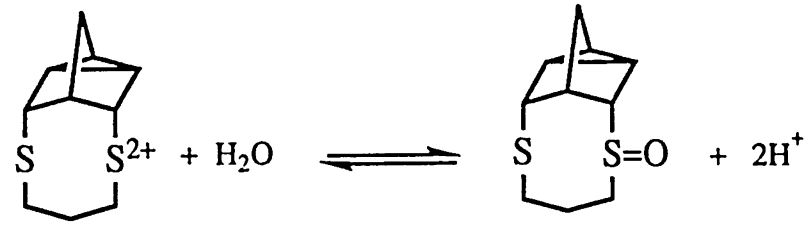

(3.31)

The apparent reversibility at higher concentrations can be rationalized in terms of the acid base chemistry as follows. As mentioned above, the dissociation of -SC_{α}-

H could lead to the decomposition of the molecule following the ET reaction. At the same time the effect of this dissociation process can be a decrease in the local pH around the electrode surface. This effect could become quite significant at higher concentrations which would correspondingly suppress further dissociation of -SC_{α}-H protons, therefore, keeping the molecular skeleton progressively intact with increasing concentration of the dithioether. At lower concentrations, the diffusion of the analyte to the electrode surface may not keep pace with the diffusion of H^+ away from the electrode surface. Therefore, at low concentration the destructive deprotonation process may not be inhibited so effectively as to manifest in the electrochemical reversibility of the system.

Electrochemistry of 2-*endo*-naphtho-6-*endo*(methylthio)bicyclo[2.2.1]heptane. The redox chemistry of compound **1.2** was studied in the same way as that of NorDTCO. This system was designed to investigate the effect of a neighboring π system of electrons on the thermodynamics as well as the kinetics of the anodic oxidation of thioether. Figure 3.12 shows a number of representative voltammograms of **1.2** run in acetonitrile.

According to the literature data the anodic waves at the more positive end of the voltammograms occur in the range of potential where naphthalenes are anodically electroactive[37]. Therefore, the first anodic peak (peak I) can be ascribed to the oxidation of the thioether function of **1.2**.

The occurrence of the anodic peak at such a low potential is indicative of thermodynamic assistance provided by the neighboring π system of electrons. However, on the reverse scan no cathodic peak is observable at any scan rate even when the potential sweep was switched back after the first anodic peak. The maximum scan rate applied to the system is 20 V s^{-1}.

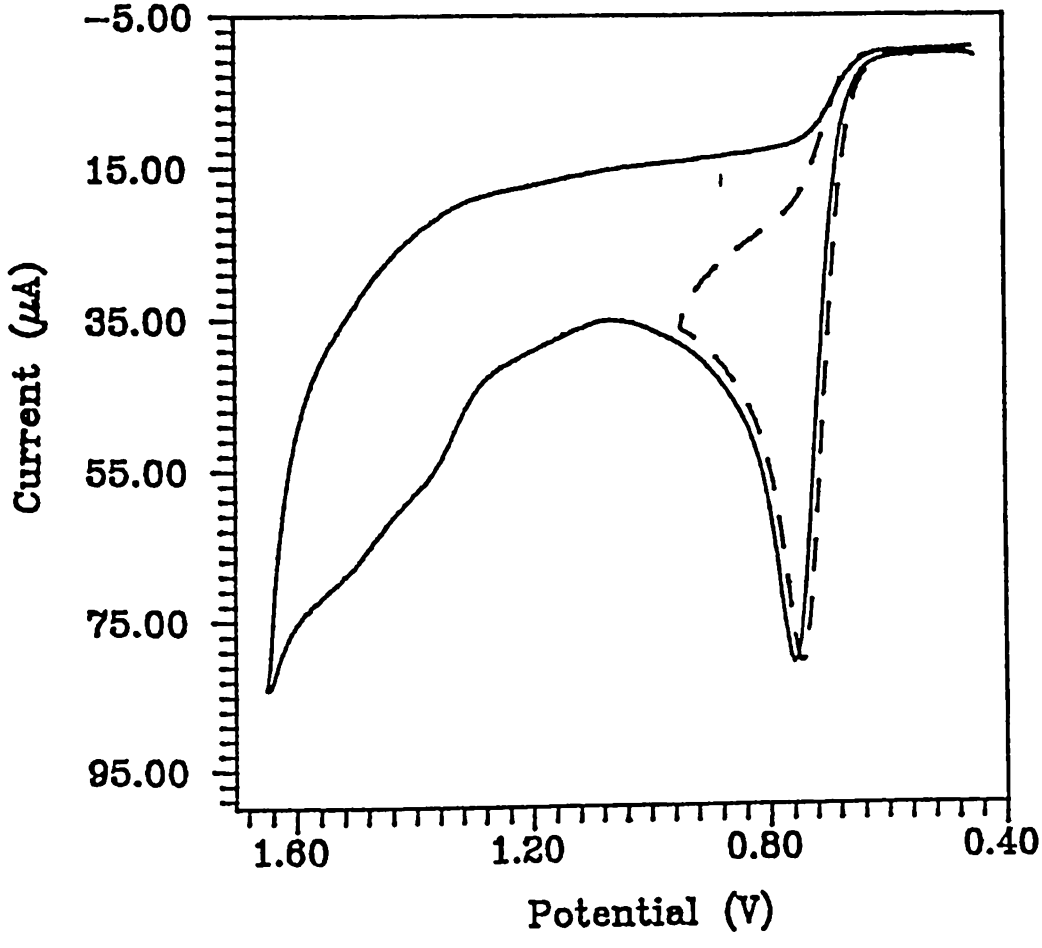

Figure 3.12. CV's of 2-*endo*-naphtho-6-*endo*(methylthio)bicyclo[2.2.1] heptane (1.0 mM) in Acetonitrile at 500 mV s^{-1} Scan Rate.

In order to circumvent the adverse effect of traces of water on the

electrochemistry of **1.2**, the voltammograms were run in a dry box under inert atmosphere. A mixed solvent system was used which was 88 % in CH_2Cl_2, 10% in trifluoroacetic anhydride, and 2% in trifluoroacetic acid. The concentration of supporting electrolyte (TBAHFP) was 0.2 M. Even under such stringent conditions no cathodic peak was recovered (Figure 3.13).

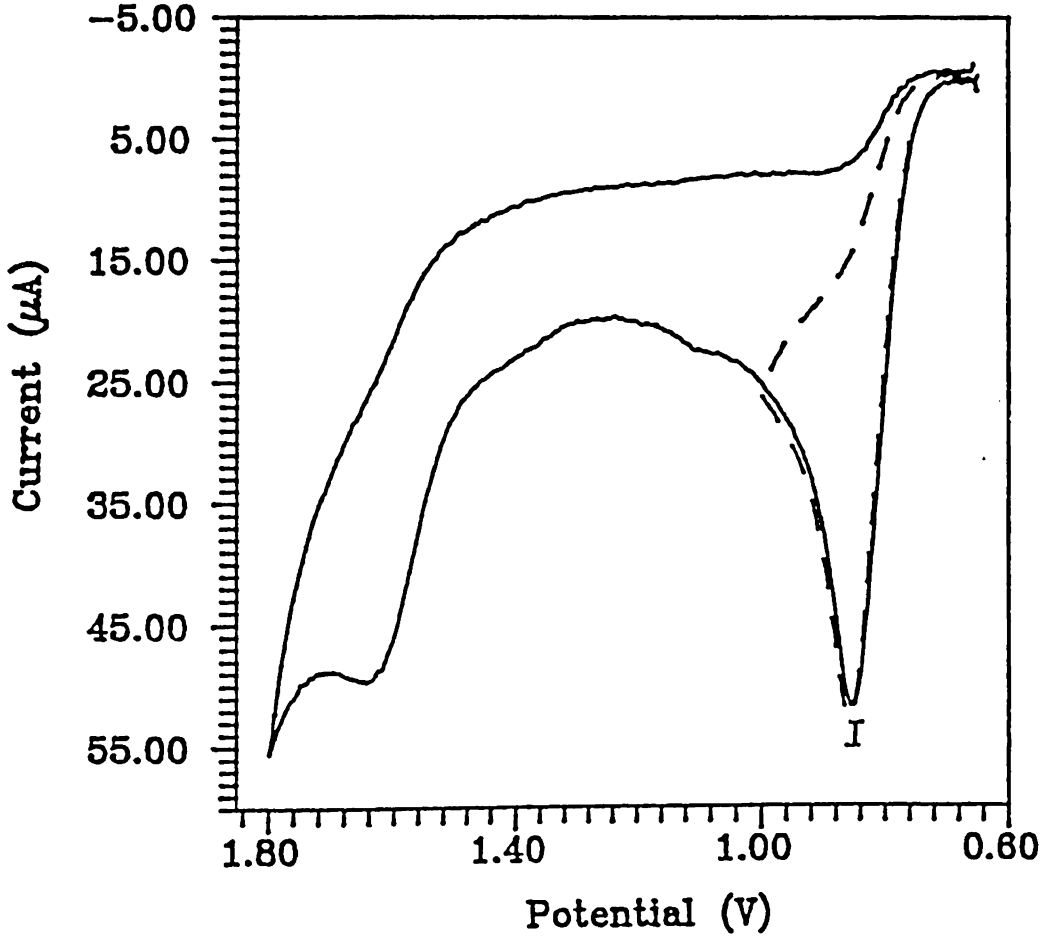

Figure 3.13. CV's of 2-*endo*-naphtho-6-*endo*(methylthio)bicyclo[2.2.1] heptane (1.0 mM) in CH_2Cl_2 which is 10% in Trifluoroacetic anhydride and 2% in Trifluoroacetic acid (Scan Rate = 500 mV s^{-1}).

This could imply that although the presence of a neighboring π system of

electrons can provide a thermodynamic driving force for the oxidation process, it cannot kinetically stabilize the initial oxidation product. This further signifies the role of a neighboring group in providing kinetic stability to the thioether cation radical through electronic interaction. In the case of NorDTCO this interaction could either be in the form of an intermolecular dimerization which presumably dominates the redox chemistry of **1.1** in acetonitrile at lower concentrations as well as lower scan rates or it could be through an intramolecular interaction between the initial oxidation product, the cation radical, and the lone pair of electrons on the neighboring sulfur. Such an intramolecular interaction could very possibly be operative in the redox chemistry of **1.1** in acetonitrile at higher scan rates and possibly in methylene chloride such that it does not lead to an intimate S-S bonding but the two sulfurs maintain an equilibrium bonding-nonbonding environment.

Internal Referencing of the Electrochemical measurements in nonaqueous media. One of the advantages of doing electrochemistry in aqueous medium is the access to reliable and universal reference electrodes. The growing popularity of electrochemical techniques among physical organic and organometallic chemists has rendered non-aqueous electrochemistry commonplace. However, such studies have more often been plagued by the choice of reference electrode. In a large number of cases the SCE has been used as reference but its drawback is the possibility of contamination of the electrolysis solution with water from the reference electrode as well as an unknown

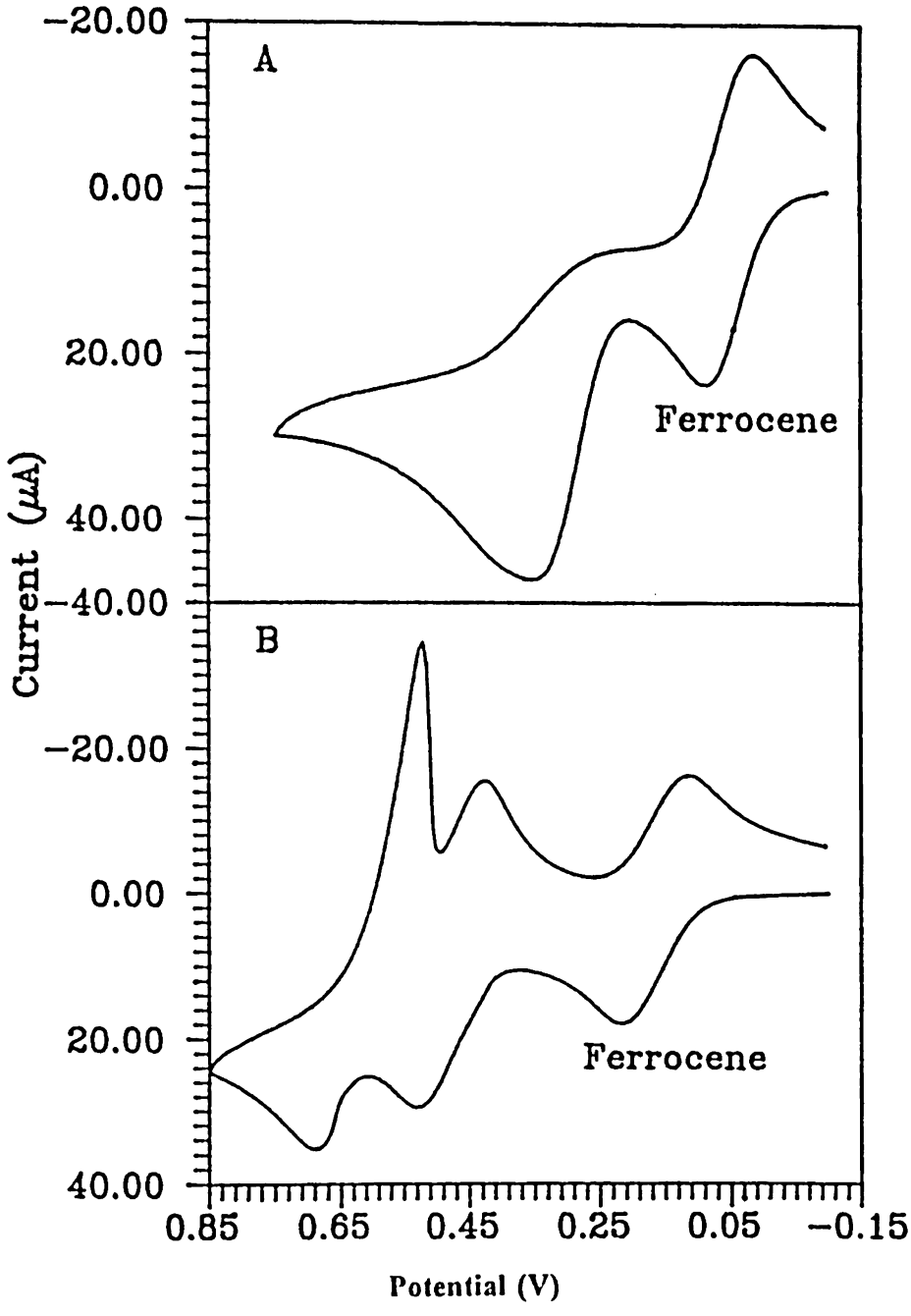

Figure 3.14. Internal referencing of the voltammetric data with ferrocene. (A) (1.0 mM NorDTCO + 5.12 mM DTBP) in CH_3CN (B) 0.8 mM NorDTCO in CH_2Cl_2. (0.1 M in TBAHFP, on glassy carbon vs Ag/(0.1 M $AgNO_3$ in CH_3CN).

or poorly defined liquid junction potential. A wide array of other electrodes have been used and a number of formal potentials are reported in the literature. The potentials of these electrodes cannot be related to each other or sometimes can hardly be reproduced. In order to overcome this problem the use of internal standard has been recommended[38].

The internal standard employed in these studies in both methylene chloride and acetonitrile has been ferrocene. Although in these studies Ag/0.1M $AgNO_3/CH_3CN$ has been used exclusively as a reference electrode, the measurements have always been cross-checked with ferrocene. Ferrocene was added to the analyte solution at the end of each experiment. No shift in the peak potentials relative to the reference electrode or a distortion of cyclic voltammogram of Fc^+/Fc couple has been observed. This also suggests the stability and reliability of the reference electrode used in these studies. Figure 3.14 shows some representative voltammograms of the analyte solutions spiked with ferrocene.

CHAPTER 4

ELECTROCHEMICAL STUDY OF REDOX ASSOCIATED CONFORMATIONAL CHANGES IN THE $[Cu^{II}(TTCN)_2]$ COMPLEX

Introduction

Copper complexes with sulfur containing ligands have been implicated in a number of important chemical and physiological systems: as synergistic deactivators in plastics, hydrocarbon oils, and rubbers; as potential models for copper binding sites in blue copper proteins; and as metallotherapeuticals of demonstrated anticancer, antibacterial, or antiviral activity[1]. In addition, their diverse structural pattern and coordination mode has stimulated interest in their structural chemistry.

In this chapter a detailed investigation of the electron transfer properties of copper-thioether systems will be presented. Also one of the major objectives of this chapter is to show how the structural constraints in the ligand conformation affect the electronic and structural properties of the metal ion in a complex molecule. The ligand of interest in this study is the tridentate macrocyclic thioether, 1,4,7-trithiacyclononane (TTCN).

The remarkable feature of TTCN is its small size. When the lengths of intermethylene chains between donor atoms in tridentate macrocyclic ligands are not sufficiently long, the ligand tends to coordinate facially because all three donor atoms are compelled to orient such as to coordinate to a single central metal ion. This kind of orientation enhances further the coordination capability of the ligand.

The x-ray crystallographic data of TTCN have shown the molecule to adopt a [3 3 3] conformation with all three sulfur atoms *endodentate*[2]. Such a conformation preorganizes the ligand for facial coordination with metal atoms. Both condensed and gas phase studies have shown that the molecule retains this structure[2,3]. This has been further supported by the cyclic voltammetric data of a number of metal complexes with TTCN[4].

The propensity of the TTCN macrocycle to retain the endodentate [3 3 3] conformation is also evident from the fact that, with the exception of one or two cases, the metal atom receives more than one bite from the same TTCN macrocycle. In $[Au^{I}(TTCN)_2]$ one of the TTCN units is shown to act as a monodentate ligand and this has been ascribed to a compromise between two extreme stereochemical tendencies at the metal center i.e. linear on the part of Au(I) and tetrahedral on the part of the ligand[5].

In view of the presumed structural rigidity of TTCN , $[Cu^{II/I}(TTCN)_2]$ was believed until recently to be an electrochemically reversible system[6]. However, Cu(II) complexes are structurally dominated by octahedral geometries whereas Cu(I) complexes are predominantly tetrahedral. Clarkson *et al.* in 1989 reported the crystal structure of a binuclear Cu(I)-TTCN complex ($[Cu^{I}_2(TTCN)_3]$) in which two Cu(I) centers, each one capped by a terminal TTCN molecule, are bridged by a central TTCN molecule showing that the bridging TTCN molecule no longer retains its endodentate [3 3 3] conformation[7]. The conformation adopted by the monodentate

TTCN ring in the Au(I) complex and the bridging TTCN ligand in the Cu(I) complex is the same [1 2 2 2 2] conformation (with a local approximate $\underline{C}_2$ axis of symmetry).

Despite the significantly different coordination geometries of Cu(II) and Cu(I) cations, a number of copper proteins involved in electron transport in biological systems accommodate these differences. This has inspired research into characterization of the metal center. The facile electron transfer in these proteins has been accomplished by (i) geometrical preorganization of the metal binding site in a near-entatic state and (ii) by an exquisite selection of the ligand system about the metal center such that both the oxidized and reduced states will be stabilized[8]. The disputed involvement of the thioether ligand from methionine in the electron transfer process of blue copper proteins[9] has prompted a high level of interest in the synthesis of model compounds and in the kinetics and mechanisms of the redox reactions of these compounds[10]. It is almost impossible for copper proteins to be mimicked completely in a single model compound, however, the rigidity of the inner sphere can be achieved by using macrocyclic ligands of appropriate ring size.

Although the homoleptic thioether complexes are clearly not models for the blue copper proteins, their redox chemistry has provided very useful information about the electron transfer reactions involving copper-thioether coordination[11]. The macrocyclic effect has played the most important role in coordinating crown thioethers despite their poor coordination capability[12] to a wide variety of metal atoms, sometimes with very unusual oxidation states[13,14].

In view of the stereochemical preferences of Cu(II) and Cu(I) the reversibility of electron transfer can be improved by restricting the flexibility of the macrocycles but at the same time the macrocycle should also be amenable to coordination with both Cu(II) and Cu(I).

Discussion

Structural Properties of Copper-TTCN Complexes.

$[Cu^{II}(TTCN)_2]$ and the Jahn-Teller Effect. The d^9 configuration of Cu(II) has powerful implications on its coordination geometry due to the Jahn-Teller effect. Generally the coordination sphere acquires a greater degree of rigidity upon engaging the *d* orbital in bonding such that transition metals like Ni(II) are used in template syntheses. However, the Jahn-Teller effect confers greater stereochemical plasticity to the coordination sphere of Cu(II) which in turn allows the ligand system to control significantly the structural characteristics of the metal center[15].

The earlier studies in our labs have shown that $[Cu^{II}(TTCN)_2]$ shows minimal Jahn-Teller distortion (Cu-S range over 0.04 Å)[16]. The sum of Cu-S bond lengths in $[Cu^{II}(TTCN)_2]$ compare closely with that of $[Cu^{II}(HTCOD)]$. The latter shows a clear-cut elongation[17].

The possibility of dynamic Jahn-Teller distortion has been supported by the low temperature EPR studies[18,19]. It has not been possible to obtain decisive evidence for the observable Jahn-Teller distortion in the $[Cu^{II}(TTCN)_2]$ chromophore through

temperature variation [19]. We, therefore, decided to try to enhance the possibility of Jahn-Teller distortion in the chromophore by changing the lattice parameters. The cation was crystallized with a chiral counter anion, (+)-3-bromocamphor-10-sulfonate. Neither this nor collection of the crystallographic data at liquid nitrogen temperature revealed any significant variation in Cu-S distances which could indicate a recognizable Jahn-Teller distortion.

The Jahn-Teller theorem requires that any nonlinear system with an electronically degenerate ground state undergo a distortion of its nuclear framework in order to remove the degeneracy[20-22]. It is obvious from the crystallographic data (Tables A1.3) that the intracyclic angles, S-Cu-S, are smaller than 90°, whereas the corresponding intercyclic angles are greater than 90°. Also S-Cu-S angles for the S atoms at the inversion points are smaller than 180°. This indicates that the smaller size of the TTCN ring already has a compressing effect on the octahedral coordination geometry of the chromophore. The overall symmetry of $[Cu^{II}(TTCN)_2]$ has been determined as C_i by Wijnands who has carried out an extensive study of the Jahn-Teller effect in crystals of hexacoordinated Cu(II) complexes[23]. So it is possible that such a low overall symmetry and the compression of the core chromophore more than compensates for the Jahn-Teller stabilization energy.

It is interesting to note that the crystal structure of the chromophore with the chiral counter ion at low temperature (Figure 4.1 A,B) is highly disordered. Another interesting feature of the crystal structure is the presence of three anions per molecule.

Figure 4.1. Crystal structure of $[Cu(TTCN)_2](CamphSO_3)_3.H_3O.3CH_2Cl_2$. The disordered cation ($[Cu^{II}(TTCN)_2]$) (A) ORTEP drawing (B) PLUTO drawing (C) The anion assembly ($(CamphSO_3)_3$) (D) The disordered anion ($CamphSO_3$).

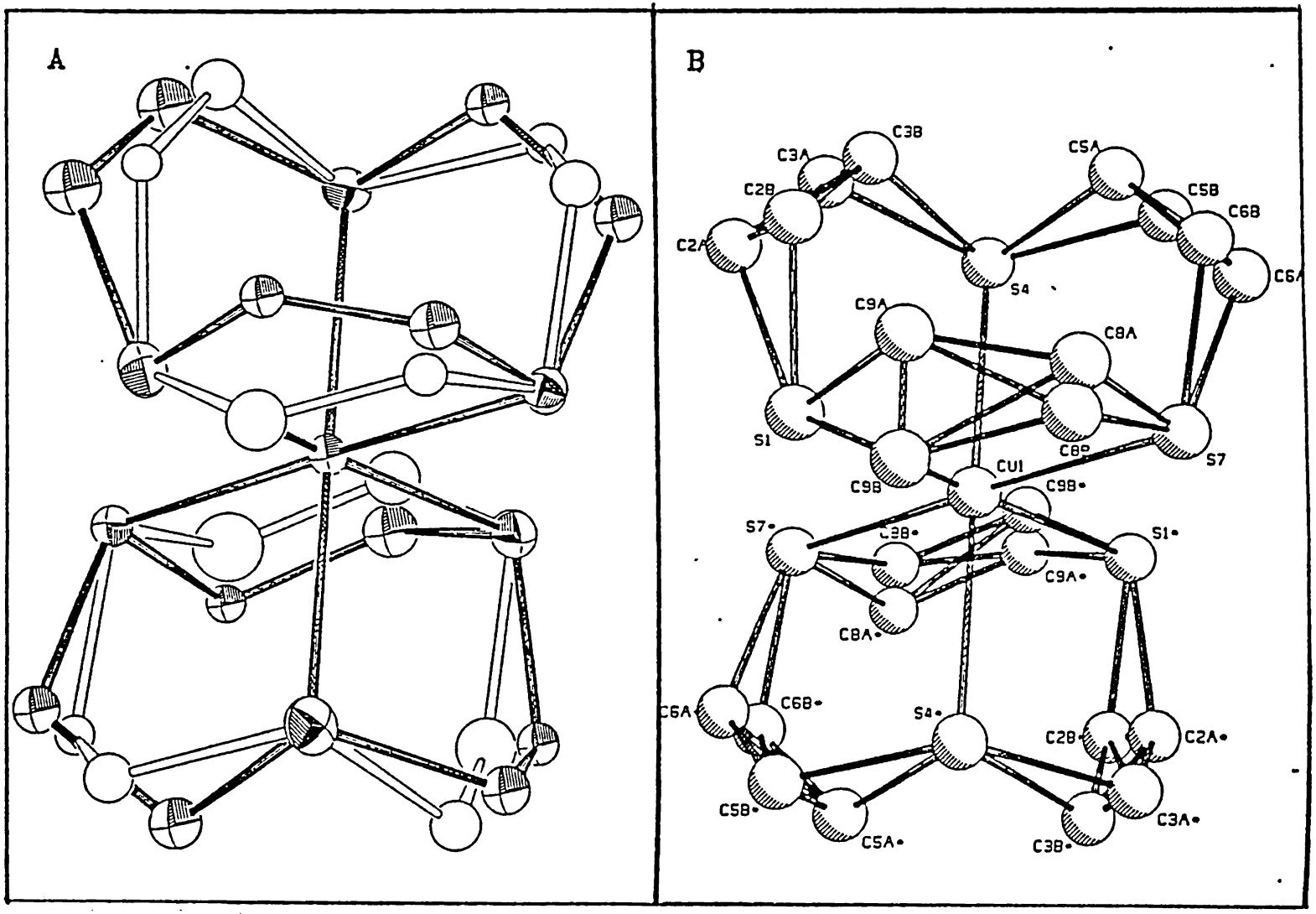
A
B
C3B
C3A
C5A
C2B
C5B
C6B
C2A
C6A
S4
C9A
C8A
S1
C8B
S7
C9B
CU1
C9B•
S7•
C8B•
S1•
C9A•
C8A•
C6A
C6B•
S4•
C2B•
C2A•
C5B•
C3A•
C5A•
C3B•

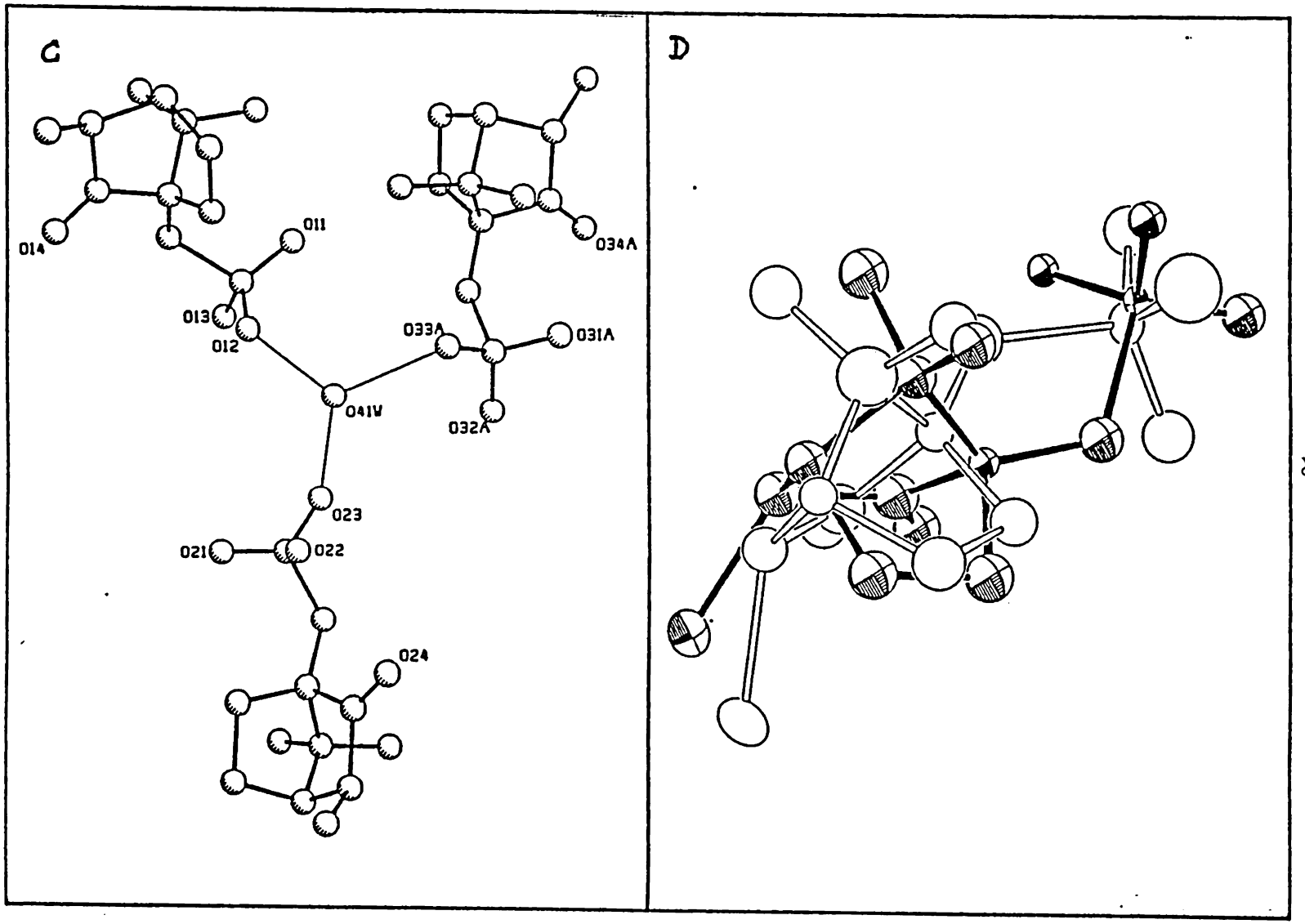
C
014
011
013
012
033A
031A
034A
041W
032A
023
021
022
024
D

All the three anions orient themselves almost equidistant about an H_3O^+ ion found in the crystal lattice (Figure 4.1 C). One of the anions also shows a high degree of disorder (Figure 4.1 D).

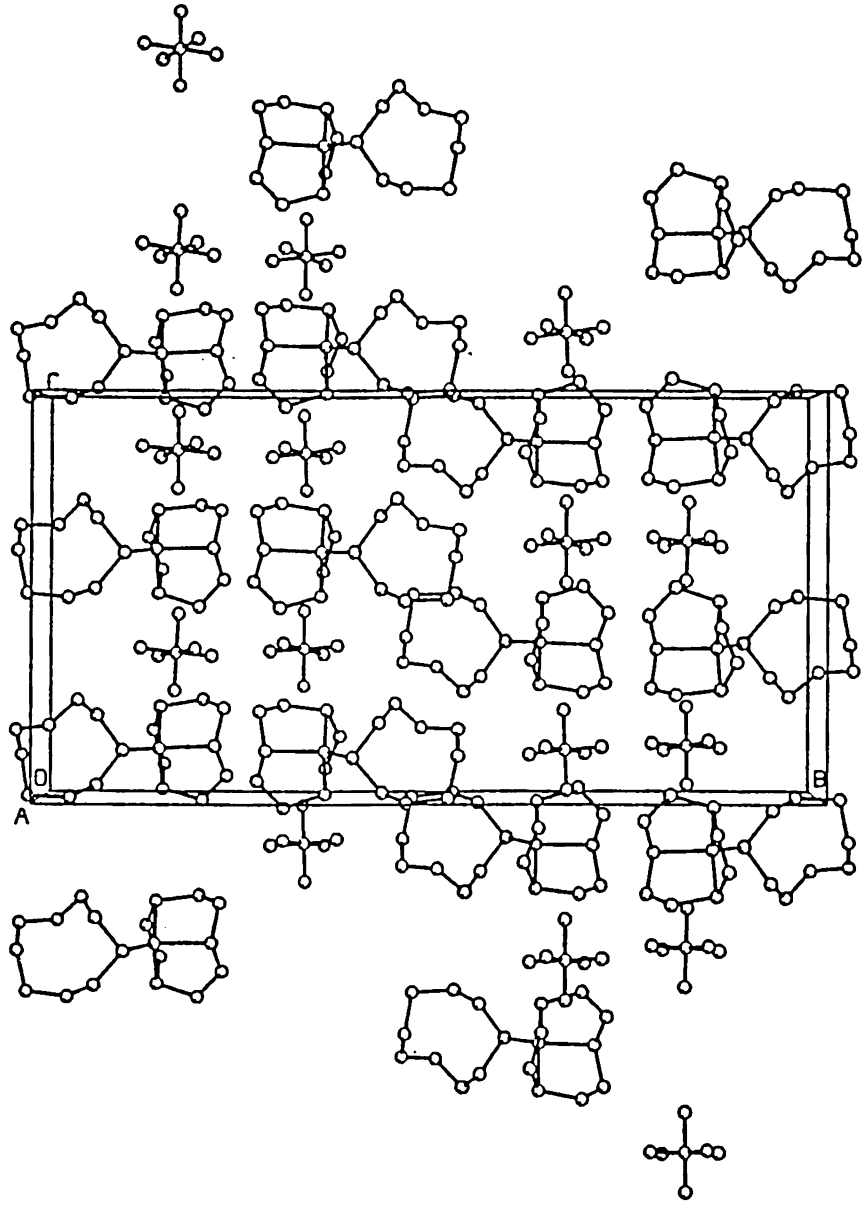

Figure 4.2. Packing of the Unit Cell of $[Cu(TTCN)_2]PF_6$.

$[Cu^{I}(TTCN)_2]$. $[Cu(TTCN)_2](PF_6)$ crystallizes in space group $P2_1/n$ of the monoclinic system with two formula units per unit cell. Packing of the unit cell is shown in Figure 4.2. The two molecular units in the unit cell differ from each other mainly in the ligation of the monodentate TTCN ligand although the conformation of these ligands is the same (Figure 4.3).

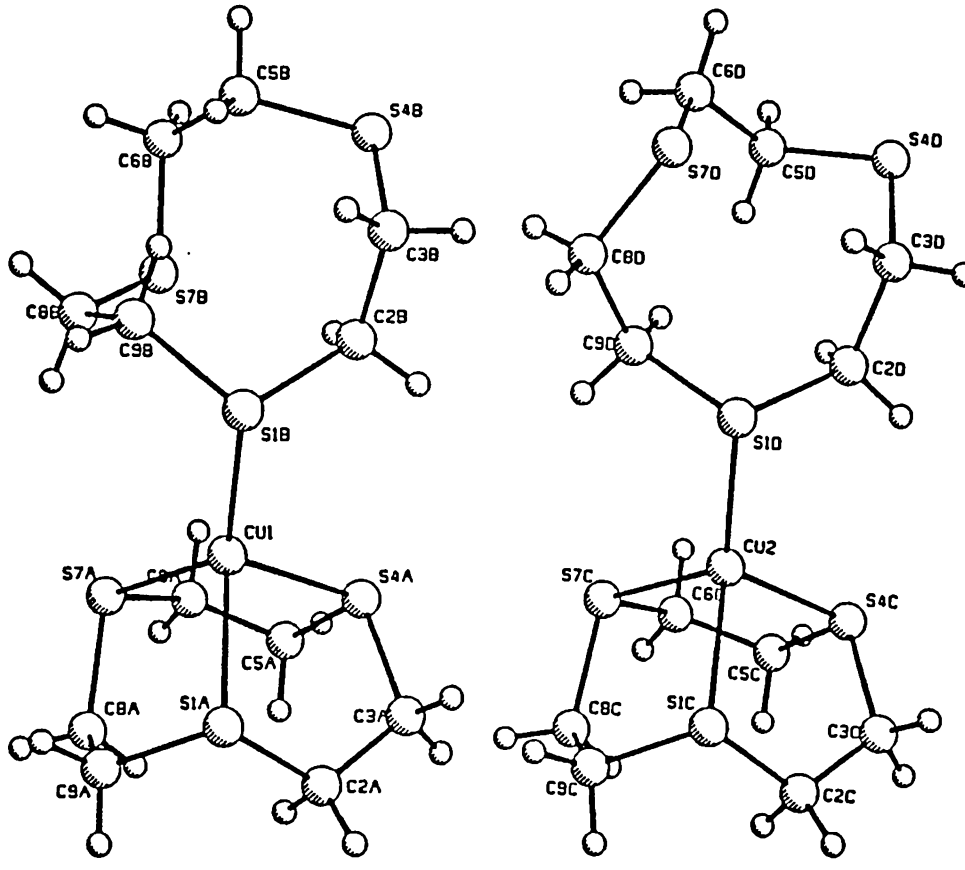

Figure 4.3. Structure of the two Molecular Units of $[Cu^{I}(TTCN)_2]$ Cation (PLUTO Drawing).

The conformation of the monodentate ligand is substantially different from the

[1 2 2 2 2] conformation observed in the monodentate ring in $[Au(TTCN)_2]PF_6$[5], the bridging ring in $[Cu_2(TTCN)_3](BF_4)_2.H_2O$ and the commonly observed endodentate [3 3 3] conformation. It appears that TTCN is a more flexible ligand than previously suggested but the relative importance of conformational constraints of the ligand in determining coordination geometry in metal complexes has not as yet been fully clarified. The coordination about Cu(I) in both the molecular units corresponds to a distorted tetrahedral geometry (Table A2.4).

In any case it is obvious from the torsion angles of the crystallographic data and Figure 4.3 that the uncoordinated sulfurs in the singly coordinated macrocycle are directed outward relative to the coordinated sulfur and are thus prone to attack by another appropriate metal ion. In order to effect the chelation, the macrocycle has to undergo significant conformational changes which can jeopardize the bonding between the coordinated sulfur of the same ring and Cu(I). Further, the free TTCN macrocycle apparently prefers the endodentate conformation. Thus the coordination of the two dissociated sulfurs to another transition metal ion presumably forces the third and Cu(I) coordinated sulfur to move towards an endodentate [3 3 3] conformation regardless of whether there is a strong interaction between this sulfur and the newly coordinated metal ion. This effect was seen when $[Cu(TTCN)_2]PF_6$ was reacted with nickel (II), cobalt (II), and palladium (II), yielding $[Ni^{II}(TTCN)_2]$, $[Co^{II}(TTCN)_2]$, and $[Pd^{II}(TTCN)_2]$ substitution products respectively[16,24] rather than the expected trinuclear complexes. This was confirmed by the electronic spectra of the reaction products and

the crystallaographic studies of the Co(II) substitution product. Moreover, the instability of the trinuclear complexes can also be ascribed to non-bonded repulsive interactions.

Electrochemistry of $[Cu^{II/I}(TTCN)_2]$ system at pH 3. An electron transfer (ET) reaction would, in principle, be expected to trigger structural changes in the reactant molecule. There has been a common tendency to conclude from the nearly reversible voltammetric behavior that there must be little or no structural change following the ET reaction. As a matter of fact the observation of a reversible wave under a certain set of conditions could mean that the structural changes accompanying ET are chemically reversible and fast on the time scale of the experiment. In the present work we have shown electrochemically that TTCN does undergo conformational change to adjust to the geometrical requirements of the oxidation state of the central metal atom, therefore, hampering the reversibility of the ET process. The conformation of the monodentate ligand can even be utilized for further coordination with another suitable metal ion to the available sulfur atoms for a short period of time.

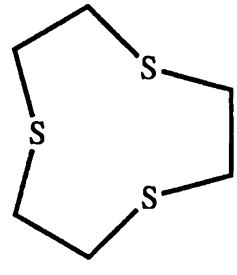

L: TTCN

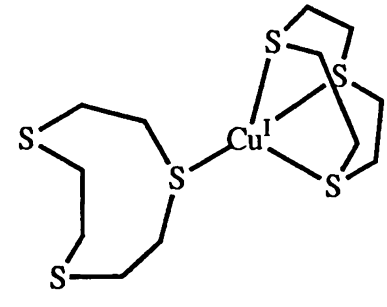

ML; $[Cu^{I}(TTCN)_2]$

Figure 4.4. Variation in the cyclic voltammograms of 1.0 mM $[Cu^{II}(TTCN)_2]$ as a function of free Cu(II) concentration and scan rate (ν) (0.1 M in $NaBF_4$, pH 3, on glassy carbon vs Ag/(AgCl Satd. NaCl)).

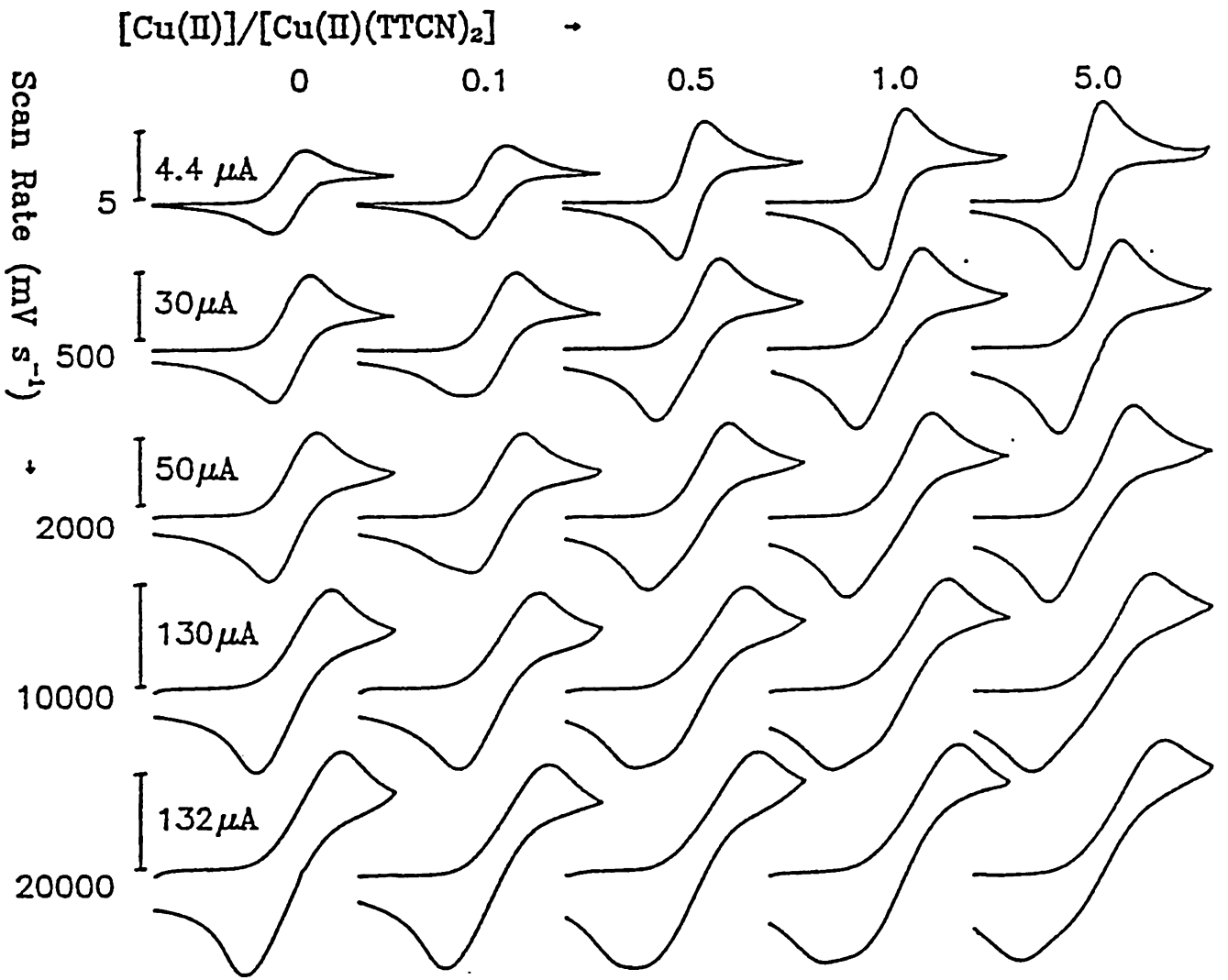
[Cu(II)]/[Cu(II)(TTCN)2] →
0
0.1
0.5
1.0
5.0
Scan Rate (mV s-1) →
5
500
2000
10000
20000
4.4 μA
30μA
50μA
130μA
132μA

Figure 4.4 summarizes the cyclic voltammetric (CV) behavior of the title system at various scan rates (ν). The CV data show only one well defined electron transfer step at all scan rates examined up to 135 V s^{-1}. The CV curves at ν around 10 mV s^{-1} or less are practically reversible with virtually identical formal potentials ($E^{\circ\prime}$) for both the reduction of $[Cu^{II}(TTCN)_2]$ as well as oxidation of $[Cu^{I}(TTCN)_2]$. With increasing ν, however, the peak separation (ΔE) increases due to the finite electron transfer rate and/or increased solution resistance. The invariance of the shape of the CVs indicates consistent mechanistic characteristics of the electron transfer process over the range of experimental conditions employed, especially the time scale of the experiment.

Both the reduction of $[Cu^{II}(TTCN)_2]$ as well as the oxidation of $[Cu^{I}(TTCN)_2]$ at the RDE at a scan rate of 5 mV s^{-1} and a rotation speed (f) of 100 rpm produced the typical sigmoidal i-E curves (Figure 4.5). Levich plots (i_ℓ vs $\omega^{1/2}$, where $\omega = 2\pi f/60$) afforded straight lines for both cathodic and anodic processes up to 3600 rpm suggesting that the electron transfer is a mass transfer controlled process. A diffusion coefficient of 5.3 x 10^{-6} cm^2 s^{-1} was estimated for both $[Cu^{II}(TTCN)_2]$ and $[Cu^{I}(TTCN)_2]$.

The number of electrons (n) involved in this redox process was calculated to be unity from the exhaustive electrolysis of 0.026 mmols of $[Cu^{II}(TTCN)_2]$ at a constant potential of 200 mV. The electrolysis was carried out at a glassy carbon RDE at 1600 rpm until the current decayed to < 0.5% of the initial current.

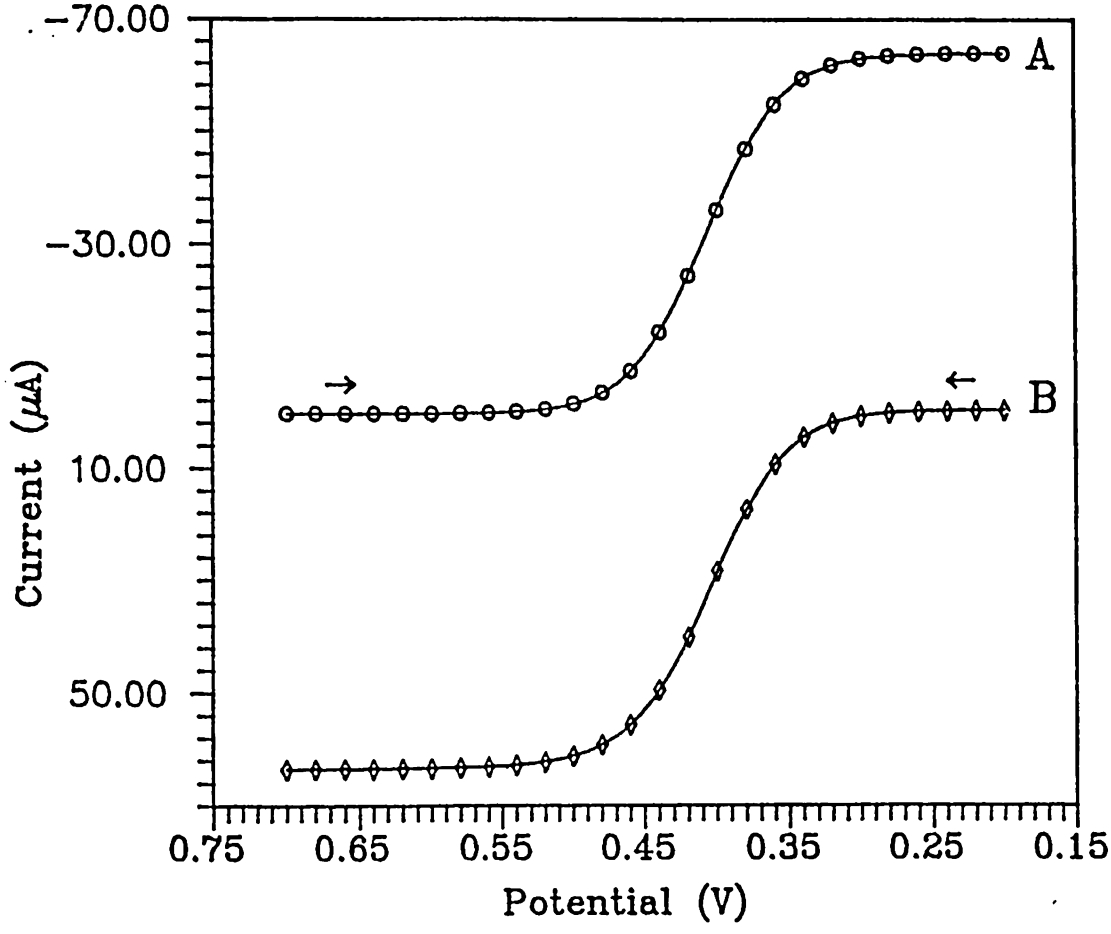

Figure 4.5. RDE Voltammograms at 100 rpm (A) 1.0 mM $[Cu^{II}(TTCN)_2]$ (B) 1.0 mM $[Cu^{I}(TTCN)_2]$

The above electrochemical behavior can be accounted for in terms of a quasi-reversible one-electron process corresponding to the following redox reaction:

$$[Cu^{II}L_2] + e^- \rightleftharpoons [Cu^{I}L_2] \qquad (4.1)$$

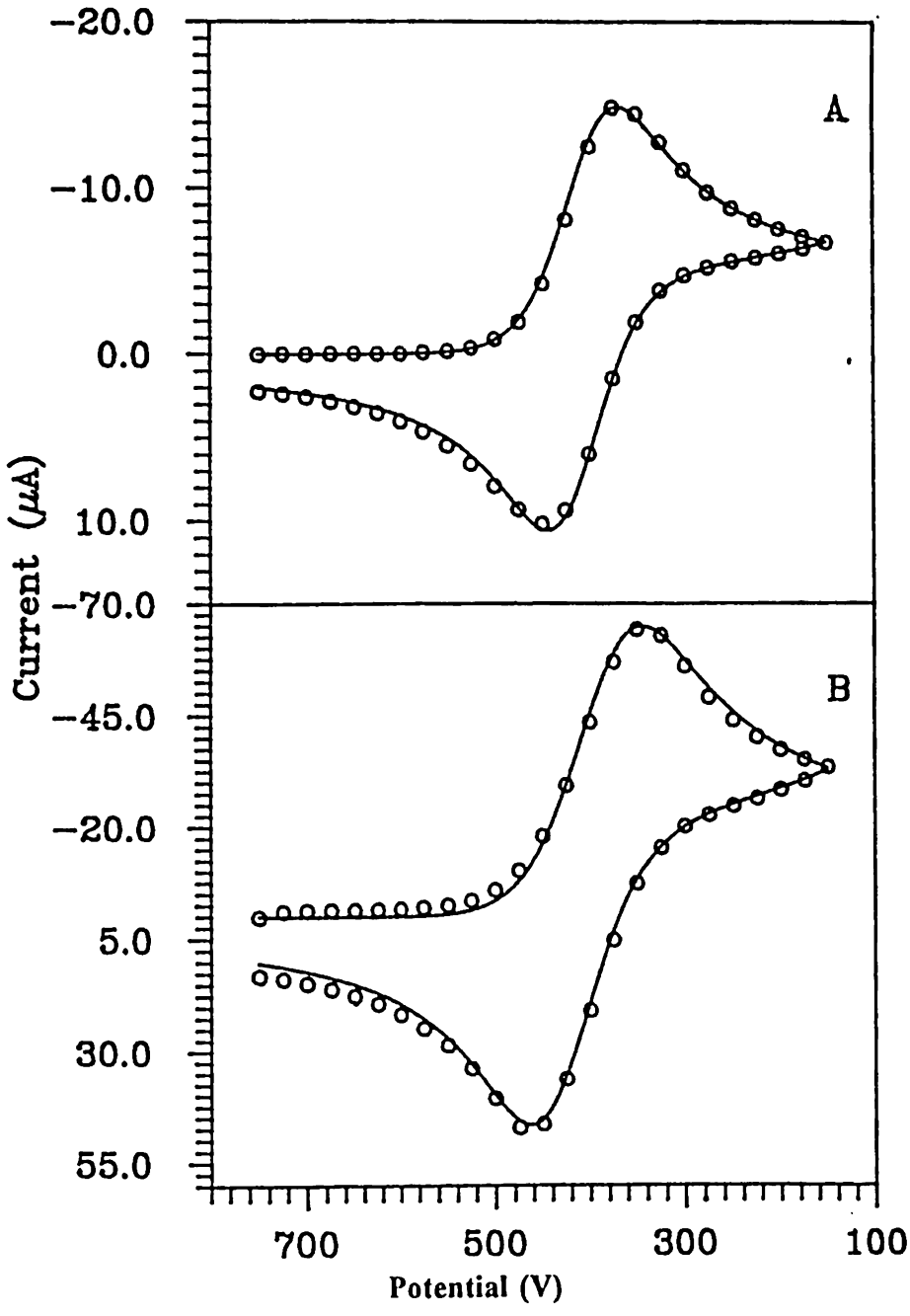

Figure 4.6. Digitally Simulated Voltammograms of 1.0 mM $[Cu^{II}(TTCN)_2]$: Experimental (ooo); Theoretical (—). (A) at 100 mV s^{-1}; (B) at 1,500 mV s^{-1}. independent analysis of 10 voltammograms at ν = 5 - 1000 mV s^{-1} resulted in $E^{\circ'}_1$

The cyclic voltammetric data are indicative of almost strict adherence to a simple one electron transfer process as indicated by the close fit of the experimental and digitally simulated voltammograms of Figure 4.6. Digital simulation of the voltammetric data for the kinetic and thermodynamic parameters of the redox process corresponding to Eq. 4.1 was carried out by using a curve-fitting method[25]. The formal redox potential ($E^{\circ\prime}_1$), the heterogeneous rate constant (K_{sh}), and the cathodic electron transfer coefficient (α_1) were adjusted to give the best fit to the voltammograms. The = 0.408 ± 0.002 V, K_{sh} = 0.0134 ± 0.001 cm s^{-1} and α_1 = 0.45 ± 0.04. The refined curves calculated with these values, however failed to reproduce the experimental voltammgrams run at scan rates higher than 1 V s^{-1}. A steady increase in the value of K_{sh} was observed with increasing scan rate for $2 < \nu < 10$ V s^{-1} above which a constant value of 2.3 x 10^{-2} cm s^{-1} was obtained from the digital simulation. This behavior is indicative of a transition between two different rate limiting processes.

It will be necessary to account for the changes in coordination geometry associated with ET. If the redox state linked conformational changes are rapid and/or if the resulting species have similar redox potentials to those of the primary redox products, then it may not be possible to detect these conformational equilibria. Several additional electrochemical experiments were conducted to clarify this point. The kinetic parameters obtained for the electron transfer step from double step chronocoulometric experiments[26] over a range of 5 ms $< \tau \leq$ 100 ms are in close agreement with those obtained from the CV data. However, the data obtained at τ =

5 ms are indicative of a follow-up chemical step with a homogeneous first order rate constant of 470 s^{-1}.

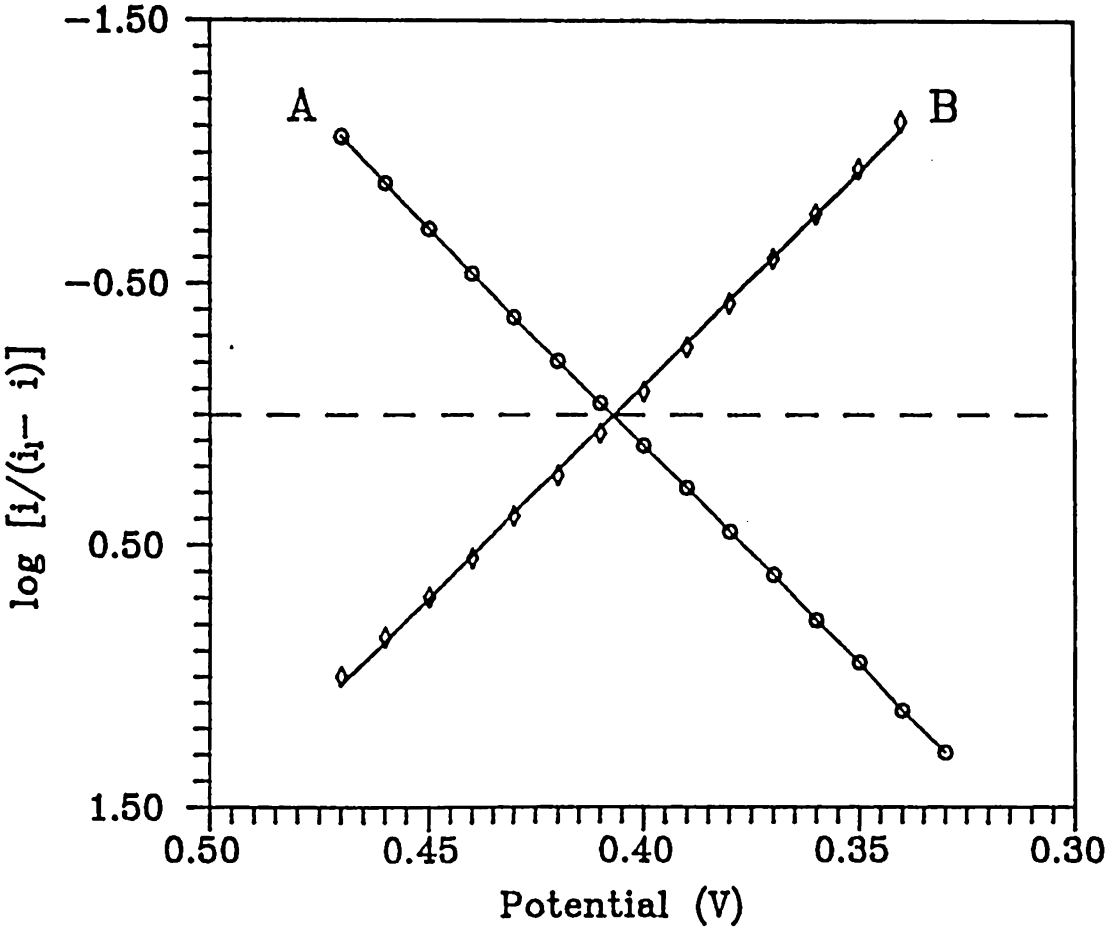

Figure 4.7. log Plots of the RDE Voltammograms at 100 rpm: (A) 1.0 mM $[Cu^{II}(TTCN)_2]$; (B) 1.0 mM $[Cu^{I}(TTCN)_2]$.

The i - E data for the RDE at 100 rpm plotted as $\log(i/i_\ell - i)$ vs electrode potential for both the oxidation of $[Cu^{I}(TTCN)_2]$ and reduction of $[Cu^{II}(TTCN)_2]$ yielded straight lines with a theoretical Nernst slope of 59 mV and a half-wave potential of 408 mV (Figure 4.7), in exact agreement with cyclic voltammetric data.

However, when the rotation speed is increased from 100 rpm up to 1600 rpm, a decrease of 10 mV is observed in the formal potential corresponding to the reduction of $[Cu^{II}(TTCN)_2]$, while an increase of essentially the same amount is observed in the oxidation of $[Cu^{I}(TTCN)_2]$, amounting to a total difference in the formal potentials of 20 mV. The slopes of the log plots corresponding to different rotation speeds remain essentially constant with a slight increase at high rotation speeds. While this difference may be due to the finite electron transfer rate, it is more likely attributable to the fact that the one electron oxidation and the corresponding reduction do not involve the same species.

It is unlikely that uncompensated resistance in the aqueous medium employed will affect determination of the heterogeneous rate constant. The effect of the uncompensated solution resistance would be a decreased k_{sh} at higher ν whereas the results from CV data, RDE, and chronocoulometry all indicate the contrary. Similarly in the presence of significant uncompensated resistance k_{sh} will decrease with increasing concentration. The thermodynamic and kinetic parameters calculated from the digital simulation for the $[Cu^{II/I}(TTCN)_2]$ did not depend on the concentration.

The negative shift in the formal potential corresponding to the reduction of $[Cu^{II}(TTCN)_2]$, with increasing rotation speed is indicative of the generation of an intermediate species (possibly octahedral Cu(I) which is less stable than the final product demonstrated to be tetrahedral Cu(I). Similarly the positive shift in the formal potential corresponding to the oxidation of $[Cu^{I}(TTCN)_2]$ indicates a preference for

octahedral Cu(II). These observations suggest a complex mechanistic pathway for the electron transfer. Accordingly, the square mechanism outlined in Scheme 4.1 is proposed. A similar mechanism has already been proposed for the $[Cu^{II/I}([14]aneS_4)]$ system[27,28].

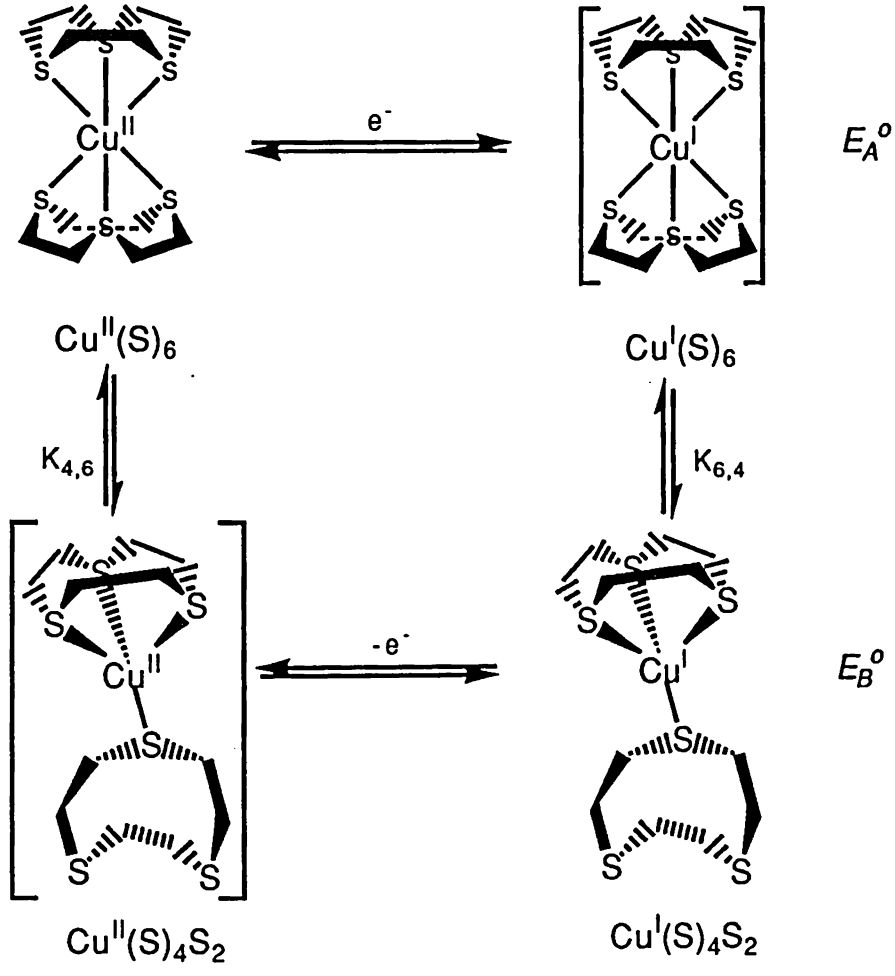

Scheme 4.1. Proposed Square Mechanism for the ET Reaction of the $[Cu^{II/I}(TTCN)_2]$ System.

Relatively slow scan rates provide sufficient time for the reduced complex to

undergo the structural changes consistent with the coordination geometry requirements of Cu(I). Thus the product of the reduction process being a structurally different species should be electrochemically different from the oxidized form. However, the redox potentials of the two copper complexes in different oxidation states are apparently too close to be resolved and one can only see the time averaged voltammograms of the entire system.

The conformational changes imposed on the complex by the reduction process will result not only in ligand dissociation but would also induce conformational changes in the partially dissociated macrocyclic ligand. This can also explain qualitatively the closeness of the two redox potentials $E^{\circ\prime}_{A}$ and $E^{\circ\prime}_{B}$ if the chemical steps are considered as intermolecular reactions involving ligand dissociation equilibria[29] between Cu(I) and the sulfur atoms of its monodentate TTCN ring. $E^{\circ\prime}_{A}$ and $E^{\circ\prime}_{B}$ represent the formal potentials for the reduction of $[Cu^{II}(TTCN)_2]$ and oxidation of $[Cu^{I}(TTCN)_2]$, respectively which do not include any structural readjustment. The high restoring force of the endodentate conformation and the proximity of the dissociated sulfurs to the copper ion would tend to keep the equilibrium to the left. This ligand rich inner sphere would anchimerically favor faster ligand binding[17]. The crowding of the ligand about Cu(I), a d^{10} transition metal ion, would destabilize the system so as to favor Cu(II) which can accommodate a coordination number of 6[30]. However, sulfur being a soft base has greater affinity for Cu(I) than Cu(II) and, therefore, the Cu(I) oxidation state would be favored. An

interplay between the ring-size effect, the macrocyclic effect, and the electronic effect is apparently responsible for such anomalous electrochemistry.

The observed values of the formal potentials and their dependence on the rotation speed can also be explained thermodynamically by considering the following two limiting cases both for the reduction of $[Cu^{II}(TTCN)_2]$ and oxidation of $[Cu^{I}(TTCN)_2]$ such that no kinetic complications are involved. (i) The system is completely electrochemically controlled and no structural readjustment is involved on the time scale of the experiment. (ii) The time scale of the experiment is such that the system is chemically controlled and complete equilibrium is achieved.

Subscripts *oct* and *tet* will be used to represent octahedral and tetrahedral coordination geometry respectively, whereas square brackets in the equation will represent the bulk concentrations of the corresponding species while subscripted concentrations to represent the electrode surface concentrations. The reduction of $[Cu^{II}(TTCN)_2]$ can be treated thermodynamically as follows:

$$[Cu^{II}L_2]_{oct} + e^- \rightleftarrows [Cu^{I}L_2]_{oct} \qquad E^{\circ\prime}_A \qquad (4.2)$$

The Nernst equation corresponding to Eq. 4.2 can be written as Eq. 4.3

$$E_A = E^{\circ\prime}_A + (RT/F) \ln\{[Cu^{II}L_2]_{o,oct}/[Cu^{I}L_2]_{o,oct}\} \qquad (4.3)$$

The chemical step following the electrochemical reduction of $[Cu^{II}(TTCN)_2]$ can be represented by the following equilibrium process.

$$[Cu^{I}L_2]_{oct} \rightleftarrows [Cu^{I}L_2]_{tet} \qquad K_{6,4} \qquad (4.4)$$

The equilibrium constant $K_{6,4}$ can be expressed as

$$K_{6,4} = [Cu^{I}L_2]_{tet}/[Cu^{I}L_2]_{oct} \qquad (4.5)$$

The overall reduction process can be represented as Eq.4.6 and the corresponding Nernst equation as Eq. 4.7.

$$[Cu^{II}L_2]_{oct} + e^- \rightleftarrows [Cu^{I}L_2]_{tet} \qquad E^{\circ\prime}_1 \qquad (4.6)$$

$$E_1 = E^{\circ\prime}_1 + (RT/F)\ \ln\{[Cu^{II}L_2]_{o,oct}/[Cu^{I}L_2]_{o,tet}\} \qquad (4.7)$$

By combining Eqs. 4.3, 4.5, and 4.7 it can now be shown for the reduction process that

$$E^{\circ\prime}_1 = E^{\circ\prime}_A + (RT/F)\ \ln K_{6,4} \qquad (4.8)$$

Similarly the following relationship can be established for the oxidation of $[Cu^{I}(TTCN)_2]_{tet}$.

$$E^{\circ\prime}_2 = E^{\circ\prime}_B - (RT/F)\ \ln K_{4,6} \qquad (4.9)$$

$E^{\circ\prime}_1$ and $E^{\circ\prime}_2$ are the formal potentials for the corresponding reduction and oxidation processes including the coupled conformational changes. When complete chemical equilibrium is achieved, $E^{\circ\prime}_1$ and $E^{\circ\prime}_2$ are equal. Moreover, in view of the stereochemical preferences of Cu(II) and Cu(I), it is safe to assume that $K_{6,4}$ and $K_{4,6}$ >> 1. It is obvious from the above treatment that the formal potential $E^{\circ\prime}_1$ corresponding to the reduction process where complete equilibrium is achieved should be more positive than $E^{\circ\prime}_A$. In the case of oxidation, $E^{\circ\prime}_2$ should be smaller than $E^{\circ\prime}_B$.

Electrochemistry of $[Cu^{II}(TTCN)_2$ in the presence of Cu(II)(aq) at pH 3.

Cyclic voltammetry, RDE, and chronocoulometry results are all suggestive of conformational changes following electron transfer as outlined in Scheme 4.1. The conformational readjustment imposed upon the complex by the oxidation state of the copper ion can however be stabilized, at least momentarily, by introducing an appropriate metal ion into the solution. Thus the electrochemistry of the system was carried out in aqueous medium in the presence of different concentrations of added Cu(II).

Cu(II) is much harder to reduce than the complex (reduction of $Cu(II)_{aq}$ occurs below 0.120 V) and, therefore, does not interfere or overlap with the electrochemistry of the complex. Moreover, the stereochemical plasticity of a d^9 system allows Cu(II) to adopt to a variable coordination number as well as coordination geometry. Passing to the right across the first row of Figure 4.4 (increasing added Cu(II)), the cyclic voltammograms gradually become sharper and increase in height. The separation between the cathodic and anodic peaks narrows and the apparent half wave potential gradually shifts to more positive values, but the process remains essentially reversible.

A plot of the cathodic peak current (i_{pc}) vs the ratio $[Cu(II)]/[Cu^{II}(TTCN)_2]$ results in a linear increase in the peak current initially which finally levels off at a value 1.842 times that of the complex alone (Figure 4.8 A). This value is very close to the theoretical value of 1.837 ($n^{3/2}$) for a reversible ET step of 1.5 electrons[31]. The inflection point corresponds to a concentration ratio of 0.5. Similarly from the RDE experiments a plot of the limiting current ($i_{\ell DISC}$) vs the concentration ratio resulted in a current ratio of 1.5 and concentration ratio of 0.5 at the inflection point (Figure 4.8 B).

The total number of electrons involved in the overall reduction process of the mixture was determined from the CPE of 0.025 mmol of $[Cu^{II}(TTCN)_2]$ in the presence of 0.13 mmol of Cu(II) at 200 mV. The electrolysis resulted in an "*n*" value of 1.45 which compares with the theoretical value of 1.5.

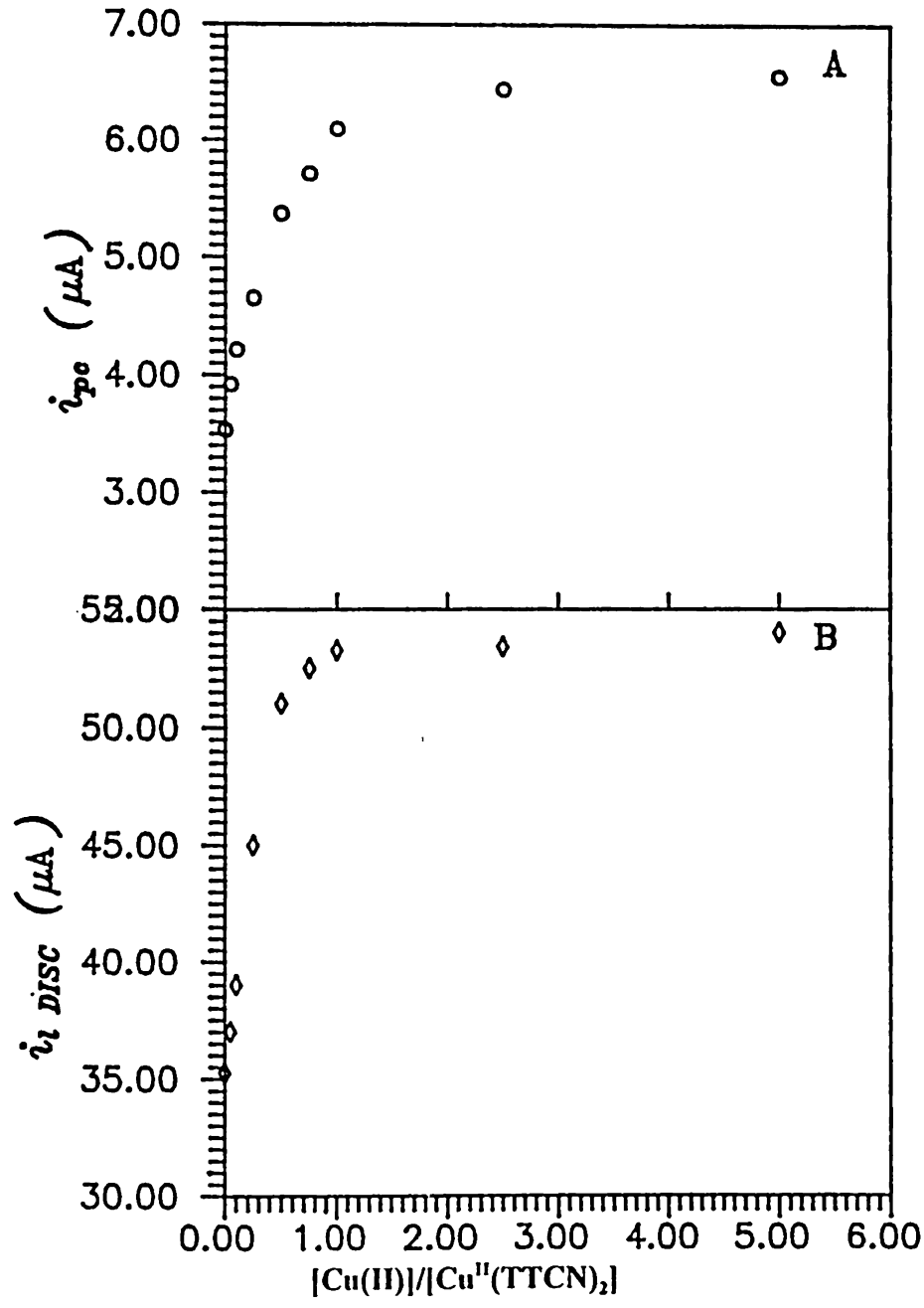

Figure 4.8. Titration of 1.0 mM [Cu^{II}(TTCN)$_2$]: Variation of (A) Cathodic Peak Current; (B) Cathodic Limiting Current, with [Cu(II)].

Figure 4.9 shows the Levich plots corresponding to the reduction of 1 mM

{$Cu^{II}(TTCN)_2$] with varying concentrations of Cu(II). The initial slopes of the plots for the mixtures are characteristic of 1.5 electrons but at high rotation speed, depending on the relative concentration of Cu(II), they decrease and converge with the Levich plot for the simple reduction of [$Cu^{II}(TTCN)_2$]. Exactly the same dependence of the plots of i_{tRING} vs $\omega^{1/2}$ on [Cu(II)]/[$Cu^{II}(TTCN)_2$] was seen. Thus changing the

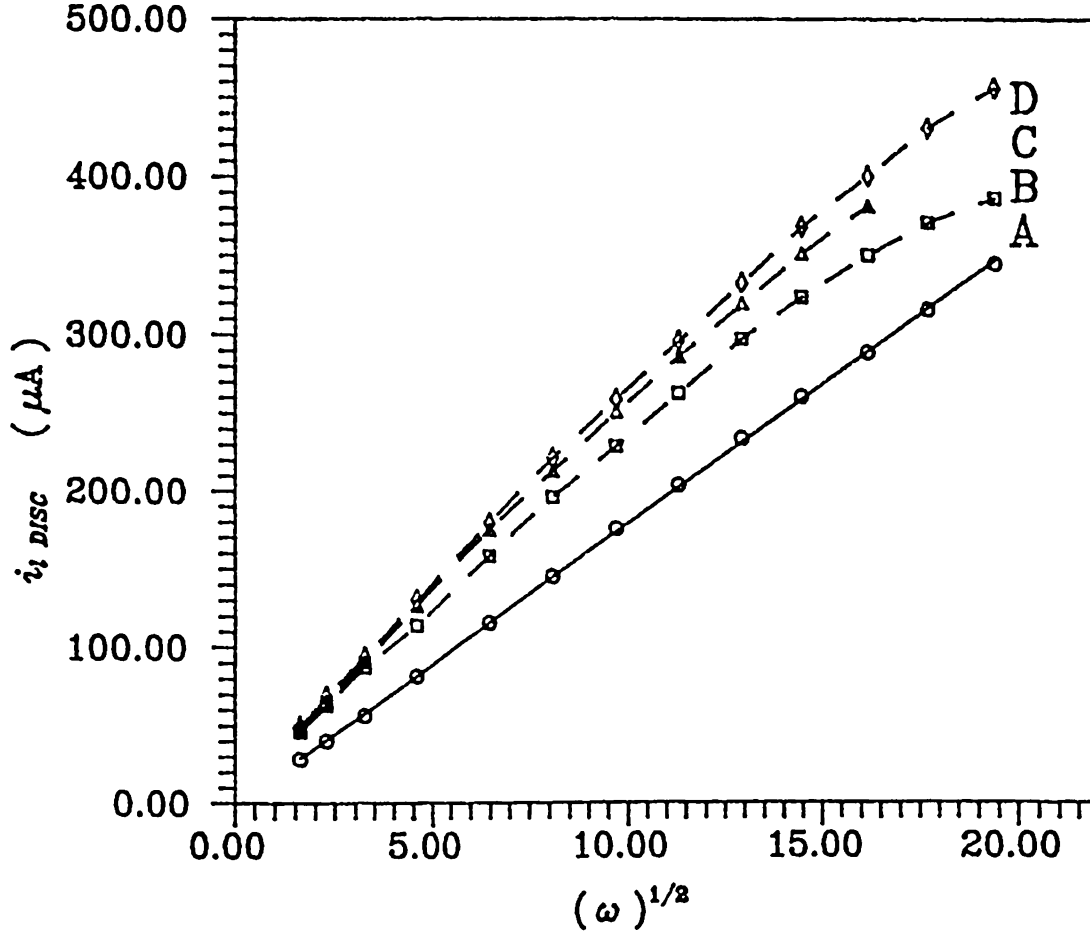

Figure 4.9. Variation of the Levich Plot of 1.0 mM [$Cu^{II}(TTCN)_2$] with [Cu(II)]: (A) No Cu(II) (B) 1.0 mM [Cu(II)] (C) 2.5 mM [Cu(II)] (D) 5.0 mM [Cu(II)].

time scale of the experiment illustrates the influence of the following chemical reaction. At high scan rates (Figure 4.4 Row 4) it is also possible to observe the partial resolution of the consecutive one electron steps.

These results support the reaction resulting in the formation of the trinuclear complex shown below.

$$2\ ML + Cu(II) \underset{k_b}{\overset{k_f}{\rightleftharpoons}} [Cu^{II}(ML)_2] \qquad K_1 \qquad (4.10)$$

where ML represents $[Cu^{I}(TTCN)_2]$. The corresponding equilibrium constant can be expressed as

$$K_1 = [Cu^{II}(ML)_2]/\{[Cu(II)][ML]^2\} \qquad (4.11)$$

The trinuclear complex ($[Cu^{II}(ML)_2]^{4+}$) then undergoes a 1 electron reduction at the electrode surface at a potential positive to the formal potential of $[Cu^{II}(TTCN)_2]$:

$$[Cu^{II}(ML)_2] + e^- \rightleftharpoons [Cu^{I}(ML)_2] \qquad E^{\circ\prime}_3 \qquad (4.12)$$

The Nernst equation for Eq. 4.12 can be written as

$$E_3 = E^{\circ\prime}_3 + (RT/F) \ln \{[Cu^{II}(ML)_2]_o/[Cu^{I}(ML)_2]_o\} \qquad (4.13)$$

For the sake of simplicity , in addition to the assumption that $K_{6,4} >> 1$, it is further assumed that the presence of Cu(II) in solution would shift the equilibrium further to the right such that only Eq. 4.6 can be considered as an electrochemical step preceding the chemical reaction between $[Cu^{I}(TTCN)_2]$ and Cu(II). Slow scan rates provide enough time for the processes of Eq. 4.10 to attain equilibrium thus ensuring complete chemical reversibility. The observation that only one redox process is evident for any composition of the test solution and the positive shift in the peak potentials coupled with decreased peak separation (ΔE) and increased i_p's with increasing Cu(II) concentration suggest that the formal potential for the redox process of Eq. 4.12 ($E^{\circ\prime}_3$ should be more positive than $E^{\circ\prime}_1$ of Eq. 4.6. Therefore, for a sufficiently positive $E^{\circ\prime}_3$ relative to $E^{\circ\prime}_1$ and excess Cu(II) present, a one-step reduction (n = 1.5 electrons) is expected for the redox process:

$$2[Cu^{II}L_2] + Cu(II) + 3e^- \rightleftharpoons [Cu^{I}(ML)_2] \qquad E^{\circ\prime}_4 \qquad (4.14)$$

For a relatively higher scan rate and lower Cu(II) concentration e.g., the bottom row of Figure 4.4, the process is dominated by ET; the chemical interactions do not have enough time to take place and only the simple one electron reduction of $[Cu^{II}(TTCN)_2]$ is observed.

Digital simulation, based on a ECE mechanism, failed to closely reproduce the experimental curves. This indicates that some other process might also be operative.

It can be assumed that the chemical step following the first ET step is not a diffusion limited reaction. Therefore, some $[Cu^{I}(TTCN)_2]$ produced at the electrode surface can diffuse into the solution before interacting with the free copper at the electrode surface and produce the trinuclear complex in solution according to Eq. 4.10. This complex can then diffuse back to the electrode and undergo electrochemical reduction. At the same time the complex can undergo solution electron transfer with the diffusing $[Cu^{I}(TTCN)_2]$ according to Eq. 4.15[32]. In that case K_2 must also be considered in calculation of the corresponding kinetic and thermodynamic parameters.

$$[Cu^{I}L_2] + [Cu^{II}(ML)_2] \rightleftharpoons [Cu^{I}(ML)_2] + [Cu^{II}L_2] \qquad K_2 \qquad (4.15)$$

When Eq. 4.15 was included in the simulation program, the analysis of five voltammograms at different scan rates and Cu(II) concentrations reproduced very closely the experimental voltammograms as shown in Figure 4.10.

Because of the complex nature of the proposed follow-up chemical reaction, represented by Eq. 4.10, no direct theoretical analysis of the i - E curves was attempted. However, the digital simulation was carried out first for the apparently reversible slow scan rate voltammograms of a number of mixture compositions. It was assumed that a 5 mV s^{-1} scan rate is slow enough to allow the follow-up chemical reaction to attain equilibrium. Fixing the electrochemical parameters already determined for the redox process preceding the chemical step of Eq. 4.10, preliminary

calculations indicated that the generated i - E curves at a given K_1K_2were practically independent of K_2 as long as $K_2 > 10$ which would be the case when $(E^{\circ\prime}_3 - E^{\circ\prime}_1)$ > 60 mV. This may be ascribed to the statistical correlation between K_1 and K_2. Since

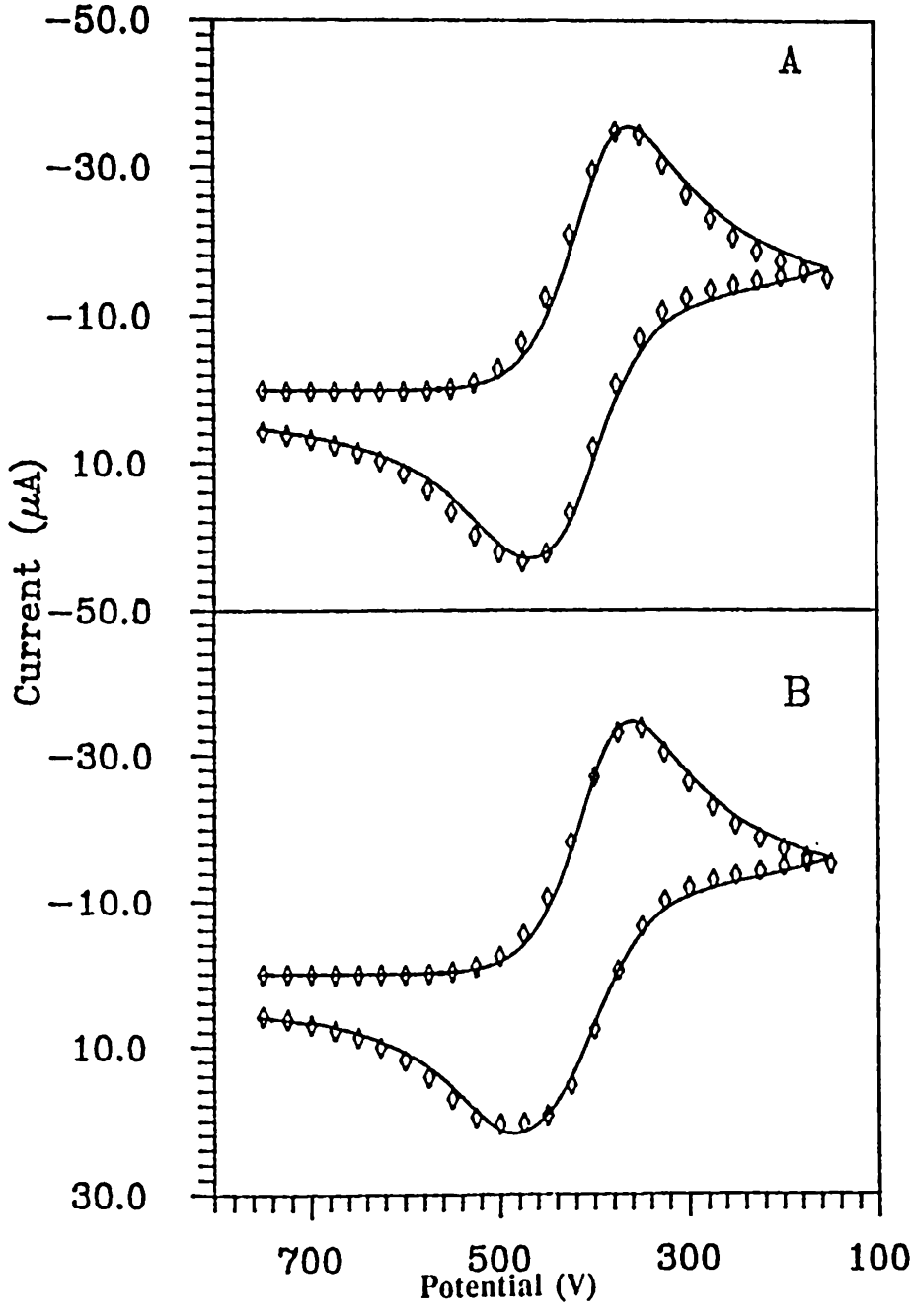

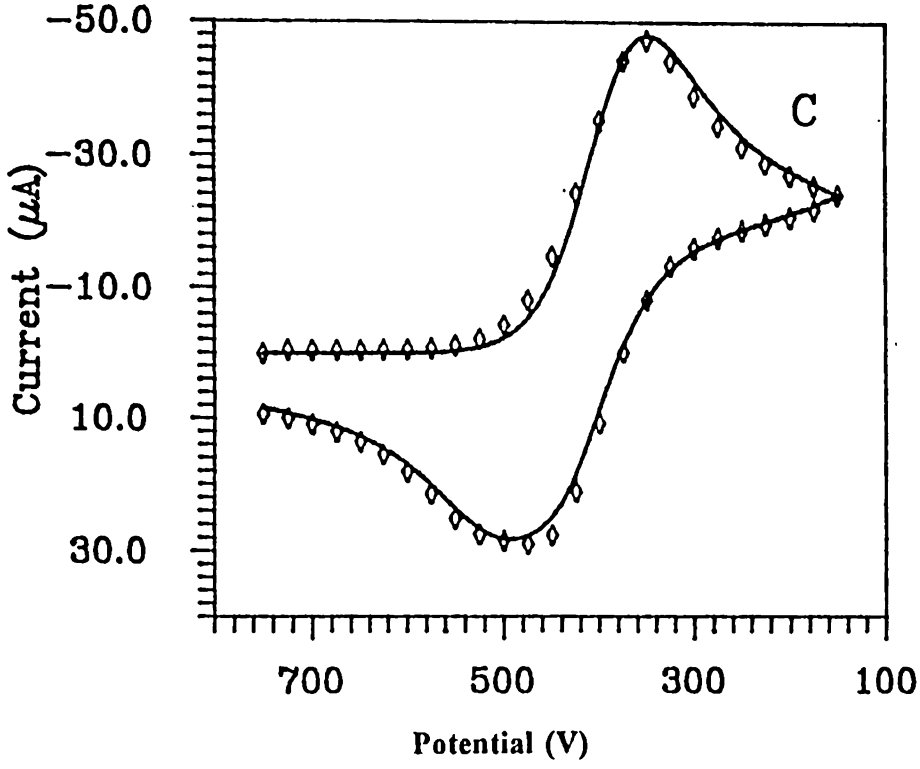

Figure 4.10. Digitally Simulated Voltammograms of 1.0 mM $[Cu^{II}(TTCN)_2]$: Experimental (◇◇◇); Theoretical (—). (A) 0.05 mM Cu(II) at 500 mV s^{-1}; (B) 0.1 mM Cu(II) at 500 mV s^{-1}; (C) 0.1 mM Cu(II) at 1,000 mV s^{-1} Scan Rate.

the independent estimation of K_1K_2 is difficult, the adjustment of K_1K_2 was allowed to get the best fit. For the digital simulation the diffusion coefficients were set as $D_1 = D_2 = 5.3 \times 10^{-6}$ cm^2 s^{-1}, $D_3 = D_4 = 4.6 \times 10^{-6}$ cm^2 s^{-1} and $D_{Cu(II)} = 7.0 \times 10^{-6}$ cm^2 s^{-1}. In this way the analysis gave $K_1K_2 = 5.87 \times 10^7$ M^{-2}, where D_1, D_2, D_3, and D_4 are the diffusion coefficients of $[Cu^{II}L_2]$, $[Cu^{I}L_2]$, $[Cu^{II}(ML)_2]$, and $[Cu^{I}(ML)_2]$, respectively.

It is obvious from Figure 4.4 that the shape of the cyclic voltammograms depends strongly both on the relative concentration of added Cu(II) and the scan rate. The changes associated with these parameters can be explained in terms of the

kinetics of the ET (Eq. 4.1 and 4.12) and the follow-up chemical step (Eq. 4.10). Our model specifies that the solution electron transfer reaction of Eq. 4.15 is in equilibrium on the time scale of relatively slower scan rate ($\nu < 2$ V s^{-1}).

The kinetic and thermodynamic parameters corresponding to Eq. 4.10 and Eq. 4.12 were calculated from the digital simulation. This was done by adjusting the ET rate constant (k_{sh3}), the cathodic transfer coefficient (α_3) and $E^{\circ\prime}_3$ corresponding to the redox process of Eq. 4.12, and the forward rate constant (k_f) corresponding to Eq. 4.10. In this way the values obtained are $E^{\circ\prime}_3 \approx 0.60$ V, $\alpha_3 \approx 0.5$, $k_{sh3} \approx 0.01$ cm s^{-1}, and $k_f \approx 2 \times 10^8$ M^{-2} s^{-1}. The validity and consistency of these values is manifested in the close fit of the calculated curves with the experimental voltammograms. The set of estimated values of various constants can explain the entire spectrum of voltammograms at $\nu < 2$ V s^{-1} shown in Figure 4.4.

These are obviously quite complicated systems and care must be taken to see if the digital simulation can discriminate the proposed mechanisms from several alternative mechanisms. The fact that the simulations failed to consistently reproduce the experimental curves for a number of alternative mechanisms justifies our model. Those alternative mechanistic schemes involved (i) no solution electron transfer; (ii) a direct two electron oxidation of the trinuclear complex [$Cu^{I}_2Cu^{II}(TTCN)_4$]) to two [$Cu^{II}(TTCN)_2$] and free Cu(II); or (iii) the generation of a dinuclear intermediate from the interaction between [$Cu^{I}(TTCN)_2$] and Cu(II) followed by the formation of the trinuclear complex.

Spectral Analysis of the Electrolyzed Mixture. The electronic spectrum of $[Cu^{II}(TTCN)_2]$ over a wavelength range of 850 - 300 nm gives a single symmetrical peak at 444 nm. No change in the spectral behavior of $[Cu^{II}(TTCN)_2]$ over a period of 24 h at room temperature was observed upon titration with Cu(II). A mixture, 2 mM in $[Cu^{II}(TTCN)_2]$ and 10 mM in Cu(II), was electrolyzed at 200 mV vs Ag/AgCl, until the current decayed to about 3% of the initial current. The spectrum of the electrolyzed mixture was run immediately after the electrolysis (Figure 4.11). The appearance of a new peak at 370 nm where there is no absorbance from the free copper or the $[Cu^{II}(TTCN)_2]$ complex, is a clear indication of the production of a new species. The peak at 440 nm can be ascribed to the absorption due to the unelectrolyzed or regenerated $[Cu^{II}(TTCN)_2]$ and the 370 nm peak to the trinuclear complex. The 370 nm peak of the electrolyzed mixture appears at almost the same position as that assigned to $S(\sigma) \rightarrow Cu(II)$ charge transfer where L = [12]aneS$_4$, and [14]aneS$_4$[27,33].

The increase in the intensity of the 440 nm peak with time (Figure 4.11) indicates the regeneration of the original complex either by the decomposition of the trinuclear complex or through autoxidation, most likely the former. Moreover, the completely reduced trinuclear complex, supposing that all the copper centers have tetrahedral geometry, could be subject to high steric repulsion which would make it to be easily attacked by the Cu(II) ion leading to the regeneration of $[Cu^{II}(TTCN)_2]$ complex.

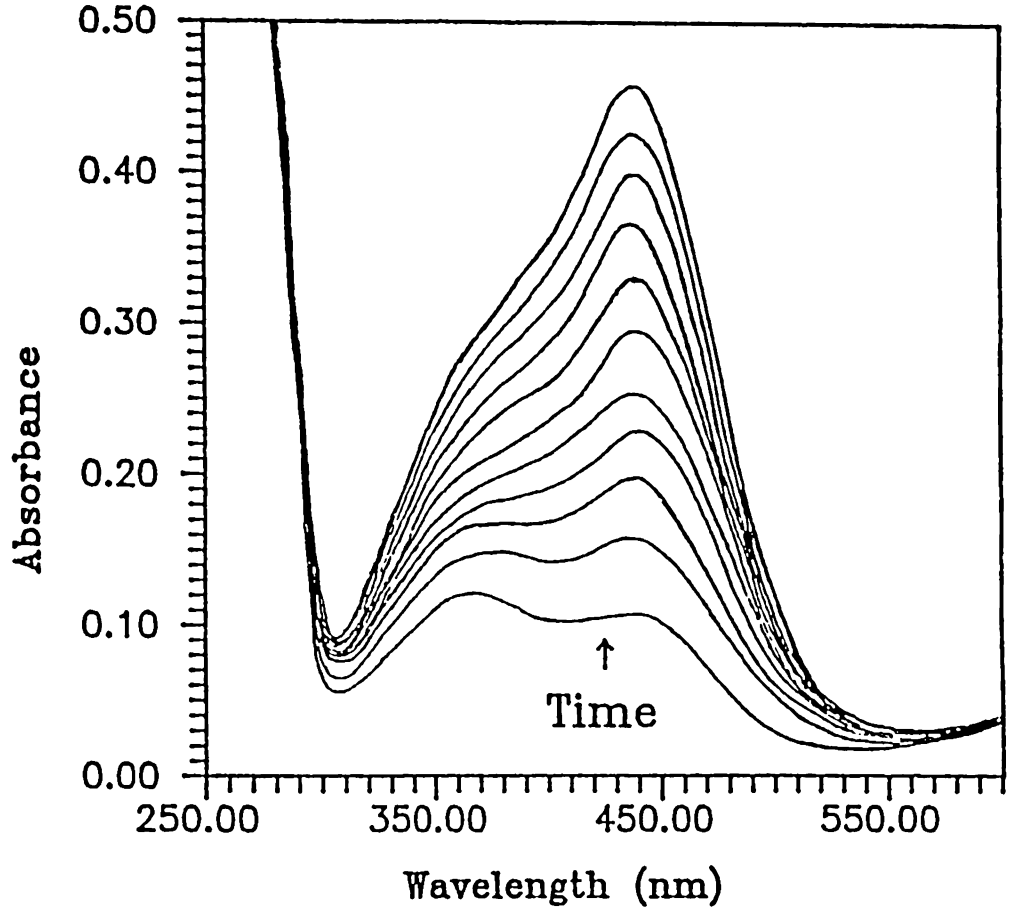

Figure 4.11. Time Dependent Spectral Changes in 5:1 [Cu(II)] : $[Cu^{II}(TTCN)_2]$ Mixture after CPE; (*at time 0 and at 3 h intervals*).

Considering all of the above observations, the mechanism outlined in Scheme 4.2 is proposed here for the ET reaction of *bis*(1,4,7-trithiacyclononane)copper (II) in the presence of free copper.

The fact that the intermediate trinuclear complex has a relatively more positive redox potential ($E^{\circ\prime}_3$) compared with that of $[Cu^{II}(TTCN)_2]$ ($E^{\circ\prime}_1$) can be explained as follows. Cyclic thioethers tend to stabilize Cu(II) better than acyclic thioethers[12]. This

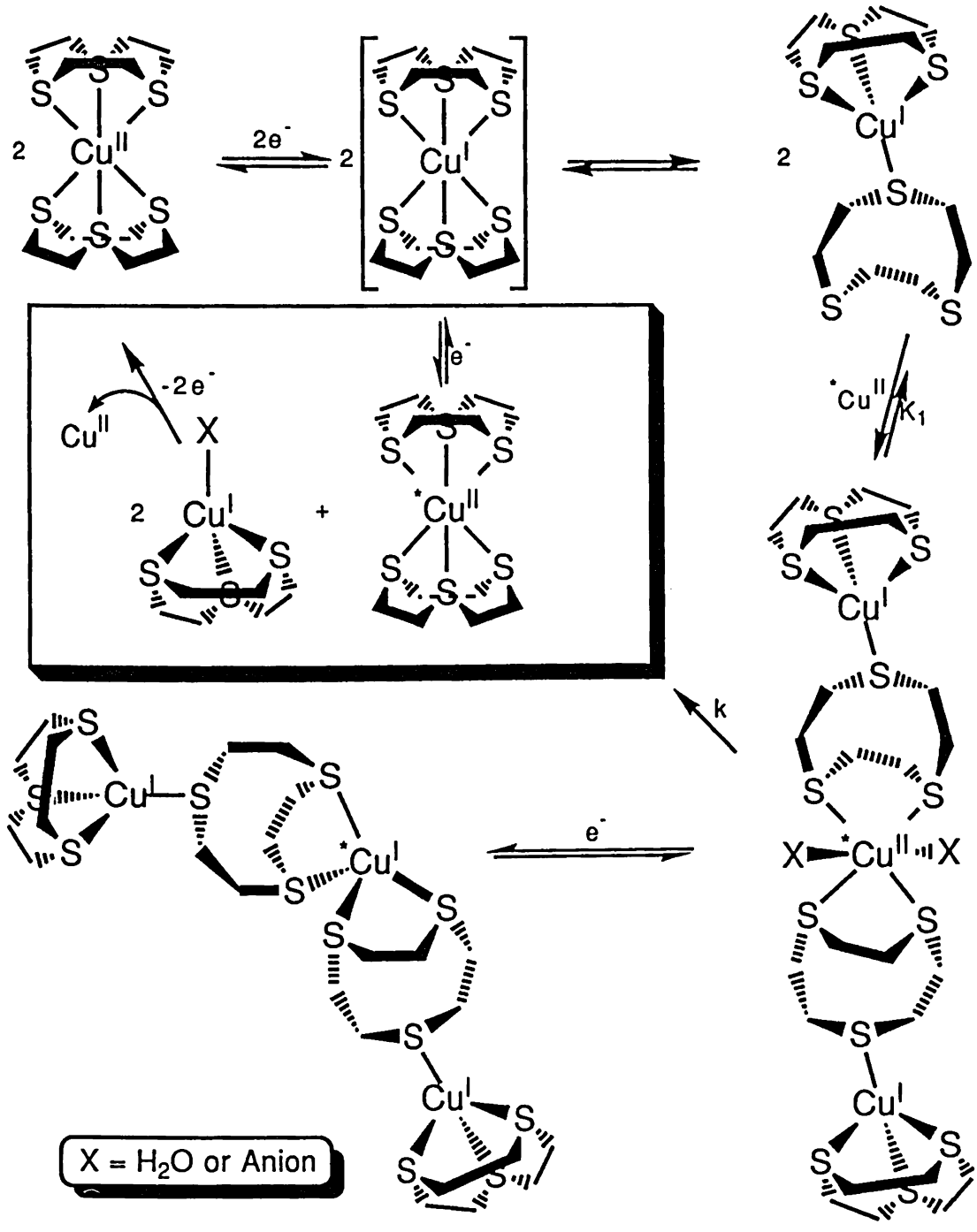

Scheme 4.2. The proposed mechanism for heterogeneous ET of $[Cu^{II}(TTCN)_2]$ followed by interaction with Cu(II) and subsequent ET of the trinuclear complex.

tendency is more obvious in the case of TTCN because the sulfurs are quite rigidly preorganized for facial coordination. However, the greater affinity of Cu(I) for thioether would cause the redox potential of $[Cu^{II}(TTCN)_2]$ to be relatively high as compared with the *ammine* and *oxo-* analogues[34], but not as high as those of the acyclic or more flexible macrocyclic thioethers[12]. In the trinuclear complex the terminal $[Cu^{I}(TTCN)_2]$ units appear to behave as bidentate ligands for the central copper atom. The loss of the macrocyclic effect would result in a higher redox potential of the central copper, however, the rigidity of this bidentate ligand may be considered responsible for the relatively small shift. This coordination of the uncomplexed sulfur atoms of the $[Cu^{I}(TTCN)_2]$ complex provides further evidence that the geometry of this complex in solution is at least similar if not the same as that determined unequivocally in the solid state by X-ray crystallographic methods.

Potentiometric analysis. Based on the proposed mechanisms, a mathematical analysis can be carried out for the potentiometric titration of $[Cu^{I}(TTCN)_2]$, generated at the electrode surface, with Cu(II).

Comparing Eq. 4.10 and Eq. 4.7, it is obvious that the effect of adding free copper to the solution is a progressive shift of the apparent formal potential of the process to a more positive value until the equilibrium is driven completely to the right at high concentrations of added copper. The value of such a limiting formal potential can mathematically be predicted by correlating $E^{\circ\prime}_4$ of Eq. 4.14 with K_1.

Under the conditions that [Cu(II)] >> $[Cu^{II}(TTCN)_2]/2$ and K_1 >> 1, the complex $[Cu^{II}(TTCN)_2]$ would be almost completely converted to $[Cu^{I}_3(TTCN)_4]^{3+}$ at the electrode surface upon reduction at low scan rate. The Nernst equation for Eq. 4.14 can then be written as Eq. 4.16.

$$E_4 = E^{\circ\prime}_4 + (RT/3F)\ \ln\{[Cu^{II}L_2]_s^2[Cu(II)]/[Cu^{I}(ML)_2]_s\} \qquad (4.16)$$

Eqs. 4.7, 4.11, 4.13, and 4.16 can be combined to obtain Eq. 4.17 for the limiting value of the formal potential corresponding to Eq. 4.14 under complete formation of $[Cu^{I}_2Cu^{II}(TTCN)_4]^{4+}$ (Eq. 4.10).

$$E^{\circ\prime}_4 = \{(2E^{\circ\prime}_1 + E^{\circ\prime}_3)/3\} + (RT/3F)\ \ln K_1 \qquad (4.17)$$

However, when [Cu(II)] is not very high as compared to $[Cu^{II}(TTCN)_2]$, Eq. 4.15 cannot be ignored. The equilibrium constant corresponding to Eq. 4.15 can be represented as

$$K_2 = \{[Cu^{II}L_2][Cu^{I}(ML)_2]\}/\{[Cu^{I}L_2][Cu^{II}(ML)_2]\}$$
$$= \mathrm{Exp}\{(F/RT)\ (E^{\circ\prime}_3 - E^{\circ\prime}_1)\} \qquad (4.18)$$

Taking the solution electron transfer into account, Eq. 4.16 can be modified

to Eq. 4.19

$$E^{\circ\prime}_4 = E^{\circ\prime}_1 + (RT/3F)\ \ln K_1K_2 \qquad (4.19)$$

Under the conditions that $[Cu(II)]_\circ \approx [Cu(II)]_{Eq} \approx [Cu(II)]$, where subscript "Eq" represents the equilibrium concentration, the following equation for the potentiometric titration can be obtained.

$$E^{\circ\prime}_{app} - E^{\circ\prime}_1 = (RT/3F)\ \ln(K_1K_2[Cu(II)][Cu^{II}L_2]) \qquad (4.20)$$

where $E^{\circ\prime}_{app} = E^{\circ\prime}_4 + (RT/3F)\ \ln([Cu(II)][Cu^{II}(TTCN)_2])$, is an apparent formal potential for a particular composition of the mixture and will have the same numerical value as the electrode potential at half reduction when $[Cu^{II}L_2]_\circ = [Cu^{II}(TTCN)_2]/2$ and $[Cu^{II}(ML)_2]_\circ = [Cu^{II}(TTCN)_2]/4$.

Estimating $E_{1/2,app}$ as $(E_{pa} + E_{pc})/2$ from the apparently reversible voltammograms run at 5 mV s^{-1}, a plot of $(E^{\circ\prime}_{app} - E^{\circ\prime}_1)$ vs log([Cu(II)]) affords a straight line in the range of $[Cu(II)]/[Cu^{II}(TTCN)_2] \approx 0.25 - 0.75$ (Figure 4.12). The experimental slope of this line segment is 16.8 mV. This slope is somewhat smaller than the theoretical value of 19.7 mV. While this difference can be ascribed to the assumption concerning $[Cu(II)]_\circ$ and $[Cu(II)]_{aq}$, the possibility of further formation of other copper complexes at much higher Cu(II) concentration cannot be ruled out.

Moreover, for a complete and successful theoretical analysis a detailed knowledge of the kinetics and thermodynamics of the decomposition of the trinuclear complex (Scheme 4.2) is needed. The existence of this competing chemical process has been strongly supported by our results with some other Cu(I)-TTCN system. These studies have indicated that the decomposition product, $[Cu^{I}(TTCN)X]$ ($X = H_2O$, A^-) has about the same redox potential as calculated for the trinuclear complex under the same set of experimental conditions. This makes the two pathways electrochemically indistinguishable from each other.

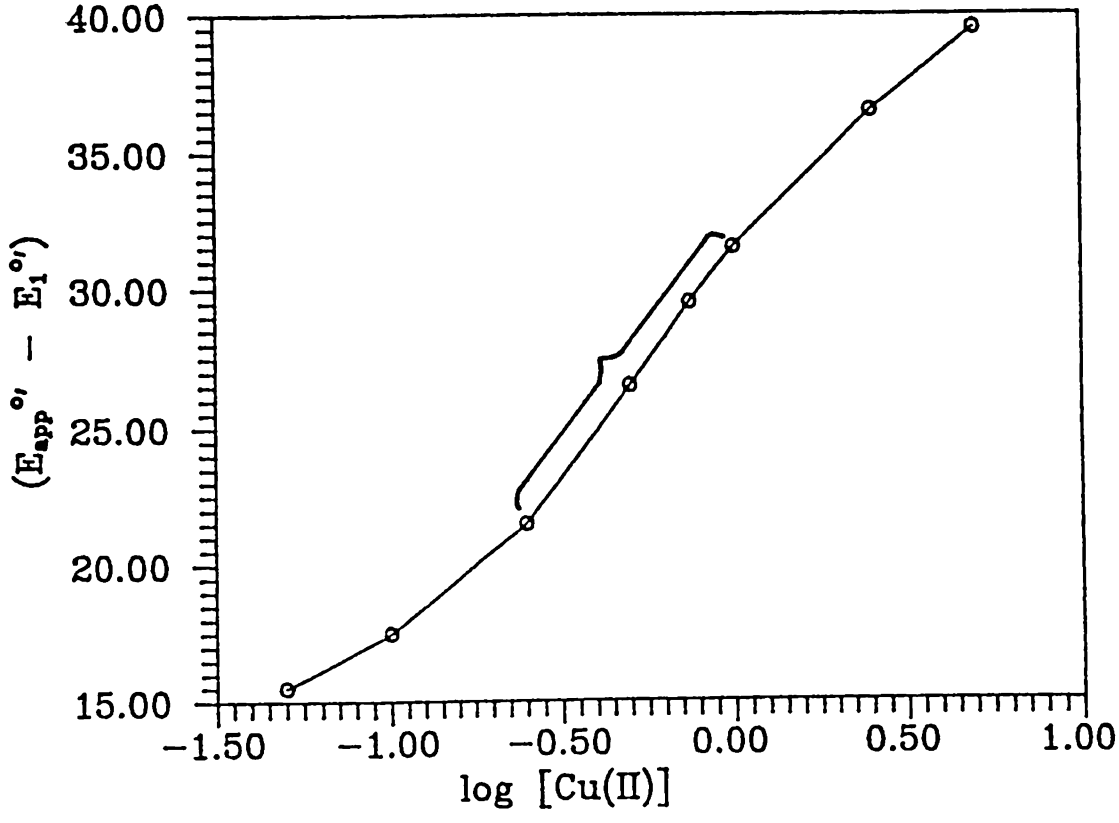

Figure 4.12. Variation of $E_{app}^{o'}$ of $[Cu^{II}(TTCN)_2]$ with [Cu(II)].

CHAPTER 5

COORDINATION DYNAMICS OF COPPER(I)-TTCN COMPLEXES AS STUDIED BY ELECTROCHEMISTRY, PULSE RADIOLYSIS AND DYNAMIC NMR SPECTROSCOPY.

Introduction

Our electrochemical study of the redox properties of $[Cu^{II}(TTCN)_2]$ indicated that the ultimate redox couple involves two, most probably conformationally, different species. This was supported by the x-ray crystallographic studies which has shown that unlike the octahedral $[Cu^{II}(TTCN)_2]$ complex, the $[Cu^{I}(TTCN)_2]$ complex is tetrahedral. Chronocoulometry of the complex with a 5 ms pulse indicated a short lived (on the electrochemical time scale) intermediate species before the complex assumes the most stable structure, corresponding to the respective oxidation state. In order to study closely the changes in coordination as a function of the oxidation state of copper and conformational rigidity of the monodentate ligand, a number of copper(I)-thioether complexes (**1.5 - 1.8**) were prepared. Further investigation of redox state-coupled conformational changes was facilitated by employing pulse radiolysis. In all of these complexes, except $[Cu^{I}(HTCOD)]$ (HTCOD = hexathiacyclooctadecane), one of the ligands is the tridentate TTCN molecule. The fourth coordination site on Cu(I) is occupied by a thioether ligand from TTCN, 1-sulfoxide-2,4-dithiacyclononane (SODTCN), 1,4-dithiane, pentamethylene sulfide (PMS) or tetrahydrothiophene (THT).

Pulse radiolysis, in conjunction with cyclic voltammetry and dynamic nuclear magnetic resonance spectroscopy, is employed in this work to study the intermediate(s) produced as a consequence of the oxidation of Cu(I) complexes (**1.5 - 1.8**). Extensive electrochemical studies of **1.5** and **1.6** are also presented here to understand the redox mechanisms of these complexes. Variable temperature NMR of **1.5** has also been carried out to study the dynamics of its conformational changes in solution.

Pulse radiolysis is the radiation-chemical analogue of flash photolysis. In pulse radiolysis free radicals are produced by the injection of energy from a transient beam of high energy (0.6 - 10 MeV) electrons which lose their energy to the electrons in the molecular orbitals of the target molecule. This results in the excitation or ionization of the molecules[1]. In water ionization dominates and the secondary electrons produced in these ionizations can cause further ionization and excitation. The electrons with relatively low energy (100 eV) have their energy deposited within a relatively small volume, creating a spur with a number of ions, electrons, and free radicals in relatively close proximity. The distribution of radicals per spur depends on the initial energy of the primary electrons and the medium irradiated. For 1 MeV electrons in water at 25°C, about half the spurs contain only one ion pair.

Secondary electrons in water normally lose their energy in a time period of about one picosecond (ps) before they become localized and get hydrated[1]. The hydrated electron (e^-_{aq}) has a characteristic spectrum which is developed at 10 ps, and

the yield of e^-_{aq} at this time is 0.5 μmol j^{-1} of energy absorbed. On the ps time scale the positive ions, resulting from the ionization, undergo ion-molecule reactions and, like the electron, become solvated.

$$H_2O^+ + H_2O \rightarrow H_3O^+ + {}^{\cdot}OH \qquad (5.1)$$

whereas the excited molecules may dissociate.

$$H_2O^* \rightarrow {}^{\cdot}H + {}^{\cdot}OH \qquad (5.2)$$

From this point in time outward diffusion of the reactive species competes with geminate reactions within the spurs, and the spur structures are effectively dissipated at about 50 ns. The geminate reactions

$$e^-_{aq} + {}^{\cdot}OH \rightarrow OH^- \text{ and } e^-_{aq} + H_3O^+ \rightarrow {}^{\cdot}H \qquad (5.3)$$

cause the yield of electrons to fall from 0.50 to 0.28 μmol j^{-1}. The following reactions can also occur during that time,

$${}^{\cdot}H + {}^{\cdot}H \rightarrow H_2 \text{ and } {}^{\cdot}OH + {}^{\cdot}OH \rightarrow H_2O_2 \qquad (5.4)$$

The stoichiometry of the radiolysis of water at 1 μs after the passage of the primary electrons is described by the following equation[2]:

$$0.43\ H_2O \rightarrow 0.28\ e^-_{aq} + 0.05\ {}^{\cdot}H + 0.29\ {}^{\cdot}OH + 0.28\ H_3O^+ + 0.05\ H_2 + 0.07\ H_2O_2 \quad (5.5)$$

On the molecular scale the above equation can be represented as

$$H_2O \rightarrow e^-_{aq}(2.75) + {}^{\cdot}OH(2.75) + {}^{\cdot}H(0.60) + H_3O^+(2.75) + H_2(0.45) + H_2O_2(0.75) \quad (5.6)$$

where the numbers in parentheses are *G* values which represent the number of molecules formed per 100 eV of energy absorbed in the solution[3].

Since the hydroxyl radical is a strong oxidant while the hydrated electron is a reductant, therefore, it is often convenient to introduce species like alcohols to scavenge for example ·OH or to convert it into a reducing species by the addition of sodium formate.

$$^{\cdot}OH + HCOO^- \rightarrow H_2 + {}^{\cdot}CO_2^- \quad (5.7)$$

Similarly the hydrated electron can also be converted to hydroxy radical with nitrous oxide

$$e^-_{aq} + N_2O + H_2O \rightarrow {}^{\cdot}OH + {}^{\cdot}OH + N_2 \quad (5.8)$$

thus producing mainly oxidizing species.

Results

X-ray Crystallography of Selected Copper(I) Complexes.

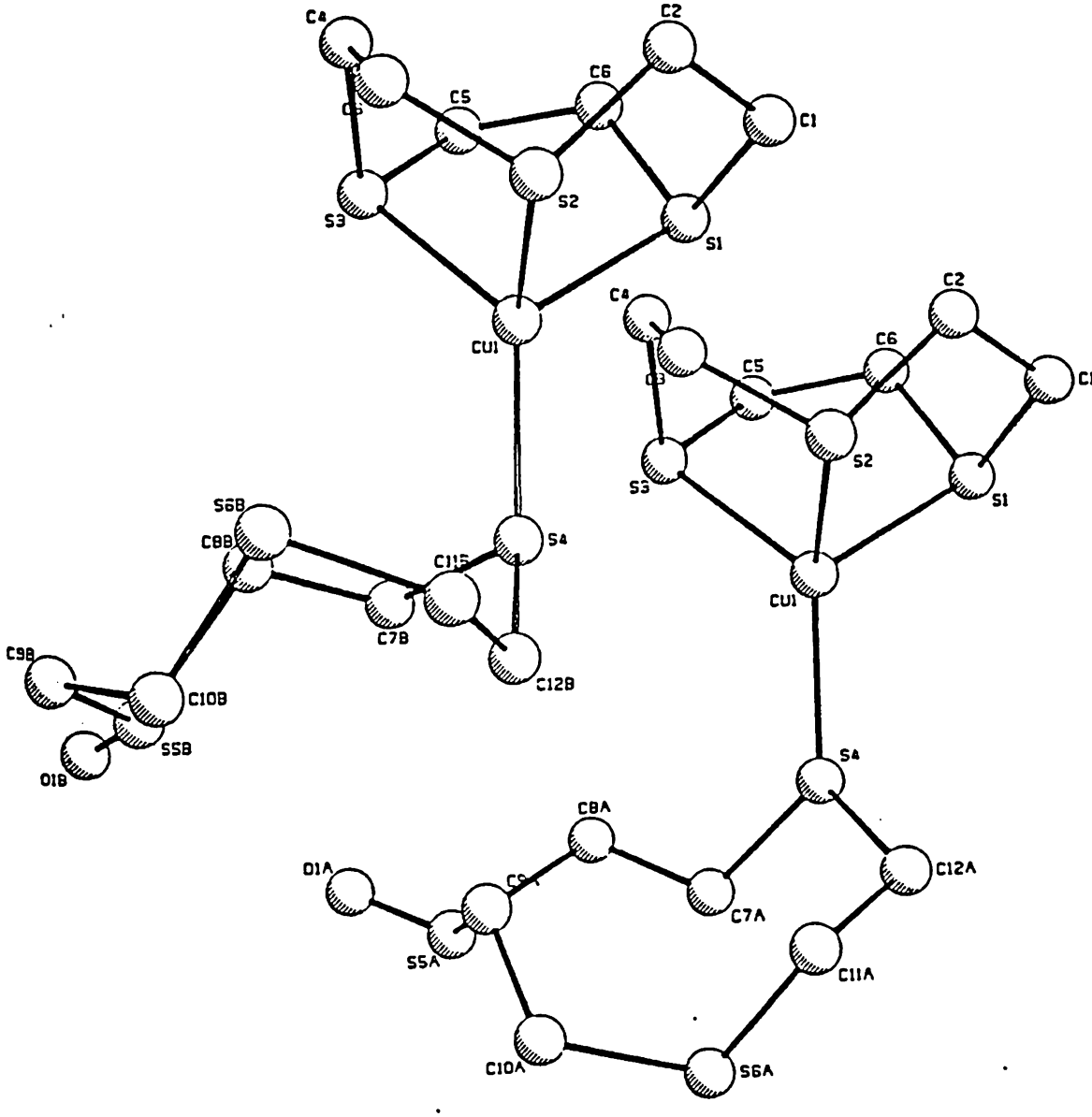

Figure 5.1. Structures of the two Molecular Units of [Cu^{I}(TTCN)(SODTCN)] (PLUTO Drawing).

[Cu^{I}(TTCN)(SODTN)]PF_6. The complex molecule crystallizes in space group *P2$_1$/n* of the monoclinic system. Like the [Cu^{I}(TTCN)$_2$], the unit cell of [Cu^{I}(TTCN)(SODTCN)] is composed of two different molecular units (Figure 5.1). Superposition of the two units reveal high degree of disorder in the SODTCN ring (Figure 5.2). This kind of behavior is proving to be frequent in TTCN complexes[4].

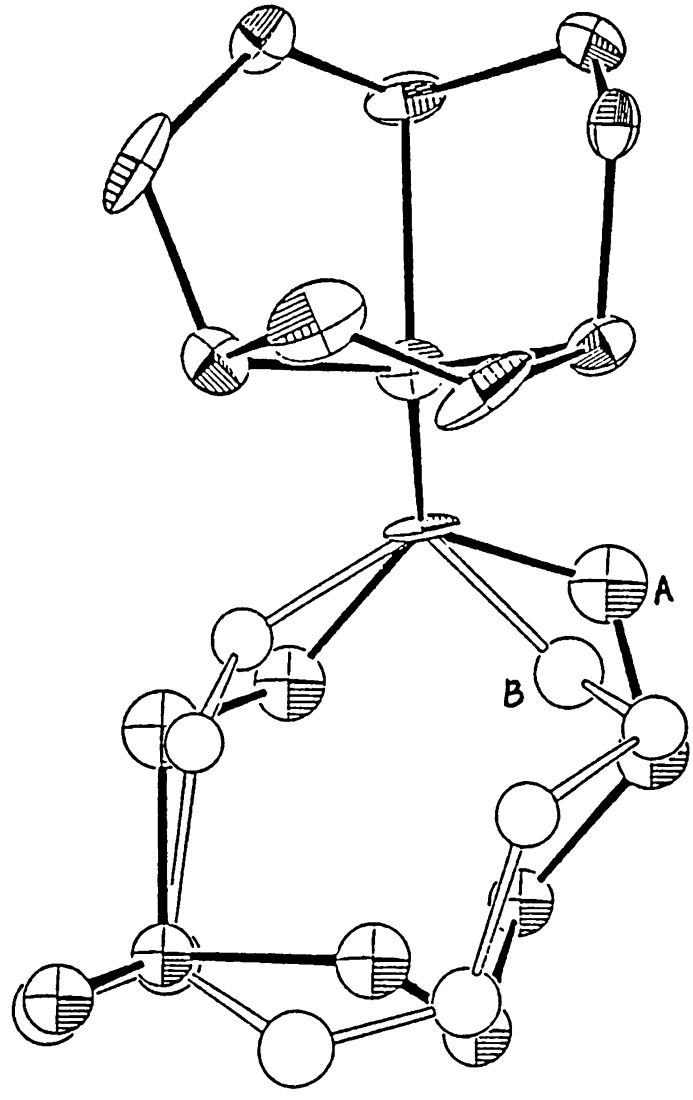

Figure 5.2. ORTEP Drawing of [Cu^{I}(TTCN)(SODTCN)] cation showing the disorder in SODTCN ring. Conformation A: Hatched; Conformation B: Blank

[(TTCN)Cu(1,4-Dithiane)Cu(TTCN)](PF$_6$)$_2$. The binuclear Cu(I) complex, [(Cu(TTCN))$_2$(1,4-dithiane)](PF$_6$)2 crystallizes in space group C2/c of the monoclinic system with a center of symmetry. The asymmetric unit contains two half PF_6 anions per half complex molecule. Several short CH—F contacts are present probably due to weak hydrogen bonding (Figure 5.3).

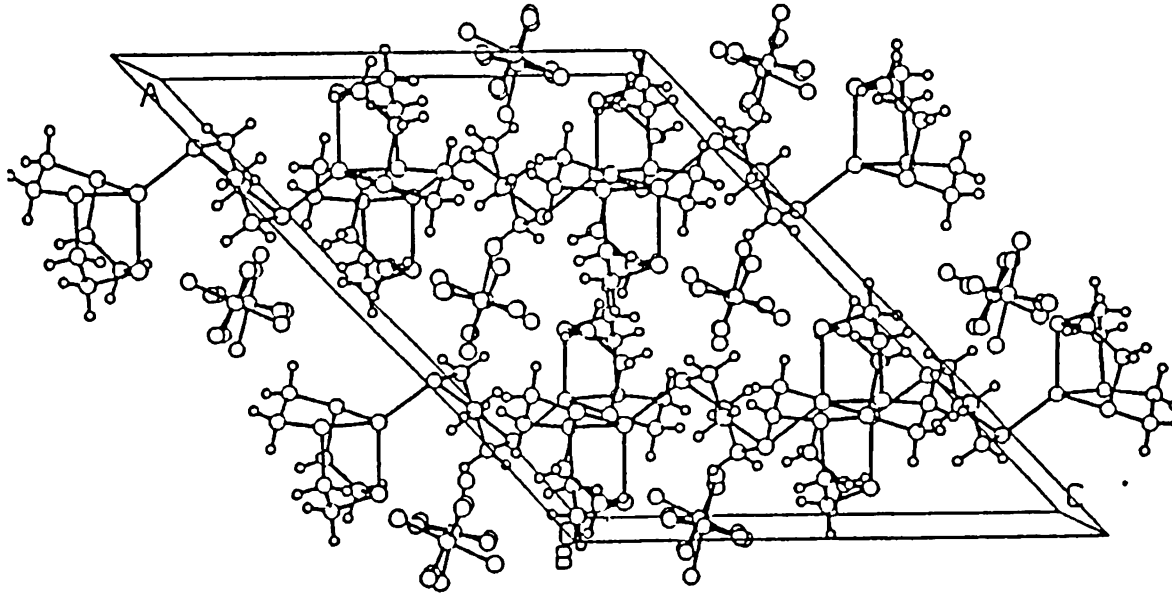

Figure 5.3. Packing of the Unit Cell of [(Cu(TTCN))$_2$(1,4-Dithiane)](PF$_6$)$_2$.

Interestingly the coordination of the bridging 1,4-dithiane to Cu(I) is axial (Figure 5.4). Comparing the Cu(I)—S (monodentate thioether) bond lengths (Tables A2.2, A3.2, A4.2) and interligand SCuS bond angles (Tables A2.3, A3.3, A4.3), it is

obvious that the coordination of the monodentate TTCN to Cu(I) does not have any special effect on the coordination of the tridentate TTCN. Comparing the Cu(I)—S bond lengths of the monodentate ligand with those of the tridentate TTCN indicates

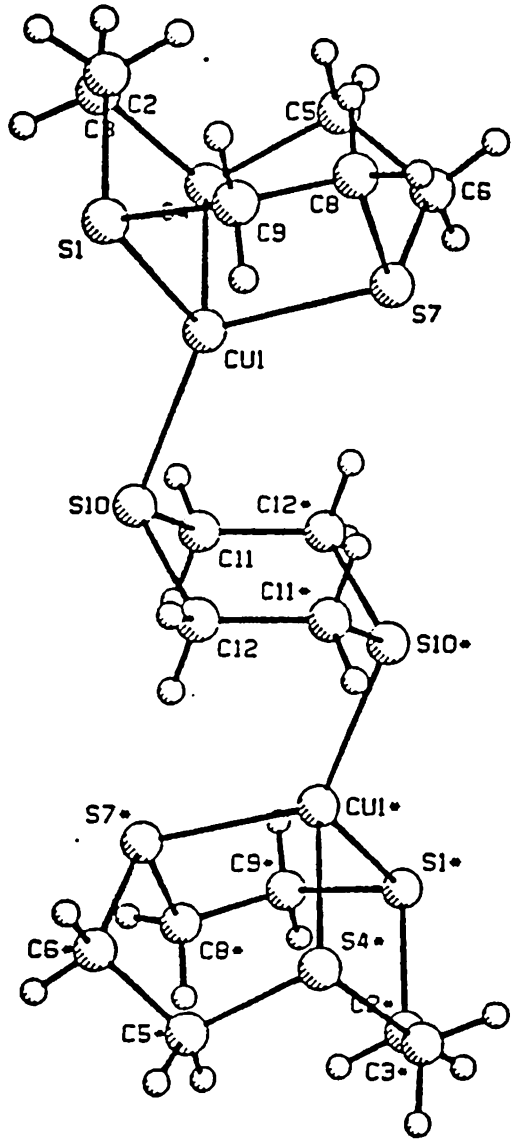

Figure 5.4. Crystal structure of $[(Cu^{I}(TTCN))_2(1,4\text{-dithiane})]$ cation (PLUTO drawing).

a significant effect of the smaller ring size of TTCN on the positioning of the metal ion facially coordinated to the tridentate TTCN ring. The relatively longer bonds between Cu(I) and the tridentate TTCN sulfurs indicate that the small size of the ring prevents the metal atom from approaching closely to the coordination sites on the ligand. This is in accordance with the conclusion arrived at by Busch and coworkers[5] that the tetrathia crown ether must contain 14 atoms to be wide enough to accommodate a first row transition metal ion such as Cu(II). TTCN being the smallest crown thioether can afford only facial coordination. This would result in smaller intraligand and larger interligand S-Cu-S bond angles which is obvious from Table A4.3. Consequently the complex would have a compressed coordination geometry which might also be playing a role in the spectral properties of the $[Cu^{II}(TTCN)_2]$ chromophore which apparently lacks the Jahn-Teller distortion as discussed in Chapter 4.

NMR Spectroscopy of $[Cu^{I}(TTCN)_2]$.

NMR spectra of the title complex were run at room temperature in CD_3CN, $(CD_3)_2SO$, CD_2Cl_2, and D_2O. Virtually no difference in the spectral behavior was noticed as the solvent was changed. Further studies were then carried out in CD_3CN to see the effect of concentration as well as temperature on the NMR spectral properties of $[Cu^{I}(TTCN)_2]$.

The effect of concentration. Both H^1 and C^{13} NMR spectra of $[Cu^{I}(TTCN)_2]$

in deuterated acetonitrile indicated dependence of the line width ($\Delta\nu$) on the concentration of the complex as well as the presence of free TTCN added to the solution. The results are listed in Table 5.1.

[complex] (mM)	[TTCN] (mM)	$\Delta\nu$ (H^1) (Hz)	$\Delta\nu$ (C^{13}) (Hz)
2.0	-	13.6	-
10.0	-	3.8	13.7
100.0	-	1.2	2.1
5.0	12.0	2.4	-
12.0	12.0	2.2	6.6
100.0	100.0	0.9	1.3

Table 5.1. Variation of the NMR line width with $[Cu^{I}(TTCN)_2]$ and [TTCN] in deuterated acetonitrile at room temperature.

The effect of temperature. The H^1 NMR spectrum of $[Cu^{I}(TTCN)_2]$ in CD_3CN as a function of temperature is shown in Figure 5.5. It is obvious from Figure 5.5 that as the temperature is lowered, the peak begins to broaden. The broadening of the peak continues initially and then begins to resolve into 3 bands around 243°K. $\Delta\nu$ at the coalescence temperature corresponds to 175 Hz. The three bands can be ultimately resolved at 225°K below which the solution freezes. From the integral, the ratio between the peaks was determined to be 12:7:5.

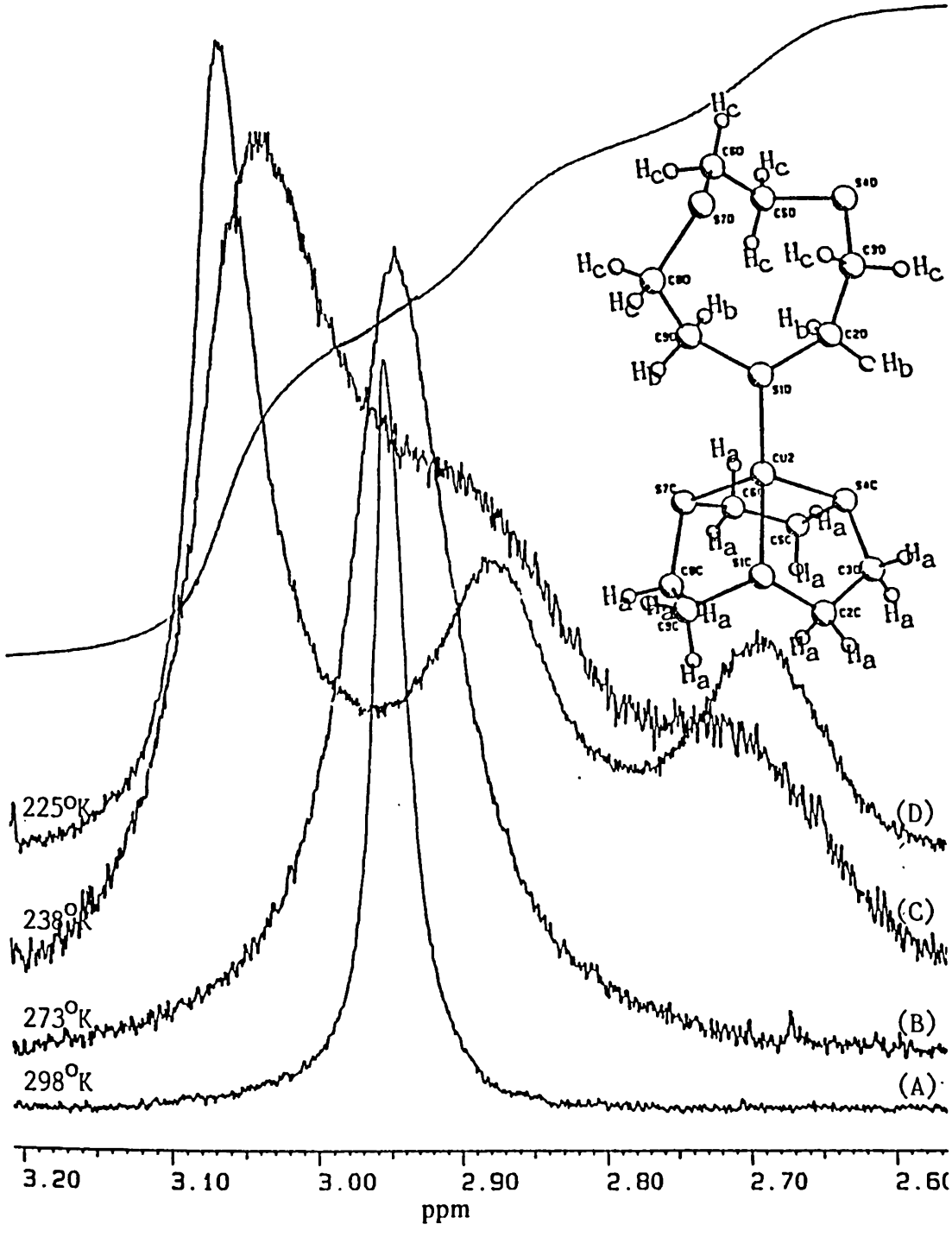

Figure 5.5. Variation of the proton magnetic resonance spectra of $[Cu^{I}(TTCN)_2]$ with temperature in deuterated acetonitrile. (A) 298°K (B) 273°K (C) 238°K (D) 225°K

At the coalescence temperature the residence time (τ_{Res}) is given by $\tau_{Res} = (\pi\Delta\nu\sqrt{2})^{-1}$ or ca. 1.3 ms. This would correspond to a first order rate constant of ca. 385 s^{-1} ($k_1 = 1/(2\tau_{Res})$). The approximate value for the free energy of activation ($\Delta G^{\ddagger}$) was calculated to be 11.25 kcal mol^{-1} by employing the following equation[6].

$$\Delta G^{\ddagger} = 2.303\ RT(10.319 + \log T - \log k_1) \qquad (5.9)$$

Caution: These are very crude estimates and may not have quantitative significance. Nevertheless, qualitatively the NMR studies demonstrate clearly the existence of an extremely fluxional conformation of the complex.

Electrochemistry of Copper-TTCN Complexes under Modified Conditions.

The effect of pH and concentration.

$[Cu^{II}(TTCN)_2]$: The coordination of TTCN to Cu(II) has been shown to be exceptionally stable. This complex was studied spectrophotometrically at different pH values in the range of pH 3 - 11 over a period of 24 h. No detectable changes in the spectral behavior were noticed in the visible region. However the complex precipitated at neutral and basic pH, causing a little decrease in pH. Cyclic voltammetry of the complex did not show any change with pH except for a decreased voltammetric current at neutral or basic pH. This could be ascribed to the decrease in concentration due to the precipitation.

$[Cu^{I}(TTCN)_2]$: Unlike the $[Cu^{II}(TTCN)_2]$ complex, $[Cu^{I}(TTCN)_2]$ does not precipitate at higher pH and its electrochemistry is very sensitive to changes in the

pH. Figure 5.6 shows a number of voltammograms of $[Cu^{I}(TTCN)_2]$ run under different pH conditions.The negative shift in the formal potential with increasing pH in Fig 5.6 is a clear indication of the involvement of pH in the electron transfer

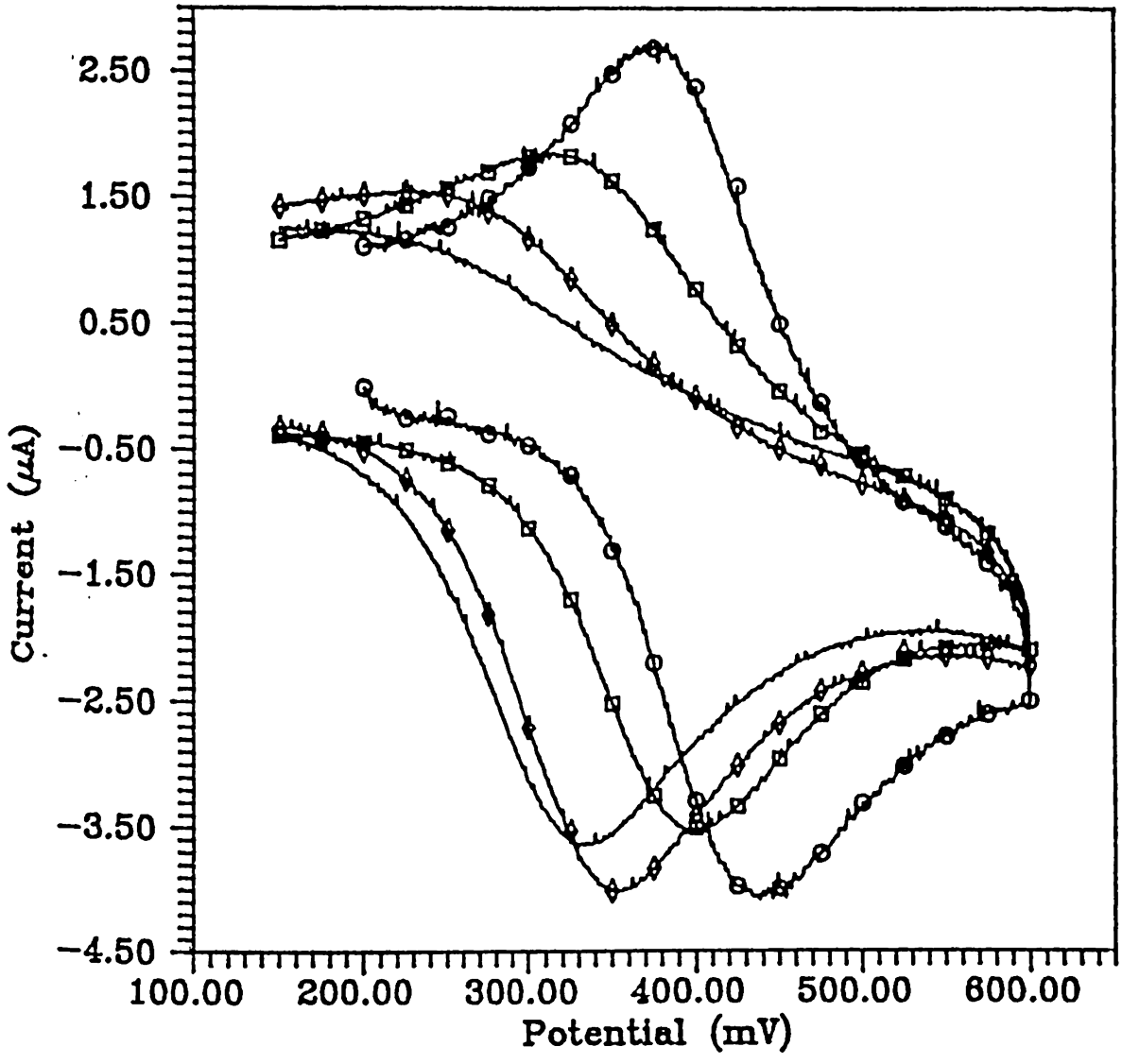

Figure 5.6. Variation of the cyclic voltammograms of $[Cu^{I}(TTCN)_2]$ with pH (0.1 M in $NaBF_4$ at glassy carbon vs Ag/(AgCl, Satd. NaCl). (○○○) pH 3; (□□□) pH 6; (◊◊◊) pH7; (—) pH 8.5.

mechanism of the complex. Also the incremental suppression and finally the disappearance of the reverse (cathodic) peak with increasing pH suggests drastic chemical changes in the molecule following the ET step.

Although there is a minor negative shift in the anodic peak potential with increasing concentration of $[Cu^{I}(TTCN)_2]$ but the shift is not significant enough to provide any mechanistic conclusions. The same may be said of the cathodic peak potential.

The effect of structural variations.

Electrochemistry of [Cu^{I}(TTCN)(SODTCN)] (1.5). Like $[Cu^{I}(TTCN)_2]$, the cyclic voltammetry of $[Cu^{I}(TTCN)(SODTCN)]$ did not show any significant dependence on the concentration of the complex. The trend in variation in the cyclic voltammograms as a function of pH was also the same for both $[Cu^{I}(TTCN)_2]$ and $[Cu^{I}(TTCN)(SODTCN)]$.

However the striking difference in the electrochemistry of the two molecules is evident from Figure 5.7. Figure 5.7 also shows that the cathodic peaks for $[Cu^{I}(TTCN)_2]$ (Figure 5.7A) and $[Cu^{I}(TTCN)(SODTCN)]$ (Figure 5.7B) coincide. This could indicate a common reducible species resulting from the oxidation of either one of these complexes. Figure 5.7 further shows that these peaks also coincide with the cathodic peak corresponding to $[Cu^{II}(TTCN)_2]$ (Figure 5.7C), therefore, $[Cu^{II}(TTCN)_2]$ could possibly be the common intermediate.

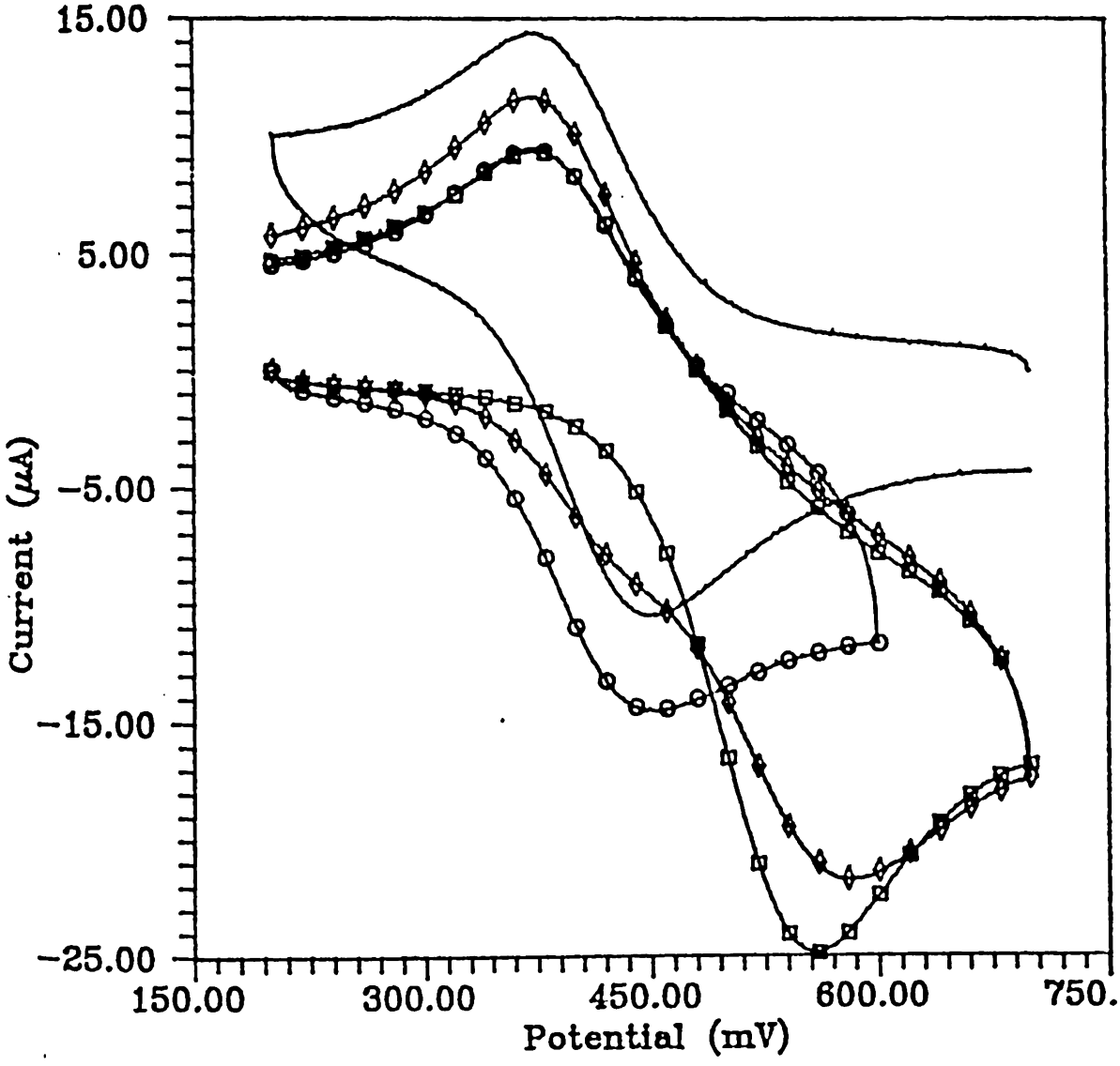

Figure 5.7. Cyclic voltammograms of (A) $[Cu^{I}(TTCN)_2]$ (ooo); (B) $[Cu^{I}(TTCN)(SODTCN)]$ (□□□); (C) $[Cu^{II}(TTCN)_2]$ (—); (D) $[Cu^{I}(TTCN)(SODTCN)]$ + TTCN (◊◊◊) (0.1 M in $NaBF_4$, pH 3 at glassy carbon vs Ag/(AgCl, Satd. NaCl).

Figure 5.7D shows the voltammogram of $[Cu^{I}(TTCN)(SODTCN)]$ run in the presence of free TTCN. It is interesting to see a new anodic wave exactly at the same position as that of $[Cu^{I}(TTCN)_2]$ besides the one at higher potential corresponding to the oxidation of the original complex.

Figure 5.8 shows cyclic voltammograms of 0.5 mM [Cu^{I}(TTCN)(SODTCN)] solution before electrolysis (A); after oxidative exhaustive electrolysis (B); and after reductive re-electrolysis of the oxidatively electrolyzed solution (C).

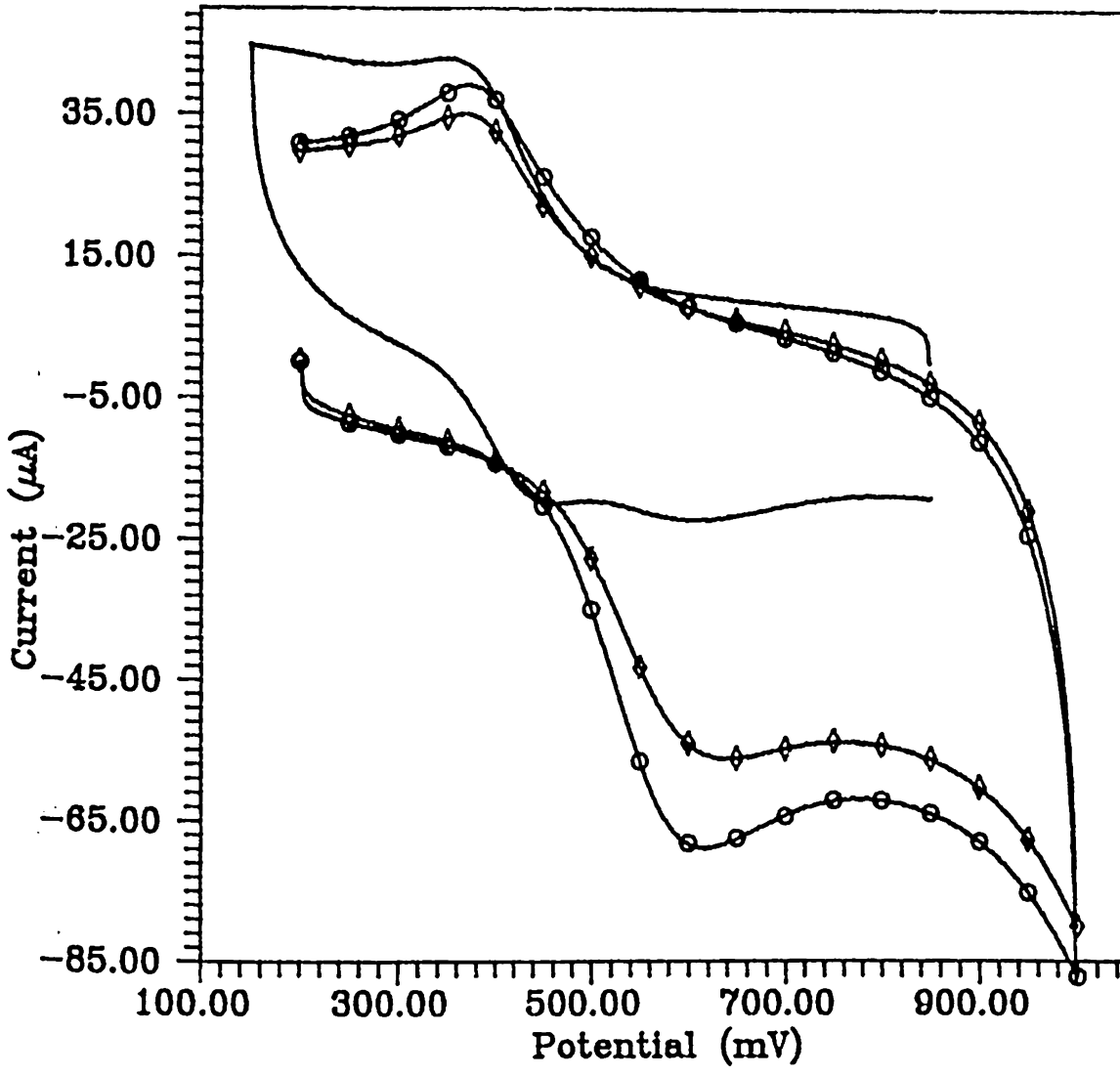

Figure 5.8. Cyclic voltammograms of [Cu^{I}(TTCN)(SODTCN] (A) before electrolysis (ooo); (B) after electrolysis (—) (C) after re-electrolysis of B (◊◊◊) (0.1 M in $NaBF_4$, pH 3 at glassy carbon vs Ag/(AgCl, Satd. NaCl).

[(TTCN)Cu^{I}(1,4-dithiane)Cu^{I}(TTCN)] (1.6) and [Cu^{I}(TTCN)(THT)] (1.7). The cyclic voltammograms of **1.6** and **1.7** were run in 0.1 M $NaBF_4$ aqueous solution on glassy carbon vs Ag/(AgCl, satd. NaCl) at pH 3. The voltammograms of both **1.6** and **1.7** were virtually the same as those of **1.5** under the same set of conditions.

Pulse Radiolysis of the Copper-TTCN Complexes.

Reaction of hydroxyl radicals with [Cu(I)(TTCN)$_2$].

Optical spectra. Pulse irradiation of N_2O-saturated water leads to the formation of hydroxyl radicals and hydrogen atoms with the radiation chemical yields G = 6.0 and G = 0.6, respectively (the G-value denotes the number of species produced per 100 eV absorbed energy; G = 1.0 corresponds to 0.1036 μM species per 1 J absorbed energy). Application of 1.55 MeV electron pulse of ca. 1 μs duration to N_2O-saturated 1.0×10^{-4} M [Cu^{I}(TTCN)$_2$] aqueous solution at pH 4.0 resulted in an optical absorption band with λ_{max} at 365 nm immediately after the pulse (Figure 5.9, band A) which subsequently decayed with first order kinetics characterized by $\tau_{1/2}$ = 4.7 ms and a radiation chemical yield, $G \times \varepsilon_{365}$ = 15,400 ± 1,100 M^{-1} cm^{-1}. The decay is followed by the build-up of another absorption band with λ_{max} = 445 nm which had a radiation chemical yield $G \times \varepsilon_{445}$ = 31,625 ± 1,375 M^{-1} cm^{-1} (Figure 5.9, band B). [Cu^{II}(TTCN)$_2$] is known to have λ_{max} at 445 nm with ε_{445} = 4,692 M^{-1} cm^{-1}, therefore the 445 nm band is assigned to [Cu^{II}(TTCN)$_2$] chromophore[7].

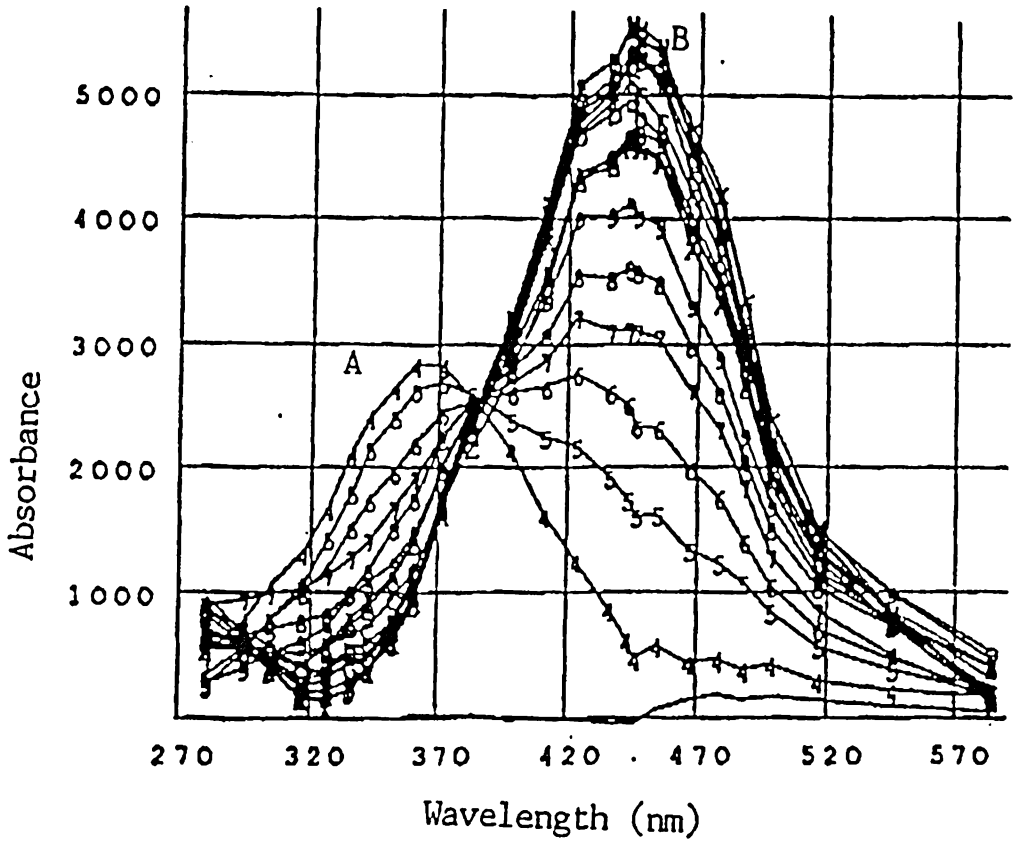

Figure 5.9. Time resolved spectra of the pulse irradiated N_2O-saturated 1.0×10^{-4} M $[Cu^{I}(TTCN)_2]$ solution at pH 4.0 as a function of time.

The presence of a single isosbestic point at $\lambda = 395$ nm suggests that the species absorbing at 365 nm converts into the species absorbing at 445 nm ($[Cu^{II}(TTCN)_2]$) in a 1:1 stoichiometry. From the $G \times \varepsilon_{445}$, $G_{[Cu^{II}(TTCN)2]}$ can be calculated to be 6.7 ± 0.3. This is equal to the sum of the radiation chemical yields of both hydroxyl radical and hydrogen atom. Preliminary results from a separate set of experiments have shown that, indeed, the reaction of hydrogen atoms with $[Cu^{I}(TTCN)_2]$ leads to the formation of $[Cu^{II}(TTCN)_2]$. The underlying mechanisms are, however, different. It is evident though that the formation of $[Cu^{II}(TTCN)_2]$ by

the oxidation of $[Cu^{I}(TTCN)_2]$ proceeds, as evidenced by the pulse radiolysis, via a relatively long-lived intermediate absorbing at λ_{max} = 365 nm. From now on the transient species absorbing at 365 nm is referred to as $[Cu^{II}(TTCN)L]$.

Variation of the concentration of $[Cu^{I}(TTCN)_2]$. Variation of the initial concentration of $[Cu^{I}(TTCN)_2]$ did not alter the characteristic features of the optical absorption. Also no influence on the yield and rate of formation of the 365 nm species ($[Cu^{II}(TTCN)L]$) was observed over a concentration range of 2.5×10^{-5} - 3×10^{-4} M $[Cu^{I}(TTCN)_2]$. However, both the yield and the formation kinetics of the 445 nm species ($[Cu^{II}(TTCN)_2]$) were affected such that higher yields and faster rates of formation of $[Cu^{II}(TTCN)_2]$ were obtained at higher initial concentrations of $[Cu^{I}(TTCN)_2]$. The respective yields of both $[Cu^{II}(TTCN)L]$ and $[Cu^{II}(TTCN)_2]$ are listed in Table 5.2.

	Yield (G = 5.5)		
$[Cu^{I}(TTCN)_2]$	365 nm	445 nm	445:365
2.5×10^{-5} M	1400	2400	1.7
5.0×10^{-5} M	1600	3100	1.9
7.5×10^{-5} M	1600	4000	2.5
1.0×10^{-4} M	2600	6000	2.3

Table 5.2. Radiation chemical yields of $[Cu^{II}(TTCN)L]$ and $[Cu^{II}(TTCN)_2]$

Variation of pH. Pulse radiolysis of N_2O-saturated 1×10^{-4} M $[Cu^{I}(TTCN)_2]$ aqueous solution did not show any significant change in the yields or kinetics of the

species discussed so far in the pH range of 3.0 - 5.0 (G x ε = 31,625 ± 1,375). However at pH 6.0 the final yield of $[Cu^{II}(TTCN)_2]$ reduced drastically (G x ε = 4,400 M^{-1} cm^{-1}) whereas the initial yield as well as the rate constant for the decay of species $[Cu^{II}(TTCN)L]$ remained unaffected. No change in specific conductivity of the solution concurrent with the formation of $[Cu^{II}(TTCN)L]$, was observed. At pH > 6 the intermediate $[Cu^{II}(TTCN)L]$ is still formed however the yield of $[Cu^{II}(TTCN)_2]$ is negligible.

$[Cu^{I}(TTCN)_2]$ in the presence of excess TTCN. Pulse irradiation of N_2O-saturated aqueous solution, pH 4.0, which is 5.0 x 10^{-5} M in $[Cu^{I}(TTCN)_2]$ and 2 x 10^{-4} M in TTCN, generated the transient spectrum, immediately after the pulse (Figure 5.10A). This spectrum shows the absorption band characteristic of species $[Cu^{II}(TTCN)L]$ and an additional absorption peak at λ_{max} = 540 nm. The absorption at 540 nm is assigned to the three-electron sulfur-sulfur bonded radical cation[8] formed by the reaction of the hydroxyl radical with free TTCN (Eq. 5.10).

$$HO^{\bullet} + TTCN \rightarrow [>S\therefore S^{+}<]_{TTCN} + {}^{-}OH \qquad (5.10)$$

The final yields of $[Cu^{II}(TTCN)L]$ in this process is G x ε = 11,550 M^{-1} cm^{-1}. However the ratio of species $[Cu^{II}(TTCN)L]$ and $[>S\therefore S^{+}<]_{TTCN}$, formed immediately after the pulse, depended both on the initial concentration of $[Cu^{I}(TTCN)_2]$ and TTCN.

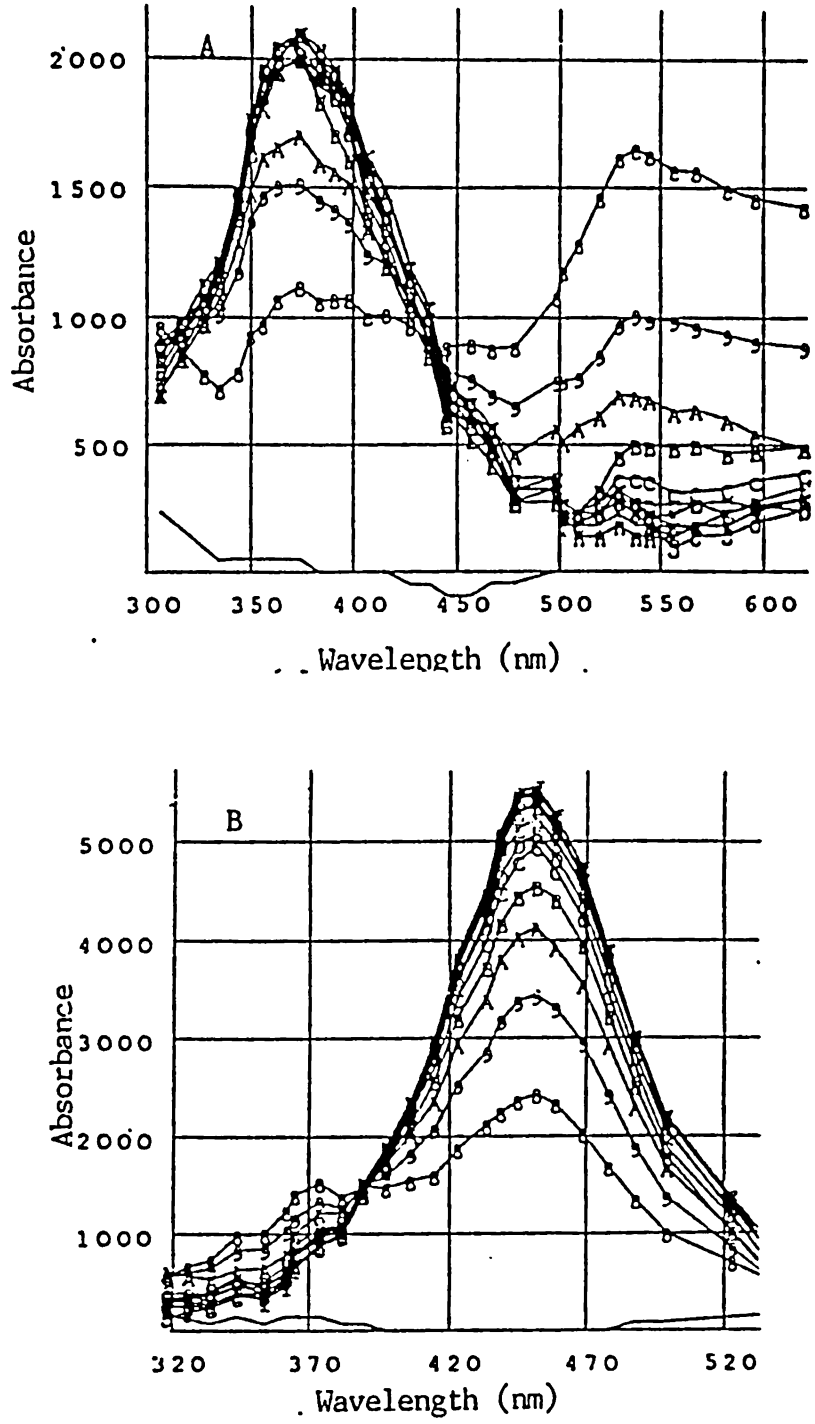

Figure 5.10. Time resolved spectra of the pulse irradiated N_2O-saturated aqueous solution which is 5 x 10^{-5} M in $[Cu^{I}(TTCN)_2]$ and 2 x 10^{-4} M in TTCN at pH 4.0 as a function of time. (A) Short time scale (200 μs); (B) long time scale (100 ms).

The disappearance of TTCN radical cation followed first-order kinetics with concomitant formation of species $[Cu^{II}(TTCN)L]$. Subsequently, on a slower time-scale, $[Cu^{II}(TTCN)L]$ converts into $[Cu^{II}(TTCN)_2]$ with first order kinetics being dependent on the concentration of TTCN (Figure 5.10B). A plot of the observed first-order rate constant vs [TTCN] yielded a straight line the slope of which corresponded to a rate constant of 8.4×10^5 M^{-1} s^{-1}.

$[Cu^{I}(TTCN)_2$ in the presence of excess dimethylsulfide (DMS) and diethylsulfide (DES). Similar results as with free TTCN are obtained if $[Cu^{I}(TTCN)_2]$ is oxidized in the presence of excess DMS or DES. Pulse irradiation of N_2O-saturated aqueous solution, pH 4.0, 1.0×10^{-4} M in $[Cu^{I}(TTCN)_2]$ and 1.0×10^{-3} M in DES led primarily to the formation of the characteristic dimeric radical cation from DES (reaction 5.11) and subsequently to $[Cu^{II}(TTCN)_2]$ via $[Cu^{II}(TTCN)L]$.

$$HO^{\cdot} + 2\ (H_5C_2)_2S \rightarrow (H_5C_2)_2S\therefore S(C_2H_5)_2]^{+} + {}^{-}OH \qquad (5.11)$$

Other Copper(I)-thioether complexes

$[(TTCN)Cu^{I}$(1,4-dithiane)$Cu^{I}(TTCN)]$ (1.6) and $[Cu^{I}(TTCN)(THT)]$ (1.7). Pulse irradiation of N_2O-saturated 1.0×10^{-4} M solution of **1.6** at pH 4 resulted in the formation of species $[Cu^{II}(TTCN)L]$ with full radiation chemical yield, ($G \times \varepsilon$ = 11,550 ± 1,650 M^{-1} cm^{-1}). The transient decayed with a half life ($\tau_{1/2}$) of 23 ms into yet an unidentified product without the formation of $[Cu^{II}(TTCN)_2]$. However, the same experiment carried out in the presence of additional amounts of free TTCN (1.0

x 10^{-4} M) produced [$Cu^{II}(TTCN)_2$] with full radiation chemical yield. Similar results were obtained from the pulse radiolysis of **1.7**.

[Cu^{I}(HTCOD)] (1.8). Pulse irradiation of N_2O-saturated 1.0 x 10^{-4} M solution of **1.8** at pH 4 leads to the formation of a species, within 5 μs after the pulse, which absorbs at λ_{max} = 450 nm. No stable intermediate is observed at 365 nm. Nevertheless, monitoring of the absorbance vs time trace at 386 nm revealed a species absorbing at this wavelength. This transient species is formed within a time period much shorter (ca. 1 μs) than the time required for the complete build-up of the spectrum which peaks at λ_{max}= 450 nm. This may imply that in the wake of radiolysis a species comparable with [Cu^{II}(TTCN)L] might be formed which decays rather rapidly to a stable compound which absorbs at λ_{max}= 450 nm. Similar observations were made at pH 8.5. Thus the oxidation of **1.8** apparently does not show any dependence on pH unlike the copper(I)-TTCN complexes. The spectral similarity of the end product of the oxidation of **1.8** and the copper(I)-(TTCN) complexes suggest that the oxidation of **1.8** leads to the formation of a species, most probably [Cu^{II}(HTCOD)], which has a primary coordination sphere comparable with that of [$Cu^{II}(TTCN)_2$].

Discussion

Despite their different stereochemical properties [$Cu^{II}(TTCN)_2$] and [$Cu^{I}(TTCN)_2$] are cyclic voltammetrically indistinguishable from each other at pH 3. This can be ascribed to the easy availability of the sulfurs and the suitable endodentate

conformation of TTCN for the coordination of Cu(II) at six sites, on one hand, and sufficient flexibility of the ring accompanied by the "soft" nature of sulfur suitable for Cu(I) coordination at 4 sites on the other hand. The lack of sensitivity of the cyclic voltammograms of $[Cu^{II/I}(TTCN)_2]$ system toward the concentration of the analyte apparently advocates such versatility of the coordination sphere of the system.

The fact that a basic aqueous solution of the Cu(I) complex, left exposed to air, did not develop any color over a period of more than a month indicates that the complex is resistant to autoxidation at higher pH. A similar test at pH ~ 3 developed a yellow color over a period of several hours and a solution of the complex in 1% HBF_4 turned yellow immediately. These observations suggest that although the coordination of Cu(I) to four thioether sulfurs provides high thermodynamic stability to Cu(I) state as manifested in the relatively high redox potential of the $[Cu^{II/I}(TTCN)_2]$ complex, its kinetic stability might change with pH. Since the $^{\cdot}OH$ or H_2O are not favorite ligands for Cu(I), they may not be posing any threat to the integrity of the complex as long as it remains in Cu(I) state. However the inherent tendency of TTCN to be predominantly in the [3 3 3] endodentate conformation would tend to favor Cu(II) state by putting 6 ligand sites around the metal ion. In basic, neutral, or slightly acidic solutions this effect could be counteracted by necessity of competition of thioether sulfurs with the more favored *oxo* ligands for Cu(II). Under very acidic conditions the uncoordinated sulfurs can attack very easily, providing a driving force for the oxidation of $[Cu^{I}(TTCN)_2]$ complex.

The presumed conformational versatility of the coordination sphere can be hampered by occupying the fourth coordination site on Cu(I) by a thioether ligand which cannot provide the favorable macrocyclic stabilizing effect (complexes **1.5 - 1.7**). The crystallographic data has shown that the Cu — S (monodentate TTCN) distance compares well with that of any other monodentate thioether reported here as well as with that reported by Clarkson *et al*[9]. This indicates that at least in the solid state monodentate coordination of TTCN or SODTCN to Cu(I) is not very different from that of simple thioethers.

It is obvious from Figure 5.7 that the coordination of SODTN renders the system less reversible and harder to oxidize. This can be ascribed to the structural constraints imposed on the ligand by converting one of the three sulfurs to sulfoxide. The effect of sulfoxidation on the conformation of the ring can be appreciated by comparing the C — SO bond distance (1.92 ± 0.01 Å) and the ∠ C(SO)C bond angle (96.0 ± 0.3°) in SODTCN with those of the monodentate TTCN ring (1.82 ± 0.01 Å and 103.0 ± 0.9° respectively). The presence of oxygen on sulfur along with conformational distortion in the ring could make it harder for SODTCN ring to revert to a conformation suitable for the facial coordination. Therefore, the effect of coordination of SODTCN to Cu(I) would be to make the oxidation of [Cu^{I}(TTCN)(SODTC)] harder. Because SODTCN is apparently incapable of adopting the appropriate endodentate conformation, the oxidation of [Cu^{I}(TTCN)(SODTCN)] would result in a substitutionally labile Cu(II) complex. Consequently this would

constitute an electrochemically irreversible system.

Unlike the cyclic voltammetry pulse radiolysis experiments on a much shorter time scale indicated a remarkable influence of the concentration of $[Cu^{I}(TTCN)_2]$ on the formation kinetics of $[Cu^{II}(TTCN)_2]$. This obviously suggests that the latter is not merely formed via the conformational rearrangement of TTCN ligands within the coordination sphere of species $[Cu^{II}(TTCN)L]$ but involves a second $[Cu^{I}(TTCN)_2]$. Since the redox process is not followed by an intramolecular reorganization, therefore, conformational versatility may not be a controlling factor in defining the redox properties $[Cu^{II/I}(TTCN)_2]$ system.

Figure 5.11 shows plots of the first-order rate constants as a function of the concentration of $[Cu^{I}(TTCN)_2]$ for the decay of the 365 nm band (Figure 5.11A) and the development of the 445 nm band (Figure 5.11B). From the slopes of the straight lines, bimolecular rate constants are calculated as $k_{(\lambda 365)} = 5.3 \times 10^5\ M^{-1}\ s^{-1}$ and $k_{(\lambda 445)} = 5.1 \times 10^5\ M^{-1}\ s^{-1}$ for the conversion of the species absorbing at 365 nm into $[Cu^{II}(TTCN)_2]$. The intercept corresponds to an unimolecular process with $k = 40\ s^{-1}$. Such a dependence of the pulse radiolysis results on the concentration of $[Cu^{I}(TTCN)_2]$ can be explained by invoking reactions 5.12 - 5.15.

$$HO^{\bullet} + [Cu^{I}(TTCN)_2] \rightarrow [Cu^{II}(TTCN)L] \qquad (5.12)$$

$$[Cu^{II}(TTCN)L] + [Cu^{I}(TTCN)_2] \rightarrow [Cu^{II}(TTCN)_2] + [Cu^{I}(TTCN)L] \qquad (5.13)$$

$$[Cu^{II}(TTCN)L] \rightarrow [Cu^{II}(TTCN)_2] \qquad (5.14)$$

$$[Cu^{II}(TTCN)L] \rightarrow \text{Other Products} \qquad (5.15)$$

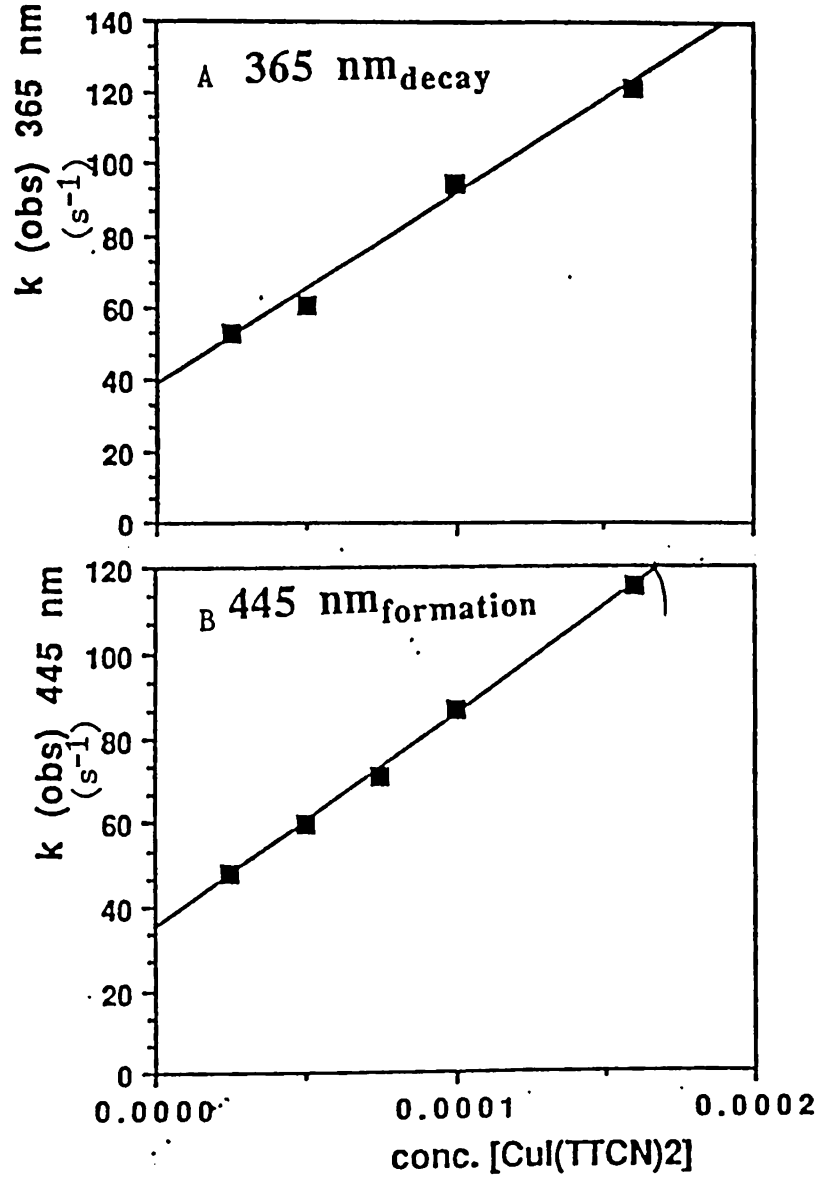

Figure 5.11. Plots of the first-order rate constants as a function of the concentration of $[Cu^{I}(TTCN)_2]$ for the decay of the 365 nm band (A) and the development of the 445 nm band (B).

The formation of $[Cu^{II}(TTCN)L]$ did not depend on the pH of the medium up

to pH 5 but at pH ≥ 6 the formation of $[Cu^{II}(TTCN)_2]$ was progressively suppressed until it became negligible. This clearly suggests the involvement of protons in the production of $[Cu^{II}(TTCN)_2]$. Therefore, the formation of $[Cu^{II}(TTCN)_2]$ represented by Eq. 5.13 rather requires a protonation step and can accordingly be written as Eq. 5.16.

$$[Cu^{II}(TTCN)L] + [Cu^{I}(TTCN)_2] \xrightarrow{H^+} [Cu^{II}(TTCN)_2] + [Cu^{I}(TTCN)L] \quad (5.16)$$

Under the conditions where protonation essentially does not occure (pH ≥ 6), the species $[Cu^{II}(TTCN)L]$ undergoes a decay via different mechanisms which do not lead to the formation of $[Cu^{II}(TTCN)_2]$. The rate constant k_{16}, corresponding to reaction 5.16 can be calculated from the slope of Figure 5.12 to be $(5.2 \pm 0.1) \times 10^5$ M^{-1} s^{-1} whereas the intercept represents $k_{14} + k_{15} = 40$ s^{-1}.

Upon oxidation of $[Cu^{I}(TTCN)_2]$, the singly coordinated exodentate TTCN has to regain the endodentate conformation before it can compete effectively with *oxo* ligands (H_3O^+, H_2O, ^-OH) for coordination. Cu(II) complexes are inherently labile and specially thioethers coordinate very weakly to Cu(II) in dipolar solvents[10]. Since the exodentate TTCN does not inhibit the substitution immediately after the oxidation of the complex, it is possible that the oxidation might be immediately followed by the formation of a transitory substitution product before TTCN can regain the endodentate conformation. Another explanation is that the high electron density on Cu(I) forces one of the TTCN units to switch to the exodentate conformation normally prevented

by the small size of TTCN ring which would tend to keep it endodentate. These competing forces might be balanced by a constant conformational flux either through an exchange of conformation between the two conformationally different ligands or through an exchange of coordination site on the same ligand or an intricate combination of the two. Upon oxidation such a fluxional conformation of the complex might be interrupted by the formation of a transitory (depending on the experimental conditions) substitution product. This concept of fluxional conformation has been supported by variable temperature NMR studies in acetonitrile.

The dependence of the NMR line width on the concentration of $[Cu^{I}(TTCN)_2]$ or TTCN at room temperature (Table 5.1) is too complicated to be unequivocally explained. The reason for the complex relationship could be that at room temperature several kinetic processes are operative. (i) The intramolecular exchange of conformation between the monodentate and tridentate TTCN ligands. (ii) The exchange of coordination sites on the monodentate ligand. (iii) The intermolecular exchange of the monodentate ligand between two $[Cu^{I}(TTCN)_2]$ complex ions which could be either through an associative (A) or a dissociative (D) process. (iv) Substitution of the monodentate TTCN by the solvent (CD_3CN). However the consistency of the spectral properties in a variety of solvents minimizes the significance of the solvent in the kinetics of the system. The observed dependence of the NMR line width on the concentration may be due to the presence of a relatively slow dissociative mechanism compared to the intramolecular conformational

rearrangements. The presence of excess ligand or complex in solution might have the effect of reversing this process rather than enhancing the exchange process so as to localize the resonance.

The effect of lowering the temperature on the NMR spectral properties of the system (Figure 5.5) can provide some useful qualitative information. The fact that one can see only one peak at temperature > -30°C in a system in which the two TTCN units would seem to have different conformations could indicate a fast conformational flux both within the monodentate ligand and between the monodentate and the tridentate ligands. This flux can be frozen by further lowering the temperature which has nicely been demonstrated by the resolution of the single peak into three bands with intensity ratio of 12:7:5. Thus the resonance at $\delta \simeq 3.05$ is assigned to the protons at the tridentate TTCN (H_a), at $\delta \simeq 2.68$ to the four Cu^I-SC α-protons (H_b) and the resonance at $\delta \simeq 2.86$ to the rest of the protons (H_c) (Figure 5.5).

The cyclic voltammetric data collected under different pH conditions provide further evidence in favor of the formation of a substitution product following the oxidation of $[Cu^I(TTCN)_2]$. The shift in the anodic peak potential can be ascribed predominantly to kinetic factors. Kinetically the effect of a chemical change following the ET step would be a continual consumption of the oxidation product which would obviously shift the potential profile of the oxidation peak to a less positive value. The disappearance of the cathodic peak with increasing pH may suggest that the oxidation step is followed by a chemical reaction involving $^{\cdot}OH$ and the product of this reaction

is a species which is electroinactive in the experimental potential range.

When cyclic voltammograms of $[Cu^{I}(TTCN)_2]$ were run in the presence of free TTCN, both the anodic and cathodic peaks shifted to less positive potential by about 10 mV with an apparent increase in the slope of the peaks. Due to its smaller size TTCN has a tendency to adopt the endodentate conformation. This conformation (ML_6 coordination) is the dominant mode of coordination in its complexes with a wide variety of metal ions. Consequently TTCN has greater affinity for Cu(II) than any other thioether which is reflected in the relatively less positive formal potential of $[Cu^{II/I}(TTCN)_2]$ system compared with the systems involving more flexible or acyclic thioethers[11,12]. The shift in the potential profile associated with the sharpening of the peaks can be explained if we assume that the oxidation step is followed by a dissociative chemical reaction. The presence of excess free TTCN will tend to suppress such a reaction.

All the observations and arguments presented so far suggest that in aqueous medium the oxidation of Cu(I)-TTCN complexes labilize the Cu-S (monodentate thioether) coordination. Consequently the monodentate thioether is substituted by an *oxo* ligand from the mediom (H_3O^+, H_2O, $^{\cdot}OH$) or through adduct fromation of $[Cu^{I}(TTCN)_2]$, for example, with $^{\cdot}OH$. The inertness/stability of this coordinate bond toward resubstitution by the thioether depends on the degree of protonation of the *oxo* ligand and hence on the pH of the medium. From these studies, however, it is still hard to decide whether the substitution takes place via an associative or dissociative

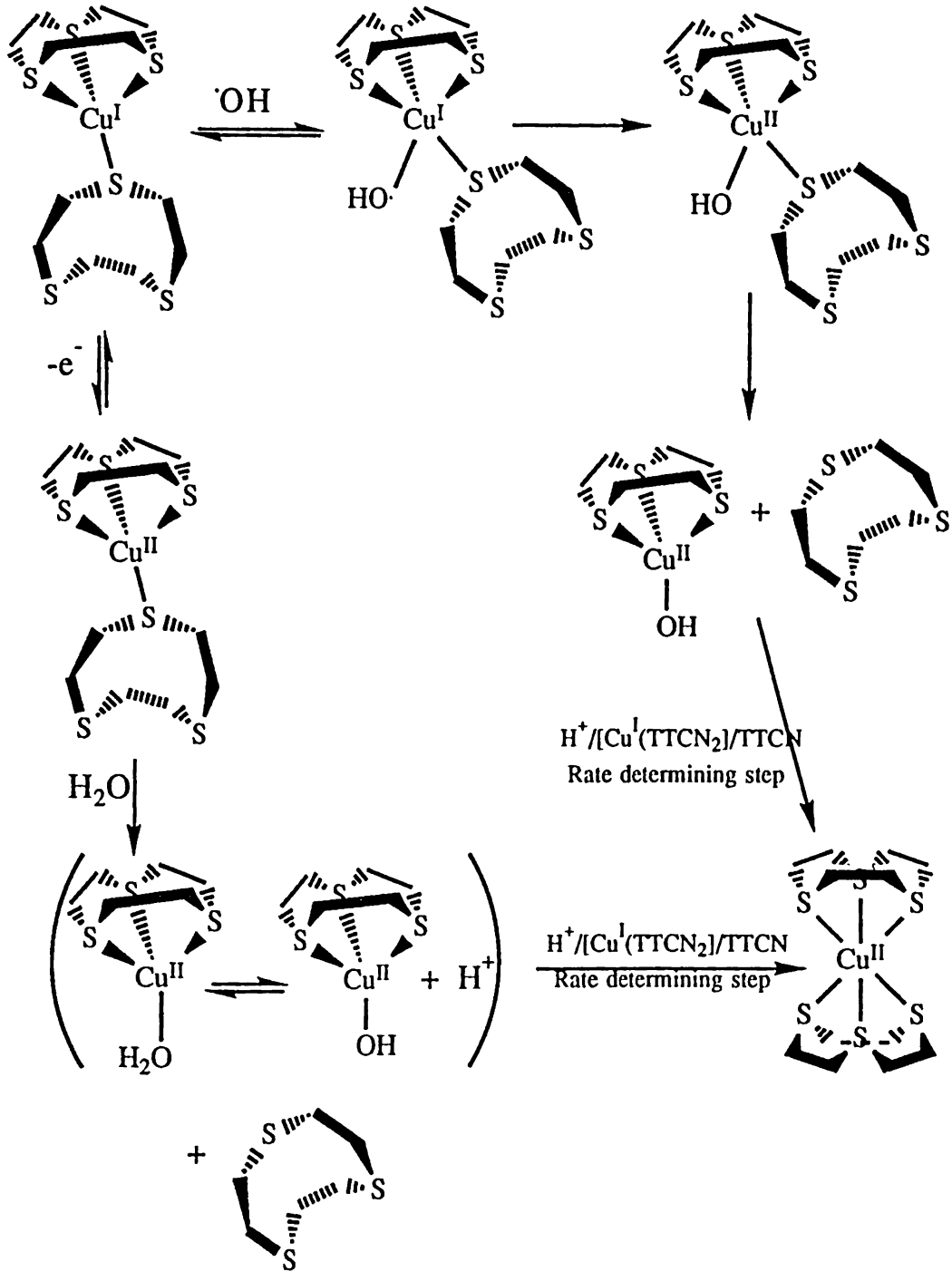

Scheme 5.1. The proposed mechanisms for the oxidation of $[Cu^{I}(TTCN)_2]$ by ·OH and by electrode.

mechanism. It is also possible that the oxidation by $^{\bullet}OH$ and by the electrode could proceed through basically different routes. Scheme 5.1 depicts the most probable mechanism of oxidation of $[Cu^{I}(TTCN)_2]$ based on these studies.

The latest studies have shown a transitory absorption band at 540 nm in the pulse radiolysis of $[Cu^{I}(TTCN)_2]$. This band can be ascribed to the sulfur-sulfur three-electron bonded radical cation of TTCN. It has been already mentioned that the kinetics of the decay of $[Cu^{I}(TTCN)L]$ strongly depend on the concentration of $[Cu^{I}(TTCN)_2]$. Therefore, the formation of the 540 nm species in the pulse radiolysis of pure $[Cu^{I}(TTCN)_2]$ can be justified in terms of the dissociation equilibrium: $[Cu^{I}(TTCN)_2] \rightleftharpoons [Cu^{I}(TTCN)H_2O] + TTCN$ [13]. Further studies are underway.

The intermolecular nature of the reaction following the oxidation of $[Cu^{I}(TTCN)_2]$ is strongly supported by experiments in which the oxidation with $^{\bullet}OH$ is carried out in the presence of excess free TTCN. $[Cu^{II}(TTCN)L]$,thus generated, subsequently converts to $[Cu^{II}(TTCN)_2]$ on a slower time scale (Figure 5.10B). The first-order kinetics of this conversion is dependent on the concentration of TTCN (Eq. 5.17).

$$[Cu^{II}(TTCN)L] \xrightarrow{H^{+}/TTCN} [Cu^{II}(TTCN)_2] \qquad (5.17)$$

A plot of the observed first-order rate constant vs [TTCN] gave a straight line. The slope of this line corresponds to the rate constant for reaction 5.17. In the presence of free TTCN the rate constant (k_{17}) for the formation of $[Cu^{II}(TTCN)_2]$ from

$[Cu^{II}(TTCN)L]$, regardless of its source, has almost a constant value which is 8.4 x 10^5 M^{-1} s^{-1} for $[Cu^{I}(TTCN)_2]$; 5.9 x 10^5 M^{-1} s^{-1} for $[(Cu^{I}(TTCN))_2(1,4\text{-dithiane})]$ and 7.2 x 10^5 M^{-1} s^{-1} for $[Cu^{I}(TTCN)(PMS)]$ as the starting material.

It is interesting to see that the formation of $[Cu^{II}(TTCN)L]$ from the pulse radiolysis of $[Cu^{I}(TTCN)_2]$ followed the same kinetics in the presence of excess DES and DMS as that in the presence of excess TTCN. This suggests that in the presence of excess TTCN, $[Cu^{II}(TTCN)L]$ is formed by the oxidation of $[Cu^{I}(TTCN)_2]$ by the TTCN radical cation (Eq. 5.10) according to reaction 5.18.

$$[>S\therefore S^{+}<]_{TTCN} + [Cu^{I}(TTCN)_2] \rightarrow TTCN + [Cu^{II}(TTCN)L] \qquad (5.18)$$

The rate constant for reaction 5.18 was obtained by plotting the observed first-order rate constant for the disappearance of TTCN radical cation as a function of $[Cu^{I}(TTCN)_2]$. The slope of the resulting straight line yielded $k_{18} = 2.0 \times 10^8$ M^{-1} s^{-1}. A similar reaction can be presented for the pulse radiolysis of $[Cu^{I}(TTCN)_2]$ in the presence of DES (Eq. 5.19).

$$(H_5C_2)_2S\therefore S(C_2H_5)_2]^{+} + [Cu^{I}(TTCN)_2] \rightarrow 2\,(H_5C_2)_2S + [Cu^{II}(TTCN)L] \qquad (5.19)$$

A plot of the observed first-order rate constant for the disappearance of the dimeric thioether radical cation and the build-up of species $[Cu^{II}(TTCN)L]$ as a function of

$[Cu^{I}(TTCN)_2]$ yielded $k_{19} = 2.0 \times 10^8\ M^{-1}\ s^{-1}$. Species $[Cu^{II}(TTCN)L]$ can then react with a second $[Cu^{I}(TTCN)_2]$ to yield $[Cu^{II}(TTCN)_2]$ (rate constant = $4.4 \times 10^5\ M^{-1}\ s^{-1}$).

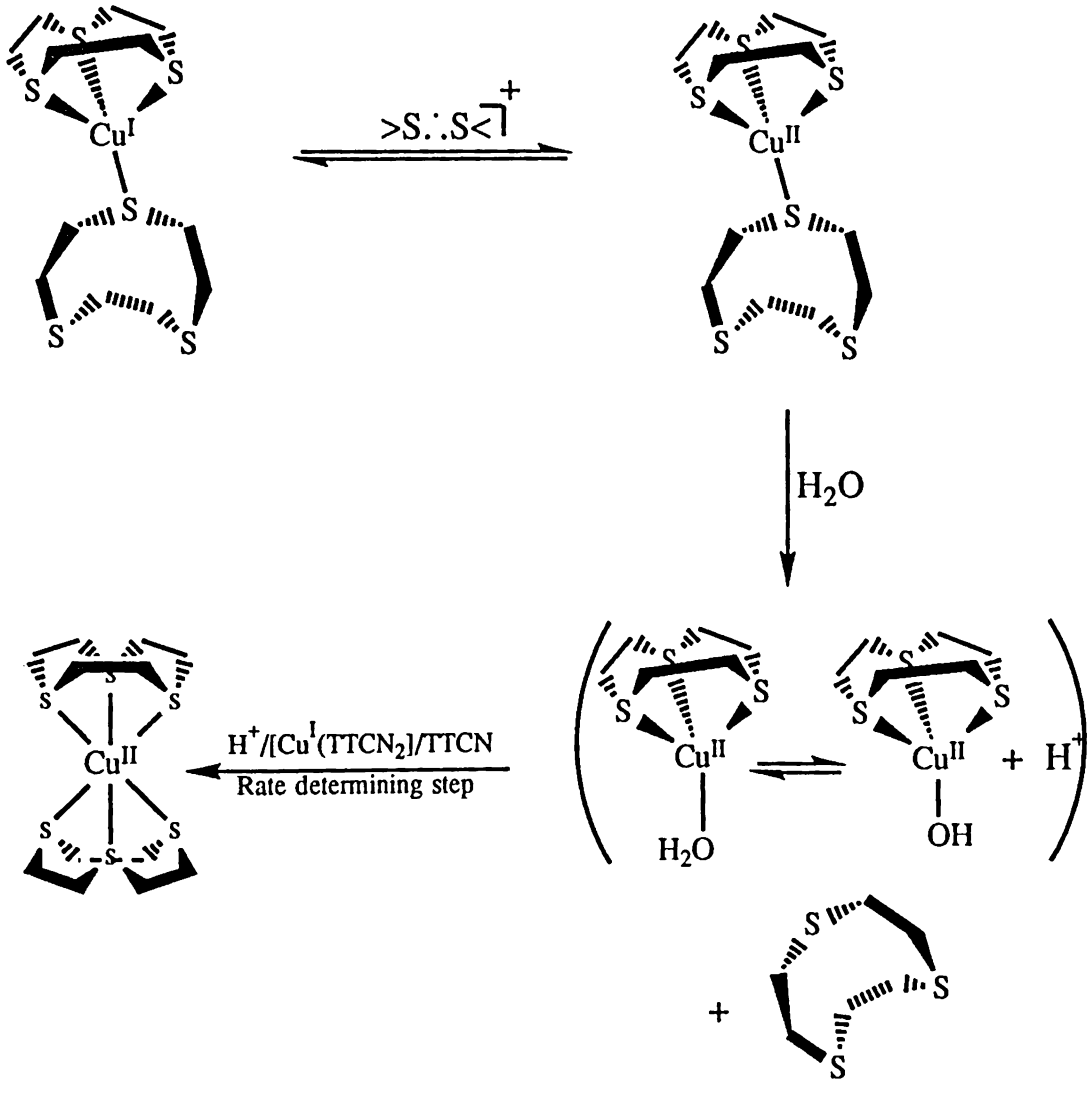

Scheme 5.2. The proposed mechanism for the oxidation of $[Cu^{I}(TTCN)_2]$ by >S.:S< radical cation, produced by pulse radiolysis of the free thioether.

The same sequence applies if DMS is employed instead of DES. Based on these observations the following mechanism is presented for the pulse radiolysis of $[Cu^{I}(TTCN)_2]$ in the presence of excess TTCN (Scheme 5.2). Nevertheless, Scheme 5.2 applies to complexes **1.6 - 1.8** as well as when excess DES or DMS is present.

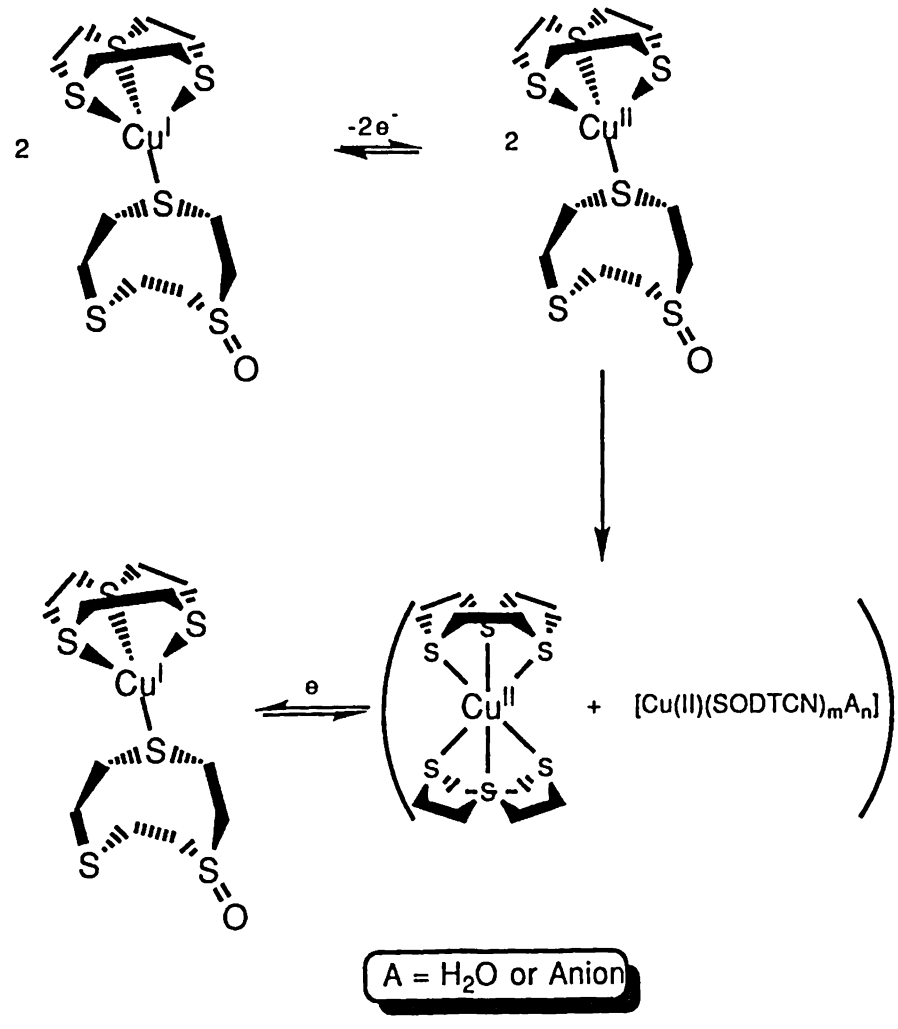

Scheme 5.3 The proposed mechanism for the heterogenous electron transfer reaction of $[Cu^{I}(TTCN)(SODTCN)$.

In Figure 5.8B one can obviously see that the exhaustive electrolysis of $[Cu^{I}(TTCN)(SODTCN)]$ results in the generation of new species which are electrochemically different from the original complex. This can be explained by assuming that upon oxidation Cu(II) cannot hold the conformationally strained SODTCN which can, therefore, be substituted by water or anion to form $[Cu^{II}(TTCN)A_3]$ (A = H_2O , anion). Two such units might interact to produce the kinetically stable $[Cu^{II}(TTCN)_2]$ and an unknown species as shown in Scheme 5.3.

Figure 5.8C is a voltammogram which was recorded after re-electrolyzing the oxidized analyte solution which is exactly the same as that of the original $[Cu^{I}(TTCN)(SODTCN)]$ cation. The scan rate dependence of the voltammogram 5.9C was also the same as that of the original compound. This is a clear indication of an exchange between the monodentate SODTCN and a TTCN molecule in solution because neither TTCN nor SODTCN is electroactive in the experimental potential range.

CHAPTER 6

ELECTROCHEMISTRY AND COORDINATION CHEMISTRY OF METHIONINE

Introduction

In this chapter a brief account of the coordination and electrochemistry of methionine will be presented. Methionine is one the most important biological thioether. In the form of S-adenosylmethionine it is involved in biological methylation processes. In biological protein-synthesis the first step in the initiation process is the formation of an N-formyl-L-methionine-transfer RNA complex. Methionine is also found in the coordination sphere of many of the proteins involved in biological electron transfer. It has been mentioned in Chapter 3 that sulfoxidation is one of the major routes of thioether metabolism in biological systems.

The oxidation of methionine and other amino sulfides by the Mn^{2+}-sulfite-O_2 system is postulated to involve a sequence of one-electron oxidation steps[1]. The data suggest that a γ-amino function is essential for efficient oxidation. Dehydromethionine which has been identified as the product of anodic oxidation of methionine[2] and a by-product of the photooxidation of methionine[3], and which is easily hydrolyzed to the sulfoxide in buffered solution[3], is a likely intermediate in the Mn^{2+}-sulfite-O_2 oxidation of methionine.

Discussion

Structural properties of $[Co(en)_2(Met)](ClO_4)_2$. The complex crystallizes in $P2_1/c$

of the monoclinic system. There are two independent molecules in the crystallographic asymmetric unit. The two molecules are related by a pseudo-center of symmetry (Figure 6.1). Analysis of the structures revealed that structure A has a Δ configuration while the configuration of structure B is Λ. The two structures are mirror images of each other.

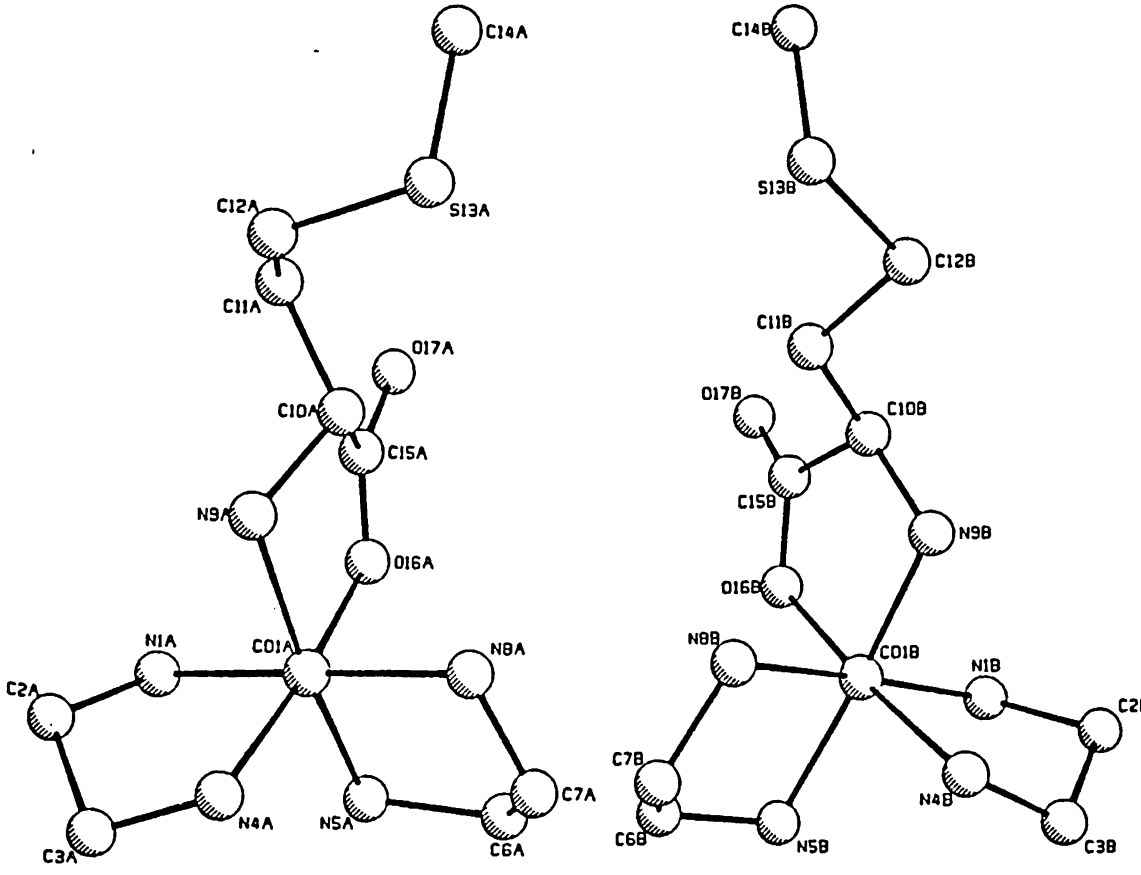

Figure 6.1. Structures of the two molecular units of $[Co^{III}(en)_2(Met)]$ cation (PLUTO drawing). (A) Δ configuration (B) Λ configuration.

Although stereochemical purity is not a concern here, it is interesting to see that both the enantiomers crystallize together in a single unit cell. This could indicate

equal stabilities of both the structural units and, therefore, kinetic discrimination of the two enantiomers in the synthesis may not be achievable. For mixed diamine-α-amino-acid-cobalt (III) species such as the bis(ethylenediamine) series, the tendency toward stereoselective reaction is relatively small[4,5]. Nevertheless, the observed stereoselectivity with L-glutamic acid has been ascribed to the possibility of "three-point attachment" of the ligand involving a hydrogen bonding interaction between the γ-carboxylate and a diamine-ring nitrogen. Molecular models have shown that such three-point attachment with L-glutamate is sterically favorable only for the Δ and not for the Λ configuration of the cation[6].

Due to the unsymmetrical nature of the chelating end of methionine (N,O) each absolute configuration could further have two different isomeric forms arising from the relative positions of the chelating ends. The crystal structure, however, revealed only two enantiomeric forms. This could mean that the relative position of methionine in the coordination sphere of the complex does not change and rather it is the absolute overall configuration of the complex that is racemized. If this is true then the enantiomeric discrimination regarding the preferential conformation of methionine can be achieved by undertaking the synthesis with optically pure starting materials.

Electrochemistry of Methionine. In Figure 6.1 several voltammograms of methionine (1.0 mM) are presented under different pH conditions. All the anodic oxidations were carried out on glassy carbon vs Ag/AgCl. The acid-base equilibria of methionine are shown in Eq. 6.1 and 6.2.

$$_3HC\text{-}S\text{-}CH_2\text{-}CH_2\text{-}\underset{\underset{NH_3^+}{|}}{CH}\text{-}COOH \xrightleftharpoons{(pK_a = 2.2)} {}_3HC\text{-}S\text{-}CH_2\text{-}CH_2\text{-}\underset{\underset{NH_3^+}{|}}{CH}\text{-}COO^- + H^+ \qquad (6.1)$$

$$_3HC\text{-}S\text{-}CH_2\text{-}CH_2\text{-}\underset{\underset{NH_3^+}{|}}{CH}\text{-}COOH \xrightleftharpoons{(pK_a = 9.2)} {}_3HC\text{-}S\text{-}CH_2\text{-}CH_2\text{-}\underset{\underset{NH_2}{|}}{CH}\text{-}COO^- + H^+ \qquad (6.2)$$

The isoelectric point of methionine is 5.75. At neutral pH methionine is present as zwitterion in which the glycinic end of the amino acid has both positively charged ammonium and negatively charged carboxylate functional groups. There is a possibility of the involvement of these functional groups, electrostatically, in the anodic oxidation of the methylthio function of methionine.

In Figure 6.2 voltammogram I was run at pH 8.2 in 0.1M aqueous sodium bicarbonate solution. At this pH methionine will be present as zwitterion. Taking this as a reference point one can see the remarkable effect of pH on the thermodynamics of thioether oxidation.

The immediate result of the oxidation process would be to generate a positive charge on the thioether end. The effect of a pH value higher than the pK_a of both ammonium and carboxylate would be to neutralize the positive charge on the ammonium. This would relieve the electrostatic hindrance to the oxidation of thioether offered by the positively charged ammonium and consequently the oxidation process should be facilitated. This is demonstrated in Figure 6.2, voltammogram II which was run at pH 12.2 in 0.05 M aqueous sodium carbonate solution.

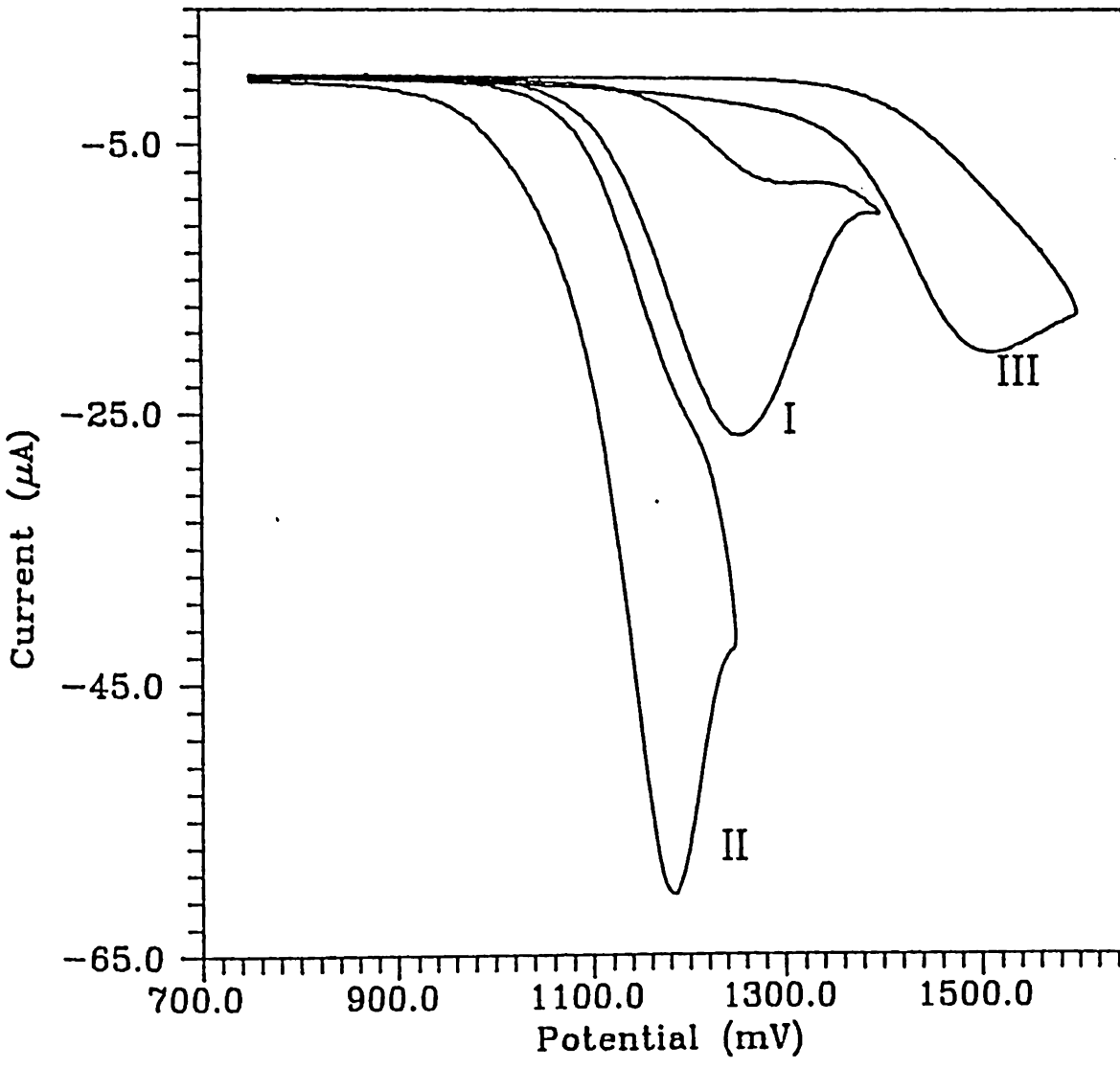

Figure 6.2. Variation of the Cyclic voltammograms of methionine with pH on glassy carbon vs Ag/(AgCl, satd. NaCl) at 100 mV s^{-1} scan rate. (I) pH 8.2 (II) pH 12.2 (III) pH 2.1.

Voltammogram III in Figure 6.2, which was run in 0.1 M aqueous $NaBF_4$ solution, shows the effect of lowering the pH to 2.1 at which point both the carboxylate and amino functions will be protonated. As a consequence the favorable

involvement of the negatively charged carboxylate in the oxidation of the thioether is not possible and, therefore, the interaction with the positively charged ammonium would suggest a more difficult oxidation than at neutral pH. These results could indicate a through-space interaction, which is a well-established concept, between the two ends of methionine. Therefore , it is logical to look into the possibility of electronic communication across the two ends of methionine by holding them rigidly in position. The positioning of the two end at fixed positions relative to each other has been achieved by synthesizing the norbornyl analog of methionine. The communication between the two ends can be studied by coordinating them to appropriate transition metal ions. Therefore it is imperative to develop a synthetic strategy for a binuclear complex using methionine as a model bridging ligand. The synthesis of such complex has been reported in Chapter 2. The main theme of this chapter is to characterize the methionine-bridged binuclear complex and pave the way for future work in this area.

Electrochemistry of $[Co^{III}(en)_2(Met)]$ Complex. Figure 6.3 shows the cyclic voltammogram for the anodic oxidation of the thioether moiety of methionine coordinated to Co(III) through the carboxylate and amino functions. The oxidation of the complexed methionine was found not to depend on pH but the oxidation takes place at a relatively high potential. No significant driving force is now derived from an interaction of the thioether moiety with a neighboring groups now involved in coordination with Co(III). Moreover, the coordination of Co(III) also introduces a high

positive charge into the system which could have an adverse effect on the oxidation process.

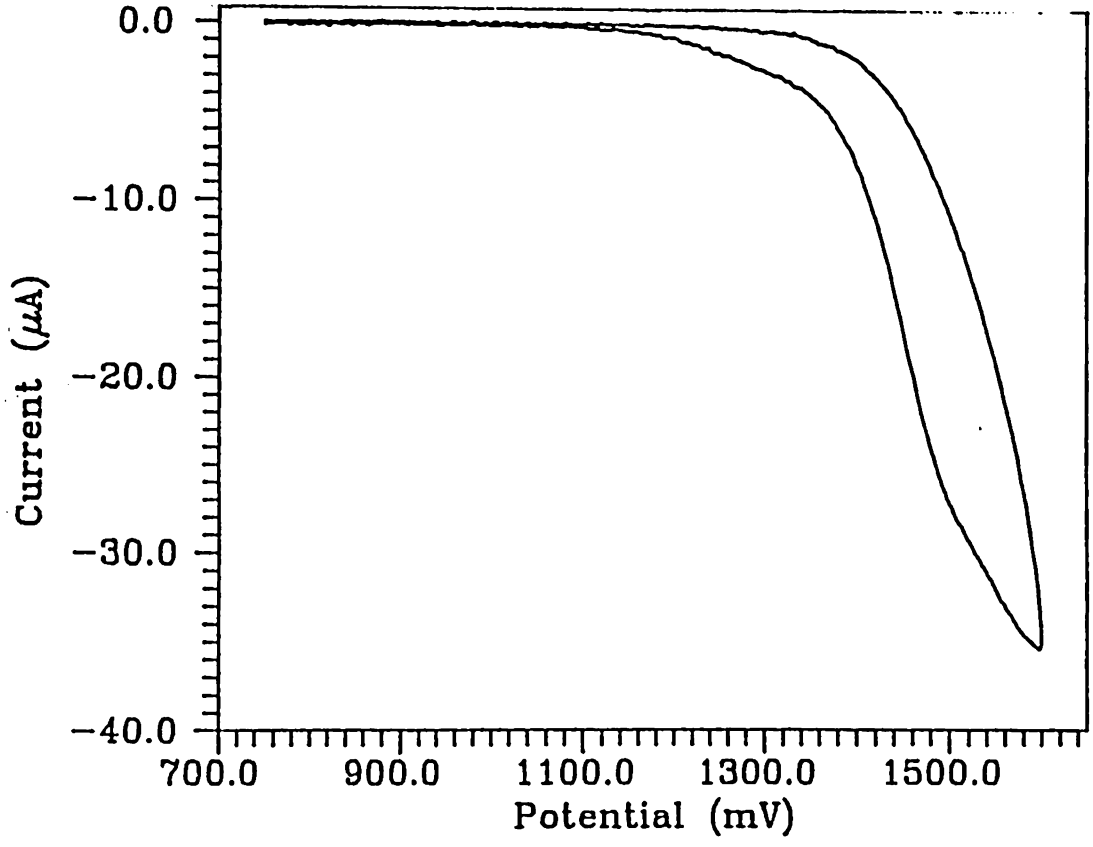

Figure 6.3. Cyclic voltammogram of the thioether moiety of $[Co^{III}(en)_2(Met)]$ at glassy carbon vs Ag/(AgCl, satd. NaCl) at 100 mV s^{-1} scan rate.

In Figure 6.4 shows a voltammogram of the methionine-coordinated Co(III) complex in aqueous solution, which is 0.1 M in $NaBF_4$, on glassy carbon vs Ag/(AgCl, satd. NaCl). The system is highly irreversible due the extremely high thermodynamic stability of Co(II) aquo complex. This would leads to the release of cobalt from its primary coordination sphere, upon reduction, to form the Co(II) aquo

complex.

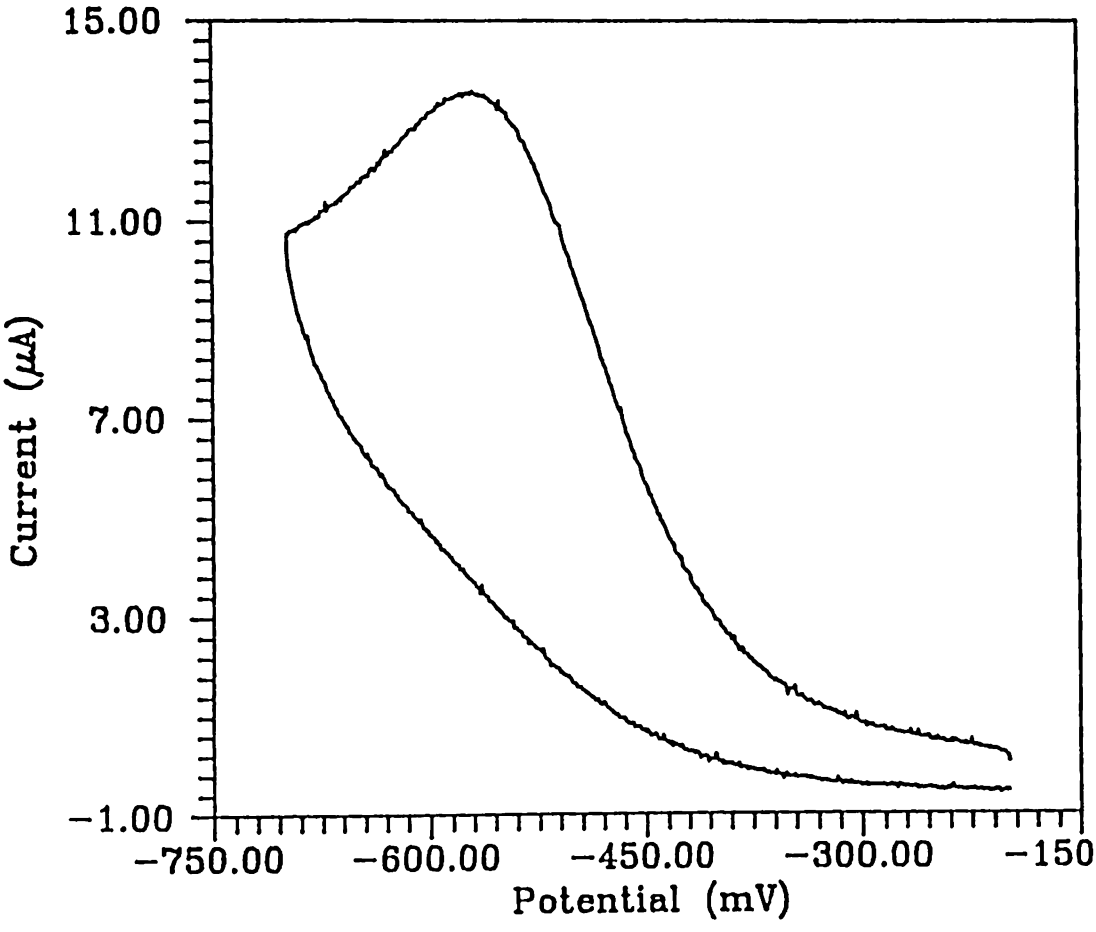

Figure 6.4. Cyclic voltammogram of $[Co^{III}(en)_2(Met)]$ at glassy carbon vs Ag/(AgCl, satd. NaCl) at 100 mV s^{-1} scan rate.

Electrochemistry of $[(en)_2Co^{III}(Met)Ru^{II}(NH_3)_5]$. The cyclic voltammogram of Co(III) moiety in the methionine bridged binuclear complex was exactly the same as in the unbridged complex. This might be an indication of the lack of interaction between the two metal centers.

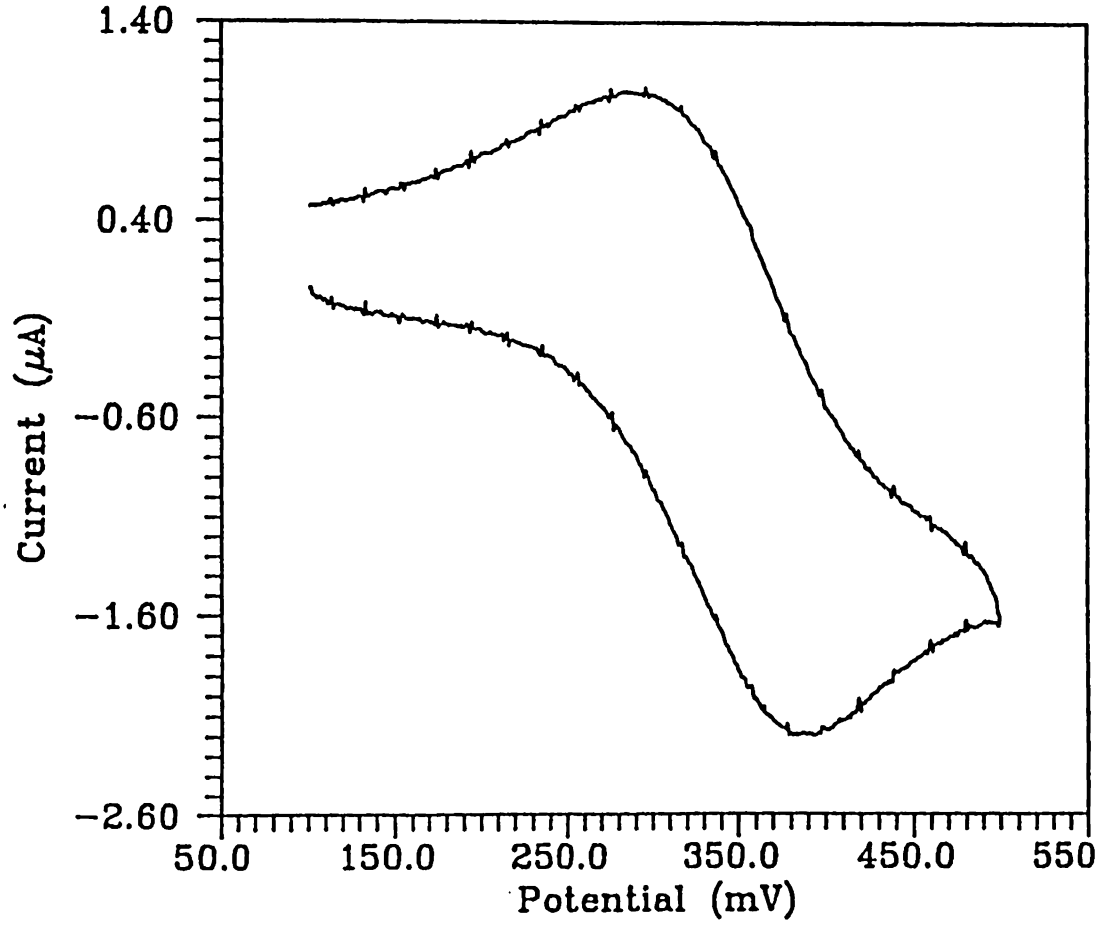

Figure 6.5. Cyclic voltammogram of Ru(III/II) end of the binuclear $[(en)_2Co^{III}(Met)Ru^{II}(NH_3)_5]$ complex at glassy carbon vs Ag/(AgCl, satd. NaCl) at 10 mV s^{-1} scan rate.

The literature value for the formal potential for the thioether bonded $[(NH_3)_5Ru^{III/II}(Met)]$ is 0.53 V vs NHE[7]. Comparing this value to the peak potential of the Co-methionine complex, there is roughly 0.8 V potential gap between the two centers, therefore, a thermodynamic driving force for the intramolecular ET does not seem to be likely. Figure 6.5 shows the cyclic voltammogram of methionine bridged Ru(II) on Glassy carbon. The formal potential is 338 mV vs Ag/ AgCl compared to

the approximately -0.45 V for the cobalt end of the complex. This was anticipated because the nature of the ligand site in methionine (ammine, carboxylate, thioether) is such that it would tend to keep the potentials of the two metal centers far away from each other. Thioether being a soft ligand will tend to stabilize Ru(II), therefore pushing the formal potential to a relatively positive value whereas carboxylate and ammine tend to favor the high oxidation state due to its harder nature. This would, therefore, make it relatively harder to reduce the coordinated Co(III). The unsymmetrical nature of the bridge between the two centers, which are already different metal ions, may make them too different to be put in Class II of the Robin and Day's classification[8].

The thermodynamic hinderance to the communication between the two metal centers can in principle be overcome in the following ways:

1. The gap between the formal potentials can be narrowed down by modifying the metal centers. One possibility is to synthesize a ruthenium homobinuclear complex. However the redox for Ru(III/II)N_5O species in general is such that the potential gap might still be quite large[9-11]. Another option could be a ruthenium-osmium[12] heterobinuclear complex bridged by methionine.

2. A wide range of ligand systems can be utilized to overcome the thermodynamic barrier. The strategy would be to prepare a ruthenium homobinuclear complex with ligand system on the metal center coordinated to the glycinic end of methionine such that it would tend to favor the lower oxidation state such as O-phen

and bipy[13-18]. This would cause a positive shift in the formal potential of the corresponding metal center. Another choice would be to coordinate the metal center to be complexed with the thioether end to a ligand system that would favor higher oxidation state such as Hedta[19-21], however the ruthenium Hedta complexes are substitutionally labile[19,22,23]. If the gap is still high then a proper combination of any of the above approaches can be utilized.

REFERENCES

Chapter 1.

1. Edwards, J. O. *J. Am. Chem. Soc.*, **1956**, *78*, 141.

2. Pearson, R. G. *J. Am. Chem. Soc.*, **1963**, *85*, 3533.

3. Janssen, M. J. "*Sulfur in Organic and Inorganic Chemistry*" Senning, A. Ed., Marcel Dekker: New York, 1972, Vol. 3; p 355.

4. Tagaki, W. "*Organic Chemistry of Sulfur*" Oae, S. Ed., Plenum: New York, 1977, p 231.

5. Fuson, R. C.; Price, C. C.; Burness, D. M. *J. Org. Chem.*, **1946**, *11*, 475.

6. Gundermann, K.-D. *Angew. Chem. Int. Ed.*, **1963**, *2*, 674.

7. Steffen, L. K. Ph.D. Dissertation, University of Arizona: 1990.

8. Asmus K.-D. "*Sulfur-Centered Reactive Intermediates in Chemistry and Biology*" Chatgilialoglu, C.; Asmus, K.-D. Eds., Plenum: New York, Nato ASI Series, Series A, Vol. 197; p 155.

9. Holland, H. L. *Organic Synthesis with Oxidative Enzymes*, VCH: New York, 1992, p 255.

10. Schroll, G.; Lawesson, S.-O. "*Sulfur in Organic and Inorganic Chemistry*" Senning, A. Ed., Marcel Dekker: New York, 1972, Vol. 2, p 171.

11. Takano, T.; Trus, B. L.; Mandel, N.; Mandel, G.; Kallai, O. B.; Swanson, R; Dickerson, R. E. *J. Biol. Chem.*, **1977**, *252*, 776.

12. Colman, P. M.; Freeman, H. C.; Guss, J. M.; Murata, M.; Norris, V. A.; Ramshaw, J. A. M.; Venkatappa, M. P. *Nature* **1978**, *272*, 319.

13. Adman, E. T.; Jensen, L. H. *Israel J. Chem.* **1981**, *21*, 8.

14. Murray, S. G.; Hartley, F. R. *Chem. Rev.*, **1981**, 365.

15. Celinkaya, B.; Hitchcock, P. B. Lappert, M. F.; Pye, P. L.; Shaw, D. B. *J.*

Chem. Soc., Dalton Trans., **1979**, 434.

16. DeSimone, R. E.; Glick, M. D. *J. Am. Chem. Soc.*, **1975**, *97*, 942.

17. DeSimone, R. E.; Glick, M. D. *J. Coord. Chem.*, **1976**, *5*, 181.

18. DeSimone, R. E.; Tighe, T. M. *J. Inorg. Nucl. Chem.*, **1976**, *38*, 1623.

19. Rawle, S. C.; Admans, G.; Cooper, S. R. *J. Chem. Soc., Dalton Trans.*, **1988**, 93.

20. Alcock, N. W.; Herron, N.; Moore, P. *J. Chem. Soc., Chem. Commun.*, **1976**, 886.

21. Nikles, D. E.; Anderson,, A. B.; Urbach, F. L. "*Copper Coordination Chemistry: Biochemical and Inorganic Perspectives*"; Karlin, K. D.; Zubieta, J. Eds., Adinine Press: New York, 1983; p 203.

22. Cooper, S. R.; Rawle, S. C. *Struct. Bonding*, **1989**, *72*, 1.

23. Blake, A. J.; Schroder, M. "*Advances in Inorganic Chemistry*"; Sykes, A. G. Ed., Academic Press: New York, 1990, Vol. 35; p 1.

24. Hancock, R. D. "*Progress in Inorganic Chemistry*" Lippard, S. J. Ed., John Wiley: New York, 1989, Vol. 37, p 187.

25. Marcus, R. A. *Ann. Rev. Phys. Chem.*, **1964**, *15*, 155.

26. Marcus, R. A. *J.Phys. Chem.*, **1956**, *24*, 966.

27. Marcus, R. A.; Sutin, N. *Biochem. Biophys. Acta*, **1985**, *811*, 265.

28. Taube, H. *Electron Transfer Reactions of Complex Ions in Solution*; Academic Press: New York, 1970.

29. Sutin, N. *Acc. Chem. Res.* **1968**, *1*, 225.

30. Isied, S. S.; Taube, H. *J. Am. Chem. Soc.* **1973**, *95*, 8198 .

31. Beinert, H. *Coord. Chem. Rev.* **1980**, *33*, 55.

Chapter 2.

1. Kubas, G. J. *Inorganic Syntheses* **1990**, *28*, 68.

2. Clarkson, J. A.;Yagbasan, R.; Blower, P. J.; Cooper, S. R. *J. Chem. Soc. Chem. Commun.* **1989**, 1244.

3. Hartman, J. A. R.; Cooper, S. R. *J. Am. Chem. Soc.* **1986**, *108*, 1202.

4. Lawrence, G. A.; Sargeson, A. M. *Inorganic Syntheses* **1986**, *24*, 279.

5. Sargeson, A. M.; Searle, G. H. *Inorg. Chem.* **1967**, *6*, 787.

6. Springborg, J.; Schaffer, C. E. *Inorganic Syntheses*, **1973**, *14*, 63.

7. Feldberg, S. W." *Electroanalytical Chemistry*"; Bard, A. J. Ed.; Mercell Dekker: New York, 1969, Vol. 3, p 199.

8. Kowalik, J.; Osborne, M. R. "*Methods for Unconstrained Optimization Problems* "; Elsevier: Amsterdam, 1968.

9. Kano, K.; Konse, T.; Uno, B.; Kubota, T. "*Redox Chemistry and Interfacial Behavior of Biological Molecules*"; Dryhurst, G.; Niki, K. Eds.; Plenum Press: New York, 1987; p 267.

10. Stout, G. H.; Jensen, L. H. "*X-ray Structure Determination*"; Wiley: New York, 2nd Ed. 1989, p 168.

11. Johnson, C. K. ORTEP II. Report ORNL-5138. Oak Ridge National Laboratory, Oak Ridge, Tennessee, 1976.

12. Motherwell, S.; Clegg, W. PLUTO. Program for Plotting Molecular and Crystal Structures. Univ. of Cambridge, England, 1978.

13. Cromer, D. T.; Weber, J. T. "*International Tables for X-ray Crystallography*"; The Kynoch Press: Birmingham, England, 1974, Vol IV, Table 2.2A.

14. Ibers, J. A.; Hamilton, W. C. *Acta Cryst.* **1964**, *17*, 781.

15. Cromer, D. T. "*International Tables for X-ray Crystallography*"; The Kynoch Press: Birmingham, England, 1974, Vol IV, Table 2.3.1.

16. TEXAN - TEXRAY Structure Analysis Package; Molecular Structure Corporation, 1985.

17. Takusagawa, F. "*Crystallographic Computing System: KUDNA*", Department of Chemistry, The University of Kansas, 1984.

18. Beurskens, P. T. *Technical Report 1984/1: Crystallography Laboratory, Toernooiveld, 6525 Ed.* Nijmegen, Netherlands.

19. Calbrese, J. C. Ph. D. Thesis, University of Wisconsin at Madison, 1972.

Chapter 3.

1. Saytzeff, A. *Liebigs Ann. Chem.* **1866**, *139*, 354.

2. Saytzeff, A. *Liebigs Ann. Chem.* **1867**, *144*, 148.

3. Bravo, P.; Resnati, G.; Viani, F. *Tetrahedron Lett.* **1985**, *26*, 2913.

4. Solladie, G. *Synthesis* **1981**, 185.

5. Solladie, G.; Zimmerman, R.; Bartsch, R. *Synthesis* **1985**, 662.

6. Steffen, L. K. Ph.D. Dissertation, University of Arizona: 1990.

7. Hawkins, D. R. Ed. *Biotransformations*, Vol. 1; Royal Society of Chemistry: London, 1988.

8. Clare, N. T. *Aust. Vet. J.*, **1940**, *23*, 340.

9. Smith, R. V.; Davis, P. J.; Kerr, K. M. *J. Pharm. Sci.*, **1983**, *72*, 733.

10. Bartle, K. D.; Lee, M. L.; Wise, S. A. *Chem. Soc. Rev.*, **1981**, *10*, 113.

11. Klein, J.; Beyer, M.; van Afferden, M.; Hodek, W,; Pfeifer, F.; Seewald, H.; Wolff-Fischer, E.; Jüntgen, H. *Biotechnology*, Rehm, H.-J.; Reed, G. Eds.; Verlag Chemie: Weinheim, 1988, Vol 6b; p 545.

12. Schenck, G. O.; Krauch, C. H. *Angew. Chem.*, **1962**, *74*, 510.

13. Foote, C. S.; Peters, J. W. *Int. Congr. Pure App. Chem., Spec. Lect. 23rd* **1971**, *4*, 129.

14. Sysak, P. K.; Foote, C. S.; Ching, T.-Y. *Photochem. Photobiol.* **1977**, *26*, 19.

15. Weil, L.; Gordon, W. G.; Buchert, A. R. *Arch. Biochem. Biophys.* **1951**, *33*, 90.

16. Forbes, W. F.; Savige, W. E. *Photochem. Photobiol.* **1962**, *1*, 77.

17. Jori, G.; Gennari, G.; Folin, M. *Photochem. Photobiol.* **1974**, *19*, 79.

18. Ericksen, J.; Foote, C. S.; Parker, T. L. *J. Am. Chem. Soc.* **1977**, *99*, 6455.

19. Tezuka, T.; Miazaki, H.; Suzuki, H. *Tetrahedron Lett.* **1978**, 1959.

20. Sinnreich, D.; Lind, H.; Batzer, H. *Tetrahedron Lett.* **1976**, 3541.

21. Glass, R. S.; Andruski, S. W.; Broeker, J. L.; Firouzabadi, H.; Steffen, L. K.; Wilson, G. S. *J. Am. Chem Soc.* **1989**, *111*, 4036.

22. Glass, R. S.; Hojjatie, M.; Sabahi, M.; Steffen, L. K.; Wilson, G. S. *J. Org. Chem.* **1990** *55*, 3798.

23. Hammerich, O.; Ørsted, H. C. "*Organic Electrochemistry an Introduction and a Guide*" Lund, H.; Baizer, M. M. Eds. Marcel Dekker: New York, 1991, 3rd Ed. p 121.

24. Greef, R.; Peat, R.; Peter, L. M.; Pletcher, D.; Robinson, J. "*Instrumental Methods in Electrochemistry*" Ellis Horwood: Chichester, 1985.

25. Imbeaux, J. C.; Savéant, J. M. *J. Electroanal. Chem.* **1973**, *44*, 169.

26. Ammar, F.; Savéant, J. M. *J. Electroanal. Chem.* **1973**, *47*, 215.

27. Wilson, G. S.; Swanson, D. D.; Klug, J. T.; Glass, R. S.; Ryan, M. D.; Musker, W. K. *J. Am. Chem. Soc.* **1979**, *101*, 1040.

28. Ryan, M. D.; Swanson, D. D.; Glass, R. S.; Wilson, G. S.; *J. Phys. Chem.* **1981**, *85*, 1069.

29. Pierce, D. T.; Geiger, W. E. *J. Am. Chem. Soc.* **1989**, *111*, 7636.

30. Astruc, D.; Lacoste, M.; Toupet, L. *J. Chem. Soc., Chem. Commun.* **1990**, 558.

31. Krejčík, M.; Vlček, A. A. *Inorg. Chem.* **1992**, *31*, 2390.

32. Glass, R. S. Private communication.

33. Evans D. H.; O'Connell, K. M.; Petersen, R. A.; Kelly, M. J. *J. Chem. Educ.* **1983**, *60*, 290.

34. Hammerich, O.; Parker, V. D. *J. Chem. Soc., Chem. Commun.* **1974**, 245.

35. Pierce, D. T.; Geiger, W. E. *J. Am. Chem. Soc.* **1992**, *114*, 6063.

36. Nelsen, S. F. "*Electroorganic Synthesis: Festschrift for Manuel M. Baizer*" Little, R. D.; Weinberg, N. L. Eds., Marcel Dekker: New York, 1991, p 11.

37. Mann, C. K.; Barnes, K. K. "*Electroanalytical Reactions in Nonaqueous Systems*" In *Monographs in Electroanalytical Chemistry and Electrochemistry*; Bard, A. J. Ed. Marcel Dekker: New York, 1970.

38. Gagné, R. R.; Koval, C. A.; Lisensky, G. C. *Inorg. Chem.* **1980**, *19*, 2854.

Chapter 4.

1. Karlin, K. D.; Zubieta, J. *Inorg. Persp. Biol. Med.*, **1979**, *2*, 127.

2. Glass, R. S.; Wilson, G. S.; Setzer, W. N. *J. Am. Chem. Soc.* **1980**, *102*, 5068.

3. Setzer, W. N.; Coleman, B. R.; Wilson, G. S.; Glass, R. S. *Tetrahedron*, **1981**, *37*, 2743.

4. Swanson, D. D. Ph. D. Thesis, University of Arizona, 1985.

5. Blake, A. J.; Gould, R. O.; Greig, J. A.; Holder, A. J.; Hyde, T. I.; Schroeder, M. *J. Chem. Soc., Chem. Commun.*, **1989**, 876.

6. Cooper, S. R.; Rawle, S. C. *Struct. Bonding*, **1989**, *72*, 1.

7. Clarkson, J. A.; Yagbasan, R.; Blower, P. J.; Cooper, S. R. *J. Chem. Soc., Chem. Commun.* **1989**, 1244.

8. Colman, P. M.; Freeman, H. C.; Guss, J. M.; Murata, M.; Norris, V. A.; Ramshaw, J. A. M.; Venkatappa, M. P. *Nature*, **1978**, *272*, 319.

9. Solomon, E. I.; Gewirth, A. A.; Cohn, S. L. *ACS Symp. Ser.*, **1986**, *307*, 236.

10. Karlin, K. D.; Zubieta, J. Eds. *Biological and Inorganic Copper Chemistry* Vol.2; Adenine Press: New York, 1986.

11. Rorabacher, D. B.; Martin, M. J.; Koenigbauer, M. J.; Malik, M.; Schroeder, R. R.; Endicott, J. F.; Ochramowycz, L. A. *Copper Coordination Chemistry: Biological and Chemical Perspectives*; Karlin, K. D.; Zubieta, J. Eds., Adinine Press: New York, 1983; p 167.

12. Murray, S. G.; Hartley, F. R. *Chem. Rev.*, **1981**, *81*, 365.

13. Westerby, B. C.; Juntunen, K. L.; Luggett, G. H.; Pet, V. B.; Koenigbauer, M. J.; Purgett, M. D.; Taschner, M. J.; Ochrymowycz, L. A.; Rorabacher, DB *Inorg. Chem.*, **1991**, *30*, 2109 and references therein.

14. Blake, A. J.; Schroder, M. *Advances in Inorganic Chemistry*; Sykes, A. G., Ed.; Academic Press: New York, 1990, Vol. 35; p 1.

15. Jameson, R. F. *Metal Ions in Biological Systems*; Sigel, H. Ed. Marcel Dekker: New York, 1981, Vol. 12, p 1.

16. Setzer, W. N.; Ogle, C. A.; Wilson, G. S.; Glass, R. S. *Inorg. Chem.*, **1983**, *22*, 266.

17. Hartman, J. R.; Cooper, S. R. *J. Am. Chem. Soc.*, **1986**, *108*, 1202.

18. Reinen, D.; Ozarowski, A.; Jakob, B.; Pebler, J.; Stratemeier, H. Wieghardt, K.; Tolksdorf, I. *Inorg. Chem.*, **1987**, *26*, 4010.

19. Glass, R. S.; Steffen. L. K.; Swanson, D. D.; Wilson, G. S.; de Gelder, R.; de Graaff, R. A. G. Reedijk, J. *Inorg. Chim. Acta*, **in press.**

20. Jahn, H. A.; Teller, E. *Proc. R. Soc. London, Ser. A*, **1937**,*161*, 220.

21. Bersuker, I. B. *The Jahn-Teller Effect and Vibronic Interactions in Chemistry*, Plenum: New York, 1984.

22. Engelman, R. *The Jahn-Teller Effect in Molecules and Crystals* Wiley-Interscience: London, 1972.

23. Wijnands, P. E. M. Ph. D. Thesis, Leiden University, The Netherlands, 1989.

24. Wieghardt, K.; Kuppers, H.-J.; Raabe, E.; Kruger, C. *Angew. Chem., Int. Ed. Engl.*, **1986**, *25*, 1101.

25. Feldberg, S. W." *Electroanalytical Chemistry*"; Bard, A. J. Ed.; Mercell Dekker: New York, 1969, Vol. 3, p 199.

26. Christie, J. H. *J. Electroanal. Chem.* **1967**, *13*, 79.

27. Bernardo, M. M.; Schroeder, R. R,; Rorabacher, D. B. *Inorg. Chem.*, **1991**, *30*, 1241.

28. Bernardo, M. M.; Robandt, P. V.; Schroeder, R. R.; Rorabacher, D. B. *J. Am. Chem. Soc.*, **1989**, *111*, 1224.

29. Geiger, W. E. *Prog. Inorg. Chem.*; Lippard, S. J. Ed.; John Wiley: New York, 1985; Vol. 33, p 275.

30. Brill A. S.; Martin, R. B.; Williams, J. P *Electronic Aspects of Biochemistry*; Pullman, B. Ed.; Academic Press: New York, 1964; p 519.

31. Bard, A. J.; Faulkner, L. R. *Electroanalytical Methods: Fundamentals and Applications*; Wiley: New York, 1980.

32. Evans, D. H. *Chem. Rev.*, **1990**, *90*, 739.

33. Jones, T.E.; Rorabacher, D. B.; Ochrymowycz, L.A. *J. Am. Chem. Soc.* **1975**, *97*, 7485.

34. Root, M. J.; Sullivan, B. P.; Meyer, T. J.; Deutsch, E. *Inorg. Chem.* **1985**, *24*, 2731.

Chapter 5.

1. Draganic I. G.; Draganic, Z. D. *The Radiation Chemistry of Water*; Academic Press: New York, 1971.

2. Klassen, N. V. *Radiation Chemistry Principles and Applications*; Farhataziz; Rodgers, M. A. J. Eds.; VCH Publishers: New York, 1987, p 29.

3. Buxton, G. V. *Radiation Chemistry Principles and Applications*; Farhataziz; Rodgers, M. A. J. Eds.; VCH Publishers: New York, 1987, p 321.

4. Bell, M. N.; Blake, A. J.; Christie, R. M.; Gould, R. O.; Holder, A. J.; Hude, T. I.; Schröder, M.; Yellowless, L. J. *J. Chem. Soc. Dalton Trans.* **1992**, 2971.

5. Busch, D. H.; Farmery, K.; Goedken, V. L.; Katovic, V.; Meynyk, A. C.; Sperati, C. R.; Tokel, N. *Adv. Chem. Ser.* **1971**, *No. 100*, 44.

6. Bovey, F. A. *Nuclear Magnetic Resonance Spectroscopy*; Academic Press: New York, 2nd Ed. 1988, p 257.

7. Swanson, D. D. Ph. D. Thesis, University of Arizona, 1985.

8. Asmus, K.-D. Unpublished data.

9. Clarkson, J. A.; Yagbasan, R.; Blower, P. J.; Cooper, S. R. *J. Chem. Soc., Chem. Commun.* **1989**, 1244.

10. Amundsen, A. R.; Whelan, J.; Bosnich, B. *J. Am. Chem. Soc.* **1977**, *99*, 6730.

11. Rorabacher, D. B.; Martin, M. J.; Koenigbauer, M. J.; Malik, M.; Schroeder, R. R.; Endicott, J. F.; Ochramowycz, L. A. *Copper Coordination Chemistry: Biological and Chemical Perspectives*; Karlin, K. D.; Zubieta, J. Eds., Adinine Press: New York, 1983; p 167.

12. Zanello, P. *Stereochemistry of Organometallic and inorganic compounds: Stereochemical Control, Bonding and Steric Rearrangements*; Bernal, I. Ed., Elsevier: Amsterdam, 1990, Vol. 4, p 181.

13. Olmstead, M. M.; Musker, W. K.; Kessler, R. M. *Transition Met. Chem.* **1982**, *7*, 140.

Chapter 6.

1. Sysak, P. K.; Foote, C. S.; Ching, T.-Y. *Photochem. Photobiol.* **1977**, *26*, 19.

2. Yang, S. F. *Biochemistry* **1970**, *9*, 5008.

3. Mann, S. *Fresenius' Z. Anal. Chem.* **1960**, *173*, 112.

4. Buckingam, D. A.; Dekkers, A. M.; Sargeson, A. M.; Marzilli, L. G. *Inorg. Chem.* **1973**, *12*, 1207.

5. Liu, C. T.; Douglas, B. E. *Inorg. Chem.* **1964**, *3*, 1356.

6. Gillard, R. D.; Payne, N. C.; Robertson, G. B. *J. Chem. Soc. (A)*, **1970**, 2579.

7. Kuehn, C. G.; Taube, H. *J. Am. Chem. Soc.* **1976**, *98*, 689.

8. Creutz, C. "*Progress in Inorganic Chemistry.*" Lippard, S.J. Ed., John Wiley: New York, 1983, Vol. 30, p 1.

9. Matsubara, T.; Ford, P. C. *Inorg. Chem.* **1976**, *15*, 1107.

10. Stanbury, D. M.; Hass, A; Taube, H. *Inorg. Chem.* **1980**, 518.

11. Richardson, D. E. *Inorg. Chem.* **1990**, 3213.

12. Lay, P. A.; Harman, W. D. *"Advances in Inorganic Chemistry"*, Sykes, A. G., Ed.; Academic Press: New York, 1991, Vol. 37, p 219.

13. Sutton, J. E.; Sutton, P. M.; Taube, H. *Inorg. Chem.* **1979**, 1017.

14. Moyer, B. A.; Meyer, T. J. *Inorg. Chem.* **1981**, *20*, 436.

15. Tinnemans, A. H. A.; Timmer, K.; Reinten, M.; Kraaijkamp, J. G.; Alberts, A. H.; Van Der Linden, J. G. M.; Schmitz, J. E. J.; Saaman, A. A. *Inorg. Chem.* **1981**, *20*, 3698.

16. Dawson, J. H.; Kendrick, M. J.; Kintner, E. T. "*Frontiers in Bioinorganic Chemistry*", Xavier, A. V., Ed.; VCH: Weinheim (F. R. G.), 1986, p 704.

17. Jameson, D. L.; Blaho, J. K.; Kruger, K. T.; Goldsby, K. A. *Inorg. Chem.*

1989, *28*, 4314.

18. Rillema, D. P.; Blanton, C. B.; Shaver, R. J.; Jackman, D. C.; Boldaji, M.; Bundy, S.; Worl, L. A.; Meyer, T. J. *Inorg. Chem.*, **1992**, 1600.

19. Matsubara, T.; Creutz, C. *Inorg. Chem.* **1979**, *18*, 1956.

20. Khan, T.; Hussain, A.; Ramachandraiah, G.; Moiz, M. A. *Inorg. Chem.* **1986**, *25*, 3023.

21. Zhang, S.; Holl, L. A.; Shepherd, R. E. *Inorg. Chem.* **1990**, *29*, 1012.

22. Matsubara, T.; Cruetz, C. *J. Am. Chem. Soc.* **1978**, *100*, 6255.

23. Ogino, H.; Katsuyama, T.; Ito, S. *Bull. Chem. Soc. Jpn.* **1990**, *63*, 1370.

APPENDIX

X-RAY CRYSTALLOGRAPHIC DATA

(Throughout this report the convention for determining the sign of torsion angle is that by numbering the atoms in a row as 1, 2, 3, and 4, the sign is positive if, when looking from atom 2 to atom 3, a clockwise motion of atom 1 would superimpose it on atom 4.)

Table A1.1

Crystal Data for $[Cu^{II}(TTCN)_2](CamphSO_3)_3.H_3O.3CH_2Cl_2$.

Molecular Formula	$CuS_9C_{45}H_{75}Br_3O_{13}Cl_6$
Formula Weight	1628.59
Space Group	$P2_12_12_1$ (#19)
a, Å	16.340 (2)
b, Å	34.379 (4)
c, Å	11.427 (1)
V, Å^3	6419.1 (7)
Z	4
d_{calcd}, g. cm^{-3}	1.685
$\mu_{(CuK\alpha}$, cm^{-1}	82.21
p-factor	0.07
R	0.083 for all data 0.059 for 3σ(F) data
R_w	0.079 for all data 0.063 for 3σ(F) data
GOF	1.12

Table A1.2

Selected Bond Distances for $[Cu^{II}(TTCN)_2](CamphSO_3)_3.H_3O.3CH_2Cl_2$

Conformation A			Conformation B		
Atom	Atom	Distance (Å)	Atom	Atom	Distance (Å)
Cu_1	S_1	2.361 (3)	Cu_1	S_1	2.361 (3)
Cu_1	S_4	2.428 (3)	Cu_1	S_4	2.428 (3)
Cu_1	S_7	2.515 (3)	Cu_1	S_7	2.515 (3)
Cu_1	S_1*	2.359 (3)	Cu_1	S_1*	2.359 (3)
Cu_1	S_4*	2.444 (3)	Cu_1	S_4*	2.444 (3)
Cu_1	S_7*	2.491 (2)	Cu_1	S_7*	2.491 (2)
S_1	C_{2A}	1.83 (1)	S_1	C_{2B}	1.80 (1)
S_1	C_{9A}	1.82 (1)	S_1	C_{9B}	1.81 (1)
S_4	C_{3A}	1.83 (1)	S_1	C_{3B}	1.81 (1)
S_4	C_{5A}	1.83 (1)	S_1	C_{5B}	1.827 (9)
S_7	C_{6A}	1.81 (1)	S_1	C_{6B}	1.84 (1)
S_7	C_{8A}	1.80 (1)	S_1	C_{8B}	1.83 (1)

Table A1.2 contd.

S_1*	C_{2A}*	1.815 (9)	S_1*	C_{2B}*	1.82 (1)
S_1*	C_{9A}*	1.836 (9)	S_1*	C_{9B}*	1.84 (1)
S_4*	C_{3A}*	1.84 (1)	S_4*	C_{3B}*	1.81 (1)
S_4*	C_{5A}*	1.84 (1)	S_4*	C_{5B}*	1.82 (1)
S_7*	C_{6A}*	1.84 (1)	S_7*	C_{6B}*	1.82 (1)
S_7*	C_{8A}*	1.83 (1)	S_7*	C_{8B}*	1.83 (1)

Table A1.3

Selected Bond Angles for $[Cu^{II}(TTCN)_2](CamphSO_3)_3.H_3O.3CH_2Cl_2$ (°)

Atom	Atom	Atom	Angle	Atom	Atom	Atom	Angle
S_1	Cu_1	S_4	88.3(1)	S_1*	Cu_1	S_4*	89.2(1)
S_4	Cu_1	S_7	87.9(1)	S_4*	Cu_1	S_7*	86.3(1)
S_1	Cu_1	S_7	87.7(1)	S_1*	Cu_1	S_7*	87.0(1)
S_1	Cu_1	S_1*	178.5(1)	S_4	Cu_1	S_1*	90.4(1)
S_1	Cu_1	S_4*	92.1(1)	S_4	Cu_1	S_4*	179.5(1)
S_1	Cu_1	S_7*	92.3(1)	S_4	Cu_1	S_7*	94.09(9)
S_7	Cu_1	S_1*	93.0(1)	S_7	Cu_1	S_4*	91.7(1)
S_7	Cu_1	S_7*	178.0(1)				
Cu_1	S_1	C_{2A}	102.8(4)	Cu_1	S_1	C_{2B}	105.8(4)
Cu_1	S_1	C_{9A}	105.7(4)	Cu_1	S_1	C_{9B}	98.0(5)
Cu_1	S_4	C_{3A}	102.0(4)	Cu_1	S_4	C_{3B}	104.2(4)
Cu_1	S_4	C_{5A}	102.2(4)	Cu_1	S_4	C_{5B}	98.8(5)
Cu_1	S_7	C_{6A}	96.5(4)	Cu_1	S_7	C_{6B}	100.8(5)
Cu_1	S_7	C_{8A}	103.0(3)	Cu_1	S_7	C_{8B}	99.7(3)

Table A1.4. Torsion angles for $[Cu^{II}(TTCN)_2](CamphSO_3)_3.H_3O.3CH_2Cl_2$.

Atom	-	Atom	-	Atom	-	Atom	Angle
S4	-	CU1	-	S1	-	C2A	19.8(5)
S4	-	CU1	-	S1	-	C9A	-83.1(5)
S7	-	CU1	-	S1	-	C2A	107.8(5)
S7	-	CU1	-	S1	-	C9A	4.9(4)
S1*	-	CU1	-	S1	-	C2A	-9.0(4)
S1*	-	CU1	-	S1	-	C9A	-112.0(4)
S4*	-	CU1	-	S1	-	C2A	-160.6(5)
S4*	-	CU1	-	S1	-	C9A	96.5(5)
S7*	-	CU1	-	S1	-	C2A	-74.2(5)
S7*	-	CU1	-	S1	-	C9A	-177.1(4)
S1	-	CU1	-	S4	-	C3A	-18.6(4)
S1	-	CU1	-	S4	-	C5A	82.0(4)
S7	-	CU1	-	S4	-	C3A	-106.4(5)
S7	-	CU1	-	S4	-	C5A	-5.8(3)
S1*	-	CU1	-	S4	-	C3A	160.7(4)
S1*	-	CU1	-	S4	-	C5A	-98.7(4)
S4*	-	CU1	-	S4	-	C3A	-146.9(4)
S4*	-	CU1	-	S4	-	C5A	-46.3(4)
S7*	-	CU1	-	S4	-	C3A	73.6(5)
S7*	-	CU1	-	S4	-	C5A	174.2(3)
S1	-	CU1	-	S7	-	C6A	-106.9(4)
S1	-	CU1	-	S7	-	C8A	1.4(3)
S4	-	CU1	-	S7	-	C6A	-18.5(4)
S4	-	CU1	-	S7	-	C8A	89.8(6)
S1*	-	CU1	-	S7	-	C6A	71.8(4)
S1*	-	CU1	-	S7	-	C8A	-179.9(3)
S4*	-	CU1	-	S7	-	C6A	161.2(4)
S4*	-	CU1	-	S7	-	C8A	-90.6(6)

Table A1.4 contd.

Atom	-	Atom	-	Atom	-	Atom	Angle
S7*	-	CU1	-	S7	-	C6A	162.5(4)
S7*	-	CU1	-	S7	-	C8A	-89.2(3)
S1	-	CU1	-	S1*	-	C2A*	-153.5(3)
S1	-	CU1	-	S1*	-	C9A*	-46.4(4)
S4	-	CU1	-	S1*	-	C2A*	177.6(4)
S4	-	CU1	-	S1*	-	C9A*	-75.2(5)
S7	-	CU1	-	S1*	-	C2A*	89.8(5)
S7	-	CU1	-	S1*	-	C9A*	-163.1(4)
S4*	-	CU1	-	S1*	-	C2A*	-1.9(3)
S4*	-	CU1	-	S1*	-	C9A*	105.2(5)
S7*	-	CU1	-	S1*	-	C2A*	-88.3(5)
S7*	-	CU1	-	S1*	-	C9A*	18.8(4)
S1	-	CU1	-	S4*	-	C3A*	-157.9(3)
S1	-	CU1	-	S4*	-	C5A*	100.0(4)
S4	-	CU1	-	S4*	-	C3A*	-29.6(3)
S4	-	CU1	-	S4*	-	C5A*	-131.7(3)
S7	-	CU1	-	S4*	-	C3A*	-70.2(3)
S7	-	CU1	-	S4*	-	C5A*	-172.3(3)
S1*	-	CU1	-	S4*	-	C3A*	22.8(3)
S1*	-	CU1	-	S4*	-	C5A*	-79.3(4)
S7*	-	CU1	-	S4*	-	C3A*	109.9(3)
S7*	-	CU1	-	S4*	-	C5A*	7.8(3)
S1	-	CU1	-	S7*	-	C6A*	-75.1(4)
S1	-	CU1	-	S7*	-	C8A*	-178.8(3)
S4	-	CU1	-	S7*	-	C6A*	-163.6(3)
S4	-	CU1	-	S7*	-	C8A*	92.7(4)
S7	-	CU1	-	S7*	-	C6A*	15.4(3)
S7	-	CU1	-	S7*	-	C8A*	-88.3(3)

Table A1.4 contd.

Atom	-	Atom	-	Atom	-	Atom	Angle
S1*	-	CU1	-	S7*	-	C6A*	106.2(4)
S1*	-	CU1	-	S7*	-	C8A*	2.5(3)
S4*	-	CU1	-	S7*	-	C6A*	16.8(3)
S4*	-	CU1	-	S7*	-	C8A*	-86.9(4)
CU1	-	S1	-	C2A	-	C3A	-18.5(6)
C9A	-	S1	-	C2A	-	C3A	89.9(9)
CU1	-	S1	-	C9A	-	C8A	-13.0(6)
C2A	-	S1	-	C9A	-	C8A	-119.(1)
CU1	-	S4	-	C3A	-	C2A	13.5(6)
C5A	-	S4	-	C3A	-	C2A	-90.8(9)
CU1	-	S4	-	C5A	-	C6A	36.0(5)
C3A	-	S4	-	C5A	-	C6A	140.0(9)
CU1	-	S7	-	C6A	-	C5A	48.8(5)
C8A	-	S7	-	C6A	-	C5A	-56.8(8)
CU1	-	S7	-	C8A	-	C9A	-9.8(5)
C6A	-	S7	-	C8A	-	C9A	91.1(9)
S1	-	C2A	-	C3A	-	S4	3.2(5)
S4	-	C5A	-	C6A	-	S7	-61.6(4)
S7	-	C8A	-	C9A	-	S1	16.2(5)
CU1	-	S1*	-	C2A*	-	C3A*	-26.2(5)
C9A*	-	S1*	-	C2A*	-	C3A*	-132.8(8)
CU1	-	S1*	-	C9A*	-	C8A*	-44.9(5)
C2A*	-	S1*	-	C9A*	-	C8A*	63.2(8)
CU1	-	S4*	-	C3A*	-	C2A*	-48.2(4)
C5A*	-	S4*	-	C3A*	-	C2A*	56.6(7)
CU1	-	S4*	-	C5A*	-	C6A*	-38.2(4)
C3A*	-	S4*	-	C5A*	-	C6A*	-136.9(8)
CU1	-	S7*	-	C6A*	-	C5A*	-46.5(4)

Table A1.4 contd.

Atom	-	Atom	-	Atom	-	Atom	Angle
C8A*	-	S7*	-	C6A*	-	C5A*	58.8(7)
CU1	-	S7*	-	C8A*	-	C9A*	-29.6(3)
C6A*	-	S7*	-	C8A*	-	C9A*	-132.5(8)
S1*	-	C2A*	-	C3A*	-	S4*	53.5(4)
S4*	-	C5A*	-	C6A*	-	S7*	59.7(4)
S7*	-	C8A*	-	C9A*	-	S1*	51.7(4)
S4	-	CU1	-	S1	-	C2B	-7.4(3)
S4	-	CU1	-	S1	-	C9B	-118.1(7)
S7	-	CU1	-	S1	-	C2B	80.6(6)
S7	-	CU1	-	S1	-	C9B	-30.2(6)
S1*	-	CU1	-	S1	-	C2B	-36.3(4)
S1*	-	CU1	-	S1	-	C9B	-147.0(5)
S4*	-	CU1	-	S1	-	C2B	172.2(4)
S4*	-	CU1	-	S1	-	C9B	61.4(7)
S7*	-	CU1	-	S1	-	C2B	-101.4(6)
S7*	-	CU1	-	S1	-	C9B	147.8(6)
S1	-	CU1	-	S4	-	C3B	1.3(4)
S1	-	CU1	-	S4	-	C5B	107.9(5)
S7	-	CU1	-	S4	-	C3B	-86.4(7)
S7	-	CU1	-	S4	-	C5B	20.2(4)
S1*	-	CU1	-	S4	-	C3B	-179.4(4)
S1*	-	CU1	-	S4	-	C5B	-72.8(5)
S4*	-	CU1	-	S4	-	C3B	-127.0(4)
S4*	-	CU1	-	S4	-	C5B	-20.4(5)
S7*	-	CU1	-	S4	-	C3B	93.5(7)
S7*	-	CU1	-	S4	-	C5B	-159.8(5)
S1	-	CU1	-	S7	-	C6B	-85.5(5)
S1	-	CU1	-	S7	-	C8B	15.8(6)

Table A1.4 contd.

Atom	-	Atom	-	Atom	-	Atom	Angle
S4	-	CU1	-	S7	-	C6B	2.9(5)
S4	-	CU1	-	S7	-	C8B	104.2(7)
S1*	-	CU1	-	S7	-	C6B	93.2(5)
S1*	-	CU1	-	S7	-	C8B	-165.5(6)
S4*	-	CU1	-	S7	-	C6B	-177.5(5)
S4*	-	CU1	-	S7	-	C8B	-76.2(7)
S7*	-	CU1	-	S7	-	C6B	-176.1(5)
S7*	-	CU1	-	S7	-	C8B	-74.8(3)
S1	-	CU1	-	S1*	-	C2B*	-136.6(6)
S1	-	CU1	-	S1*	-	C9B*	-32.6(6)
S4	-	CU1	-	S1*	-	C2B*	-165.5(6)
S4	-	CU1	-	S1*	-	C9B*	-61.5(9)
S7	-	CU1	-	S1*	-	C2B*	107.(1)
S7	-	CU1	-	S1*	-	C9B*	-149.4(8)
S4*	-	CU1	-	S1*	-	C2B*	14.9(6)
S4*	-	CU1	-	S1*	-	C9B*	118.9(9)
S7*	-	CU1	-	S1*	-	C2B*	-71.(1)
S7*	-	CU1	-	S1*	-	C9B*	32.6(8)
S1	-	CU1	-	S4*	-	C3B*	-177.0(5)
S1	-	CU1	-	S4*	-	C5B*	69.9(6)
S4	-	CU1	-	S4*	-	C3B*	-48.7(5)
S4	-	CU1	-	S4*	-	C5B*	-161.9(7)
S7	-	CU1	-	S4*	-	C3B*	-89.3(8)
S7	-	CU1	-	S4*	-	C5B*	157.6(6)
S1*	-	CU1	-	S4*	-	C3B*	3.7(5)
S1*	-	CU1	-	S4*	-	C5B*	-109.5(6)
S7*	-	CU1	-	S4*	-	C3B*	90.8(8)
S7*	-	CU1	-	S4*	-	C5B*	-22.4(6)

Table A1.4 contd.

Atom	-	Atom	-	Atom	-	Atom	Angle
S1	-	CU1	-	S7*	-	C6B*	-92.5(6)
S1	-	CU1	-	S7*	-	C8B*	165.1(9)
S4	-	CU1	-	S7*	-	C6B*	179.0(6)
S4	-	CU1	-	S7*	-	C8B*	77.(1)
S7	-	CU1	-	S7*	-	C6B*	-2.0(6)
S7	-	CU1	-	S7*	-	C8B*	-104.4(4)
S1*	-	CU1	-	S7*	-	C6B*	88.8(6)
S1*	-	CU1	-	S7*	-	C8B*	-13.6(9)
S4*	-	CU1	-	S7*	-	C6B*	-0.6(6)
S4*	-	CU1	-	S7*	-	C8B*	-103.(1)
CU1	-	S1	-	C2B	-	C3B	14.3(5)
C9B	-	S1	-	C2B	-	C3B	118.(1)
CU1	-	S1	-	C9B	-	C8B	47.7(7)
C2B	-	S1	-	C9B	-	C8B	-62.(1)
CU1	-	S4	-	C3B	-	C2B	7.0(4)
C5B	-	S4	-	C3B	-	C2B	-96.(1)
CU1	-	S4	-	C5B	-	C6B	-49.1(6)
C3B	-	S4	-	C5B	-	C6B	58.0(8)
CU1	-	S7	-	C6B	-	C5B	-32.3(5)
C8B	-	S7	-	C6B	-	C5B	-134.1(9)
CU1	-	S7	-	C8B	-	C9B	7.7(5)
C6B	-	S7	-	C8B	-	C9B	110.(1)
S1	-	C2B	-	C3B	-	S4	-15.0(3)
S4	-	C5B	-	C6B	-	S7	58.5(5)
S7	-	C8B	-	C9B	-	S1	-39.3(4)
CU1	-	S1*	-	C2B*	-	C3B*	-37.3(8)
C9B*	-	S1*	-	C2B*	-	C3B*	-137.(1)
CU1	-	S1*	-	C9B*	-	C8B*	-55.(1)

Table A1.4 contd.

Atom	-	Atom	-	Atom	-	Atom	Angle
C2B*	-	S1*	-	C9B*	-	C8B*	48.(1)
CU1	-	S4*	-	C3B*	-	C2B*	-27.5(5)
C5B*	-	S4*	-	C3B*	-	C2B*	78.(1)
CU1	-	S4*	-	C5B*	-	C6B*	49.5(7)
C3B*	-	S4*	-	C5B*	-	C6B*	-57.(1)
CU1	-	S7*	-	C6B*	-	C5B*	30.2(6)
C8B*	-	S7*	-	C6B*	-	C5B*	134.(1)
CU1	-	S7*	-	C8B*	-	C9B*	-15.6(6)
C6B*	-	S7*	-	C8B*	-	C9B*	-120.(1)
S1*	-	C2B*	-	C3B*	-	S4*	46.0(5)
S4*	-	C5B*	-	C6B*	-	S7*	-56.5(6)
S7*	-	C8B*	-	C9B*	-	S1*	49.8(5)

Table A1.5. Fractional coordinates and equivalent isotropic thermal parameters. (The thermal parameters are of the form, $B = 8\pi^2\bar{U}^2$)

ATOM	X	Y	Z	B	Occ.
CU1	0.68658(8)	0.74844(4)	1.2495(1)	2.20	1.00
S1	0.6141(2)	0.6951(1)	1.1706(3)	3.87	1.00
S4	0.5567(2)	0.78203(8)	1.2709(2)	2.92	1.00
S7	0.6628(2)	0.71937(9)	1.4486(2)	3.08	1.00
C2A	0.5175(9)	0.7170(4)	1.125(2)	4.43	0.55
C3A	0.4906(9)	0.7546(4)	1.171(2)	4.15	0.55
C5A	0.5174(7)	0.7618(5)	1.4084(9)	2.55	0.55
C6A	0.5864(9)	0.7543(5)	1.496(1)	3.10	0.55
C8A	0.608(1)	0.6751(4)	1.416(1)	3.47	0.55
C9A	0.577(1)	0.6676(4)	1.2956(8)	2.78	0.55
C2B	0.5074(6)	0.7065(4)	1.189(2)	2.04	0.45
C3B	0.4819(7)	0.7474(4)	1.219(2)	3.60	0.45
C5B	0.547(1)	0.7795(5)	1.4300(8)	2.26	0.45
C6B	0.5610(9)	0.7391(5)	1.483(2)	3.28	0.45
C8B	0.632(2)	0.6701(3)	1.406(1)	2.61	0.45
C9B	0.641(2)	0.6594(4)	1.281(1)	5.20	0.45
S1*	0.7563(2)	0.8028(1)	1.3265(3)	3.79	1.00
S4*	0.8176(2)	0.71476(9)	1.2299(3)	4.05	1.00
S7*	0.7146(2)	0.77596(8)	1.0519(2)	2.57	1.00
C2A*	0.8627(5)	0.7877(3)	1.331(1)	2.36	0.65
C3A*	0.8721(8)	0.7437(3)	1.341(1)	3.10	0.65
C5A*	0.8612(6)	0.7356(5)	1.0953(9)	3.61	0.65
C6A*	0.7951(8)	0.7424(4)	1.0024(9)	2.94	0.65
C8A*	0.7751(9)	0.8195(3)	1.0849(8)	2.10	0.65
C9A*	0.754(1)	0.8372(3)	1.2035(8)	4.08	0.65

Table A1.5 contd.

ATOM	X	Y	Z	B	Occ.
C2B*	0.8621(8)	0.7921(4)	1.287(3)	4.80	0.35
C3B*	0.8878(9)	0.7495(5)	1.294(3)	3.43	0.35
C5B*	0.828(2)	0.7148(6)	1.0714(9)	3.10	0.35
C6B*	0.814(1)	0.7549(7)	1.016(2)	2.00	0.35
C8B*	0.747(2)	0.8254(4)	1.089(1)	6.85	0.35
C9B*	0.726(2)	0.8377(4)	1.212(1)	4.07	0.35
BR11	0.64683(9)	0.92733(4)	0.1069(1)	5.08	1.00
S11	0.3422(2)	0.85537(8)	0.4459(2)	2.70	1.00
O11	0.2765(6)	0.8798(3)	0.4194(9)	5.17	1.00
O12	0.3524(7)	0.8244(3)	0.362(1)	6.88	1.00
O13	0.3433(7)	0.8379(4)	0.5579(9)	7.33	1.00
O14	0.6016(5)	0.8793(3)	0.3472(8)	4.39	1.00
C11	0.4587(7)	0.9022(3)	0.3236(9)	2.50	1.00
C12	0.5532(7)	0.9032(3)	0.3110(9)	2.84	1.00
C13	0.5725(7)	0.9396(3)	0.237(1)	3.36	1.00
C14	0.4853(7)	0.9545(3)	0.201(1)	3.00	1.00
C15	0.4478(9)	0.9215(4)	0.118(1)	4.08	1.00
C16	0.4288(7)	0.8874(3)	0.2054(9)	2.67	1.00
C17	0.4386(7)	0.9475(4)	0.316(1)	3.14	1.00
C18	0.4762(8)	0.9712(4)	0.417(1)	3.78	1.00
C19	0.3474(9)	0.9556(3)	0.306(1)	3.91	1.00
C20	0.4387(8)	0.8816(5)	0.440(1)	5.00	1.00
BR21	0.82828(9)	0.96565(4)	0.9303(1)	4.45	1.00
S21	0.8139(2)	0.81210(9)	0.6671(3)	3.65	1.00
O21	0.8877(6)	0.8118(3)	0.6051(8)	5.33	1.00
O22	0.8268(5)	0.8121(2)	0.7927(7)	3.67	1.00

Table A1.5 contd.

ATOM	X	Y	Z	B	Occ.
O23	0.7586(7)	0.7799(3)	0.6313(9)	5.47	1.00
O24	0.7304(5)	0.8845(2)	0.8627(7)	3.24	1.00
C21	0.7899(6)	0.8935(3)	0.6698(8)	1.68	1.00
C22	0.7574(6)	0.9046(3)	0.7901(9)	2.00	1.00
C23	0.7651(7)	0.9497(3)	0.796(1)	2.66	1.00
C24	0.7975(8)	0.9602(4)	0.670(1)	3.90	1.00
C25	0.8896(9)	0.9466(4)	0.669(1)	5.00	1.00
C26	0.8829(8)	0.9010(4)	0.673(1)	4.31	1.00
C27	0.7554(7)	0.9291(3)	0.594(1)	3.15	1.00
C28	0.6635(8)	0.9315(3)	0.600(1)	3.39	1.00
C29	0.7834(9)	0.9283(4)	0.468(1)	4.07	1.00
C30	0.7563(6)	0.8544(3)	0.6247(8)	2.15	1.00
BR31A	0.9098(2)	0.97803(7)	0.2366(2)	5.47	0.60
S31A	1.0669(6)	0.8068(3)	0.1777(8)	1.98	0.60
O31A	0.9982(6)	0.8146(3)	0.1026(9)	2.53	0.60
O32A	1.0530(8)	0.7715(3)	0.242(1)	4.75	0.60
O33A	1.1447(6)	0.8081(4)	0.119(1)	3.43	0.60
O34A	0.9121(7)	0.8846(5)	0.258(2)	5.62	0.60
C31A	1.0611(6)	0.8870(3)	0.242(1)	2.46	0.60
C32A	0.9708(6)	0.8999(4)	0.222(2)	5.46	0.60
C33A	0.9804(7)	0.9402(3)	0.162(1)	5.36	0.60
C34A	1.0755(8)	0.9484(3)	0.155(1)	4.85	0.60
C35A	1.101(1)	0.9550(4)	0.286(1)	5.96	0.60
C36A	1.089(1)	0.9144(4)	0.346(1)	6.10	0.60
C37A	1.1049(7)	0.9041(4)	0.135(1)	4.64	0.60
C38A	1.067(1)	0.8916(6)	0.019(1)	5.89	0.60

Table A1.5 contd.

ATOM	X	Y	Z	B	Occ.
C39A	1.1967(8)	0.9018(7)	0.141(2)	5.35	0.60
C40A	1.071(1)	0.8461(3)	0.281(1)	4.93	0.60
BR31B	0.9630(3)	0.9899(1)	0.3409(4)	5.93	0.40
S31B	1.046(1)	0.8091(4)	0.191(1)	3.44	0.40
O31B	1.014(2)	0.8093(7)	0.308(1)	6.47	0.40
O32B	1.008(1)	0.7818(6)	0.112(2)	5.84	0.40
O33B	1.134(1)	0.805(1)	0.195(3)	11.21	0.40
O34B	0.897(1)	0.9100(7)	0.208(2)	5.84	0.40
C31B	1.044(1)	0.8928(4)	0.190(2)	3.63	0.40
C32B	0.966(1)	0.9191(5)	0.205(3)	6.32	0.40
C33B	1.001(1)	0.9603(5)	0.206(2)	5.29	0.40
C34B	1.097(1)	0.9562(5)	0.190(2)	3.71	0.40
C35B	1.126(2)	0.9375(8)	0.310(2)	7.42	0.40
C36B	1.088(2)	0.8951(8)	0.309(2)	5.84	0.40
C37B	1.101(1)	0.9185(6)	0.110(2)	9.08	0.40
C38B	1.065(2)	0.923(1)	-0.009(2)	6.71	0.40
C39B	1.188(1)	0.902(1)	0.114(3)	5.92	0.40
C40B	1.023(2)	0.8560(4)	0.131(2)	6.71	0.40
O41W	0.2622(5)	0.7812(2)	0.2582(8)	3.64	1.00
CL51	0.5407(2)	0.8323(1)	0.7119(3)	3.82	1.00
CL52	0.5423(2)	0.83151(9)	0.9676(3)	3.69	1.00
C51	0.5887(7)	0.8140(3)	0.839(1)	2.84	1.00
CL61	0.1049(3)	0.9411(1)	0.6607(4)	5.65	1.00
CL62	0.2089(3)	0.9941(1)	0.5322(4)	7.58	1.00
C61	0.199(1)	0.9484(6)	0.602(2)	8.48	1.00
CL71	0.4132(4)	0.9340(2)	0.7598(5)	8.42	1.00
CL72	0.2836(4)	0.8901(2)	0.8665(6)	10.11	1.00
C71	0.371(1)	0.8880(5)	0.786(2)	8.68	1.00

Table A2.1

Crystal Data for $[Cu^{I}(TTCN)_2](PF_6)$.

Molecular Formula	$CuS_6C_{12}H_{24}PF_6$
Formula Weight	569.19
Space Group	$P2_1/n$ (#14)
a, Å	8.608 (3)
b, Å	31.041 (8)
c, Å	16.008 (4)
β°	90.88 (2)
V, Å^3	4277 (4)
Z	8
d_{calcd}, g. cm^{-3}	1.768
$\mu_{(CuK\alpha}$, cm^{-1}	80.46
p-factor	0.10
R	0.089
R_w	0.136
GOF	2.21

Table A2.2

Selected Bond Distances for $[Cu^{I}(TTCN)_2](PF_6)$ (Å)

Atom	Atom	Distance	Atom	Atom	Distance
Cu_1	S_{1A}	2.332(6)	Cu_2	S_{1C}	2.288(7)
Cu_1	S_{4A}	2.327(5)	Cu_2	S_{4C}	2.317(6)
Cu_1	S_{7A}	2.300(6)	Cu_2	S_{7C}	2.334(7)
Cu_1	S_{1B}	2.224(6)	Cu_2	S_{1D}	2.246(6)
S_{1B}	C_{2B}	1.91(2)	S_{1D}	C_{2D}	1.86(2)
S_{1B}	C_{9B}	1.77(2)	S_{1D}	C_{9D}	1.78(2)
S_{4B}	C_{3B}	1.82(3)	S_{4D}	C_{3D}	1.80(2)
S_{4B}	C_{5B}	1.76(2)	S_{4D}	C_{5D}	1.74(2)
S_{7B}	C_{6B}	1.78(2)	S_{7D}	C_{6D}	1.81(3)
S_{7B}	C_{8B}	1.79(2)	S_{7D}	C_{8D}	1.79(2)

Table A2.3

Selected Bond Angles for $[Cu^{I}(TTCN)_2]PF_6$ (°)

Atom	Atom	Atom	Angle	Atom	Atom	Atom	Angle
S_{1A}	Cu_1	S_{4A}	92.9(2)	S_{1A}	Cu_1	S_{1B}	117.0(2)
S_{4A}	Cu_1	S_{7A}	94.0(2)	S_{4A}	Cu_1	S_{1B}	119.4(2)
S_{7A}	Cu_1	S_{1A}	93.4(2)	S_{7A}	Cu_1	S_{1B}	131.2(2)
S_{1C}	Cu_2	S_{4C}	94.5(2)	S_{1C}	Cu_2	S_{1D}	120.5(2)
S_{4C}	Cu_2	S_{7C}	93.6(2)	S_{4C}	Cu_2	S_{1D}	122.8(2)
S_{7C}	Cu_2	S_{1C}	94.0(2)	S_{7C}	Cu_2	S_{1D}	123.8(2)
Cu_1	S_{1A}	C_{2A}	98.6(8)	Cu_2	S_{1C}	C_{2C}	97.9(7)
Cu_1	S_{1A}	C_{9A}	96.7(8)	Cu_2	S_{1C}	C_{9C}	99.0(1)
Cu_1	S_{4A}	C_{3A}	98.4(7)	Cu_2	S_{4C}	C_{3C}	96.5(8)
Cu_1	S_{4A}	C_{5A}	98.6(6)	Cu_2	S_{4C}	C_{5C}	99.5(7)
Cu_1	S_{7A}	C_{6A}	97.5(8)	Cu_2	S_{7C}	C_{6C}	99.0(1)
Cu_1	S_{7A}	C_{8A}	100.5(8)	Cu_2	S_{7C}	C_{8C}	101.7(9)
Cu_1	S_{1B}	C_{2B}	100.1(7)	Cu_2	S_{1D}	C_{2D}	97.5(7)
Cu_1	S_{1B}	C_{9B}	113.0(7)	Cu_2	S_{1D}	C_{9D}	102.3(8)

Table A2.3 contd.

C_{9B}	S_{1B}	C_{2B}	103.9(8)	C_{9D}	S_{1D}	C_{2D}	103.6(9)
S_{1B}	C_{2B}	C_{3B}	115.0(2)	S_{1D}	C_{2D}	C_{3D}	113.0(1)
C_{2B}	C_{3B}	S_{4B}	113.0(2)	C_{2D}	C_{3D}	S_{4D}	115.0(2)
C_{3B}	C_{4B}	C_{5B}	103.0(1)	C_{3D}	S_{4D}	C_{5D}	105.0(1)
S_{4B}	S_{5B}	C_{6B}	120.0(2)	S_{4D}	C_{5D}	C_{6D}	118.0(2)
C_{5B}	C_{6B}	S_{7B}	116.0(2)	C_{5D}	C_{6D}	S_{7D}	117.0(2)
C_{6B}	C_{7B}	C_{8B}	102.0(1)	C_{6D}	S_{7D}	C_{8D}	102.0(1)
S_{7B}	S_{8B}	C_{9B}	115.0(1)	S_{7D}	C_{8D}	C_{9D}	118.0(1)
C_{8B}	C_{9B}	S_{1B}	121.0(1)	C_{8D}	S_{9D}	S_{1D}	119.0(2)

Table A2.4

Torsion Angles of the Monodentate TTCN in $[Cu^{I}(TTCN)_2]PF_6$ (°)

Atom	Atom	Atom	Atom	Angle
S_{1B}	C_{2B}	C_{3B}	S_{4B}	-122 (2)
S_{4D}	C_{3D}	C_{2D}	S_{1D}	-122 (1)
S_{1B}	C_{9B}	C_{8B}	S_{7B}	-61 (2)
S_{4D}	C_{5D}	C_{6D}	S_{7D}	-60 (2)
C_{2B}	S_{1B}	C_{9B}	C_{8B}	76 (2)
C_{3D}	S_{4D}	C_{5D}	C_{6D}	76 (2)
C_{2B}	C_{3B}	S_{4B}	C_{5B}	85 (2)
C_{3D}	C_{2D}	S_{1D}	C_{9D}	83 (2)
C_{3B}	C_{2B}	S_{1B}	C_{9B}	60 (2)
C_{2D}	C_{3D}	S_{4D}	C_{5D}	58 (2)
C_{3B}	S_{4B}	C_{5B}	C_{6B}	-103 (2)
C_{2D}	S_{1D}	C_{9D}	C_{8D}	-102 (2)

Table A2.4 contd.

S_{4B}	C_{5B}	C_{6B}	S_{7B}	54 (3)
S_{1D}	C_{9D}	C_{8D}	S_{7D}	57 (2)
C_{5B}	C_{6B}	S_{7B}	C_{8B}	79 (2)
C_{9D}	C_{8D}	S_{7D}	C_{6D}	73 (2)
C_{6B}	S_{7B}	C_{8B}	C_{9B}	-79 (2)
C_{8D}	S_{7D}	C_{6D}	C_{5D}	-78 (2)

Table A2.5. Fractional coordinates and B_{eq} for $[Cu^{I}(TTCN)_2]PF_6$

atom	x	y	z	B(eq)
Cu(1)	0.5296(3)	0.3622(1)	0.1171(2)	3.3(1)
S(1A)	0.5487(6)	0.2873(2)	0.1190(3)	4.1(3)
C(2A)	0.407(3)	0.2754(7)	0.039(1)	6(1)
C(3A)	0.384(3)	0.308(1)	-0.029(1)	7(2)
S(4A)	0.3554(7)	0.3620(2)	0.0045(3)	4.2(3)
C(5A)	0.173(2)	0.3611(8)	0.063(1)	5(1)
C(6A)	0.177(3)	0.3796(7)	0.146(1)	6(1)
S(7A)	0.3379(7)	0.3635(2)	0.2156(3)	4.4(3)
C(8A)	0.303(3)	0.3070(9)	0.228(1)	6(1)
C(9A)	0.437(3)	0.2788(7)	0.214(1)	6(1)
S(1B)	0.7503(6)	0.3991(2)	0.1077(3)	3.6(2)
C(2B)	0.697(3)	0.4376(7)	0.019(1)	5(1)
C(3B)	0.817(4)	0.469(1)	-0.003(1)	8(2)
S(4B)	0.7508(8)	0.5246(2)	0.0065(4)	6.0(3)
C(5B)	0.784(4)	0.5362(8)	0.113(2)	7(2)
C(6B)	0.647(3)	0.5364(7)	0.174(1)	6(1)
S(7B)	0.5322(7)	0.4889(2)	0.1766(3)	5.3(3)
C(8B)	0.651(3)	0.4541(6)	0.239(1)	4(1)
C(9B)	0.785(3)	0.4336(6)	0.194(1)	3.4(9)
Cu(2)	0.5234(4)	0.3574(1)	0.6106(2)	3.8(2)
S(1C)	0.5521(7)	0.2842(2)	0.6170(3)	4.7(3)
C(2C)	0.414(4)	0.2704(7)	0.538(2)	8(2)
C(3C)	0.377(3)	0.302(1)	0.473(1)	7(1)
S(4C)	0.3440(8)	0.3555(2)	0.5012(3)	5.3(3)

Table A2.5 contd.

atom	x	y	z	B(eq)
C(5C)	0.163(3)	0.3569(9)	0.561(1)	6(1)
C(6C)	0.172(4)	0.371(1)	0.649(2)	12(2)
S(7C)	0.3329(8)	0.3593(2)	0.7127(3)	4.9(3)
C(8C)	0.301(3)	0.3027(8)	0.732(1)	6(1)
C(9C)	0.437(3)	0.274(1)	0.711(2)	7(2)
S(1D)	0.7326(6)	0.4007(2)	0.6106(3)	3.9(3)
C(2D)	0.673(3)	0.4353(7)	0.521(1)	4(1)
C(3D)	0.802(3)	0.4668(7)	0.493(1)	4(1)
S(4D)	0.7506(7)	0.5229(2)	0.4961(3)	4.9(3)
C(5D)	0.699(3)	0.5326(7)	0.599(1)	5(1)
C(6D)	0.829(3)	0.5367(7)	0.664(1)	6(1)
S(7D)	0.9544(7)	0.4903(2)	0.6786(3)	4.5(3)
C(8D)	0.836(3)	0.4559(6)	0.741(1)	4(1)
C(9D)	0.700(3)	0.4341(7)	0.699(1)	4(1)
P(1A)	0.3451(7)	0.1697(2)	0.3620(3)	3.6(3)
F(1A)	0.254(2)	0.2143(4)	0.3526(8)	7.0(8)
F(2A)	0.435(2)	0.1256(5)	0.376(1)	10(1)
F(3A)	0.502(2)	0.1965(5)	0.3746(9)	8(1)
F(4A)	0.186(2)	0.1438(5)	0.351(1)	9(1)
F(5A)	0.316(2)	0.1721(5)	0.4575(7)	8.2(9)
F(6A)	0.369(2)	0.1682(5)	0.2663(7)	8(1)
P(1B)	0.3367(7)	0.1706(2)	0.8649(3)	3.7(3)
F(1B)	0.252(2)	0.2156(4)	0.8569(8)	6.8(8)
F(2B)	0.424(2)	0.1262(5)	0.8737(9)	8.2(9)
F(3B)	0.495(2)	0.1966(5)	0.8804(8)	7.5(9)

Table A2.5 contd.

atom	x	y	z	B(eq)
F(4B)	0.179(2)	0.1454(5)	0.848(1)	8(1)
F(5B)	0.307(2)	0.1706(4)	0.9598(7)	7.0(8)
F(6B)	0.363(2)	0.1707(4)	0.7687(7)	8.0(9)
H(1)	0.4338	0.2492	0.0139	7.2
H(2)	0.3084	0.2723	0.0660	7.2
H(3)	0.4742	0.3075	-0.0621	8.4
H(4)	0.2962	0.2998	-0.0612	8.4
H(5)	0.0975	0.3771	0.0301	5.6
H(6)	0.1401	0.3325	0.0675	5.6
H(7)	0.1855	0.4106	0.1385	6.8
H(8)	0.0837	0.3732	0.1715	6.8
H(9)	0.2663	0.3021	0.2830	7.1
H(10)	0.2229	0.2987	0.1888	7.1
H(11)	0.4050	0.2499	0.2142	6.9
H(12)	0.5094	0.2833	0.2602	6.9
H(13)	0.6773	0.4203	-0.0301	5.4
H(14)	0.6063	0.4524	0.0331	5.4
H(15)	0.9051	0.4658	0.0324	9.4
H(16)	0.8471	0.4651	-0.0598	9.4
H(17)	0.8594	0.5169	0.1321	8.3
H(18)	0.8271	0.5651	0.1135	8.3
H(19)	0.6909	0.5403	0.2289	7.1
H(20)	0.5813	0.5598	0.1610	7.1
H(21)	0.6909	0.4701	0.2856	4.8
H(22)	0.5865	0.4314	0.2601	4.8

Table A2.5 contd.

atom	x	y	z	B(eq)
H(23)	0.8429	0.4170	0.2350	4.3
H(24)	0.8497	0.4564	0.1755	4.3
H(25)	0.4544	0.2459	0.5094	9.9
H(26)	0.3209	0.2629	0.5645	9.9
H(27)	0.4582	0.3025	0.4353	8.1
H(28)	0.2831	0.2927	0.4467	8.1
H(29)	0.0906	0.3734	0.5324	7.2
H(30)	0.1272	0.3273	0.5649	7.2
H(31)	0.1680	0.4032	0.6452	12.6
H(32)	0.0816	0.3625	0.6760	12.6
H(33)	0.2761	0.2989	0.7878	7.0
H(34)	0.2130	0.2941	0.6970	7.0
H(35)	0.3927	0.2449	0.7036	8.9
H(36)	0.5033	0.2736	0.7572	8.9
H(37)	0.6421	0.4178	0.4750	5.7
H(38)	0.5844	0.4525	0.5370	5.7
H(39)	0.8907	0.4622	0.5286	5.3
H(40)	0.8296	0.4594	0.4370	5.3
H(41)	0.6436	0.5588	0.5987	6.0
H(42)	0.6351	0.5096	0.6150	6.0
H(43)	0.8929	0.5606	0.6508	7.4
H(44)	0.7814	0.5423	0.7172	7.4
H(45)	0.9036	0.4327	0.7607	5.3
H(46)	0.8014	0.4715	0.7865	5.3
H(47)	0.6321	0.4572	0.6792	5.5
H(48)	0.6469	0.4178	0.7385	5.5

Table A3.1

Crystal Data for $[Cu^{I}(TTCN)(SODTCN)](PF_6)$.

Molecular Formula	$CuS_6C_{12}H_{24}PF_6O$
Formula Weight	585.19
Space Group	$P2_1/n$ (#4)
a, Å	7.939 (2)
b, Å	8.688 (3)
c, Å	15.964 (4)
β°	102.94 (4)
V, Å^3	1073 (1)
Z	2
d_{calcd}, g. cm^{-3}	1.811
$\mu_{(CuK\alpha}$, cm^{-1}	80.70
p-factor	0.10
R	0.078
R_w	0.075
GOF	1.12

Table A3.2

Selected Bond Distances of $[Cu^{I}(TTCN)(SODTCN)]PF_6$ (Å)

Atom	Atom	Distance	Atom	Atom	Distance
Cu_1	S_1	2.320(2)	Cu_1	S_4	2.215(2)
Cu_1	S_2	2.281(2)			
Cu_1	S_3	2.299(3)			
S_4	C_{7A}	1.82(1)	S_4	C_{7B}	1.82(1)
S_4	C_{12A}	1.824(9)	S_4	C_{12B}	1.824(8)
S_{6A}	C_{10A}	1.83(1)	S_{6B}	C_{10B}	1.83(1)
S_{6A}	C_{11A}	1.82(1)	S_{6B}	C_{11B}	1.82(1)
S_{5A}	C_{8A}	1.92(1)	S_{5B}	C_{8B}	1.93(1)
S_{5A}	C_{9A}	1.911(9)	S_{5B}	C_{9B}	1.92(1)

Table A3.3

Selected Bond Angles for $[Cu^{I}(TTCN)(SODTCN)]PF_6$ (°)

Atom	Atom	Atom	Angle	Atom	Atom	Atom	Angle
S_1	Cu_1	S_2	93.9(1)	S_1	Cu_1	S_4	116.68(9)
S_2	Cu_1	S_3	93.5(1)	S_2	Cu_1	S_4	124.8(1)
S_3	Cu_1	S_1	93.5(1)	S_3	Cu_1	S_4	126.2(1)
Cu_1	S_1	C_1	97.9(3)	Cu_1	S_1	C_6	100.8(3)
Cu_1	S_2	C_2	99.6(3)	Cu_1	S_3	C_4	103.2(5)
Cu_1	S_2	C_3	97.3(4)	Cu_1	S_3	C_5	100.9(4)
Cu_1	S_4	C_{7A}	131.3(1)	Cu_1	S_4	C_{7B}	112.0(3)
Cu_1	S_4	C_{12A}	120.3(3)	Cu_1	S_4	C_{12B}	125.4(3)
C_{8A}	S_{5A}	C_{9A}	96.3(5)	C_{8B}	S_{5B}	C_{9B}	95.7(6)
O_{1A}	S_{5A}	C_{8A}	112.7(7)	O_{1B}	S_{5B}	C_{8B}	121.9(7)
O_{1A}	S_{5A}	C_{9A}	115.3(7)	O_{1B}	S_{5B}	C_{9B}	123.5(9)
S_{5A}	C_{9A}	C_{10A}	110.2(7)	S_{5B}	C_{9B}	C_{10B}	109.7(8)
S_{6A}	C_{11A}	C_{12A}	114.3(7)	S_{6B}	C_{11B}	C_{12B}	114.5(5)
C_{9A}	C_{10A}	S_{6A}	114.3(7)	C_{9B}	C_{10B}	S_{6A}	113.9(7)
C_{10A}	S_{6A}	C_{11A}	102.7(6)	C_{10B}	S_{6B}	C_{11B}	102.4(5)

Table A3.4

Torsion angles for SODTCN in $[Cu^{I}(TTCN)(SODTCN)]PF_6$ (°)

Atom	Atom	Atom	Atom	Angle
S_1	Cu_1	S_4	C_{7A}	-120.1(3)
S_1	Cu_1	S_4	C_{12A}	90.4(2)
S_2	Cu_1	S_4	C_{7A}	123.7(3)
S_2	Cu_1	S_4	C_{12A}	-25.8(4)
S_3	Cu_1	S_4	C_{7A}	-3.1(3)
S_3	Cu_1	S_4	C_{12A}	-152.6(4)
S_1	Cu_1	S_4	C_{7B}	-110.5(3)
S_1	Cu_1	S_4	C_{12B}	123.7(2)
S_2	Cu_1	S_4	C_{7B}	133.3(3)
S_2	Cu_1	S_4	C_{12B}	7.5(2)
S_3	Cu_1	S_4	C_{7B}	6.4(3)
S_3	Cu_1	S_4	C_{12B}	-119.4(2)
Cu_1	S_4	C_{7A}	C_{8A}	-9.6(5)
Cu_1	S_4	C_{12A}	C_{11A}	106.2(7)

Table A3.4 contd.

Cu_1	S_4	C_{7B}	C_{8B}	-58.0(5)
Cu_1	S_4	C_{12B}	C_{11B}	22.6(4)
S_4	C_{7A}	C_{8A}	S_{5A}	-126.3(5)
S_{5A}	C_{9A}	C_{10A}	S_{6A}	74.0(4)
S_{6A}	C_{11A}	C_{12A}	S_4	62.7(2)
S_4	C_{7B}	C_{8B}	S_{5B}	-123.9(4)
S_{5B}	C_{9B}	C_{10B}	S_{6B}	88.8(5)
S_{6B}	C_{11B}	C_{12B}	S_4	58.0(3)
C_{12A}	S_4	C_{7A}	C_{8A}	-143.6(6)
C_{7A}	S_4	C_{12A}	C_{11A}	-50.8(5)
C_{9A}	S_{5A}	C_{8A}	C_{7A}	58.6(4)
C_{8A}	S_{5A}	C_{9A}	C_{10A}	-106.3(7)
C_{11A}	S_{6A}	C_{10A}	C_{9A}	71.5(6)
C_{10A}	S_{6A}	C_{11A}	C_{12A}	-130.0(5)
C_{12B}	S_4	C_{7B}	C_{8B}	79.2(5)
C_{7B}	S_4	C_{12B}	C_{11B}	-106.8(5)

Table A3.4 contd.

C_{9B}	S_{5B}	C_{8B}	C_{7B}	128.9(5)
C_{8B}	S_{5B}	C_{9B}	C_{10B}	-70.9(5)
C_{11B}	S_{6B}	C_{10B}	C_{9B}	-141.2(7)
C_{10B}	S_{6B}	C_{11B}	C_{12B}	70.4(5)
O_{1A}	S_{5A}	C_{8A}	C_{7A}	179.4(9)
O_{1A}	S_{5A}	C_{9A}	C_{10A}	134.9(9)
O_{1B}	S_{5B}	C_{8B}	C_{7B}	-95.0(1)
O_{1B}	S_{5B}	C_{9B}	C_{10B}	154.0(1)

Table A3.5. Fractional coordinates and equivalent isotropic thermal parameters. (The thermal parameters are of the form, $B = 8\pi^2\bar{U}^2$)

ATOM	X	Y	Z	B
CU1	0.3964(2)	0.330300(0)	0.77864(8)	5.64
S1	0.4788(4)	0.3078(4)	0.9270(2)	5.95
S2	0.1891(3)	0.5098(3)	0.7829(2)	5.39
S3	0.6038(4)	0.5116(3)	0.7723(2)	5.98
C1	0.289(2)	0.402(2)	0.9534(7)	9.44
C2	0.234(1)	0.545(2)	0.9018(8)	7.87
C3	0.294(2)	0.666(1)	0.7496(8)	9.02
C4	0.495(2)	0.694(2)	0.7853(9)	9.49
C5	0.743(1)	0.494(2)	0.880(1)	8.83
C6	0.645(1)	0.448(1)	0.9507(6)	5.64
S4	0.3523(3)	0.1133(3)	0.7044(1)	4.48
S5A	0.5083(8)	0.1620(9)	0.4672(4)	5.26
S6A	0.1469(7)	-0.0521(7)	0.5084(4)	6.04
C7A	0.455(1)	0.035(1)	0.6223(9)	7.60
C8A	0.574(1)	0.147(2)	0.5905(5)	8.29
C9A	0.2765(9)	0.229(1)	0.4613(9)	7.71
C10A	0.150(1)	0.099(1)	0.4294(6)	6.58
C11A	0.0417(8)	0.042(2)	0.5850(5)	7.10
C12A	0.138(1)	0.026(2)	0.6785(5)	8.64
O1A	0.601(1)	0.254(1)	0.4373(7)	6.60
S5B	0.505(1)	0.119(1)	0.4671(4)	6.55
S6B	0.1442(6)	0.3371(7)	0.5351(3)	5.76
C7B	0.5176(9)	0.080(1)	0.6435(7)	5.37
C8B	0.534(1)	0.207(1)	0.5803(7)	4.69
C9B	0.333(1)	0.263(2)	0.4112(8)	8.32

Table A3.5 contd.

ATOM	X	Y	Z	B
C10B	0.164(1)	0.233(2)	0.4385(7)	6.74
C11B	0.0393(8)	0.196(1)	0.5910(6)	5.74
C12B	0.153(1)	0.061(1)	0.6282(4)	6.75
O1B	0.617(1)	0.084(2)	0.4409(7)	7.01
P1	0.9284(3)	0.0121(3)	0.8436(1)	4.29
F1	0.905(1)	0.153(1)	0.7859(5)	10.02
F2	0.7392(9)	0.011(1)	0.8441(3)	9.19
F3	0.933(1)	-0.1314(8)	0.8984(5)	10.40
F4	1.1221(8)	0.0132(9)	0.8450(3)	6.92
F5	0.973(1)	0.111(1)	0.9321(4)	9.29
F6	0.889(1)	-0.0988(9)	0.7573(4)	10.65

Table A4.1

Crystal Data for $[(Cu^{I}(TTCN))_2(1,4\text{-Dithiane})](PF_6)_2$.

Empirical Formula	$CuS_4C_8H_{16}PF_6$
Formula Weight	448.96
Molecular Weight	897.92
Space Group	C2/c (#15)
a, Å	19.832 (6)
b, Å	13.396 (2)
c, Å	15.815 (4)
β°	133.57 (1)
V, Å^3	3044 (1)
Z	8
d_{calcd}, g. cm^{-3}	1.959
$\mu_{(CuK\alpha}$, cm^{-1}	86.25
p-factor	0.15
R	0.041
R_w	0.044
GOF	1.08

Table A4.2

Selected Bond Lengths for $[(Cu^{I}(TTCN))_2(1,4\text{-Dithiane})](PF_6)_2$ (Å)

Atom	Atom	Distance
Cu_1	S_1	2.323 (1)
Cu_1	S_4	2.311 (1)
Cu_1	S_7	2.320 (2)
Cu_1	S_{10}	2.223 (1)
S_1	C_2	1.840 (4)
S_1	C_9	1.826 (4)
S_4	C_3	1.826 (4)
S_4	C_5	1.798 (5)
S_7	C_6	1.834 (5)
S_7	C_8	1.833 (4)
S_{10}	C_{11}	1.807 (4)
S_{10}	C_{12}	1.805 (4)

Table A4.3

Selected Bond Angles for $[(Cu^{I}(TTCN))_2(1,4\text{-Dithiane})](PF_6)_2$ (°)

Atom	Atom	Atom	Angle	Atom	Atom	Atom	Angle
S_1	Cu_1	S_4	94.48(4)	S_1	Cu_1	S_{10}	119.29(4)
S_4	Cu_1	S_7	94.06(4)	S_4	Cu_1	S_{10}	119.31(4)
S_7	Cu_1	S_1	94.29(4)	S_7	Cu_1	S_{10}	127.72(5)
Cu_1	S_1	C_2	99.10(1)	Cu_1	S_1	C_9	102.3(2)
Cu_1	S_4	C_3	96.8(1)	Cu_1	S_4	C_5	100.1(1)
Cu_1	S_7	C_6	97.5(2)	Cu_1	S_7	C_8	98.81(2)
Cu_1	S_{10}	C_{11}	106.4(2)	Cu_1	S_{10}	C_{12}	110.0(2)
S_1	C_2	C_3	112.6(3)	S_7	C_6	C_5	115.5(3)
S_4	C_3	C_2	115.6(3)	S_7	C_8	C_9	113.6(3)
S_4	C_5	C_6	115.2(3)	S_1	C_9	C_8	115.9(3)
S_{10}	C_{11}	C_{12}*	114.0(3)	S_{10}	C_{12}	C_{11}*	115.3(3)
C_2	S_1	C_9	102.3(2)	C_3	S_4	C_5	102.9(2)
C_6	S_7	C_8	102.1(2)				

Table A4.4

Torsion Angles for $[(Cu^{I}(TTCN))_2(1,4\text{-Dithiane})](PF_6)_2$

Atom	Atom	Atom	Atom	Angle (°)
S_1	Cu_1	S_4	C_3	-15.5 (2)
S_1	Cu_1	S_4	C_5	89.0 (2)
S_1	Cu_1	S_7	C_6	-109.4 (2)
S_1	Cu_1	S_7	C_8	-5.9 (1)
S_4	Cu_1	S_1	C_2	-6.5 (1)
S_4	Cu_1	S_1	C_9	-110.1 (1)
S_4	Cu_1	S_7	C_6	-14.6 (2)
S_4	Cu_1	S_7	C_8	88.9 (1)
S_7	Cu_1	S_1	C_2	87.9 (1)
S_7	Cu_1	S_1	C_9	-15.6 (1)
S_7	Cu_1	S_4	C_3	-110.2 (2)
S_7	Cu_1	S_4	C_5	-5.7 (2)
S_1	Cu_1	S_{10}	C_{11}	162.3 (2)
S_1	Cu_1	S_{10}	C_{12}	-90.4 (2)

Table A4.4 contd.

S_4	Cu_1	S_{10}	C_{11}	47.6 (2)
S_4	Cu_1	S_{10}	C_{12}	154.9 (2)
S_7	Cu_1	S_{10}	C_{11}	-74.9 (2)
S_7	Cu_1	S_{10}	C_{12}	32.5 (2)
S_{10}	Cu_1	S_1	C_2	117.9 (2)
S_{10}	Cu_1	S_1	C_9	-138.6 (1)
S_{10}	Cu_1	S_4	C_3	111.8 (2)
S_{10}	Cu_1	S_4	C_5	-143.7 (2)
S_{10}	Cu_1	S_7	C_6	117.9 (2)
S_{10}	Cu_1	S_7	C_8	-138.6 (1)
Cu_1	S_1	C_2	C_3	33.6 (3)
Cu_1	S_1	C_9	C_8	42.5 (3)
Cu_1	S_4	C_3	C_2	42.5 (3)
Cu_1	S_4	C_5	C_6	31.3 (3)
Cu_1	S_7	C_6	C_5	38.4 (4)
Cu_1	S_7	C_8	C_9	33.3 (3)

Table A4.4 contd.

Cu_1	S_{10}	C_{11}	C_{12}	57.9 (3)
Cu_1	S_{10}	C_{12}	C_{11}	-54.2 (4)
S_1	C_2	C_3	S_4	-55.1 (4)
C_2	C_3	S_4	C_5	-59.5 (4)
C_3	S_4	C_5	C_6	130.8 (3)
S_4	C_5	C_6	S_7	-50.6 (4)
C_5	C_6	S_7	C_8	-62.3 (4)
C_6	S_7	C_8	C_9	133.0 (3)
S_1	C_9	C_8	S_7	-55.3 (4)
C_2	S_1	C_9	C_8	-58.3 (3)
C_3	C_2	S_1	C_9	132.1 (3)

Table A4.5. Fractional coordinates and B_{eq} for $[(Cu^{I}(TTCN))_2(1,4\text{-dithiane})](PF_6)_2$

atom	x	y	z	B(eq)
Cu(1)	0.27235(4)	0.22348(4)	0.20990(4)	1.52(4)
S(1)	0.27812(7)	0.10428(7)	0.32146(8)	1.42(4)
S(4)	0.24012(7)	0.35426(7)	0.27269(9)	1.72(4)
S(7)	0.43159(7)	0.25192(7)	0.34809(8)	1.67(5)
S(10)	0.18086(7)	0.19786(7)	0.01959(8)	1.56(4)
C(2)	0.2680(3)	0.1871(3)	0.4051(4)	1.7(1)
C(3)	0.2065(3)	0.2783(3)	0.3345(4)	1.9(2)
C(5)	0.3564(3)	0.3928(3)	0.3995(4)	2.1(2)
C(6)	0.4288(3)	0.3772(3)	0.3923(4)	2.0(2)
C(8)	0.4631(3)	0.1742(3)	0.4663(4)	1.7(1)
C(9)	0.4035(3)	0.0826(3)	0.4241(4)	1.6(1)
C(11)	0.1657(3)	0.3179(3)	-0.0437(4)	2.0(2)
C(12)	0.2445(3)	0.1333(3)	-0.0072(4)	1.8(2)
H(1)	0.229(2)	0.146(2)	0.411(2)	-1.1(5)
H(2)	0.330(3)	0.208(3)	0.480(4)	0.6(7)
H(3)	0.216(3)	0.317(3)	0.395(4)	1.1(8)
H(4)	0.131(3)	0.265(3)	0.259(4)	1.2(8)
H(5)	0.357(3)	0.463(5)	0.404(4)	3(1)
H(6)	0.382(4)	0.364(5)	0.469(5)	4(1)
H(7)	0.491(3)	0.395(4)	0.454(4)	2(1)
H(8)	0.420(2)	0.413(3)	0.341(3)	0.5(8)
H(9)	0.555(4)	0.140(6)	0.564(6)	5(1)
H(10)	0.460(3)	0.199(3)	0.515(4)	1.0(8)
H(11)	0.414(2)	0.051(3)	0.487(3)	-0.5(6)

Table A4.5 contd.

atom	x	y	z	B(eq)
H(12)	0.401(5)	0.029(6)	0.363(6)	6(2)
H(15)	0.205(3)	0.131(3)	-0.083(4)	1.0(8)
H(13)	0.129(2)	0.297(2)	-0.120(3)	-0.9(6)
H(14)	0.137(2)	0.366(3)	-0.024(3)	0.5(7)
H(16)	0.267(3)	0.080(4)	0.033(3)	0.7(8)
P(1)	1/2	0.0392(1)	3/4	1.27(5)
F(1)	0.5198(2)	-0.0460(2)	0.6978(2)	2.18(9)
F(2)	0.3922(2)	0.0398(2)	0.6316(2)	2.00(8)
F(3)	0.5189(2)	0.1225(2)	0.6966(2)	2.21(9)
P(2)	1/2	0.4101(1)	3/4	2.05(6)
F(4)	0.5707(2)	0.3259(2)	0.8427(2)	2.8(1)
F(5)	0.4524(2)	0.4099(2)	0.8005(2)	3.5(1)
F(6)	0.5710(3)	0.4929(2)	0.8428(3)	5.0(1)

Table A5.1

Crystal Data for $[Co^{III}(en)_2(Met)](ClO_4)_2.H_2O$.

Empirical Formula	$CoCl_2SO_{11}N_5C_9H_{28}$
Molecular Weight	544.25
Space Group	$P2_1$ (#4)
a, Å	9.582 (2)
b, Å	11.554 (2)
c, Å	19.988 (6)
β°	98.85 (2)
V, Å^3	2186.5 (8)
Z	4
d_{calcd}, g. cm^{-3}	1.622
$\mu_{(CuK\alpha}$, cm^{-1}	101.96
p-factor	0.10
R	0.074
R_w	0.104
GOF	1.60

Table A5.2

Selected Bond Distances for $[Co^{III}(en)_2(Met)](ClO_4)_2$ (Å)

Atom	Atom	Distance	Atom	Atom	Distance
Co_{1A}	N_{1A}	1.99 (2)	Co_{1B}	N_{1B}	1.92 (2)
Co_{1A}	N_{4A}	1.89 (2)	Co_{1B}	N_{4B}	2.03 (2)
Co_{1A}	N_{5A}	1.95 (2)	Co_{1B}	N_{5B}	1.99 (2)
Co_{1A}	N_{8A}	1.97 (2)	Co_{1B}	N_{8B}	2.00 (2)
Co_{1A}	N_{9A}	1.97 (2)	Co_{1B}	N_{9B}	1.95 (2)
Co_{1A}	O_{16A}	1.97 (1)	Co_{1B}	O_{16B}	1.82 (2)

Table A5.3

Selected Bond Angles for $[Co^{III}(en)(Met)](ClO_4)_2$ (°)

Atom	Atom	Atom	Angle	Atom	Atom	Atom	Angle
N_{1A}	Co_{1A}	N_{4A}	84.9(8)	N_{1B}	Co_{1B}	N_{4B}	85.0(1)
N_{1A}	Co_{1A}	N_{5A}	87.0(7)	N_{1B}	Co_{1B}	N_{5B}	96.0(8)
N_{1A}	Co_{1A}	N_{8A}	174.2(8)	N_{1B}	Co_{1B}	N_{8B}	175.0(1)
N_{1A}	Co_{1A}	N_{9A}	90.2(7)	N_{1B}	Co_{1B}	N_{9B}	92.8(9)
N_{4A}	Co_{1A}	N_{5A}	91.8(8)	N_{4B}	Co_{1B}	N_{5B}	90.5(8)
N_{4A}	Co_{1A}	N_{8A}	98.7(9)	N_{4B}	Co_{1B}	N_{8B}	89.4(8)
N_{4A}	Co_{1A}	N_{9A}	99.8(8)	N_{4B}	Co_{1B}	N_{9B}	86.8(7)
N_{5A}	Co_{1A}	N_{8A}	88.3(8)	N_{5B}	Co_{1B}	N_{8B}	84.1(7)
N_{5A}	Co_{1A}	N_{9A}	167.8(8)	N_{5B}	Co_{1B}	N_{9B}	170.5(9)
N_{8A}	Co_{1A}	N_{9A}	93.6(8)	N_{8B}	Co_{1B}	N_{9B}	86.8(7)
N_{1A}	Co_{1A}	O_{16A}	85.0(6)	N_{1B}	Co_{1B}	O_{16B}	94.6(9)
N_{4A}	Co_{1A}	O_{16A}	169.8(7)	N_{4B}	Co_{1B}	O_{16B}	174.9(8)
N_{5A}	Co_{1A}	O_{16A}	85.6(7)	N_{5B}	Co_{1B}	O_{16B}	94.5(8)

Table A5.3 Contd.

N_{8A}	Co_{1A}	O_{16A}	91.2(7)	N_{8B}	Co_{1B}	O_{16B}	90.6(8)
N_{9A}	Co_{1A}	O_{16A}	82.3(7)	N_{9B}	Co_{1B}	O_{16B}	88.2(7)
Co_{1A}	N_{1A}	C_{2A}	109.0(2)	Co_{1B}	N_{1B}	C_{2B}	110.0(2)
Co_{1A}	N_{4A}	C_{3A}	117.0(2)	Co_{1B}	N_{4B}	C_{3B}	105.0(2)
Co_{1A}	N_{5A}	C_{6A}	108.0(2)	Co_{1B}	N_{5B}	C_{6B}	109.0(2)
Co_{1A}	N_{8A}	C_{7A}	106.0(1)	Co_{1B}	N_{8B}	C_{7B}	112.0(1)
Co_{1A}	N_{9A}	C_{10A}	109.0(1)	Co_{1B}	N_{9B}	C_{10B}	108.0(2)
Co_{1A}	O_{16A}	C_{15A}	116.0(1)	Co_{1B}	O_{16B}	C_{15B}	118.0(2)

Table A5.4

Torsion Angles for $[Co^{III}(en)_2(Met)](ClO_4)_2$

Conformation A

Atom	Atom	Atom	Atom	Angle (°)
Co_{1A}	N_{1A}	C_{2A}	C_{3A}	-39 (2)
Co_{1A}	N_{4A}	C_{3A}	C_{2A}	-23 (2)
Co_{1A}	N_{5A}	C_{6A}	C_{7A}	30 (2)
Co_{1A}	N_{8A}	C_{7A}	C_{6A}	37 (2)
Co_{1A}	N_{9A}	C_{10A}	C_{11A}	162 (1)
Co_{1A}	N_{9A}	C_{10A}	C_{15A}	39 (2)
Co_{1A}	O_{16A}	C_{15A}	C_{10A}	16 (2)
Co_{1A}	O_{16A}	C_{15A}	C_{17A}	179 (2)
N_{1A}	Co_{1A}	N_{4A}	C_{3A}	2 (1)
N_{1A}	Co_{1A}	N_{5A}	C_{6A}	169 (1)
N_{1A}	Co_{1A}	N_{8A}	C_{7A}	-50 (9)
N_{1A}	Co_{1A}	N_{9A}	C_{10A}	-112 (1)
N_{1A}	Co_{1A}	O_{16A}	C_{15A}	98 (1)

Table A5.4 contd.

C_{2A}	N_{1A}	Co_{1A}	N_{4A}	22 (1)
C_{2A}	N_{1A}	Co_{1A}	N_{5A}	114 (1)
C_{2A}	N_{1A}	Co_{1A}	N_{8A}	150 (8)
C_{2A}	N_{1A}	Co_{1A}	N_{9A}	-78 (1)
C_{2A}	N_{1A}	Co_{1A}	O_{16A}	-161 (1)
C_{3A}	N_{4A}	Co_{1A}	N_{5A}	-84 (2)
C_{3A}	N_{4A}	Co_{1A}	N_{8A}	-173 (1)
C_{3A}	N_{4A}	Co_{1A}	N_{9A}	92 (2)
C_{3A}	N_{4A}	Co_{1A}	O_{16A}	-9 (5)
N_{4A}	Co_{1A}	N_{5A}	C_{6A}	-106 (1)
N_{4A}	Co_{1A}	N_{8A}	C_{7A}	78 (1)
N_{4A}	Co_{1A}	N_{9A}	C_{10A}	163 (1)
N_{4A}	Co_{1A}	O_{16A}	C_{15A}	109 (4)
N_{5A}	Co_{1A}	N_{8A}	C_{7A}	-14 (1)
N_{5A}	Co_{1A}	N_{9A}	C_{10A}	-35 (4)
N_{5A}	Co_{1A}	O_{16A}	C_{15A}	-175 (1)

Table A5.4 contd.

C_{6A}	N_{5A}	Co_{1A}	N_{8A}	-8 (1)
C_{6A}	N_{5A}	Co_{1A}	N_{9A}	91 (4)
C_{6A}	N_{5A}	Co_{1A}	O_{16A}	84 (1)
C_{7A}	N_{8A}	Co_{1A}	N_{9A}	178 (1)
C_{7A}	N_{8A}	Co_{1A}	O_{16A}	-99 (1)
N_{8A}	Co_{1A}	N_{9A}	C_{10A}	64 (1)
N_{8A}	Co_{1A}	O_{16A}	C_{15A}	-87 (1)
N_{9A}	Co_{1A}	O_{16A}	C_{15A}	7 (1)
C_{10A}	N_{9A}	Co_{1A}	O_{16A}	-27 (1)

Conformation B

Atom	Atom	Atom	Atom	Angle (°)
Co_{1B}	N_{1B}	C_{2B}	C_{3B}	45 (2)
Co_{1B}	N_{4B}	C_{3B}	C_{2B}	42 (3)
Co_{1B}	N_{5B}	C_{6B}	C_{7B}	-54 (2)
Co_{1B}	N_{8B}	C_{7B}	C_{6B}	-39 (3)
Co_{1B}	N_{9B}	C_{10B}	C_{11B}	121 (2)
Co_{1B}	N_{9B}	C_{10B}	C_{15B}	-10 (3)

Table A5.4 contd.

Co_{1B}	O_{16B}	C_{15B}	C_{10B}	-1 (3)
Co_{1B}	O_{16B}	C_{15B}	C_{17B}	170 (2)
N_{1B}	Co_{1B}	N_{4B}	C_{3B}	-12 (2)
N_{1B}	Co_{1B}	N_{5B}	C_{6B}	-159 (2)
N_{1B}	Co_{1B}	N_{8B}	C_{7B}	-80 (9)
N_{1B}	Co_{1B}	N_{9B}	C_{10B}	102 (2)
N_{1B}	Co_{1B}	O_{16B}	C_{15B}	-97 (2)
C_{2B}	N_{1B}	Co_{1B}	N_{4B}	-19 (1)
C_{2B}	N_{1B}	Co_{1B}	N_{5B}	-109 (2)
C_{2B}	N_{1B}	Co_{1B}	N_{8B}	-17 (10)
C_{2B}	N_{1B}	Co_{1B}	N_{9B}	68 (2)
C_{2B}	N_{1B}	Co_{1B}	O_{16B}	156 (2)
C_{3B}	N_{4B}	Co_{1B}	N_{5B}	84 (2)
C_{3B}	N_{4B}	Co_{1B}	N_{8B}	169 (2)
C_{3B}	N_{4B}	Co_{1B}	N_{9B}	-105 (2)
C_{3B}	N_{4B}	Co_{1B}	O_{16B}	-102 (9)

Table A5.4 contd.

N_{4B}	Co_{1B}	N_{5B}	C_{6B}	116 (2)
N_{4B}	Co_{1B}	N_{8B}	C_{7B}	-79 (2)
N_{4B}	Co_{1B}	N_{9B}	C_{10B}	-172 (2)
N_{4B}	Co_{1B}	O_{16B}	C_{15B}	-7 (10)
N_{5B}	Co_{1B}	N_{8B}	C_{7B}	12 (2)
N_{5B}	Co_{1B}	N_{9B}	C_{10B}	-99 (5)
N_{5B}	Co_{1B}	O_{16B}	C_{15B}	167 (2)
C_{6B}	N_{5B}	Co_{1B}	N_{8B}	26 (2)
C_{6B}	N_{5B}	Co_{1B}	N_{9B}	42 (6)
C_{6B}	N_{5B}	Co_{1B}	O_{16B}	-64 (2)
C_{7B}	N_{8B}	Co_{1B}	N_{9B}	-166 (2)
C_{7B}	N_{8B}	Co_{1B}	O_{16B}	106 (2)
N_{8B}	Co_{1B}	N_{9B}	C_{10B}	-83 (2)
N_{8B}	Co_{1B}	O_{16B}	C_{15B}	83 (2)
N_{9B}	Co_{1B}	O_{16B}	C_{15B}	-4 (2)
C_{10B}	N_{9B}	Co_{1B}	O_{16B}	8 (2)

Table A5.5. Fractional coordinates and B_{eq} for $[(Co^{III}(en)_2(Met)](ClO_4)_2.H_2O$

atom	x	y	z	B(eq)
Co(1A)	0.1995(3)	0.4663	0.0622(2)	2.6(1)
N(1A)	0.346(2)	0.550(1)	0.0204(8)	3.8(7)
C(2A)	0.444(2)	0.466(3)	-0.001(1)	4(1)
C(3A)	0.472(2)	0.367(2)	0.053(1)	4(1)
N(4A)	0.333(2)	0.344(2)	0.075(1)	3.9(9)
N(5A)	0.280(1)	0.538(2)	0.147(1)	3.0(7)
C(6A)	0.174(2)	0.517(2)	0.201(1)	3(1)
C(7A)	0.105(2)	0.413(2)	0.185(1)	2.8(8)
N(8A)	0.053(2)	0.398(2)	0.109(1)	4(1)
N(9A)	0.100(2)	0.426(2)	-0.0282(8)	3.2(8)
C(10A)	-0.041(2)	0.491(2)	-0.0402(9)	3.3(8)
C(11A)	-0.098(2)	0.493(2)	-0.116(1)	4.0(9)
C(12A)	-0.149(2)	0.379(3)	-0.142(1)	5(1)
S(13A)	-0.3114(7)	0.3230(8)	-0.1150(4)	4.9(3)
C(14A)	-0.441(2)	0.416(3)	-0.165(1)	6(1)
C(15A)	-0.001(2)	0.610(2)	-0.008(1)	2.7(8)
O(16A)	0.089(1)	0.610(1)	0.0448(7)	2.9(5)
O(17A)	-0.083(1)	0.692(2)	-0.0277(8)	4.6(8)
Co(1B)	0.2094(3)	1.0018(3)	0.5616(2)	2.9(2)
N(1B)	0.360(2)	0.939(2)	0.520(1)	5(1)
C(2B)	0.447(3)	1.037(2)	0.494(1)	5(1)
C(3B)	0.465(3)	1.117(3)	0.552(2)	6(2)
N(4B)	0.323(2)	1.151(2)	0.5687(8)	3.6(8)
N(5B)	0.292(2)	0.960(2)	0.6560(9)	3.8(8)

Table A5.5 contd.

atom	x	y	z	B(eq)
C(6B)	0.181(3)	0.958(3)	0.697(1)	6(1)
C(7B)	0.104(4)	1.089(3)	0.683(2)	8(2)
N(8B)	0.062(2)	1.081(2)	0.6058(7)	3.1(7)
N(9B)	0.110(2)	1.062(2)	0.476(1)	3.7(8)
C(10B)	-0.007(2)	0.983(3)	0.452(1)	4(1)
C(11B)	-0.146(2)	1.027(2)	0.442(1)	6(1)
C(12B)	-0.171(3)	1.123(3)	0.379(1)	6(1)
S(13B)	-0.3413(8)	1.1747(8)	0.3804(4)	5.6(3)
C(14B)	-0.452(3)	1.078(2)	0.323(1)	5(1)
C(15B)	0.001(3)	0.870(3)	0.495(2)	4(2)
O(16B)	0.100(2)	0.873(2)	0.5479(7)	4.9(9)
O(17B)	-0.064(2)	0.783(1)	0.478(1)	3.6(8)
O(1W)	0.545(2)	0.648(2)	0.284(1)	9(1)
O(2W)	0.543(2)	0.842(3)	0.778(1)	9(1)
Cl(1C)	0.2355(8)	0.808(1)	0.3479(4)	6.6(4)
O(1C)	0.096(6)	0.836(5)	0.312(2)	24(4)
O(2C)	0.317(9)	0.894(6)	0.359(2)	44(8)
O(3C)	0.213(2)	0.770(2)	0.4095(8)	7(1)
O(4C)	0.283(4)	0.732(3)	0.308(1)	16(2)
Cl(1D)	0.7228(6)	0.6449(7)	0.1158(3)	4.0(3)
O(1D)	0.608(3)	0.620(3)	0.149(1)	12(2)
O(2D)	0.790(2)	0.546(2)	0.102(2)	11(1)
O(3D)	0.820(3)	0.712(4)	0.150(2)	18(3)
O(4D)	0.668(3)	0.692(3)	0.055(1)	13(2)
Cl(1E)	0.2452(9)	0.6644(8)	0.8428(4)	6.1(4)

Table A5.5 contd.

atom	x	y	z	B(eq)
O(1E)	0.170(5)	0.716(3)	0.791(1)	21(3)
O(2E)	0.393(3)	0.679(2)	0.844(2)	17(2)
O(3E)	0.208(3)	0.722(5)	0.898(2)	21(3)
O(4E)	0.223(2)	0.545(2)	0.839(1)	9(1)
Cl(1F)	0.7226(6)	0.8411(8)	0.6158(3)	4.8(3)
O(1F)	0.672(2)	0.825(3)	0.546(1)	12(2)
O(2F)	0.816(3)	0.921(3)	0.624(2)	17(3)
O(3F)	0.604(1)	0.870(2)	0.6470(8)	4.9(7)
O(4F)	0.776(4)	0.733(4)	0.641(3)	23(4)